UNIVERSIDAD DE CONCEPCION
ESCUELA DE GRADUADOS
CONCEPCION–CHILE

INTERACCION ENTRE FLUIDOS Y ESTRUCTURAS DELGADAS

Tesis para optar al grado de
Doctor en Ciencias Aplicadas con mención en Ingeniería Matemática

Erwin Carlos Hernández Hernández

FACULTAD DE CIENCIAS FISICAS Y MATEMATICAS
DEPARTAMENTO DE INGENIERIA MATEMATICA
2002

INTERACCION ENTRE FLUIDOS Y ESTRUCTURAS DELGADAS

Erwin Carlos Hernández Hernández

Director de Tesis: Dr. Rodolfo Rodríguez A.

Director de Programa: Dr. Norbert Heuer.

COMISION EVALUADORA

Dr. Alfredo Bermúdez, Universidad de Compostela, España

Dr. Daniele Boffi, Universidad de Pavia, Italia

COMISION EXAMINADORA

Firma: _____
Dr. Mario Durán
Pontificia Universidad Católica, Chile

Firma: _____
Dr. Ricardo Durán
Universidad de Buenos Aires, Argentina

Firma: _____
Dr. Gabriel Gatica
Universidad de Concepción, Chile

Firma: _____
Dr. Rodolfo Rodríguez
Universidad de Concepción, Chile

Fecha Examen de Grado: _____

Calificación: _____

Concepción–Diciembre 2002

AGRADECIMIENTOS

Deseo expresar mi más sincero agradecimiento a Rodolfo Rodríguez, mi director, por su motivación, confianza y contaste apoyo. Gracias a su profesionalimo y dedicación ha sabido introducirme en la matemática aplicada y, con ello, al buen término de este trabajo.

No puedo dejar pasar estas líneas sin mencionar a quien ha sido un importante pilar en mi formación, Gabriel Gatica quien es para mi un excelente profesor, dentro y fuera de las aulas.

Al Fondo Nacional de Ciencia y Tecnología (FONDECYT) por financiar este trabajo por medio del proyecto para alumnos de doctorado No. 2000114.

A todos quienes habitan el DIM, quienes a lo largo de estos años han mantenido un buen lugar de camaraderia, lleno de trabajo y alegrias. En especial a quienes hicieron más fácil mi pasar por aqui, René y Teresita.

A mis amigos del departamento de Matemática Aplicada de la U. de Santiago de Compostela, la excelente hospitalidad en las dos ocasiones que estuve allí.

A Mario y Tomás, a quienes agradezco estos años de compartir largas horas de reunión y discusión. Por decir siempre las cosas como son y nunca olvidar que "no solo de matemáticas se vive". Gracias por su amistad, la que espero mucho perdure.

Un profundo agradecimiento a toda mi familia, sin su amor y cariño, siempre presente, no hubiese sido posible finalizar este trabajo. Un abrazo muy especial a mi hermana, Marcela.

Finalmente, a la persona a quien dedico mi trabajo, la más importante en mi vida, la que me ha animado y apoyado no dejándome caer, a quien doy infinitas gracias por todo: mi Madre, IHA.

A mi Madre y mi Hijo, Ma. Angélica y Nicolás,
Con mucho Amor...

RESUMEN

El objetivo de esta tesis es desarrollar y analizar, teórica y computacionalmente, métodos numéricos para el cálculo de los modos naturales de vibración de baja frecuencia de un sistema acoplado, con interacción acústica entre un fluido compresible y una estructura delgada.

Se demuestra convergencia y se obtienen estimaciones de error óptimas en orden y regularidad para el problema acústico espectral sobre dominios curvos no convexos. Se estudian dos formulaciones del problema, usando elementos lineales a trozos y continuos para una formulación en presiones y elementos de Raviart-Thomas para una formulación en desplazamientos.

Para la estructura se usa el modelo clásico de Naghdi sobre un dominio de referencia. Para evitar el bloqueo numérico (locking), se consideran métodos de bajo orden de la familia de los MITC (Mixed Interpolation of Tensorial Component) sobre cuadriláteros. Para una placa, bajo ciertas hipótesis, se prueba convergencia y estimaciones de error válidas con constantes independientes del espesor de la misma.

Finalmente, se considera el problema acoplado utilizando elementos de Raviart-Thomas hexaédricos en el fluido e imponiendo de manera débil la condición de interfaz entre ambos medios. Se obtienen estimaciones de error óptimas para las autofunciones calculadas así como un doble orden para los autovalores.

Se presentan experimentos numéricos que corroboran el buen comportamiento de los métodos, incluso en algunos casos no cubiertos por la teoría desarrollada.

ABSTRACT

The goal of this thesis is to develop and analyze, theoretically and computationally, numerical methods for the computation of the free vibration modes of coupled systems. We consider an elasto-acoustic problem involving interaction between a compressible fluid and a thin structure.

Convergence and optimal in order and regularity error estimates are proved for the spectral acoustic problem on a curved non-convex domain. We study two different formulations of the problem. The first one is a pressure formulation which is approximated using standard piecewise linear continuous elements, and the other oner is a displacement formulation approximated using Raviart-Thomas elements.

For the thin structure, we use the classical Naghdi model over a reference domain. To avoid numerical locking, we consider a low-order method of the so called MITC (Mixed Interpolation of Tensorial Component) family on quadrilateral meshes. In the case of a plate, under mild assumptions, we obtain convergence and error estimates involving constants independent of the thickness.

Finally, we consider the coupled problem using hexahedal Raviart-Thomas elements in the fluid and a non conforming coupling on the fluid-solid interface. We obtain optimal order error estimates for the computed eigenfunctions, as well as a double order for the eigenvalues.

We report several numerical experiments to assess the performance of the methods, even in some cases not covered by the developed theory.

Contents

Introducción

Un problema importante que ocurre en aplicaciones en ingeniería proviene de las numerosas situaciones en que una estructura sólida está en contacto con un fluido. Ejemplos de esta interacción son las vibraciones de un tanque de combustible, el sonido de instrumentos musicales, propagación de ruidos en vehículos, el efecto del aire en las alas de un avión, etc.

Dependiendo del acotamiento del dominio, diferente será la naturaleza de estos problemas: en la mayoría de las situaciones el sólido es un dominio acotado, aquellos problemas en que el dominio del fluido también es acotado se llaman *problemas interiores* (por ejemplo, un tanque lleno de líquido) y cuando el dominio del fluido no es acotado se llaman *problemas exteriores* (por ejemplo, una barco flotando en el mar).

Puede observarse que el conjunto de problemas que engloba la denominación *interacción fluido-estructura* es muy diversa, sin embargo presentan dos caracterízticas comunes, esto es, por una parte involucran el estudio tanto del fluidos como de estructuras sólidas y, por otro lado, requieren establecer modelos adecuados para una resolución eficaz del problema acoplado.

En este trabajo nos enfocaremos al estudio de la resolución numérica de un problema interior de interacción fluido-estructura: el problema elastoacústico. Un problema modelo, de este tipo, consiste en determinar la respuesta dinámica de un fluido, compresible e ideal, que ocupa un dominio acotado, en contacto con una estructura elástica, ambos en pequeños desplazamientos, sujeto a fuerzas externas periódicas.

Nuestro interés radica en el cálculo de los primeros modos de vibración de un sistema elastoacústico. Principalmente, el conocimiento de estas frecuencias de vibración es necesario para evitar efectos de resonancia. Cuando una fuerza externa periódica actúa sobre un sistema dinámico, la intensidad de la respuesta dependerá de la frecuencia de la fuerza externa y será máxima cuando ésta sea igual a una de las frecuencias naturales del sistema, esto es, la raíz cuadrada de alguno de los primeros valores propios del sistema. Es decir, si la fuerza periódica externa tiene

un período cercano a los de resonancia se producirá un efecto importante sobre el sistema, lo cual podría corresponder a tensiones máximas, posibles rupturas o ruido excesivo dentro de la cavidad.

Para los problemas en que la estructura es un sólido elástico que interactúa con fluido, existe un fuerte desarrollo teórico y numérico, mucho del cual se puede encontrar en las monografías de Morand y Ohayon[68], Conca *et al.*[39] y Ohayon y Soize[69], donde también se dan métodos numéricos para la resolución de este problema y más referencias sobre el tema.

En las aplicaciones es usual que la estructura sea delgada en cuyo caso, además, la interacción entre el fluido y la estructura suele ser más fuerte. Un ejemplo típico de aplicación es la transmisión de ruidos al interior de vehículos. En nuestro trabajo consideramos estas estructuras delgadas; esto es, en general, *cáscaras* si son superficies curvas o *placas* si son superficies planas.

En lo que sigue presentamos los modelos que utilizaremos para describir el fluido y la cáscara.

Fluido.

Consideramos un *fluido acústico*, es decir, no viscoso, irrotacional y compresible. Estas hipótesis son plausibles cuando se trata de modelar la interacción acústica de un gas en contacto con un sólido (por ejemplo, transmisión de ruidos). Distintas formulaciones han sido propuestas para el análisis de problemas de interacción fluido–estructura considerando este modelo. Mas aún, como las cáscaras en general son curvas, estas formulaciones se establecen en dominios curvos, los cuales no necesariamente son convexos.

Las ecuaciones dinámicas que describen los pequeños desplazamientos de un fluido, respecto de una posición de equilibrio, al suponerlo viscoso y barotrópico, pueden obtenerse utilizando las fluctuaciones Eulerianas y Lagrangianas de éste, tanto para el problema como para las condiciones de frontera (una descripción detallada puede encontrarse en el libro de Morand y Ohayon[68]).

Si $U(x,\tau)$ y $P(x,\tau)$ representan los desplazamientos y las presiones de una partícula en la posición x en el tiempo τ, la segunda Ley de Newton se traduce en una vinculación entre estas pequeñas variaciones de presión y los pequeños desplazamientos del fluido en la forma:

$$\nabla P = -\rho_F \ddot{U},$$

donde ρ_F denota la densidad del fluido. Por otro lado, una especie de ley constitutiva, obtenida a partir de la conservación de masas, despreciando el efecto de la gravedad, se expresa como

$$P = -\rho_F c^2 \mathrm{div} U$$

donde c es la velocidad acústica o velocidad del sonido. Notemos que esta ley establece que cuando menos compresible es el fluido más alta debe ser la velocidad del sonido en él.

Con esto, las ecuaciones dinámicas del fluido son

$$\begin{aligned} \nabla P &= -\rho_F \ddot{U} \\ P &= -\rho_F c^2 \mathrm{div} U, \end{aligned}$$

para x en el dominio del fluido y el tiempo $\tau > 0$, más condiciones iniciales en $\tau = 0$.

Una solución estacionaria del problema se obtiene buscando soluciones armónicas en el tiempo de la forma

$$\begin{aligned} U(x,\tau) &= \vec{u}(x)\cos\omega\tau \\ P(x,\tau) &= p(x)\cos\omega\tau, \end{aligned}$$

donde $\vec{u}$ y p denotan los desplazamientos y las presiones como variables que sólo dependen de la posición, y ω es la frecuencia angular de vibración. Notemos que de la paridad de coseno, el caso de interés se reduce a $\omega \geq 0$. Teniendo en cuenta las expresiones anteriores, las ecuaciones que gobiernan las vibraciones libres (modos propios) de pequeña amplitud del fluido, en el dominio de las frecuencias, son:

- Ecuación de movimiento: $\nabla p = \omega^2 \rho_F \vec{u}$,
- Conservación de masa: $p = -\rho_F c^2 \mathrm{div}\vec{u}$.

Es claro que éstas ecuaciones pueden reducirse, utilizando la presión como variable o bien el desplazamiento, obteniendo una única ecuación en derivadas parciales.

El problema de determinar las vibraciones del fluido solo usualmente se trata eligiendo la presión como variable primaria, lo cual parece razonable considerando que p es una variable escalar. En este caso resulta:

$$-\rho_F \Delta p = \omega^2 \frac{\rho_F}{c^2} p.$$

Típicamente, el fluido solo se encuentra en una cavidad rígida, lo que conduce a imponer una condición homogénea sobre la derivada normal de la presión en la frontera. En cuyo caso, el problema que resulta es estudiar el cálculo de autovalores del Laplaciano con condición de Neumann homogenea en un dominio no convexo.

En el Capítulo 1 de este trabajo consideramos la aproximación por elementos finitos de este problema en un dominio no convexo. El contenido de este capítulo corresponde al artículo [56]:

- E. Hernández and R. Rodríguez, Finite element approximation of spectral problems with Neumann boundary conditions on curved domains. *Mathematics of Computation* (En prensa).

Haciendo uso de la teoría abstracta de convergencia espectral expuesta en Babuška y Osborn[7], para operadores compactos, en este artículo se ha probado convergencia y estimaciones de error óptimas para la aproximación del problema de autovalores del Laplaciano en 2D, con condiciones de Neumann, usando elementos finitos lineales a trozos y continuos en un dominio poligonal discreto Ω_h que aproxima el dominio original Ω no convexo, es decir, se tiene $\Omega_h \not\subset \Omega$. Resultados similares habian sido probados por Vanmaele y Ženíšek[82, 83] (usando la caracterización *min–max* de autovalores expuesta en Strang y Fix[80]) y por Lebaud[64], en ambos casos solo para condiciones de frontera de Dirichlet.

Para problemas acoplados, la elección de la presión para describir el fluido tiene un inconveniente, lleva a problemas de autovalores no-simétricos, cuya solución computacional involucra complicaciones a la hora de calcular los autovalores en los sistemas resultantes.

Alternativamente, el fluido ha sido descrito por diferentes variables, Everstine[47] y Olson y Bathe[70] han usado el potencial de velocidad (es decir, una función φ tal que $\partial\vec{u}/\partial\tau = \nabla\varphi$) obteniendo una formulación análoga a la anterior que involucra problemas de autovalores cuadráticos, mientras Morand y Ohayon[68] han usado la presión y el potencial de desplazamiento, conjuntamente, obteniendo problemas simétricos, pero de gran tamaño.

Otra posibilidad consiste en eliminar la presión para llegar a una ecuación en función del desplazamiento:

$$-\rho_F c^2 \nabla(\mathrm{div}\vec{u}) = \omega^2 \rho_F \vec{u},$$

lo que lleva a problemas de autovalores tambien simétricos. Sin embargo, con dos importantes dificultades.

Por un lado, la variable es vectorial lo cual requiere una aproximación por elementos finitos, en principio, más costosa.

Por otro lado, la segunda dificultad es aún mas compleja. En la formulación en desplazamientos el cero es un autovalor del sistema con autoespacio propio de dimensión infinita, cuyos elementos son nulos en el sólido y en el fluido corresponden a movimientos rotacionales que no inducen variación de la presión. Una discretización estandar de esta formulación involucra la presencia de frecuencias no nulas correspondientes a modos espúreos que no poseen sentido físico.

Una discretización alternativa ha sido introducida por Bermúdez y Rodríguez[19], la cual consiste en usar los elementos de Raviart–Thomas[75, 81] (llamados "*edge elements*" o "*face elements*", en 2D o 3D, respectivamente) para el fluido. Para problemas bidimensionales se ha probado en [12] y [74] la no existencia de modos espúreos y estimaciones de error con orden óptimo. Para ello se ha extendido la teoría espectral de operadores no compactos en [40] a métodos no conformes.

En el Capítulo 2, extendemos los resultados de [12] a un dominio curvo no necesariamente convexo. Este capítulo corresponde, principalmente, al artículo [56]:

- E. Hernández and R. Rodríguez, Finite element approximation of spectral acoustic problems on curved domains. (Enviado a Numerische Mathematik).

En él hemos considerado la formulación en desplazamientos del problema espectral de la acústica en un dominio curvo y no convexo. Hemos probado convergencia y estimaciones de error óptimas para la aproximación usando elementos de Raviart-Thomas. Tales resultados se conocen sólo para dominios poligonales ([12]).

Cáscara.

Una cáscara es un medio continuo tridimensional del cual una dimensión, el *grosor*, es pequeño comparado con las otras dos. Bajo la acción de pequeños movimientos la cáscara se deforma de acuerdo a las leyes normales de la elasticidad tridimensional.

El conocimiento de las vibraciones libres de una cáscara elástica es importante para el entendimiento general de los principios básicos de su comportamiento. Bajo la hipótesis de pequeños desplazamientos, son válidas las ecuaciones clásicas de la elasticidad lineal escrita en término de los desplazamientos. Sin embargo, al intentar simular computacionalmente una estructura delgada como un sólido tridimensional los resultados que se obtienen son de muy mala calidad (como lo ilustra el segundo ejemplo en [17]).

De hecho, si bien la literatura sobre cáscaras es muy amplia, es común admitir que los métodos computacionales utilizados no son completamente confiables (ver por ejemplo [30]). Desde el punto de vista del análisis numérico, hay serias dificultades para tratar cáscaras. En efecto, el concepto general de "cáscaras" cubre varias familias de problemas con muy marcadas diferencias en su comportamiento, dependiendo, por ejemplo, de la geometría de la superficie media, las condiciones de frontera y las cargas o fuerzas externas.

Durante los últimos años, una gran cantidad de trabajo se ha desarrollado en el tema, principalmente por las dos comunidades interesadas en resolver numericamente el problema: matemáticos numéricos e ingenieros. Pese al interés común , existe un grado de confusión entre ambas corrientes.

Como ha mencionado Chapelle en [31], en un marco general, se puede clasificar los elementos finitos para cáscaras en dos grandes familias: métodos que resultan de la discretización de los modelos matemáticos clásicos de cáscaras (métodos bidimensionales), donde el dominio de las incógnitas es la superficie media de la cáscaras (mas precisamente, necesitan una aplicación, llamada *carta*, que transforma un dominio bidimensional en la superficie media de la cáscara, ver por ejemplo [21, 33]), y métodos basados en "degenerar" un elemento finito sólido 3D en un "elemento de cáscara" usando algunas hipótesis cinemáticas para describir la variación del desplazamiento a largo del grosor de la estructura (elementos generales de cáscaras, ver [8, 11, 23]).

Los métodos clásicos son usualmente los elegidos por los matemáticos. Principalmente, porque se puede mostrar que las soluciones se aproximan con cierta precisión y, de hecho, se pueden obtener estimaciones de error *a priori* (ver [21]). Sin embargo, estos métodos requieren un abundante uso de la *carta* y, mas aún, las constantes que aparecen en las estimaciones dependen del grosor de la cáscara. Esto último, provoca lo que se conoce como *bloqueo numérico* ("*locking*"), al disminuir el grosor de la cáscara. Por otro lado, al no necesitar el uso de una carta y emplear leyes constitutivas generales 3D, los "elementos de cáscaras" entregan una mayor versatilidad al momento de usarlos. Sin embargo, debido a su construcción específica, es dificil obtener un analisis matemático general para ellos.

Recientemente, se ha obtenido una relación asintótica entre las dos familias de métodos (ver [31, 34]), lo que pone de manifiesto la necesidad de avanzar en el estudio de los métodos clasicos.

Los modelos de cáscaras clásicos más utilizados en la práctica son los de *Naghdi* y de *Koiter* (ver Bernadou[21]). Ambos toman en cuenta las deformaciones tanto de tipo membrana como de flexión. Se diferencian en que el segundo desprecia el *esfuerzo de corte tranversal* de la cáscara, al suponer que los puntos situados sobre una normal a la superficie media antes de la deformación permanecen en ésta después de la misma. Esta hipótesis es razonable para las cáscaras delgadas pero no para las moderadamente gruesas, en cuyo caso se considera el esfuerzo de corte, lo que se conoce como hipótesis de Reissner-Mindlin. Es importante hacer notar que estos modelos, se enmarcan en las hipótesis clásicas de operadores simétricos y compactos en un espacio de Hilbert. Así, el problema admite una sucesión creciente de autovalores reales, estrictamente positivos y de multiplicidad finita (ver [21]).

En lo que sigue introducimos las herramientas necesarias para describir estos modelos.

Las incógnitas, para estos modelos matemáticos, se definen en la superficie media de la cáscara, es decir sobre un dominio de referencia bidimensional que denotamos

por $\Omega \subset \mathbb{R}^2$, con frontera $\partial\Omega$ desde el cual la superficie media S se obtiene vía una *carta* $\vec{\phi}$ (también denominada mapeo),

$$\vec{\phi} : (\xi_1, \xi_2) \in \overline{\Omega} \subset \mathbb{R}^2 \longrightarrow \vec{\phi}(\xi_1, \xi_2) \in \overline{S} \subset \mathbb{R}^3,$$

donde $\overline{S} = S \cup \partial S$ con $\partial S = \vec{\phi}(\partial\Omega)$. Asumimos que tanto $\vec{\phi}$ como $\partial\Omega$ son suficientemente regulares. En particular, asumimos que todos los puntos de la superficie media $S = \vec{\phi}(\overline{\Omega})$ son regulares.

Con el propósito de introducir el modelo y el problema de vibraciones correspondiente, necesitamos algunas definiciones y notaciones clásicas de la geometría diferencial (ver Bernadou[21]).

Denotemos por $\vec{a}_\alpha$, $\alpha = 1, 2$, la base covariante del plano tangente a la superficie media en el punto $\vec{\phi}(\xi_1, \xi_2)$ (ver Figura 1), esto es

$$\vec{a}_\alpha = \vec{\phi}_{,\alpha} = \frac{\partial \vec{\phi}}{\partial \xi_\alpha}, \quad \alpha = 1, 2,$$

y la base contravariante $\vec{a}^\beta$, dada por

$$\vec{a}_\alpha \cdot \vec{a}^\beta = \delta_\alpha^\beta = \begin{cases} 1 & \alpha = \beta, \\ 0 & \alpha \neq \beta, \end{cases}$$

donde $\alpha, \beta \in \{1, 2\}$. El vector normal unitario a la superficie media en el punto $\vec{\phi}(\xi_1, \xi_2)$ es

$$\vec{a}_3 = \frac{\vec{a}_1 \times \vec{a}_2}{|\vec{a}_1 \times \vec{a}_2|},$$

donde $|\cdot|$ denota la norma euclideana en el espacio $\mathbb{R}^3$.

Entonces podemos definir la cáscara sin deformar $\mathcal{C}$, de grosor constante t, como el subconjunto cerrado de $\mathbb{R}^3$ formado por todos los puntos situados a una distancia $\xi_3 \in [-\frac{t}{2}, \frac{t}{2}]$ desde el punto $\vec{\phi}(\xi_1, \xi_2)$, en la dirección de $\vec{a}_3$, para todo punto $(\xi_1, \xi_2) \in \overline{\Omega}$, esto es

$$\mathcal{C} := \Big\{ M \in \mathbb{R}^3 : \ M = \vec{\phi}(\xi_1, \xi_2) + \xi_3 \vec{a}_3, \ (\xi_1, \xi_2) \in \overline{\Omega}, \ -\frac{t}{2} \leq \xi_3 \leq \frac{t}{2} \Big\}.$$

En lo que sigue, las letras griegas $\alpha, \beta, \ldots$ denotan índices que toman valores en el conjunto {1,2}, las letras latinas $i, j, \ldots$ para índices en el conjunto {1,2,3}. Usamos también la clásica convención sobre los índices repetidos (conocida como notación de Einstein), es decir índices repetidos indican sumatoria sobre ellos.

Denotamos por $a_{\alpha\beta}$ la *primera forma fundamental* de la superficie, que está dada por

$$a_{\alpha\beta} = \vec{a}_\alpha \cdot \vec{a}_\beta,$$

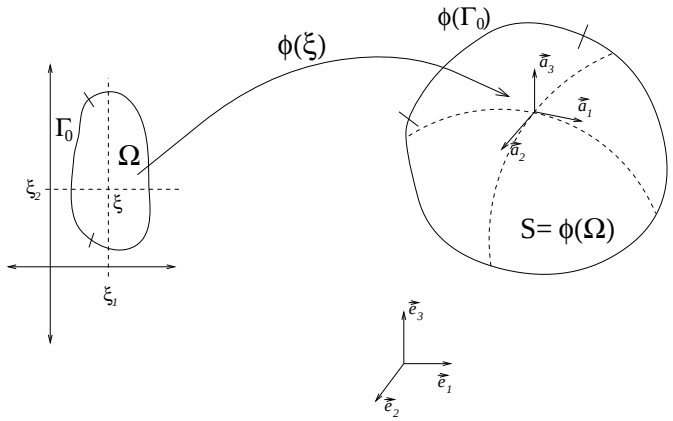

Figure 1: Definición de la superficie media.

o bien, alternativamente, en su forma contravariante

$$a^{\alpha\beta} = \vec{a}^{\alpha} \cdot \vec{a}^{\beta}.$$

La *segunda* y *tercera forma fundamental* están dadas por

$$b_{\alpha\beta} = \vec{a}_3 \cdot \vec{a}_{\alpha,\beta} \qquad \text{y} \qquad c_{\alpha\beta} = b^{\lambda}_{\alpha} b_{\lambda\beta},$$

con $b^{\lambda}_{\alpha} = a^{\beta\lambda} b_{\lambda\alpha}$. Como todos los puntos son regulares, el número $a = \det(a_{\alpha\beta}) = a_{11}a_{22} - a_{12}^2$ es no nulo, luego la medida de superficie estará dada por

$$dS := |\vec{a}_1 \times \vec{a}_2| \mathrm{d}\xi_1 \mathrm{d}\xi_2 = \sqrt{a} \mathrm{d}\xi_1 \mathrm{d}\xi_2.$$

Por otro lado, las derivadas covariantes de un vector tridimensional v se definen por

$$v_{\alpha|\beta} = v_{\alpha,\beta} - \Gamma^{\lambda}_{\alpha,\beta} v_{\lambda},$$

donde $\Gamma^{\lambda}_{\alpha,\beta}$ representa los *símbolos de Christoffel* , que están dados por

$$\Gamma^{\lambda}_{\alpha,\beta} = \Gamma^{\lambda}_{\beta,\alpha} = \vec{a}^{\lambda} \cdot \vec{a}_{\beta,\alpha} = \vec{a}^{\lambda} \cdot \vec{a}_{\alpha,\beta}$$

Como hemos mencionado, los modelos clásicos de cáscaras están basados en hipótesis cinemáticas, las cuales se usan para describir el desplazamiento de los puntos localizados sobre una fibra del material que es ortogonal a la superficie en la configuración original (antes de la deformación), como en la Figura 2.

El modelo de Naghdi está basado en las hipótesis cinemáticas de Reissner-Mindlin, esto es que cualquier fibra normal a la superficie media permanece rígida

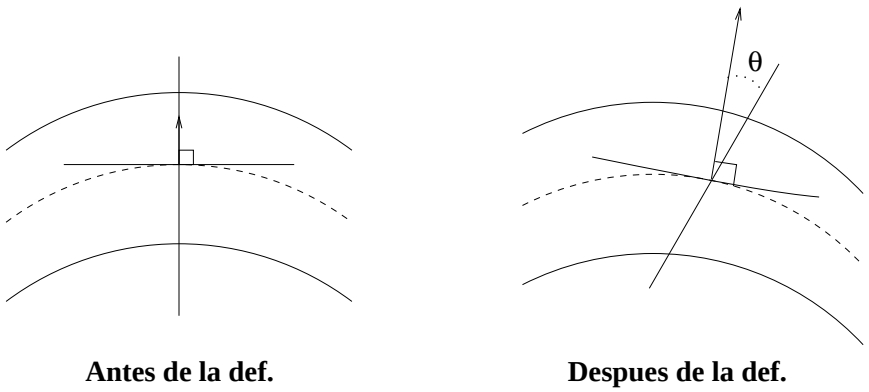

Figure 2: Aspectos geométricos de la deformación de una cáscara (sección tranversal).

durante la deformación. Los desplazamientos en cualquier punto en $\mathcal{C}$ están dados por

$$U = \vec{u}(\xi_1, \xi_2) + \xi_3 \, \underline{\theta}(\xi_1, \xi_2), \tag{1}$$

donde $\underline{\theta}$, es un vector que representa las rotaciones de la fibra normal, la cual es tangente a la superficie media en el punto de coordenadas (ξ_1, ξ_2), es decir $\underline{\theta} = \theta_\alpha \vec{a}^\alpha$ (como un vector en $\mathbb{R}^2$), y $\vec{u} = (\underline{u}, u_3)$ es el desplazamiento en la superficie media (como un vector en $\mathbb{R}^3$).

El problema de autovalores consiste en considerar las vibraciones que pueden ocurrir en una cáscara que se encuentra libre de cargas externas en todo tiempo y que está sujeta a condiciones de frontera que son independientes del tiempo. Estas son las que se conocen como *vibraciones libres* y pueden ser representadas por una expresión del tipo:

$$\tilde{U}_j(\xi_1, \xi_2, \xi_3, s) = U_j(\xi_1, \xi_2, \xi_3) \cos \omega s, \quad j = 1, 2, 3,$$

donde $\tilde{U} = (\tilde{U}_1, \tilde{U}_2, \tilde{U}_3)$ y $U = (U_1, U_2, U_3)$ son funciones (campos de desplazamientos) definidas en cualquier punto de la cáscara $\mathcal{C}$, con U independente del tiempo s y definida de acuerdo a (1). La constante ω corresponde a la *frecuencia de vibración.*

En general, al considerar modelos bidimensionales, la formulación variacional de este problema puede escribirse de la siguiente manera:
Hallar $\lambda > 0$ *y* $(\vec{u}, \underline{\theta})$*, tal que*

$$t^3 A\Big((\vec{u}, \underline{\theta}), (\vec{v}, \underline{\eta})\Big) + tD\Big((\vec{u}, \underline{\theta}), (\vec{v}, \underline{\eta})\Big) = \lambda B\Big((\vec{u}, \underline{\theta}), (\vec{v}, \underline{\eta})\Big) \quad \forall (\vec{v}, \underline{\eta}) \in \mathcal{U}, \tag{2}$$

donde $\mathcal{U}$ es el espacio en el que buscamos la solución y que contiene condiciones de frontera apropiadas, de tal manera que el problema este bien planteado. Por otro lado, $\lambda = \rho\omega^2$, donde ρ es la densidad del material. La definición de las formas bilineales A, D y B dependen del modelo que se considere, A y D son independientes del grosor t.

En la formulación de Naghdi, la forma bilineal A, corresponde al término de flexión de la cáscara (*bending term*), que esta dado por

$$A\Big((\vec{u},\underline{\theta}),(\vec{v},\underline{\eta})\Big) := \int_\Omega \frac{E^{\alpha\beta\lambda\mu}}{12}\chi_{\alpha\beta}(\vec{u},\underline{\theta})\chi_{\lambda\mu}(\vec{v},\underline{\eta})\,dS,$$

donde el operador de deformación de flexión, o tensor de curvatura de flexión χ, está dado por

$$\chi_{\lambda\mu}(\vec{v},\underline{\eta}) := \frac{1}{2}\Big[\eta_{\lambda|\mu} + \eta_{\mu|\lambda} - b^\alpha_\lambda v_{\alpha|\mu} - b^\alpha_\mu v_{\alpha|\lambda}\Big] + c_{\lambda\mu}v_3.$$

El tensor de cuarto orden, presente en la definición anterior, contiene las propiedades del material y esta definido por

$$E^{\alpha\beta\lambda\mu} := \frac{E}{2(1+\nu)}\left[a^{\alpha\lambda}a^{\beta\mu} + a^{\alpha\mu}a^{\beta\lambda} + \frac{2\nu}{1+\nu}a^{\alpha\beta}a^{\lambda\mu}\right],$$

donde E y ν, denotan el módulo de Young y el coeficiente de Poisson, respectivamente. La forma bilineal D puede escribirse como la suma de un término de membrana D^m (*membrane term*) y un término debido al corte transversal D^s (*shear term*), y están definidas por

$$\begin{aligned} D^m(\vec{u},\vec{v}) &:= \int_\Omega E^{\alpha\beta\lambda\mu}\varphi_{\alpha\beta}(\vec{u})\varphi_{\lambda\mu}(\vec{v})\,dS \\ D^s\Big((\vec{u},\underline{\theta}),(\vec{v},\underline{\eta})\Big) &:= \int_\Omega G^{\alpha\beta}\gamma_\alpha(\vec{u},\underline{\theta})\gamma_\beta(\vec{v},\underline{\eta})\,dS, \end{aligned}$$

donde, el tensor de deformación de membrana φ, el tensor de deformación de corte γ y el factor $G^{\alpha\beta}$ se definen mediante

$$\begin{aligned} \varphi_{\lambda\mu}(\vec{v}) &:= \frac{1}{2}(v_{\lambda|\mu} + v_{\mu|\lambda}) - b_{\lambda\mu}v_3, \\ \gamma_\beta(\vec{v},\underline{\eta}) &:= v_{3,\beta} + b^\lambda_\beta v_\lambda + \eta_\beta, \\ G^{\alpha\beta} &:= \frac{Ea^{\alpha\beta}}{2(1+\nu)}. \end{aligned}$$

La forma bilineal en el lado derecho de (2), correspondiente a los términos de masa, está definida por

$$B^N\Big((\vec{u},\theta),(\vec{v},\underline{\eta})\Big) = t\int_\Omega \vec{u}\cdot\vec{v}\,dS \;+\; \frac{t^3}{12}\int_\Omega \theta\cdot\underline{\eta}\,dS.$$

El modelo de Koiter está basado en las hipótesis de Kirchhoff-Love que cualquier fibra normal a la superficie media permanece rígida (como en el caso de Naghdi) y normal a la superficie deformada. Los desplazamientos pueden escribirse como:

$$U = \vec{u}(\xi_1, \xi_2) - \xi_3(\vec{u}_{3,\alpha} + b_\alpha^\lambda u_\lambda)a^\alpha, \tag{3}$$

donde, como antes, $\vec{u}(\xi_1, \xi_2)$ está definida en Ω. Si comparamos las ecuaciones (1) y (3), se puede notar que la hipótesis sobre los desplazamientos es equivalente a imponer que las rotaciones estén dadas por

$$\theta_\alpha = -(\vec{u}_{3,\alpha} + b_\alpha^\lambda u_\lambda).$$

En este caso el término de corte no aparece en la formulación, y las formas bilineales A y D están dadas por

$$A^K(\vec{u}, \vec{v}) := \int_\Omega \frac{E^{\alpha\beta\lambda\mu}}{12} \bar{\rho}_{\alpha\beta}(\vec{u})\bar{\rho}_{\lambda\mu}(\vec{v})\, dS,$$

donde el tensor de flexión es

$$\bar{\rho}_{\lambda\mu}(\vec{v}) := v_{3|\lambda\mu} - c_{\lambda\mu}v_3 + b^\alpha_{\lambda|\mu}v_\alpha + b^\alpha_\lambda v_{\alpha|\mu} + b^\alpha_\mu v_{\alpha|\lambda},$$

la parte de membrana es identica al caso anterior,

$$D^K(\vec{u}, \vec{v}) := D^m(\vec{u}, \vec{v}),$$

y, el término de masa,

$$\begin{aligned} B^K(\vec{u}, \vec{v}) &= t\int_\Omega \Big\{ \Big[1 + \frac{t^2}{12}(b^1_1 b^2_2 - b^2_1 b^1_2)\Big]\Big[a^{\alpha\beta}u_\alpha v_\beta + u_3 v_3\Big] \\ &+ \frac{t^2}{12}a^{\alpha\beta}\Big[(u_{3|\alpha} + b^\lambda_\alpha u_\lambda)(v_{3|\beta} + b^\lambda_\beta u_\lambda) \\ &+ (u_\alpha v_{3|\beta} + u_{3|\alpha}v_\beta + 2b^\lambda_\alpha u_\lambda v_\beta)b^\mu_\mu\Big]\Big\}\, dS. \end{aligned}$$

Una diferencia importante entre ambos modelos es la respectiva regularidad de los espacios en que se busca la solución. Para el modelo de Naghdi, éste es de la forma

$$\mathcal{U} := \Big\{(\vec{v}, \underline{\eta}) \in [\mathrm{H}^1(\Omega)]^5 :\ \vec{v}|_{\Gamma_0} = \vec{0},\ \underline{\eta}|_{\Gamma_0} = \underline{0}\Big\},$$

y

$$\mathcal{U}^K := \Big\{\vec{v} \in [\mathrm{H}^1(\Omega)]^2 \times \mathrm{H}^2(\Omega) :\ \vec{v}|_{\Gamma_0} = \vec{0}\Big\}.$$

para el modelo de Koiter. En ambos espacios, se ha puesto una condición de frontera suficiente para prevenir los movimientos de cuerpo rígido sobre una parte $\Gamma_0 \subset \Gamma$.

Una importante propiedad de estos modelos aparece en el libro de Bernadou[21]. Allí se muestra que se tiene una estimación del tipo

$$c_t\|V\|^2_{\mathcal{U}} \leq t^3 A(V;V) + tD(V,V) \leq C_t t\|V\|^2_{\mathcal{U}}, \quad \forall V \in \mathcal{U} \tag{4}$$

donde $\|\cdot\|_{\mathcal{U}}$ denota la norma usada por $\mathcal{U}$ de acuerdo a la naturaleza del problema, V denota simbólicamente el campo de desplazamientos para cada modelo.

Nuestro interés es estudiar cáscaras tanto delgadas como moderadamente gruesas, por ello en este trabajo nos restringimos al modelo de Naghdi. Es decir, estamos interesados en resolver el problema (2), en el que las formas bilineales son A, D^m, D^s y B^N.

Notemos que, las constantes de elipticidad y acotamiento presentes en la estimación (4) (c_t y C_t, respectivamente) dependen del parámetro de grosor t. Más aún, la constante c_t degenera cuando el grosor disminuye ($c_t \to 0$ cuando $t \to 0$. Este es el principal inconveniente a la hora de implementar métodos usuales de elementos finitos para solucionar el problema, pues por ello apararece el fenómeno de bloqueo numérico.

Para evitar el fenómeno de bloqueo, se han introducido algunos métodos especiales basados en integración reducida o interpolación mixta. De ellos, los llamados *MITC* (Mixed Interpolation of Tensorial Component), introducidos por Bathe y Dvorkin en [10], o variantes de ellos, corresponden a la familia de métodos más utilizados en la práctica.

El modelo de Reissner-Mindlin para flexión de placas, que es el más utilizado en casos de cáscaras planas moderadamente gruesas, puede ser entendido como un caso especial del modelo clásico de Naghdi, en el que el desplazamiento transversal aparece separado de los desplazamientos en el plano. Estos pueden ser escritos en término de las rotaciones de una fibra normal a la superficie media de la placa. Más precisamente, esto puede entenderse al considerar una placa cuya superficie media se genera por un mapeo del tipo $\phi(x,y) = (x,y,0)$ para (x,y) en una región Ω bidimensional, en tal caso, las expresiones resultan facilmente calculables y la independencia mencionada se nota claramente. De ésta forma, el problema de la deformación en el plano puede tratarse de manera independiente (ver [87]).

Para problemas de cargas, se han publicado un gran número de trabajos que contienen análisis matemáticos del método MITC o variantes de él, aplicado a la flexión de placas (ver, por ejemplo, [5, 9, 44], e incluso para versiones *hp* del método [79]).

En ellos se ha establecido convergencia y estimaciones de error que no dependen del grosor de la placa, lo que descarta la aparición del fenómeno de bloqueo. Sin embargo, resultados de este tipo para elementos finitos cuadrilaterales isoparamétricos,

como el original propuesto por Bathe y Dvorkin[10], no habian sido obtenidos pese a ser éstos los elementos mas comunmente utilizados en aplicaciones en ingeniería.

En el Capítulo 3, consideramos dos métodos de más bajo orden pertenecientes a la familia de MITC, sobre mallas cuadrilaterales. Este capítulo corresponde al artículo [43]:

- R. Durán, E. Hernández, L. Hervella-Nieto, E. Liberman, R. Rodríguez, Error estimates for low-order isoparametric quadrilateral finite elements for plates. (enviado a *SIAM Journal on Numerical Analysis*).

Asumiendo algunas hipótesis sobre las mallas, hemos probado estimaciones de error óptimas en orden y regularidad de la aproximación del problema de flexión de placas, usando el método original MITC4 y una variante de él, que enriquece el espacio de aproximación de las rotaciones, llamado DL4 (el número, en ambos casos, hace referencia a que se basan en cuadrilateros con 4 nodos). Haciendo uso de la teoría abstracta de convergencia en [7], también se obtienen estimaciones de error para la aproximación del problema de vibración de placas. Incluimos también resultados numéricos que muestran el buen comportamiento de los métodos, incluso en casos no cubiertos por la teoría presentada en el capítulo.

Al momento de experimentar numéricamente el problema de vibración de cáscaras usando MITC4, se debe destacar dos puntos.

Por un lado, recientemente en [5] se muestra que la extensión de los resultados de convergencia válidos para mallas rectangulares al caso de cuadrilateros generales no es muy simple y, de hecho, en algunos casos puede deteriorarse (por ejemplo cuando se usan elementos finitos no estandar en cuadrilateros generales, ver [6]), incluso cuando las mallas satifacen la hipótesis de regularidad.

Por otro lado, al aplicar estos métodos al problema de vibración de una cáscara general, se hace necesario un uso intensivo de la *carta*, lo cual, en principio, limita la gama de problemas a ser abordados.

En el Capítulo 4 estudiamos numéricamente el problema de vibraciones de una cáscara. Este capítulo corresponde principalmente al artículo [58]:

- E. Hernández, L. Hervella-Nieto, and R. Rodríguez, Computation of the vibration modes of plates and shells by low order MITC quadrilateral finite elements. (aceptado *Computers and Structures*).

Hemos testeado la eficiencia del método MITC4 para calcular las correspondientes frecuencias de vibración de una cáscara modelada por las ecuaciones de Naghdi, sobre el dominio de referencia. Para el caso de placas, extendemos los resultados numéricos presentados en el Capítulo 3 a otras condiciones de frontera usando

mallas generales, mostrando, en todos los casos, que el orden de convergencia del método es óptimo. Aplicamos tambien el método para calcular las vibraciones libres de algunos problemas tipo ("*benchmark problem*") de cáscaras, sugeridos en [33], comparando los resultados obtenidos al utilizar discretizaciones estándar por elementos finitos cuadrilaterales de más bajo orden.

Interacción.

Como hemos mencionado, cuando la estructura considerada es un sólido, el problema de interacción entre ambos medios ha sido fuertemente estudiado. No ocurre lo mismo en los casos en que la estructura es una cáscara.

Recientemente, Le Tallec y Mani en [65] han analizado un problema similar de interacción en que el fluido es considerado muy viscoso y la cáscara modelada por las ecuaciones de Koiter. El fluido, en este caso, es aproximado por métodos de elementos finitos mixtos estándar y la estructura es discretizada usando elementos finitos DKT, de los cuales no se conoce demostraciones independientes del grosor de la estructura (ver [21]).

Para el caso de interacción entre placas y fluidos, existen algunos trabajos. En Durán *et al.* [45] se ha considerado elementos triangulares DL3 para aproximar la flexión de placas y elementos tetraédricos de Raviart-Thomas para el fluido. Se ha probado, como en el caso de problemas de acoplamiento sólido–fluido, que los métodos convergen con orden óptimo y que no se presentan fenómenos de *bloqueo* cuando el grosor es pequeño. En Bermúdez *et al* [18] se ha estudiado computacionalmente este modelo en el caso de interacción amortiguada por capas de aislante entre el fluido y la placa.

En el Capítulo 5, se extienden los resultados de [45] a los métodos que hemos estudiado en los capítulos 3 y 4. El capítulo corresponde al trabajo [55]:

- E. Hernández, Approximation of the vibration modes of a plate coupled with a fluid by low-order isoparametric finite elements. En redacción.

Hemos considerado una discretización del problema acoplado por medio de elementos finitos cuadrilaterales MITC4 para la flexión de placas y elementos hexaédricos de más bajo orden de Raviart-Thomas para el fluido.

Remarcamos que los elementos finitos isoparamétricos, como los que estamos considerando, son los más utilizados en las aplicaciones en ingeniería. Mas aún, para problemas estructurales, los elementos hexaédricos aproximan mejor la solución exacta que los tetraédricos (ver [16]).

Como el fluido y la estructura están en contacto, la condición sobre la interfaz de ambos medios corresponde a la igualdad de los desplazamientos normales. Sin

embargo, como tales desplazamientos en la estructura no dependen de la coordenada en la dirección normal a la superficie media, se puede considerar que es la superficie media la que está en contacto con el fluido. Más aún, en la discretización, tal condición se impone de manera débil. Esto es, en cada cara $\mathcal{F}$ de la malla del fluido que cae sobre la superficie media de la cáscara

$$\int_{\mathcal{F}} \vec{u}_F \cdot \mathrm{n} = \int_{\mathcal{F}} \vec{u}_C \cdot \mathrm{n},$$

donde los deplazamientos en el fluido y en la cáscara se denotan por $\vec{u}_F$ y $\vec{u}_C$, respectivamente.

Esta manera de imponer la condición de acoplamiento de ambos medios, se origina en el hecho que hacerlo de forma fuerte es muy restrictivo (ver [19]). Notemos que debido a esta imposición el espacio discreto no es subespacio del espacio continuo, lo cual hace que el método sea no conforme. Igualmente, probamos estimaciones de error óptimas para el problema de vibraciones placa-fluido.

Finalmente, en el Capítulo 6, se extiende los resultados de [59]:

- E. Hernández, L. Hervella-Nieto, and R. Rodríguez, Computation of the vibration modes of plates and shells coupled with a fluid. MECOM 2002. Procedings of the First South-American Congress on Computational Mechanics, Santa Fe - Paraná, Argentina, 2002.

Testeando la eficiencia del método para calcular las correspondientes frecuencias de vibración de una cáscara cilíndrica que contiene en su interior un fluido.

Comparamos los resultados de nuestros códigos con aquellos en [63], obtenidos analíticamente por medio de expansiones en series de Fourier finitas. Además, por medio de otro ejemplo mostramos la eficiencia, en problema de interacción entre fluidos y cáscaras, del uso de modelos 2D con respecto a los modelos de elasticidad clásica 3D.

Chapter 1

Finite element approximation of spectral problems with Neumann boundary conditions on curved domains

This chapter deals with the finite element approximation of the spectral problem for the Laplace equation with Neumann boundary conditions on a curved non convex domain Ω. Convergence and optimal order error estimates are proved for standard piecewise linear continuous elements on a discrete polygonal domain $\Omega_h \not\subset \Omega$, in the framework of the abstract spectral approximation theory.

1.1 Introduction

In this chapter we analyze an elementary problem: the piecewise linear finite element approximation of eigenvalues and eigenfunctions of the Laplace operator with a Neumann boundary condition on a curved domain Ω.

Since Neumann condition is a natural condition, in principle, a conforming finite element space could be theoretically defined on a curved triangulation fitting exactly the boundary of Ω (see, for instance, Chapter 8 of [26]). Then, to effectively solve the problem, the integrals for the entries of the stiffness and mass matrices on the curved triangles should be computed by means of a quadrature rule. Thus, the method turns out to be actually non conforming.

However, for piecewise linear elements, the most usual procedure in practice is to consider a mesh $\mathcal{T}_h$ formed by straight triangles. Then, the integrals of the entries of both matrices, are actually computed on a discrete domain $\Omega_h := \bigcup\{T \in \mathcal{T}_h\}$ which

do not coincide with Ω, thus yielding also a non conforming method. As we show in this chapter, this coarser procedure leads anyway to optimal order approximation results.

When $\Omega_h \subset \Omega$, the standard theory applies almost directly. In fact, for Dirichlet boundary conditions the method turns out to be conforming since the discrete space is a subset of $H_0^1(\Omega)$ (see for instance the book by Raviart and Thomas[76]). For Neumann boundary conditions the method is not conforming, but convergence and optimal error estimates can be proved as rather straightforward consequences of standard Strang's Lemma, estimates like Lemma 5.2-3 in Raviart and Thomas' book[76] and the classical abstract spectral approximation theory by Osborn[71] (see also the monograph by Babuška and Osborn[7]).

The situation is quite different when $\Omega_h \not\subset \Omega$. The finite element approximation of the linear boundary value problem associated to the Laplace operator was extensively studied since long time ago. Different approaches have been considered for instance by Ciarlet and Raviart[38], Zlámal[88], and Scott[77] (see also [80], [22], and [86]).

However, these results do not lead to a similar analysis for the corresponding eigenvalue problem. Indeed, convergence results for a linear boundary value problem do not necessarily imply similar results for its associated spectral one. This is particularly true for non-conforming and mixed methods (see, for instance, [24, 25] for examples of methods working out for the linear boundary value problem but failing for the associated eigenvalue problem).

In fact, to apply the spectral approximation theory stated in [7], one needs convergence in L^2 norm for the involved discrete operators, as well as optimal order L^2 and H^1 convergence results for the associated linear boundary value problem with homogeneous boundary conditions. For instance, for the Dirichlet problem on a curved domain with a smooth boundary, such results have been only recently proved by Bramble and King in Proposition 1 of [27], where the transfer of non-homogeneous boundary data is analyzed.

For the eigenvalue problem, the first proof of convergence valid in the case $\Omega_h \not\subset \Omega$ was given by Vanmaele and Ženíšek[82] just a few years ago. They prove it for simple eigenvalues and Dirichlet boundary conditions by using the *min-max* characterization. These results have been further extended by the same authors to include multiple eigenvalues [83] and numerical integration effects [84] (thus allowing to considering non constant coefficients).

Around the same time, Lebaud analyzed in [64] a similar problem also for simple eigenvalues and Dirichlet boundary conditions. She allowed for non constant coefficients in the differential operator but assuming exact integration. She used

the spectral approximation theory stated in [7] and optimal convergence results like those in [27]. She proved that, when isoparametric elements of degree k are used and the eigenfunctions are sufficiently smooth, the approximation of the eigenvalues is of order $\mathcal{O}(h^{2k})$ instead of $\mathcal{O}(h^{k+1})$.

In the case of Neumann boundary conditions, to the best of the authors' knowledge, no approximation result has been proved yet for the eigenvalue problem. Moreover, it is not apparent that neither the theory in [82] nor that in [64] could be extended to provide optimal error estimates in this case. In fact, both theories rely on estimates like (4.8) in [82], which are valid for functions vanishing on $\partial\Omega_h$ or on $\partial\Omega$ like the eigenfunctions of a Dirichlet problem, but not for those of a Neumann one.

For instance, for piecewise linear elements, the techniques in [64] clearly do not apply to the Neumann problem. To see this, notice that these results depend on the estimate (4.4) of that paper:

$$\|(T - T_h)u\|_{0,2,\mathbb{R}^2} = \mathcal{O}(h^2), \tag{1.1}$$

where Tu is the solution of the Laplace equations on Ω with right hand side u, and $T_h u$ is its piecewise linear finite element approximation on Ω_h, obtained by using as right hand side the extension of u by zero outside of Ω (Tu and $T_h u$ also extended by zero outside of their domains). Estimate (1.1) is proved in [64] as a consequence of the following three inequalities:

$$\begin{aligned}
\|(T - T_h)u\|_{m,2,\Omega\cap\Omega_h} &\leq Ch^{2-m}\|Tu\|_{2,2,\Omega}, \quad \text{for } m = 0, 1, && (1.2)\\
\|Tu\|_{0,2,\Omega\setminus(\Omega\cap\Omega_h)} &\leq Ch^2\|Tu\|_{2,2,\Omega}, && (1.3)\\
\|T_h u\|_{0,2,\Omega_h\setminus(\Omega\cap\Omega_h)} &\leq Ch^2\|T_h u\|_{1,2,\Omega\cap\Omega_h}. && (1.4)
\end{aligned}$$

To the best of the authors' knowledge estimate (1.2) has not been proved for $m = 0$ and Neumann boundary conditions. Furthermore, estimate (1.4) is clearly not valid in this case.

This shows the necessity of considering a more subtle extension of the data u outside of Ω. One such extension, which preserves the eigenvalues of the Neumann problem, is introduced and analyzed in the following section.

The goal of this chapter is to analyze the piecewise linear finite element approximation of the spectral problem for the Laplace equation with Neumann boundary conditions on curved non convex domains. We prove optimal order L^2 and H^1 error estimates for the eigenfunctions, and a double order for the eigenvalues. These estimates are proved to be valid for any piecewise smooth Lipschitz domain, for which the eigenfunctions do not necessarily belong to $\mathrm{H}^2(\Omega)$.

The outline of the chapter is as follows. In §1.2 we present the model problem, the meshes to be used, the finite element approximation and some basic results. Then, in §1.3, we prove optimal order error estimates for the approximate eigenfunctions and eigenvalues in the framework of the spectral approximation theory stated in [7].

1.2 Statement of the problem

Let $\Omega \subset \mathbb{R}^2$ be a bounded open domain, in general non convex, with a piecewise smooth (v.g., $\mathcal{C}^2$) Lipschitz boundary $\Gamma := \partial\Omega$. Consider the eigenvalue problem for the shifted Laplace operator in Ω with Neumann boundary conditions:

To find $\lambda \in \mathbb{R}$ and $u \in \mathrm{H}^1(\Omega)$, $u \neq 0$, such that:

$$a(u,v) = \lambda b(u,v) \qquad \forall v \in \mathrm{H}^1(\Omega). \tag{1.5}$$

The bilinear forms $a : \mathrm{H}^1(\Omega) \times \mathrm{H}^1(\Omega) \longrightarrow \mathbb{R}$ and $b : \mathrm{L}^2(\Omega) \times \mathrm{L}^2(\Omega) \longrightarrow \mathbb{R}$ in the equation above are defined by:

$$a(v,w) := \int_\Omega (\nabla v \cdot \nabla w + vw)\ dx \qquad \forall v, w \in \mathrm{H}^1(\Omega), \tag{1.6}$$

$$b(f,g) := \int_\Omega fg\ dx \qquad \forall f, g \in \mathrm{L}^2(\Omega). \tag{1.7}$$

It is well known that problem (1.5) attains a sequence of finite multiplicity eigenvalues satisfying

$$1 = \lambda_0 < \lambda_1 \leq \cdots \leq \lambda_k \leq \cdots, \qquad \lambda_k \overset{k\to\infty}{\longrightarrow} +\infty,$$

with corresponding $\mathrm{L}^2(\Omega)$-orthonormal eigenfunctions $\{u_k\}_{k=0}^\infty$ providing a Hilbert basis of $\mathrm{H}^1(\Omega)$.

Remark 1.2.1 *We consider the bilinear form given by (1.6) instead of the standard one for the Laplace equations (i.e., $a(u,v) = \int_\Omega \nabla u \cdot \nabla v\ dx$), because the eigenvalues of both problems only differ by one and the corresponding eigenfunctions coincide. Since the same is true for the discrete problem (1.8) below, thus we avoid dealing with the standard constraints for pure Neumann problems.*

We consider a family $\{\mathcal{T}_h\}$ of standard finite element triangulations (see for instance [36]) of polygonal domains Ω_h approximating Ω, such that if $\Gamma_h := \partial\Omega_h$ and $\mathcal{N}_h$ is the set of vertices of all the triangles in $\mathcal{T}_h$, then there holds (see Figure 1.1):

- $\mathcal{N}_h \subset \bar{\Omega}_h$ and $\mathcal{N}_h \cap \Gamma_h \subset \Gamma$;

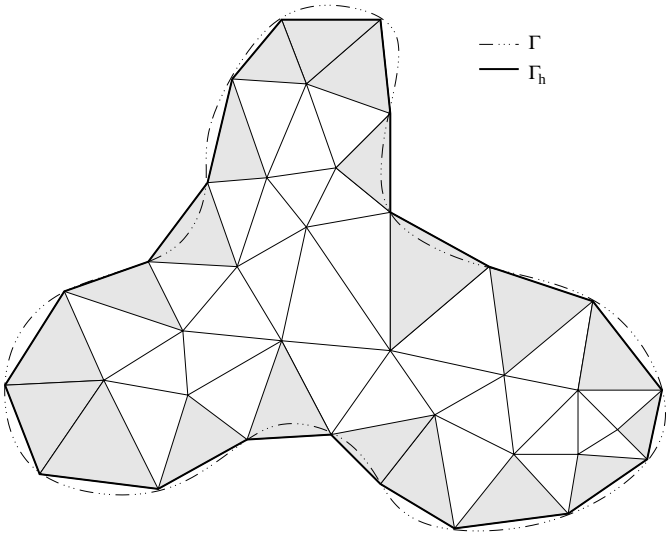

Figure 1.1: Triangulation of $\Omega_h \approx \Omega$. The shaded triangles are the *boundary* ones $T \in \mathcal{T}_h^\partial$.

- for all $T \in \mathcal{T}_h$, at most two vertices of T lie on Γ_h;

the second assumption is only made for the sake of simplicity.

As usual, h stands for the mesh-size, namely, the maximum diameter h_T of all the triangles $T \in \mathcal{T}_h$. We also assume that the family $\{\mathcal{T}_h\}$ is regular in the sense of a minimum angle condition; i.e., there exists $\theta_0 > 0$ such that, if θ_T is the smallest angle of T, then $\theta_T > \theta_0$ for all $T \in \mathcal{T}_h$ and for all the triangulations $\mathcal{T}_h$ in the family.

In what follows we will use the notation and definition introduced in [49] (see also [86]). For a given triangulation $\mathcal{T}_h$, we denote by $\mathcal{T}_h^\partial$ the subset of the so called *boundary triangles*; namely, those having an edge on Γ_h (see Figure 1.1). For one such triangle T, let P_1^T, P_2^T, and P_3^T be its three vertices, with $S_T := \overline{P_2^T P_3^T} \subset \Gamma_h$, and let Σ_T be the piece of Γ approximated by S_T (see Figure 1.2).

We denote by $\widetilde{T}$ the curved triangle of edges $\overline{P_1^T P_2^T}$, Σ_T, and $\overline{P_3^T P_1^T}$, and we call it the *ideal triangle* associated to T. For inner triangles $T \in \mathcal{T}_h \setminus \mathcal{T}_h^\partial$ we simply define $\widetilde{T} \equiv T$ as its associated ideal triangle. We denote by $\widetilde{\mathcal{T}}_h := \left\{\widetilde{T} : \ T \in \mathcal{T}_h\right\}$, the partition of Ω provided by the ideal triangles and we call it the *ideal triangulation* of Ω. We also denote $\widetilde{\mathcal{T}}_h^\partial := \left\{\widetilde{T} : \ T \in \mathcal{T}_h^\partial\right\}$, the family of ideal triangles associated to the boundary ones.

For the sake of simplicity we assume that the triangulations $\mathcal{T}_h$ are such that, for each boundary triangles $T \in \mathcal{T}_h^\partial$, either $T \subset \widetilde{T}$ or $T \supset \widetilde{T}$. Let ω_T be the domain bounded by Σ_T and S_T (see Figure 1.2). Therefore $\bigcup_{T \in \mathcal{T}_h^\partial} \omega_T = (\Omega \setminus \bar{\Omega}_h) \cup (\Omega_h \setminus \bar{\Omega})$.

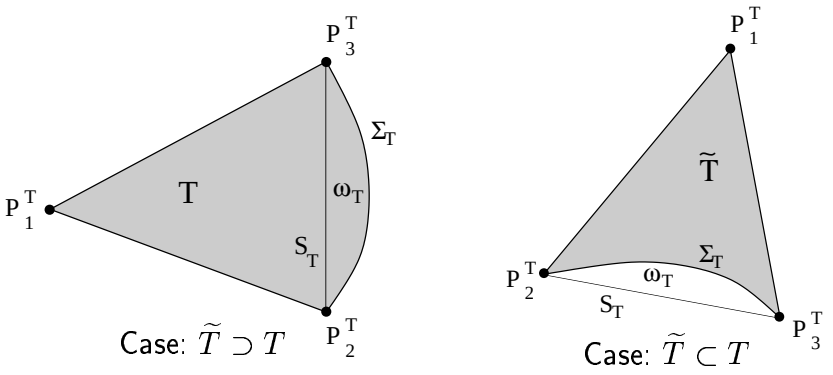

Figure 1.2: *Ideal* triangles $\widetilde{T}$.

We introduce in each domain ω_T local coordinates (γ, η), the first one along S_T and the second one normal to S_T. Let $\varphi_T(\gamma)$, $0 \leq \gamma \leq s_T := \text{length}\,(S_T)$, be a parameterization of Σ_T. We choose the orientation of η in such a way that $\varphi_T \geq 0$. Then $\Sigma_T = \{(\gamma, \eta) : \eta = \varphi_T(\gamma),\ \gamma \in [0, s_T]\}$ and $\omega_T = \{(\gamma, \eta) : 0 < \eta < \varphi_T,\ \eta \in (0, s_T)\}$ (see Figure 1.3).

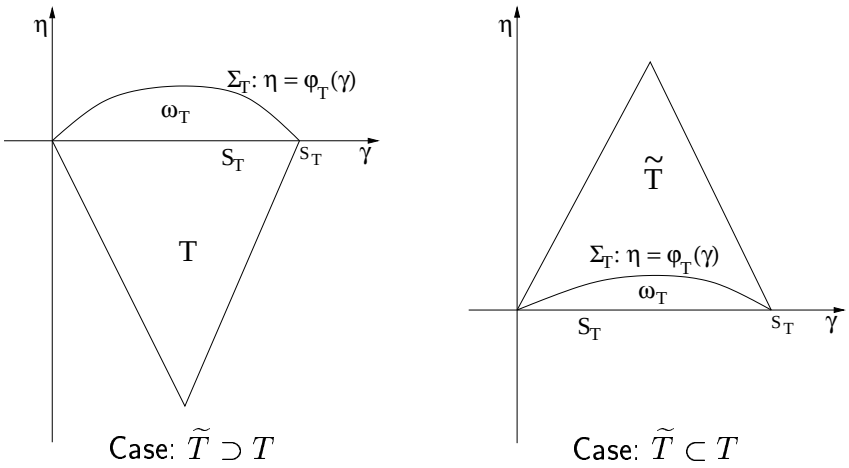

Figure 1.3: Local coordinates (γ, η).

As a consequence of the assumed smoothness of Γ, $\varphi_T \in \mathcal{C}^2([0, s_T])$ and the following estimate holds:

Lemma 1.2.1 *There exists a constant $C > 0$, independent of T, such that*

$$0 \leq \varphi_T(\gamma) \leq C s_T^2 \leq C h_T^2 \qquad \forall \gamma \in [0, s_T].$$

Proof. It is a direct consequence of standard interpolation results. □

Here and thereafter, C denotes a positive constant not necessarily the same at each occurrence, but always independent of the mesh-size h.

Consider the discretization of the spectral problem (1.5) obtained by using standard piecewise linear continuous finite elements on $\mathcal{T}_h$:

To find $\lambda_h \in \mathbb{R}$ *and* $u_h \in \mathcal{L}_h(\Omega_h)$, $u_h \neq 0$, *such that:*

$$a_h(u_h, v_h) = \lambda_h b_h(u_h, v_h) \qquad \forall v_h \in \mathcal{L}_h(\Omega_h). \tag{1.8}$$

In the equation above

$$\mathcal{L}_h(\Omega_h) := \{v_h \in \mathrm{H}^1(\Omega_h) : \ v_h|_T \in \mathcal{P}_1(T) \ \forall T \in \mathcal{T}_h\},$$

with $\mathcal{P}_1(T)$ being the space of linear functions defined on T, and the bilinear forms $a_h : \mathrm{H}^1(\Omega_h) \times \mathrm{H}^1(\Omega_h) \longrightarrow \mathbb{R}$ and $b_h : \mathrm{L}^2(\Omega_h) \times \mathrm{L}^2(\Omega_h) \longrightarrow \mathbb{R}$ are defined by:

$$a_h(v, w) := \int_{\Omega_h} (\nabla v \cdot \nabla w + vw) \ dx \qquad \forall v, w \in \mathrm{H}^1(\Omega_h), \tag{1.9}$$

$$b_h(f, g) := \int_{\Omega_h} fg \ dx \qquad \forall f, g \in \mathrm{L}^2(\Omega_h). \tag{1.10}$$

Problem (1.8) reduces to a finite dimensional generalized eigenvalue problem with symmetric positive definite matrices. It attains a finite number of eigenvalues

$$1 = \lambda_{h1} < \lambda_{h2} \leq \cdots \leq \lambda_{hm},$$

with corresponding $\mathrm{L}^2(\Omega_h)$-orthonormal eigenfunctions $\{u_{hk}\}_{k=0}^m$.

The following three basic lemmas will be used in the sequel:

Lemma 1.2.2 *There exist positive constants* c *and* C *(not depending on* T*) such that, if* $v_h \in \mathcal{P}_1(\mathbb{R}^2)$ *and* h_T *is small enough, then*

$$c\|v_h\|_{0,\widetilde{T}} \leq \|v_h\|_{0,T} \leq C\|v_h\|_{0,\widetilde{T}},$$
$$c|v_h|_{1,\widetilde{T}} \leq |v_h|_{1,T} \leq C|v_h|_{1,\widetilde{T}}.$$

Proof. Similar results have been proved in several papers (see for instance [49]). For the sake of completeness, we include an elementary proof in the case $\widetilde{T} \subset T$; the case $\widetilde{T} \supset T$ can be dealt with almost identically.

We use the notation in Figure 1.4. In particular T' is the triangle of vertices P_1^T, Q_2^T, and Q_3^T, with Q_k^T being the midpoint of the edge $\overline{P_1^T P_k^T}$, for $k = 2, 3$.

Because of Lemma 1.2.1, for h_T small enough, the triangle T' is contained in $\widetilde{T}$ as shown in Figure 1.4. Then, straightforward computations show that $\|v_h\|_{0,T} \leq C\,\|v_h\|_{0,T'}$ and $|v_h|_{1,T} = 2\,|v_h|_{1,\widetilde{T}}$. Hence, the lemma is a consequence of the fact that $T' \subset \widetilde{T} \subset T$. □

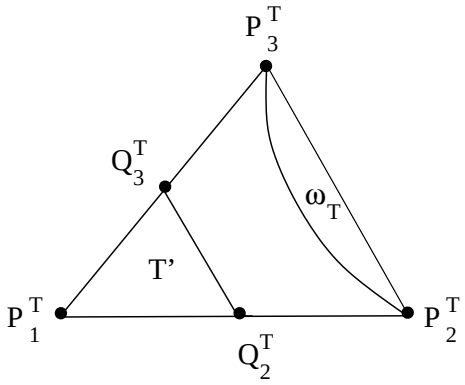

Figure 1.4: Auxiliary triangle T' (case: $\widetilde{T} \subset T$).

Lemma 1.2.3 *There exist a positive constant C such that, if h is small enough, then:*

$$\begin{aligned} \|v\|_{0,\Omega\setminus\bar{\Omega}_h} &\leq Ch^s\|v\|_{s,\Omega} \quad \forall v \in \mathrm{H}^s(\Omega) \quad (0 \leq s \leq 1), \\ \|v\|_{0,\Omega_h\setminus\bar{\Omega}} &\leq Ch^s\|v\|_{s,\Omega_h} \quad \forall v \in \mathrm{H}^s(\Omega_h) \quad (0 \leq s \leq 1). \end{aligned}$$

Proof. The two inequalities have been essentially proved in the proof of Lemma 5.2-3 in [76] for $s = 1$. Since the inequalities are clearly true for $s = 0$, they follow for $0 < s < 1$ from standard results on interpolation in Sobolev spaces (see, for instance, Theorem 1.4 in [52]). □

Lemma 1.2.4 *There exist a positive constant C such that, if h_T is small enough, then, for all $T \in \mathcal{T}_h$,*

$$\begin{aligned} \|v\|_{0,\widetilde{T}\setminus T} &\leq C\left(\|v\|_{0,T} + h_T^{2s}\|v\|_{s,\widetilde{T}}\right) \quad \forall v \in \mathrm{H}^s(\widetilde{T}) \quad (0 \leq s \leq 1), \quad \text{if } T \subset \widetilde{T}, \\ \|v\|_{0,T\setminus\widetilde{T}} &\leq C\left(\|v\|_{0,\widetilde{T}} + h_T^{2s}\|v\|_{s,T}\right) \quad \forall v \in \mathrm{H}^s(T) \quad (0 \leq s \leq 1), \quad \text{if } \widetilde{T} \subset T. \end{aligned}$$

Proof. We only include the proof of the first inequality. The second one can be obtained by applying similar arguments. We use the notation shown in Figure 1.5 for $T \subset \widetilde{T}$.

Consider polar coordinates centered at the vertex P_1^T. We assume that S_T and Σ_T are parameterized by $r = r_1(\theta)$ and $r = r_2(\theta)$, respectively, with $0 \leq \theta \leq \theta_1$. Then $\omega_T := \widetilde{T} \setminus T = \{(r,\theta) : \ r_1(\theta) < r < r_2(\theta),\ 0 < \theta < \theta_1\}$. Let d denote the distance of each point on Σ_T to S_T, as shown in Figure 1.5.

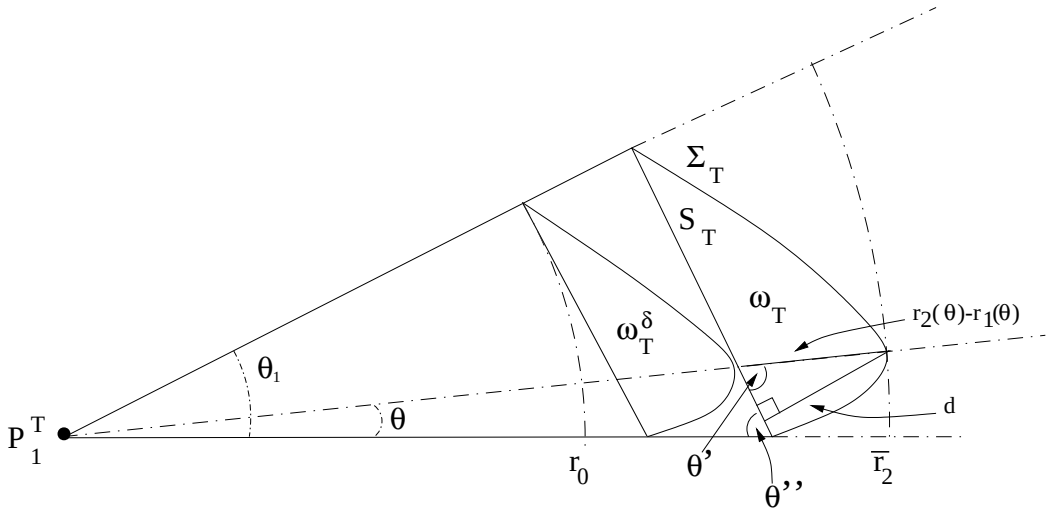

Figure 1.5: Polar coordinates on $\widetilde{T} \supset T$.

Assume that $\theta' \leq \frac{\pi}{2}$ as in Figure 1.5 (a similar argument is valid for $\theta' \geq \frac{\pi}{2}$). Since $\theta' = \theta'' + \theta$, then $\sin\theta' \geq \sin\theta'' \geq \sin\theta_T$, with θ_T being the smallest angle of T. Hence,

$$r_2(\theta) - r_1(\theta) = \frac{d}{\sin\theta'} \leq \frac{d}{\sin\theta_T}.$$

Then, because of Lemma 1.2.1 and the minimum angle condition,

$$\delta := \max_{0\leq\theta\leq\theta_1} [r_2(\theta) - r_1(\theta)] \leq Ch_T^2,$$

and, consequently, for h_T small enough,

$$\begin{aligned} r_0 &:= \min_{0\leq\theta\leq\theta_1} r_1(\theta) - \delta \geq ch_T > 0, \\ \bar{r}_2 &:= \max_{0\leq\theta\leq\theta_1} r_2(\theta) \leq Ch_T. \end{aligned}$$

Hence, for h_T small enough, $\omega_T^\delta := \{(r-\delta,\theta) : (r,\theta) \in \omega_T\} \subset T$ (see Figure 1.5).

Let $v^\delta(r,\theta) := v(r-\delta,\theta)$, for $(r,\theta) \in \omega_T$. We will prove that

$$\|v - v^\delta\|_{0,\omega_T} \leq Ch_T^{2s}\|v\|_{s,\widetilde{T}}. \tag{1.11}$$

Then the lemma follows from this inequality and the fact that, for h_T small enough, $\|v^\delta\|_{0,\omega_T} \leq C\|v\|_{0,\omega_T^\delta} \leq C\|v\|_{0,T}$.

Inequality (1.11) is clear for $s = 0$. We prove it for $s = 1$; then, for $0 < s < 1$, it follows by interpolation between Sobolev spaces.

Let $v \in \mathcal{C}^\infty(\widetilde{T})$ (we prove (1.11) for such smooth v; for any $v \in \mathrm{H}^1(\widetilde{T})$ it follows by the standard density argument). For any $(r,\theta) \in \omega_T$ we may write

$$v(r,\theta) - v^\delta(r,\theta) = \int_{r-\delta}^{r} \frac{\partial v}{\partial r}(t,\theta)\, dt.$$

Hence, applying Cauchy-Schwarz inequality and integrating on ω_T, we obtain:

$$\begin{aligned}
\|v - v^\delta\|^2_{0,\omega_T} &\leq \int_0^{\theta_1} \int_{r_1(\theta)}^{r_2(\theta)} \delta \int_{r-\delta}^{r} \left|\frac{\partial v}{\partial r}(t,\theta)\right|^2 dt\; r\, dr\; d\theta \\
&\leq \delta \int_0^{\theta_1} \left[\int_{r_0}^{r_2(\theta)} \left|\frac{\partial v}{\partial r}(t,\theta)\right|^2 \frac{t}{r_0}\, dt\right] \left[\int_{r_1(\theta)}^{r_2(\theta)} r\, dr\right] d\theta \\
&\leq \delta \int_0^{\theta_1} \left[\int_0^{r_2(\theta)} |\nabla v(t,\theta)|^2\, t\, dt\right] \frac{2\bar{r}_2}{r_0} \left[r_2(\theta) - r_1(\theta)\right] d\theta \\
&\leq C\delta^2 \|\nabla v\|^2_{0,\widetilde{T}}.
\end{aligned}$$

Thus, for $s = 1$, (1.11) is a consequence of the fact that $\delta \leq C h_T^2$. □

Consider the operator $\mathbf{T}$ defined by

$$\begin{array}{rccl}
\mathbf{T}: & \mathrm{L}^2(\Omega) & \longrightarrow & \mathrm{L}^2(\Omega) \\
& f & \longmapsto & u \in \mathrm{H}^1(\Omega):\ a(u,v) = b(f,v) \quad \forall v \in \mathrm{H}^1(\Omega),
\end{array}$$

where $a(\cdot,\cdot)$ and $b(\cdot,\cdot)$ are the bilinear forms defined in (1.6) and (1.7), respectively. By virtue of Lax-Milgram Lemma, it is clear that $\mathbf{T}$ is a well defined bounded operator and

$$\|u\|_{1,\Omega} \leq C\|f\|_{0,\Omega}. \tag{1.12}$$

Furthermore, because of the compact inclusion $\mathrm{H}^1(\Omega) \hookrightarrow \mathrm{L}^2(\Omega)$, $\mathbf{T}$ is compact. Clearly, the eigenvalues of $\mathbf{T}$ are given by $\mu_k = 1/\lambda_k$, with λ_k being the eigenvalues of problem (1.5), and the corresponding eigenfunctions u_k coincide.

As a consequence of the classical a priori estimates (see [53]), for any $f \in \mathrm{L}^2(\Omega)$, $u = \mathbf{T}f$ is known to satisfy some further regularity. In fact, $u \in \mathrm{H}^{1+r}(\Omega)$ for some $r > 0$ depending on the geometry of Ω, and there holds

$$\|u\|_{1+r,\Omega} \leq C\|f\|_{0,\Omega}. \tag{1.13}$$

For a pure Neumann problem, if Ω has no reentrant corners, then $r = 1$; otherwise $r < \frac{2\pi}{\theta}$, with θ being the largest interior angle of Ω. From now on let $r \in (0,1]$ be fixed such that (1.13) holds. Notice that, as a consequence, the eigenfunctions u_k of $\mathbf{T}$ belong to $\mathrm{H}^{1+r}(\Omega)$ and satisfy

$$\|u_k\|_{1+r,\Omega} \leq C\|u_k\|_{0,\Omega}. \tag{1.14}$$

Let $\overline{\mathbf{T}}_h$ be defined by

$$\begin{array}{rccl} \overline{\mathbf{T}}_h: & \mathrm{L}^2(\Omega_h) & \longrightarrow & \mathrm{L}^2(\Omega_h) \\ & g & \longmapsto & v_h \in \mathcal{L}_h(\Omega_h):\ a_h(v_h, w_h) = b_h(g, w_h) \quad \forall w_h \in \mathcal{L}_h(\Omega_h), \end{array}$$

with $a_h(\cdot,\cdot)$ and $b_h(\cdot,\cdot)$ as defined in (1.9) and (1.10), respectively. Clearly

$$\|v_h\|_{1,\Omega_h} \leq C\|g\|_{0,\Omega_h}. \tag{1.15}$$

The positive non-zero eigenvalues of $\overline{\mathbf{T}}_h$ are given by $\mu_{hk} = 1/\lambda_{hk}$, with λ_{hk} being those of the discrete problem (1.8) and coinciding associated eigenfunctions u_{hk}.

The spectral approximation theory stated in [7] cannot be directly applied to the operators $\overline{\mathbf{T}}_h$, since their domains $\mathrm{L}^2(\Omega_h)$ do not coincide with that of $\mathbf{T}$. So, we are going to introduce other discrete operators $\mathbf{T}_h$ defined on $\mathrm{L}^2(\Omega)$ and with spectrum also related to that of problem (1.8).

From now on, we assume that h is sufficiently small in order to Lemmas 1.2.2, 1.2.3, and 1.2.4 hold. Let

$$\mathcal{L}_h(\Omega) := \{v_h \in \mathrm{H}^1(\Omega):\ v_h|_{\widetilde{T}} \in \mathcal{P}_1(\widetilde{T})\ \forall \widetilde{T} \in \widetilde{\mathcal{T}}_h\}.$$

We consider two restriction-extension operators, one from $\mathcal{L}_h(\Omega_h)$ to $\mathcal{L}_h(\Omega)$ and the other from $\mathcal{L}_h(\Omega)$ to $\mathcal{L}_h(\Omega_h)$. Let

$$\begin{array}{rccc} \check{\mathbf{E}}: & \mathcal{L}_h(\Omega_h) & \longrightarrow & \mathcal{L}_h(\Omega) \\ & v_h & \longmapsto & \check{v}_h \end{array}$$

with

$$\check{v}_h|_{\widetilde{T}} := \begin{cases} v_h|_{\widetilde{T}} & \forall \widetilde{T} \in \widetilde{\mathcal{T}}_h:\ \widetilde{T} \subset \Omega_h, \\ \\ (v_h|_T)^{\check{}} & \forall \widetilde{T} \in \widetilde{\mathcal{T}}_h:\ \widetilde{T} \not\subset \Omega_h, \end{cases}$$

where $(v_h|_T)^{\check{}} \in \mathcal{P}_1(\widetilde{T})$ denotes the natural extension of the linear function $v_h|_T \in \mathcal{P}_1(T)$ to the larger set $\widetilde{T}$ (notice that, if $\widetilde{T} \not\subset \Omega_h$, then $T \subset \widetilde{T}$).

Let $\hat{\mathbf{E}} := \check{\mathbf{E}}^{-1}$; namely,

$$\begin{array}{rccc} \hat{\mathbf{E}}: & \mathcal{L}_h(\Omega) & \longrightarrow & \mathcal{L}_h(\Omega_h) \\ & w_h & \longmapsto & \hat{w}_h \end{array}$$

with

$$\hat{w}_h|_T := \begin{cases} w_h|_T & \forall T \in \mathcal{T}_h:\ T \subset \Omega, \\ \\ \left(w_h|_{\widetilde{T}}\right)^{\hat{}} & \forall T \in \mathcal{T}_h:\ T \not\subset \Omega, \end{cases}$$

where, $\left(w_h|_{\widetilde{T}}\right)^{\widehat{}} \in \mathcal{P}_1(T)$ denotes the natural extension of the linear function $w_h|_{\widetilde{T}} \in \mathcal{P}_1(\widetilde{T})$ to the larger set T (notice that, now, if $T \not\subset \Omega$, then $\widetilde{T} \subset T$).

As a consequence of Lemma 1.2.2, the operators $\check{\mathbf{E}}$ and $\hat{\mathbf{E}}$ are uniformly bounded in L^2 and H^1 norms. More precisely,

$$\|\check{\mathbf{E}}v_h\|_{k,\Omega} \leq C\|v_h\|_{k,\Omega_h} \qquad \forall v_h \in \mathcal{L}_h(\Omega_h), \qquad k = 0, 1, \tag{1.16}$$

$$\|\hat{\mathbf{E}}w_h\|_{k,\Omega_h} \leq C\|w_h\|_{k,\Omega} \qquad \forall w_h \in \mathcal{L}_h(\Omega), \qquad k = 0, 1. \tag{1.17}$$

We will also use the $\mathrm{L}^2(\Omega)$-projection onto $\mathcal{L}_h(\Omega)$. Let

$$\begin{array}{rccc} \mathbf{P}: & \mathrm{L}^2(\Omega) & \longrightarrow & \mathcal{L}_h(\Omega) \\ & f & \longmapsto & f_h \end{array}$$

with

$$f_h \in \mathcal{L}_h(\Omega): \qquad \int_\Omega (f_h - f) w_h \, dx = 0 \qquad \forall w_h \in \mathcal{L}_h(\Omega). \tag{1.18}$$

Clearly

$$\|f_h\|_{0,\Omega} \leq \|f\|_{0,\Omega} \qquad \forall f \in \mathrm{L}^2(\Omega). \tag{1.19}$$

Furthermore, the standard error estimate for this projection yields

$$\|f_h - f\|_{0,\Omega} \leq Ch\|f\|_{1,\Omega} \qquad \forall f \in \mathrm{H}^1(\Omega). \tag{1.20}$$

Now we are able to define the discrete operator that we will use in the sequel:

$$\begin{array}{rccc} \mathbf{T}_h: & \mathrm{L}^2(\Omega) & \longrightarrow & \mathrm{L}^2(\Omega) \\ & f & \longmapsto & \check{u}_h = \check{\mathbf{E}}\overline{\mathbf{T}}_h\hat{\mathbf{E}}\mathbf{P}f \end{array}$$

As a consequence of the estimates (1.19), (1.17), (1.15), and (1.16), the operators $\mathbf{T}_h$ are uniformly bounded. Moreover, they satisfy

$$\|\mathbf{T}_h f\|_{1,\Omega} \leq C\|f\|_{0,\Omega}. \tag{1.21}$$

The following lemma shows that the eigenvalues of $\mathbf{T}_h$ and $\overline{\mathbf{T}}_h$ coincide and the eigenfunctions of one operator are the restriction-extension of those of the other:

Lemma 1.2.5 *The non-zero eigenvalues of $\overline{\mathbf{T}}_h$ and $\mathbf{T}_h$ coincide and the respective associated eigenfunctions u_h and $\check{u}_h$ are related by $\check{u}_h = \check{\mathbf{E}}u_h$ and $u_h = \hat{\mathbf{E}}\check{u}_h$.*

Proof. Let $u_h \in \mathcal{L}_h(\Omega_h)$, $u_h \neq 0$, such that $\overline{\mathbf{T}}_h u_h = \lambda_h u_h$. Then

$$\mathbf{T}_h\check{\mathbf{E}}u_h = \check{\mathbf{E}}\overline{\mathbf{T}}_h\hat{\mathbf{E}}\mathbf{P}\check{\mathbf{E}}u_h = \check{\mathbf{E}}\overline{\mathbf{T}}_h\hat{\mathbf{E}}\check{\mathbf{E}}u_h = \check{\mathbf{E}}\overline{\mathbf{T}}_h u_h = \lambda_h\check{\mathbf{E}}u_h.$$

Conversely, let $\check{u}_h \in \mathcal{L}_h(\Omega)$, $\check{u}_h \neq 0$, such that $\mathbf{T}_h\check{u}_h = \lambda_h\check{u}_h$. Then

$$\overline{\mathbf{T}}_h\hat{\mathbf{E}}\check{u}_h = \hat{\mathbf{E}}\check{\mathbf{E}}\overline{\mathbf{T}}_h\hat{\mathbf{E}}\mathbf{P}\check{u}_h = \hat{\mathbf{E}}\mathbf{T}_h\check{u}_h = \lambda_h\hat{\mathbf{E}}\check{u}_h.$$

□

The aim of this chapter is to study how the eigenvalues and eigenfunctions of $\mathbf{T}_h$, approximate those of $\mathbf{T}$, and hence to analyze how the eigenvalue problem (1.8) allows approximating the solutions of the spectral problem (1.5).

1.3 Spectral approximation

In order to use the spectral approximation theory stated in [7], we are going to prove that the operators $\mathbf{T}_h$ converge to $\mathbf{T}$ in norm as h goes to zero. From now on and throughout the rest of the section, we use the following notation: given $f \in \mathrm{L}^2(\Omega)$, we denote $u := \mathbf{T}f$, $f_h := \mathbf{P}f$, $\hat{f}_h := \hat{\mathbf{E}}f_h$, $u_h := \overline{\mathbf{T}}_h\hat{f}_h$, and $\check{u}_h := \check{\mathbf{E}}u_h = \mathbf{T}_hf$.

We will also use in the proofs, extensions to $\Omega \cup \Omega_h$ of functions originally defined in Ω. For $v \in \mathrm{H}^s(\Omega)$ $(s > 0)$, let v^e denote an extension of v to $\mathbb{R}^2$ satisfying (see, for instance, Theorem 1.4.3.1 in [53])

$$\|v^e\|_{s,\mathbb{R}^2} \leq C\|v\|_{s,\Omega}. \tag{1.22}$$

In particular, since according to the estimate (1.13) $u \in \mathrm{H}^{1+r}(\Omega)$, then let u^e be an extension of u satisfying

$$\|u^e\|_{1+r,\mathbb{R}^2} \leq C\|u\|_{1+r,\Omega}. \tag{1.23}$$

The following lemma splits $\|(\mathbf{T}-\mathbf{T}_h)f\|_{1,\Omega} = \|u-\check{u}_h\|_{1,\Omega}$ into three terms which can be dealt with separately:

Lemma 1.3.1 *There exists a positive constant C, not depending on f, such that*

$$\|u-\check{u}_h\|_{1,\Omega} \leq C\left[\inf_{v_h\in\mathcal{L}_h(\Omega_h)}\|u^e-v_h\|_{1,\Omega_h} + \sup_{w_h\in\mathcal{L}_h(\Omega_h)}\frac{|b_h(\hat{f}_h,w_h)-a_h(u^e,w_h)|}{\|w_h\|_{1,\Omega_h}}\right] + \|u-\check{u}_h\|_{1,\Omega\setminus\bar{\Omega}_h}. \tag{1.24}$$

Proof. It is enough to notice that

$$\begin{aligned}\|u-\check{u}_h\|^2_{1,\Omega} &= \|u-u_h\|^2_{1,\Omega\cap\Omega_h} + \|u-\check{u}_h\|^2_{1,\Omega\setminus\bar{\Omega}_h}\\ &\leq \|u^e-u_h\|^2_{1,\Omega_h} + \|u-\check{u}_h\|^2_{1,\Omega\setminus\bar{\Omega}_h},\end{aligned}$$

and to use the standard techniques to deal with non conforming methods to estimate the first term (see Strang's Lemma, for instance, in [36]):

$$\|u^e - u_h\|_{1,\Omega_h} \leq 2 \inf_{v_h \in \mathcal{L}_h(\Omega_h)} \|u^e - v_h\|_{1,\Omega_h} + \sup_{w_h \in \mathcal{L}_h(\Omega_h)} \frac{|b_h(\hat{f}_h, w_h) - a_h(u^e, w_h)|}{\|w_h\|_{1,\Omega_h}}. \quad (1.25)$$

□

In what follows we give estimates of the three terms in the right hand side of (1.24). For the first one we have:

Lemma 1.3.2 *There exists a positive constant C, not depending on f, and $v_h \in \mathcal{L}_h(\Omega_h)$ such that*

$$\|u^e - v_h\|_{1,\Omega_h} \leq Ch^r \|f\|_{0,\Omega}.$$

Proof. Let $v_h \in \mathcal{L}_h(\Omega_h)$ be the Lagrange interpolant of $u^e \in \mathrm{H}^{1+r}(\Omega_h)$. Proceeding as in Example 3 of [41] we have

$$\|u^e - v_h\|_{1,\Omega_h} \leq Ch^r \|u^e\|_{1+r,\Omega_h}.$$

(See also, Theorem 2.27 in [48] for an alternative proof). So, the lemma follows from this inequality and estimates (1.23) and (1.13). □

Now we estimate the second term in the right hand side of (1.24):

Lemma 1.3.3 *There exists a positive constant C, not depending on f, such that*

$$\sup_{w_h \in \mathcal{L}_h(\Omega_h)} \frac{|b_h(\hat{f}_h, w_h) - a_h(u^e, w_h)|}{\|w_h\|_{1,\Omega_h}} \leq Ch^r \|f\|_{0,\Omega}.$$

Proof. Let $w_h \in \mathcal{L}_h(\Omega_h)$ and $\breve{w}_h = \breve{\mathbf{E}} w_h$. Since $\breve{w}_h \in \mathrm{H}^1(\Omega)$, then $a(u, \breve{w}_h) = b(f, \breve{w}_h)$, and hence

$$b_h(\hat{f}_h, w_h) - a_h(u^e, w_h) = [b_h(\hat{f}_h, w_h) - b(f, \breve{w}_h)] + [a(u, \breve{w}_h) - a_h(u^e, w_h)].$$

Because of (1.18) and the fact that $\breve{w}_h \in \mathcal{L}_h(\Omega)$, we have

$$b_h(\hat{f}_h, w_h) - b(f, \breve{w}_h) = \int_{\Omega_h} \hat{f}_h w_h \, dx - \int_{\Omega} f \breve{w}_h \, dx = \int_{\Omega_h \setminus \bar{\Omega}} \hat{f}_h w_h \, dx - \int_{\Omega \setminus \bar{\Omega}_h} f_h \breve{w}_h \, dx.$$

Analogously,

$$a(u, \breve{w}_h) - a_h(u^e, w_h) = \int_{\Omega \setminus \bar{\Omega}_h} (\nabla u \cdot \nabla \breve{w}_h + u \breve{w}_h) \, dx - \int_{\Omega_h \setminus \bar{\Omega}} (\nabla u^e \cdot \nabla w_h + u^e w_h) \, dx.$$

Now, by using Cauchy-Schwarz inequality and Lemma 1.2.3, we obtain:

$$\begin{aligned}
\left|\int_{\Omega_h\setminus\bar\Omega} \hat f_h w_h\, dx\right| &\le \|\hat f_h\|_{0,\Omega_h\setminus\bar\Omega}\, Ch\|w_h\|_{1,\Omega_h}\\
\left|\int_{\Omega\setminus\bar\Omega_h} f_h \check w_h\, dx\right| &\le \|f_h\|_{0,\Omega\setminus\bar\Omega_h}\, Ch\|\check w_h\|_{1,\Omega}\\
\left|\int_{\Omega\setminus\bar\Omega_h} (\nabla u\cdot\nabla\check w_h + u\check w_h)\, dx\right| &\le Ch^r\|u\|_{1+r,\Omega}\|\check w_h\|_{1,\Omega\setminus\bar\Omega_h}\\
\left|\int_{\Omega_h\setminus\bar\Omega} (\nabla u^e\cdot\nabla w_h + u^e w_h)\, dx\right| &\le Ch^r\|u^e\|_{1+r,\Omega_h}\|w_h\|_{1,\Omega_h\setminus\bar\Omega}
\end{aligned}$$

Finally, we conclude the lemma bounding the four right hand sides above by

$$Ch^r\|f\|_{0,\Omega}\|w_h\|_{1,\Omega_h}.$$

To do this, we use (1.17) and (1.19) for the first one, (1.16) for the second one, (1.13) and (1.16) for the third one, and (1.23) and (1.13) for the last one. □

Remark 1.3.1 *Combining estimate (1.25) in the proof of Lemma 1.3.1, with Lemmas 1.3.2 and 1.3.3, we also have*

$$\|u^e - u_h\|_{1,\Omega_h} \le Ch^r\|f\|_{0,\Omega}.$$

Now we are able to estimate the third term in (1.24):

Lemma 1.3.4 *There exists a positive constant C, not depending on f, such that*

$$\|u - \check u_h\|_{1,\Omega\setminus\bar\Omega_h} \le Ch^r\|f\|_{0,\Omega}.$$

Proof. For the L^2 norm, we use Lemma 1.2.3 and estimates (1.12) and (1.21) to obtain

$$\|u - \check u_h\|_{0,\Omega\setminus\bar\Omega_h} \le Ch\|u\|_{1,\Omega} + Ch\|\check u_h\|_{1,\Omega} \le Ch\|f\|_{0,\Omega}.$$

For the H^1 seminorm we use Lemma 1.2.4:

$$\begin{aligned}
|u - \check u_h|^2_{1,\Omega\setminus\bar\Omega_h} &= \sum_{T\in\mathcal{T}_h^\partial:\, T\subset\widetilde T} \|\nabla(u-\check u_h)\|^2_{0,\widetilde T\setminus T}\\
&\le \sum_{T\in\mathcal{T}_h^\partial:\, T\subset\widetilde T} C\left[\|\nabla(u-\check u_h)\|_{0,T} + h_T^{2r}\|\nabla(u-\check u_h)\|_{r,\widetilde T}\right]^2\\
&\le C\left[\|u^e - u_h\|^2_{1,\Omega_h} + h^{4r}\left(\|u\|^2_{1+r,\Omega} + \|\check u_h\|^2_{1,\Omega}\right)\right],
\end{aligned}$$

where we have used that $\|\nabla\check u_h\|_{r,\widetilde T} = \|\nabla\check u_h\|_{0,\widetilde T}$, since $\check u_h|_{\widetilde T}\in\mathcal{P}_1(\widetilde T)$.

Therefore the lemma follows from Remark 1.3.1, and estimates (1.13) and (1.21). □

Now we may conclude the convergence in norm of $\mathbf{T}_h$ to $\mathbf{T}$:

Lemma 1.3.5 *There exists a positive constant C such that, for all $f \in \mathrm{L}^2(\Omega)$,*

$$\|(\mathbf{T} - \mathbf{T}_h)f\|_{1,\Omega} \leq Ch^r \|f\|_{0,\Omega}.$$

Proof. It is an immediate consequence of the four previous lemmas. □

Therefore, we are able to apply the spectral approximation theory for compact operators (see [7]) to obtain optimal order error estimates for the eigenfunctions. For simplicity we state the result for a simple eigenvalue; see [7] for the general statement.

Theorem 1.3.1 *Let μ_k be the k-th (simple) eigenvalue of $\mathbf{T}$ and μ_{hk} the k-th eigenvalue of $\mathbf{T}_h$. Then, the corresponding eigenfunctions u_k and $\breve{u}_{hk}$ can be chosen such that $\|u_k\|_{0,\Omega} = \|\breve{u}_{hk}\|_{0,\Omega} = 1$ and*

$$\|u_k - \breve{u}_{hk}\|_{1,\Omega} \leq Ch^r,$$

with C a strictly positive constant.

Proof. It is a direct consequence of the convergence in norm of $\mathbf{T}_h$ to $\mathbf{T}$ and the error estimate in the previous lemma, and Lemma 7.1 in [7]. □

In the remainder of the chapter we will prove optimal order error estimates for the L^2 norm of the eigenfunctions and for the eigenvalues. To this goal, we will use a double order error estimate for $\|u - \breve{u}_h\|_{0,\Omega}$. To the best of the author's knowledge, estimates of this type have not been proved for Neumann boundary conditions on curved domains. The proofs given below for the estimate of $\|u - \breve{u}_h\|_{0,\Omega}$ are valid only for smooth right-hand sides f (namely, $f \in \mathrm{H}^1(\Omega)$). However, the obtained results suffice to yield optimal error estimates for the spectral problem without assuming any regularity.

The following two lemmas are valid for $f \in \mathrm{H}^1(\Omega)$. For such functions, we denote by f^e their bounded extensions to $\mathbb{R}^2$ satisfying (1.22) for $s = 1$; namely:

$$\|f^e\|_{1,\mathbb{R}^2} \leq C\|f\|_{1,\Omega}. \tag{1.26}$$

First we prove the following technical result:

Lemma 1.3.6 *There exists a positive constant C such that, for all $f \in \mathrm{H}^1(\Omega)$,*

$$\|\hat{f}_h - f^e\|_{0,\Omega_h \setminus \bar{\Omega}} \leq Ch\|f\|_{1,\Omega}.$$

Proof. According to Lemma 1.2.4, we have $\forall T \in \mathcal{T}_h^{\partial}$ such that $T \supset \widetilde{T}$,

$$\|\hat{f}_h - f^e\|_{0,T \setminus \widetilde{T}} \leq C\left(\|f_h - f\|_{0,\widetilde{T}} + h_T^2 \|\hat{f}_h - f^e\|_{1,T}\right).$$

From a standard local inverse inequality (see for instance [36]), we obtain

$$|\hat{f}_h|_{1,T} \leq \frac{C}{h_T}\|\hat{f}_h\|_{0,T}$$

Hence, since $\|\hat{f}_h\|_{0,T} \leq C\|f_h\|_{0,\widetilde{T}}$ because of Lemma 1.2.2, we have

$$h_T^2\|\hat{f}_h - f^e\|_{1,T} \leq h_T^2\left(\|\hat{f}_h\|_{1,T} + \|f^e\|_{1,T}\right) \leq C\left(h_T\|f_h\|_{0,\widetilde{T}} + h_T^2\|f^e\|_{1,T}\right).$$

Therefore,

$$\|\hat{f}_h - f^e\|_{0,\Omega_h\setminus\bar{\Omega}} \leq C\left(\|f_h - f\|_{0,\Omega} + h\|f_h\|_{0,\Omega} + h^2\|f^e\|_{1,\Omega_h}\right),$$

and the lemma follows from (1.20), (1.19), and (1.26). □

Now we can prove an double order $\mathrm{L}^2(\Omega)$-estimate:

Lemma 1.3.7 *There exists a positive constant C such that, for all $f \in \mathrm{H}^1(\Omega)$,*

$$\|(\mathbf{T} - \mathbf{T}_h)f\|_{0,\Omega} \leq Ch^{2r}\|f\|_{1,\Omega}.$$

Proof. Let $f \in \mathrm{H}^1(\Omega)$. Since

$$\|(\mathbf{T} - \mathbf{T}_h)f\|_{0,\Omega} = \sup_{g\in\mathrm{L}^2(\Omega)} \frac{b((\mathbf{T} - \mathbf{T}_h)f, g)}{\|g\|_{0,\Omega}},$$

then it only remains to prove that

$$|b\left((\mathbf{T} - \mathbf{T}_h)f, g\right)| \leq Ch^{2r}\|f\|_{1,\Omega}\,\|g\|_{0,\Omega} \quad \forall g \in \mathrm{L}^2(\Omega).$$

Let $g \in \mathrm{L}^2(\Omega)$ and $v = \mathbf{T}g$. We denote as above $v_h = \overline{\mathbf{T}}_h\hat{\mathbf{E}}\mathbf{P}g$ and $\check{v}_h = \check{\mathbf{E}}v_h = \mathbf{T}_h g$. Since according to (1.13) $v \in \mathrm{H}^{1+r}(\Omega)$, there exists a bounded extension v^e of v satisfying (1.22) for $s = 1 + r$.

Since a and b are symmetric and $u - \check{u}_h = (\mathbf{T} - \mathbf{T}_h)f \in \mathrm{H}^1(\Omega)$, then we have

$$b\left((\mathbf{T} - \mathbf{T}_h)f, g\right) = a(u - \check{u}_h, v) = a(u - \check{u}_h, v - \check{v}_h) + a(u - \check{u}_h, \check{v}_h).$$

Thus, from the continuity of $a(\cdot,\cdot)$ and Lemma 1.3.5, we only have to estimate the second term in the right hand side. Since $\check{v}_h \in \mathcal{L}_h(\Omega) \subset \mathrm{H}^1(\Omega)$ and $v_h \in \mathcal{L}_h(\Omega_h)$, then

$$\begin{aligned} a(u - \check{u}_h, \check{v}_h) &= b(f, \check{v}_h) - a(\check{u}_h, \check{v}_h) \\ &= \left[b(f, \check{v}_h) - b_h(\hat{f}_h, v_h)\right] + \left[a_h(u_h, v_h) - a(\check{u}_h, \check{v}_h)\right]. \end{aligned}$$

By using (1.18) and repeating the arguments in the proof of Lemma 1.3.3, we obtain

$$a(u-\breve{u}_h,\breve{v}_h)=\int_{\Omega\setminus\bar{\Omega}_h} f_h\breve{v}_h\,dx-\int_{\Omega_h\setminus\bar{\Omega}}\hat{f}_h v_h\,dx$$
$$+\int_{\Omega_h\setminus\bar{\Omega}}(\nabla u_h\cdot\nabla v_h+u_h v_h)\;dx-\int_{\Omega\setminus\bar{\Omega}_h}(\nabla\breve{u}_h\cdot\nabla\breve{v}_h+\breve{u}_h\breve{v}_h)\;dx.$$

Thus, to conclude the lemma, we estimate each term in the right hand side above. From Lemma 1.2.3 applied to $\breve{v}_h$ and f_h, (1.20), and (1.21),

$$\begin{aligned}\left|\int_{\Omega\setminus\bar{\Omega}_h} f_h\breve{v}_h\,dx\right| &\le \|f_h\|_{0,\Omega\setminus\bar{\Omega}_h}\|\breve{v}_h\|_{0,\Omega\setminus\bar{\Omega}_h}\\ &\le \left(\|f_h-f\|_{0,\Omega\setminus\bar{\Omega}_h}+\|f\|_{0,\Omega\setminus\bar{\Omega}_h}\right)Ch\|\breve{v}_h\|_{1,\Omega}\\ &\le Ch^2\|f\|_{1,\Omega}\|g\|_{0,\Omega}.\end{aligned}$$

By using Lemma 1.2.3 applied to v_h and f^e, Lemma 1.3.6, (1.16), (1.26), and (1.21),

$$\begin{aligned}\left|\int_{\Omega_h\setminus\bar{\Omega}}\hat{f}_h v_h\,dx\right| &\le \|\hat{f}_h\|_{0,\Omega_h\setminus\bar{\Omega}}\|v_h\|_{0,\Omega_h\setminus\bar{\Omega}}\\ &\le \left(\|\hat{f}_h-f^e\|_{0,\Omega_h\setminus\bar{\Omega}}+\|f^e\|_{0,\Omega_h\setminus\bar{\Omega}}\right)Ch\|v_h\|_{1,\Omega_h}\\ &\le Ch^2\left(\|f\|_{1,\Omega}+\|f^e\|_{1,\Omega_h}\right)\|\breve{v}_h\|_{1,\Omega_h}\\ &\le Ch^2\|f\|_{1,\Omega}\|g\|_{0,\Omega}.\end{aligned}$$

By using Remark 1.3.1, Lemma 1.2.3, (1.23), and (1.13),

$$\begin{aligned}\left|\int_{\Omega_h\setminus\bar{\Omega}}(\nabla u_h\cdot\nabla v_h+u_h v_h)\;dx\right| &\le \|u_h\|_{1,\Omega_h\setminus\bar{\Omega}}\|v_h\|_{1,\Omega_h\setminus\bar{\Omega}}\\ &\le \left(\|u_h-u^e\|_{1,\Omega_h\setminus\bar{\Omega}}+\|u^e\|_{1,\Omega_h\setminus\bar{\Omega}}\right)\left(\|v_h-v^e\|_{1,\Omega_h\setminus\bar{\Omega}}+\|v^e\|_{1,\Omega_h\setminus\bar{\Omega}}\right)\\ &\le \left(Ch^r\|f\|_{0,\Omega}+Ch^r\|u^e\|_{1+r,\Omega_h}\right)\left(Ch^r\|g\|_{0,\Omega}+Ch^r\|v^e\|_{1+r,\Omega_h}\right)\\ &\le Ch^{2r}\|f\|_{0,\Omega}\|g\|_{0,\Omega}.\end{aligned}$$

Finally, from Lemmas 1.3.5 and 1.2.3, and (1.13),

$$\begin{aligned}\left|\int_{\Omega\setminus\bar{\Omega}_h}(\nabla\breve{u}_h\cdot\nabla\breve{v}_h+\breve{u}_h\breve{v}_h)\;dx\right| &\le \|\breve{u}_h\|_{1,\Omega\setminus\bar{\Omega}_h}\|\breve{v}_h\|_{1,\Omega\setminus\bar{\Omega}_h}\\ &\le \left(\|\breve{u}_h-u\|_{1,\Omega\setminus\bar{\Omega}_h}+\|u\|_{1,\Omega\setminus\bar{\Omega}_h}\right)\left(\|\breve{v}_h-v\|_{1,\Omega\setminus\bar{\Omega}_h}+\|v\|_{1,\Omega\setminus\bar{\Omega}_h}\right)\\ &\le \left(Ch^r\|f\|_{0,\Omega}+Ch^r\|u\|_{1+r,\Omega}\right)\left(Ch^r\|g\|_{0,\Omega}+Ch^r\|v\|_{1+r,\Omega}\right)\\ &\le Ch^{2r}\|f\|_{0,\Omega}\|g\|_{0,\Omega}.\end{aligned}$$

□

As a consequence of this lemma we may prove a double order error estimate for the eigenfunctions in L^2 norm:

Theorem 1.3.2 *Let μ_k be the k-th (simple) eigenvalue of $\mathbf{T}$ and μ_{hk} the k-th eigenvalue of $\mathbf{T}_h$. Then, the corresponding eigenfunctions u_k and $\check{u}_{hk}$ can be chosen such that $\|u_k\|_{0,\Omega} = \|\check{u}_{hk}\|_{0,\Omega} = 1$ and*

$$\|u_k - \check{u}_{hk}\|_{0,\Omega} \leq Ch^{2r},$$

with C a strictly positive constant.

Proof. Because of the previous lemma and the estimate (1.14), the theorem is also a direct consequence of Lemma 7.1 in [7]. □

Finally, a double order of convergence for the eigenvalues can also be proved:

Theorem 1.3.3 *Let μ_k be the k-th (simple) eigenvalue of $\mathbf{T}$ and μ_{hk} the k-th eigenvalue of $\mathbf{T}_h$. Then, there exists a strictly positive constant C such that*

$$|\mu_k - \mu_{hk}| \leq Ch^{2r}.$$

Proof. Since $\mathbf{T}$ is self-adjoint with respect to $b(\cdot,\cdot)$, then Theorem 7.3 of [7] applied to our case yields

$$|\mu - \mu_h| \leq C \left[\sup_{f,g \in \mathcal{E} \subset \mathrm{L}^2(\Omega)} \frac{|b\left((\mathbf{T} - \mathbf{T}_h)f, g\right)|}{\|f\|_{0,\Omega}\, \|g\|_{0,\Omega}} + \|(\mathbf{T} - \mathbf{T}_h)|\varepsilon\|_{0,\Omega} \|(\mathbf{T} - \mathbf{T}_h^*)|\varepsilon\|_{0,\Omega} \right],$$

where $\mathcal{E}$ is the eigenspace associated to μ_k, and $\mathbf{T}_h^*$ is the adjoint operator of $\mathbf{T}_h$ with respect to $b(\cdot,\cdot)$.

Now

$$\sup_{f,g \in \mathcal{E} \subset \mathrm{L}^2(\Omega)} \frac{|b\left((\mathbf{T} - \mathbf{T}_h)f, g\right)|}{\|f\|_{0,\Omega}\, \|g\|_{0,\Omega}} = \sup_{f \in \mathcal{E}} \frac{\|(\mathbf{T} - \mathbf{T}_h)f\|_{0,\Omega}}{\|f\|_{0,\Omega}}$$

and

$$\begin{aligned} \|(\mathbf{T} - \mathbf{T}_h^*)f\|_{0,\Omega} &= \sup_{g \in \mathrm{L}^2(\Omega)} \frac{b((\mathbf{T} - \mathbf{T}_h^*)f, g)}{\|g\|_{0,\Omega}} = \sup_{g \in \mathrm{L}^2(\Omega)} \frac{b(f, (\mathbf{T} - \mathbf{T}_h)g)}{\|g\|_{0,\Omega}} \\ &\leq \|f\|_{0,\Omega} \sup_{g \in \mathrm{L}^2(\Omega)} \frac{\|(\mathbf{T} - \mathbf{T}_h)g\|_{0,\Omega}}{\|g\|_{0,\Omega}} \leq C\|f\|_{0,\Omega}, \end{aligned}$$

the last inequality because of (1.12) and (1.21).

Thus, the theorem is a consequence of Lemma 1.3.7 and estimate (1.14). □

1.4 Conclusions

We have analyzed the finite element approximation of eigenvalues and eigenfunctions of the Laplace equations with Neumann boundary conditions on curved (non convex) domains Ω. Convergence and optimal order error estimates have been proved for standard piecewise linear elements on a discrete polygonal domain $\Omega_h \not\subset \Omega$, in the framework of the abstract spectral approximation theory as stated in [7]. Similar results had been previously proved by Vanmaele and Ženíšek[82] (based on *min-max* techniques), and Lebaud [64], but in both cases only for Dirichlet boundary conditions.

Chapter 2

Finite element approximation of spectral acoustic problems on curved domains

This chapter deals with the finite element approximation of the displacement formulation of the spectral acoustic problem on a curved non convex two-dimensional domain Ω. Convergence and error estimates are proved for *Raviart-Thomas* elements on a discrete polygonal domain $\Omega_h \not\subset \Omega$ in the framework of the abstract spectral approximation theory. Similar results have been previously proved only for polygonal domains. Numerical tests confirming the theoretical results are reported.

2.1 Introduction

A considerable amount of work has been devoted during the last years to device and analyze efficient numerical tools to deal with structural-acoustic interaction problems. See for instance the monographs by Morand and Ohayon [68], Conca *et al.* [39], and Ohayon and Soize [69], where different mechanical problems involving fluid-structure interaction are treated. These references also include numerical techniques and extensive bibliographic lists.

Although the typical variable to describe an acoustic fluid is its pressure, since long time ago (see for instance [62]) practitioners recognize several advantages of using fluid displacement formulations in spectral problems involving interaction with a solid. However, this approach has also a severe drawback: the presence of spurious vibration modes when standard finite elements are used for the fluid displacements.

Several alternatives have been proposed to avoid these spurious modes (see for instance [54, 35, 85, 51]). One of them was introduced in [19] and analyzed in

[12, 74] for the structural-acoustic vibration problem. It is based on using Raviart-Thomas elements to discretize the fluid displacement field—a natural choice since the variational formulation is posed on H(div). Since then, this approach was succesfully extended to deal with other spectral problems involving, for instance, incompressible fluids [13, 14], dissipative acoustics [15, 20], interaction with slender structures [45, 18], etc.

In all these cases, optimal order error estimates have been proved for eigenvalues and eigenfunctions. However, in all the proofs, the domain has been assumed to be polygonal (or polyhedral in 3D). The main reason for this assumption was to avoid some intrinsic difficulties in the application of the standard spectral approximation theory ([7]). These difficulties arise from the variational crime committed by approximating the curved domain with a polygonal one.

Even in much simpler cases like the finite element approximation of the spectral problem for the Laplacian on a general curved domain, the number of papers with theoretical results is remarkably small. Indeed, the first rigorous proofs for this problem valid for non-convex domains have been given just a few years ago by Vanmaele and Ženíšek ([82, 83, 84]) (using the *min-max* characterization; see [80, 76]) and Lebaud ([64]) (using the abstract approximation theory; see [7]). These papers deal only with Dirichlet boundary conditions. For Neumann boundary conditions the first results have been obtained even more recently ([56]).

In the present chapter we consider the vibration problem for an acoustic fluid contained within a rigid curved cavity. In spite of the fact that this problem can be efficiently solved by using pressure variables, we consider a displacement formulation of the fluid. The reason for this is the interest of applying this approach to fluid-structure vibration problems, where this formulation is convenient as remarked above. We prove spectral convergence and error estimates for eigenfunctions and eigenvalues, the latter of double-order as usual in this kind of problems.

From the mathematical point of view, the displacement formulation of the fluid acoustic vibration problem and its discretization with Raviart-Thomas elements is completely equivalent to the discretization with these elements of the mixed formulation of the spectral problem for the Laplacian (see [2, 42]). Thus, our analysis also covers this more standard problem. Let us recall that although error estimates for this spectral problem on polygonal domains have been given in [7], some recent papers ([24, 25]) show that, even in this case, it is not immediate to extend standard results on mixed methods to spectral problems.

The outline of the chapter is as follows: in the following section we introduce the displacement formulation of the acoustic vibration problem and its discretization by Raviart-Thomas elements. In section 3, corresponding continuous and discrete

operators are defined on a same Hilbert space, which allows us to fit this problem in the framework of the abstract spectral approximation theory ([7]). Let us remark that the correct definition of these operators is a key point for curved boundaries, because the continuous and discrete problems are posed on different domains. In section 4 we prove convergence in H(div)-norm of the discrete operators to the continuous one and apply this to obtain error estimates for the eigenfunctions. Since in this case an improved order of convergence in L^2-norm cannot be expected, an additional approximation property has to be proved to obtain a double-order error estimate for the eigenvalues. Finally, in section 5, we report some numerical tests which confirm the theoretical results and exhibit the performance of the method.

Throughout the chapter C will denote a positive constant not necessarily the same at each occurrence but always independent of the mesh-size h.

2.2 Statement of the problem

We consider the problem of determining the vibrations modes of an ideal inviscid barotropic fluid contained in a rigid cavity, described by means of the fluid displacement field.

Let $\Omega \subset \mathbb{R}^2$ be the domain occupied by the fluid. We assume that Ω is a bounded open domain, in general non convex, with a Lipschitz boundary $\partial\Omega$. We denote by ν the outward unit normal to $\partial\Omega$. We also assume $\partial\Omega$ is piecewise smooth; more precisely, $\partial\Omega = \bigcup_{j=1}^{J} \Gamma_j$ with Γ_j being $\mathcal{C}^2$ curves.

Consider the spectral problem which consists in finding $\lambda \in \mathbb{R}$ and $u \neq 0$ satisfying

$$\begin{cases} -\nabla(\rho c^2 \operatorname{div} u) = \lambda \rho u & \text{in } \Omega, \\ u \cdot \nu = 0 & \text{on } \partial\Omega. \end{cases}$$

The solution of this problem are the free vibration modes of the fluid contained in Ω; u is the amplitude of the displacement oscillation and $\sqrt{\lambda}$ the natural vibration frequency. On the other hand ρ denotes the fluid density and c the acoustic speed. Without loosing generality we assume $\rho = 1$ and $c = 1$.

Let $\mathrm{H}(\mathrm{div}, \Omega) := \{v \in \mathrm{L}^2(\Omega)^2 : \ \operatorname{div} v \in \mathrm{L}^2(\Omega)\}$, which endowed with the norm defined by $\|v\|^2_{\mathrm{div},\Omega} := \|v\|^2_{0,\Omega} + \|\operatorname{div} v\|^2_{0,\Omega}$ is a Hilbert space. We denote

$$\mathcal{V} := \mathrm{H}_0(\mathrm{div}, \Omega) := \{v \in \mathrm{H}(\mathrm{div}, \Omega) : \ v \cdot \nu = 0 \text{ on } \partial\Omega\},$$

which is a closed subspace of $\mathrm{H}(\mathrm{div}, \Omega)$. Then, the variational formulation of the spectral problem above reads:

Find $\lambda \in \mathbb{R}$ *and* $u \in \mathcal{V}$, $u \neq 0$, *such that*

$$\int_\Omega \operatorname{div} u \operatorname{div} v \, dx = \lambda \int_\Omega u \cdot v \, dx \qquad \forall v \in \mathcal{V}. \tag{2.1}$$

The above problem has exactly two types of solutions (see [12]):

1. $\lambda_0 = 0$, with corresponding eigenspace

$$\mathcal{K} := \{u \in \mathrm{H}_0(\operatorname{div}, \Omega) : \ \operatorname{div} u = 0 \text{ in } \Omega\};$$

2. a sequence of finite multiplicity eigenvalues $\lambda_n > 0$, $n \in \mathbb{N}$, diverging to $+\infty$, with corresponding eigenfunctions $u_n \in \mathcal{V}$ satisfying $u_n = \nabla \varphi_n$ for some $\varphi_n \in \mathrm{H}^1(\Omega)$.

The eigenfunctions of the second type form a complete orthogonal system of the closed subspace $\mathcal{G}$ of $\mathcal{V}$, which consists of the conservative displacement fields of this space; namely,

$$\mathcal{G} := \left\{u \in \mathrm{H}_0(\operatorname{div}, \Omega) : \ u = \nabla \varphi, \ \varphi \in \mathrm{H}^1(\Omega)\right\}.$$

Notice that $\mathcal{G}$ and $\mathcal{K}$ are orthogonal in $\mathrm{L}^2(\Omega)^2$ and $\mathrm{H}(\operatorname{div}, \Omega)$.

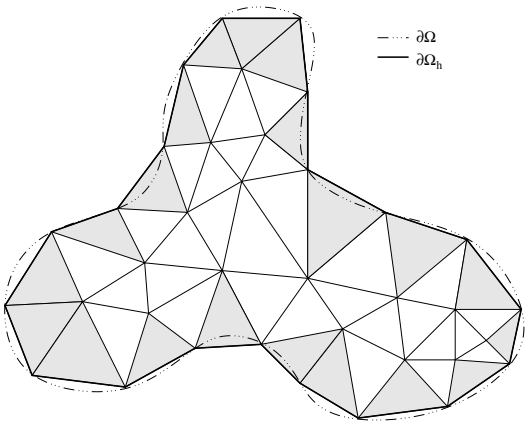

Figure 2.1: Triangulation of $\Omega_h \approx \Omega$. The shaded triangles are the *boundary* ones $T \in \mathcal{T}_h^\partial$.

We consider a family $\{\mathcal{T}_h\}$ of standard finite element triangulations of polygonal domains Ω_h approximating Ω (see for instance [36]) such that, if $\mathcal{N}_h$ is the set of vertexes of all the triangles in $\mathcal{T}_h$, then there holds (see Fig. 2.1):

- $\mathcal{N}_h \subset \bar{\Omega}_h$ and $\mathcal{N}_h \cap \partial\Omega_h \subset \partial\Omega$;

- $\mathcal{N}_h$ contains all the points where the boundary $\partial\Omega$ is not $\mathcal{C}^2$;
- for all $T \in \mathcal{T}_h$, at most two vertexes of T lie on $\partial\Omega_h$;

the third assumption is made only for the sake of simplicity.

As usual, h stands for the mesh-size, namely, the maximum diameter h_T of all the triangles $T \in \mathcal{T}_h$. We also assume that the family $\{\mathcal{T}_h\}$ is regular in the sense of a minimum angle condition; i.e., there exists $\theta_0 > 0$ such that, if θ_T is the smallest angle of T, then $\theta_T > \theta_0$ for all $T \in \mathcal{T}_h$ and for all the triangulations $\mathcal{T}_h$ in the family.

In what follows we will use some notation and definitions introduced in [49] (see also [86]). For a given triangulation $\mathcal{T}_h$, we denote by $\mathcal{T}_h^\partial$ the subset of the so called *boundary triangles*; namely, those having an edge on $\partial\Omega_h$ (see Fig. 2.1). For one such triangle T, let P_1^T, P_2^T, and P_3^T be its three vertexes, with $s_T := \overline{P_2^T P_3^T} \subset \partial\Omega_h$, and let σ_T be the piece of $\partial\Omega$ approximated by s_T (see Fig. 2.2).

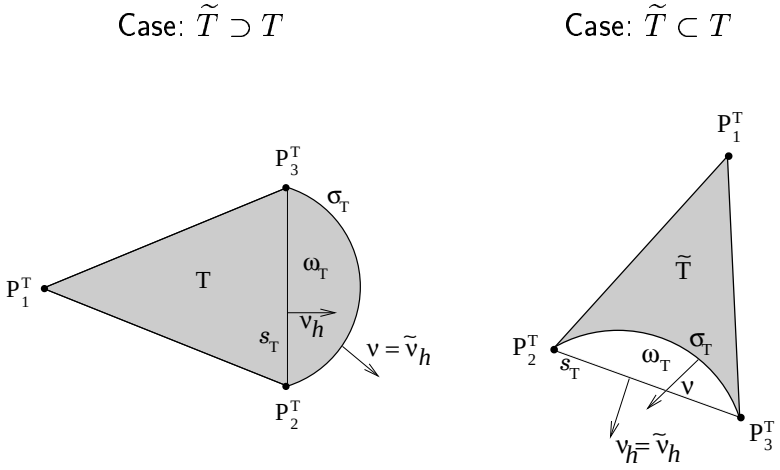

Figure 2.2: *Ideal* triangles $\widetilde{T}$.

We denote by $\widetilde{T}$ the curved triangle of edges $\overline{P_1^T P_2^T}$, σ_T, and $\overline{P_3^T P_1^T}$, and we call it the *ideal triangle* associated to T. For the sake of simplicity we assume that the triangulations $\mathcal{T}_h$ are such that, for each boundary triangle $T \in \mathcal{T}_h^\partial$, either $T \subset \widetilde{T}$ or $T \supset \widetilde{T}$.

We consider the finite dimensional space $\mathcal{V}_h$ defined by

$$\mathcal{V}_h := \{v_h \in \mathcal{R}_h(\Omega_h) : \ v_h \cdot \nu_h|_{\partial\Omega_h} = 0\},$$

where ν_h is the outward unit normal to $\partial\Omega_h$ and $\mathcal{R}_h(\Omega_h)$ is the Raviart-Thomas space (see [75])

$$\mathcal{R}_h(\Omega_h) := \{v_h \in \mathrm{H}(\mathrm{div}, \Omega_h) : \ v_h|_T \in \mathcal{RT}_0(T) \ \ \forall T \in \mathcal{T}_h\},$$

with

$$\mathcal{RT}_0(T) := \left\{ v_h \in \mathcal{P}_1(T)^2 : \ v_h(x,y) = (a+bx, c+by), \right. \\ \left. a,b,c \in \mathbb{R}, \ (x,y) \in T \right\}.$$

Then, the discretization of the spectral problem (2.1) obtained by using these elements reads:

Find $\lambda_h \in \mathbb{R}$ *and* $u_h \in \mathcal{V}_h$, $u_h \neq 0$, *such that*

$$\int_{\Omega_h} \operatorname{div} u_h \operatorname{div} v_h \, dx = \lambda_h \int_{\Omega_h} u_h \cdot v_h \, dx \qquad \forall v_h \in \mathcal{V}_h. \tag{2.2}$$

Proceeding as in [12], it is simple to prove that problem (2.2) has also two kind of solutions:

1. $\lambda_{h0} = 0$, with corresponding eigenspace

$$\mathcal{K}_h := \{ u_h \in \mathcal{V}_h : \ \operatorname{div} u_h = 0 \text{ in } \Omega_h \};$$

2. a finite set of positive eigenvalues λ_{hn}, with corresponding eigenfunctions $u_{hn} \in \mathcal{G}_h$, where $\mathcal{G}_h$ is the orthogonal complement of $\mathcal{K}_h$ in $\mathcal{V}_h$.

Notice that $\mathcal{G}_h$ and $\mathcal{K}_h$ are also orthogonal in $\mathrm{L}^2(\Omega_h)^2$; i.e.,

$$\mathcal{G}_h = \left\{ u_h \in \mathcal{V}_h : \ \int_{\Omega_h} u_h \cdot v_h \, dx = 0 \ \ \forall v_h \in \mathcal{K}_h \right\}.$$

The goal of this chapter is to prove that the solutions of the eigenvalue problem (2.2) approximate those of problem (2.1) and to establish error estimates.

2.3 Linear operators associated with the spectral problems

To study the convergence properties of problem (2.2), we will use the abstract spectral approximation theory stated in [7]. To do this we need to define, on a same fixed domain, operators A and A_h with spectra related to those of problems (2.1) and (2.2), respectively.

For each mesh $\mathcal{T}_h$ we denote

$$\widetilde{\Omega}_h := \Omega \cup \Omega_h.$$

We also denote by $\widetilde{\nu}_h$ the outward unit normal to $\widetilde{\Omega}_h$. Notice that either $\widetilde{\nu}_h = \nu_h$ or $\widetilde{\nu}_h = \nu$ (see Fig. 2.2).

We consider the operator A defined by

$$\begin{array}{rccl} A: & \mathrm{L}^2(\mathbb{R}^2)^2 & \longrightarrow & \mathrm{H}(\mathrm{div},\mathbb{R}^2) \hookrightarrow \mathrm{L}^2(\mathbb{R}^2)^2 \\ & f & \longmapsto & \overline{u}: \ \overline{u}|_\Omega = u, \end{array}$$

where $u \in \mathcal{G}$ is the solution of

$$\int_\Omega \mathrm{div}\, u \,\mathrm{div}\, v \; dx = \int_\Omega f \cdot v \; dx \quad \forall v \in \mathcal{G}, \tag{2.3}$$

and, from now on, $\overline{v}$ denotes the extension of a function v by zero from its original domain to $\mathbb{R}^2$.

This problem is well posed because the bilinear form $\int_\Omega \mathrm{div}\, u \,\mathrm{div}\, v \; dx$ is $\mathcal{V}$-elliptic on $\mathcal{G}$. Indeed, given $v \in \mathcal{G}$, let $\varphi \in \mathrm{H}^1(\Omega)$ be such that $v = \nabla\varphi$; then φ is solution of the compatible Neumann problem

$$\left\{ \begin{array}{ll} \Delta\varphi = \mathrm{div}\, v & \text{in } \Omega, \\ \dfrac{\partial\varphi}{\partial\nu} = 0 & \text{on } \partial\Omega. \end{array} \right. \tag{2.4}$$

Hence, because of Lax Milgram Lemma, there exist $C > 0$ such that

$$\|v\|_{0,\Omega} = \|\nabla\varphi\|_{0,\Omega} \leq C \, \|\mathrm{div}\, v\|_{0,\Omega} \quad \forall v \in \mathcal{G}. \tag{2.5}$$

Consequently there exist $\alpha > 0$ such that

$$\int_\Omega (\mathrm{div}\, v)^2 \; dx \geq \alpha \|v\|^2_{\mathrm{div},\Omega} \quad \forall v \in \mathcal{G}. \tag{2.6}$$

Therefore, by virtue of Lax Milgram Lemma again, it is clear that A is a well defined bounded operator and, if $\overline{u} = Af$, then

$$\|\overline{u}\|_{\mathrm{div},\mathbb{R}^2} \leq C \, \|f\|_{0,\mathbb{R}^2} \, . \tag{2.7}$$

Furthermore, as a consequence of classical a priori estimates for (2.4) (see [53]) φ attains additional regularity. Indeed, $\nabla\varphi \in \mathrm{H}^r(\Omega)^2$ and

$$\|\nabla\varphi\|_{r,\Omega} \leq C \, \|\mathrm{div}\, v\|_{0,\Omega} \, , \tag{2.8}$$

with $r \in (1/2, 1]$ (in fact, $r = 1$ if Ω has no reentrant corner, and $r < \frac{\pi}{\theta}$, with θ being the largest interior angle of Ω, otherwise). In particular, for $\overline{u} = Af$, we have that $u = \overline{u}|_\Omega \in \mathrm{H}^r(\Omega)^2$ and

$$\|u\|_{r,\Omega} \leq C \, \|\mathrm{div}\, u\|_{0,\Omega} \leq C \, \|f\|_{0,\mathbb{R}^2} \, . \tag{2.9}$$

Regarding further regularity of $\mathrm{div}\, u$ we have the following lemma:

Lemma 2.3.1 *Given $f \in \mathrm{L}^2(\mathbb{R}^2)^2$, let $u \in \mathcal{G}$ be the solution of problem (2.3). Then,*

$$\int_\Omega [\nabla(\operatorname{div} u) + f] \cdot \nabla\xi \, dx = 0 \qquad \forall \xi \in \mathrm{H}^1(\Omega). \tag{2.10}$$

Furthermore, $\operatorname{div} u \in \mathrm{H}^1(\Omega)$ *and*

$$\|\operatorname{div} u\|_{1,\Omega} \leq C \|f\|_{0,\mathbb{R}^2}, \tag{2.11}$$

with C a positive constant independent of f.

Proof. For $f \in \mathrm{L}^2(\Omega)^2$ the following decomposition holds (see [52]): $f = \nabla\psi + \eta$, with $\psi \in \mathrm{H}^1(\Omega)/\mathbb{R}$ and $\eta \in \mathcal{K}$; furthermore, $\|\nabla\psi\|_{0,\Omega} \leq C\|f\|_{0,\Omega}$ with C independent of f. Then, because of (2.3) and the $\mathrm{L}^2(\Omega)$-orthogonality of $\mathcal{K}$ and $\mathcal{G}$, we have

$$\int_\Omega \operatorname{div} u \operatorname{div} v \, dx = \int_\Omega f \cdot v \, dx = \int_\Omega \nabla\psi \cdot v \, dx \qquad \forall v \in \mathcal{G},$$

and consequently,

$$-\int_\Omega \nabla(\operatorname{div} u) \cdot v \, dx = \int_\Omega \nabla\psi \cdot v \, dx \qquad \forall v \in \mathcal{G}.$$

The above equality is valid for $v \in \mathcal{K}$ too. Hence, since $\mathcal{C}_0^\infty(\Omega) \subset \mathcal{G} \oplus \mathcal{K}$, there holds

$$\nabla(\operatorname{div} u + \psi) = 0 \quad \text{in } \Omega,$$

which together with (2.7) yield (2.11). On the other hand,

$$\int_\Omega [\nabla(\operatorname{div} u) + f] \cdot \nabla\xi \, dx = \int_\Omega \nabla(\operatorname{div} u + \psi) \cdot \nabla\xi \, dx + \int_\Omega \eta \cdot \nabla\xi \, dx = 0,$$

and we conclude the proof. □

It is simple to show that λ_n is a positive eigenvalue of (2.1) if and only if $\mu_n = 1/\lambda_n$ is a positive eigenvalue of the operator A; moreover, the corresponding associated eigenfunctions are related by $u_n = \overline{u}_n|_\Omega$. As a consequence of the previous lemma, the eigenfunctions u_n, $n \in \mathbb{N}$, satisfy $\operatorname{div} u_n \in \mathrm{H}^{1+r}(\Omega)$ and

$$\|\operatorname{div} u_n\|_{1+r,\Omega} \leq C \, \|u_n\|_{0,\Omega}, \tag{2.12}$$

with $r \in (1/2, 1]$ being the constant in (2.9).

To define the discrete analogue of the operator A, we are going to prove that the bilinear form $\int_{\Omega_h} \operatorname{div} u_h \operatorname{div} v_h \, dx$ is also $\mathcal{V}$-elliptic on $\mathcal{G}_h$. To this goal, we first recall the following two lemmas stated in [56]:

Lemma 2.3.2 *Given $T \in \mathcal{T}_h^\partial$, let ω_T be the domain bounded by σ_T and s_T (see Fig. 2.2). Then, there exists a constant $C > 0$, independent of T, such that*

$$|\omega_T| \leq C h_T^3.$$

Consequently,

$$\left|\Omega \setminus \bar{\Omega}_h\right| + \left|\Omega_h \setminus \bar{\Omega}\right| \leq C h^2.$$

Proof. The first estimate is a direct consequence of the assumed smoothness of $\partial\Omega$ and standard interpolation results (see for instance [49]). Since $(\Omega \setminus \bar{\Omega}_h) \cup (\Omega_h \setminus \bar{\Omega}) = \bigcup\{\omega_T : T \in \mathcal{T}_h^\partial\}$, we obtain the second estimate by adding $|\omega_T|$ for all $T \in \mathcal{T}_h^\partial$. □

Lemma 2.3.3 *There exists a positive constant C such that:*

$$\begin{aligned} \|v\|_{0,\Omega\setminus\bar{\Omega}_h} &\leq C h^s \|v\|_{s,\Omega} \qquad \forall v \in \mathrm{H}^s(\Omega) \qquad (0 \leq s \leq 1), \\ \|v\|_{0,\Omega_h\setminus\bar{\Omega}} &\leq C h^s \|v\|_{s,\Omega_h} \qquad \forall v \in \mathrm{H}^s(\Omega_h) \qquad (0 \leq s \leq 1). \end{aligned}$$

Proof. The two inequalities have been essentially proved in the proof of Lemma 5.2-3 in [76] for $s = 1$. Since the inequalities are clearly true for $s = 0$, they follow for $0 < s < 1$ from standard results on interpolation in Sobolev spaces (see, for instance, Theorem 1.4 in [52]). □

We also recall the definition and some properties of the Raviart-Thomas interpolant (see for example [75]). For $s > 1/2$, let

$$R : \mathrm{H}^s(\Omega_h)^2 \cap \mathrm{H}(\mathrm{div}, \Omega_h) \longrightarrow \mathcal{R}_h(\Omega_h),$$

where for each $v \in \mathrm{H}^s(\Omega_h)^2$, Rv is the unique vector field in $\mathcal{R}_h(\Omega_h)$ satisfying

$$\int_\ell Rv \cdot \nu_\ell \, ds = \int_\ell v \cdot \nu_\ell \, ds, \tag{2.13}$$

for every edge ℓ of $\mathcal{T}$ (ν_ℓ being a unit normal to ℓ). The operator R satisfies for all $T \in \mathcal{T}_h$

$$\int_T \mathrm{div}(v - Rv) \, dx = 0 \qquad \forall v \in \mathrm{H}^s(\Omega_h)^2 \cap \mathrm{H}(\mathrm{div}, \Omega_h). \tag{2.14}$$

Moreover, it is well known (see for example [75]) that for $v \in \mathrm{H}^s(\Omega_h)^2$ such that $\mathrm{div}\, v \in \mathrm{H}^s(\Omega_h)$

$$\|v - Rv\|_{0,\Omega_h} \leq C h^s \|v\|_{s,\Omega_h}, \tag{2.15}$$

$$\|\mathrm{div}(v - Rv)\|_{0,\Omega_h} \leq C h^s \|\mathrm{div}\, v\|_{s,\Omega_h}. \tag{2.16}$$

In what follows, we will use a Helmholtz decomposition of functions in $\mathcal{G}_h$ extended by zero outside Ω_h. Consider the following spaces defined in $\widetilde{\Omega}_h$:

$$\mathcal{K}(\widetilde{\Omega}_h) := \left\{ v \in \mathrm{H}_0(\mathrm{div}, \widetilde{\Omega}_h) : \ \mathrm{div}\, v = 0 \text{ in } \widetilde{\Omega}_h \right\},$$
$$\mathcal{G}(\widetilde{\Omega}_h) := \left\{ v \in \mathrm{H}_0(\mathrm{div}, \widetilde{\Omega}_h) : \ v = \nabla\varphi, \ \varphi \in \mathrm{H}^1(\widetilde{\Omega}_h) \right\}.$$

These two spaces are orthogonal in $\mathrm{H}(\mathrm{div}, \widetilde{\Omega}_h)$ and $\mathrm{L}^2(\widetilde{\Omega}_h)^2$. Notice that the inclusions $\mathcal{K} \hookrightarrow \mathcal{K}(\widetilde{\Omega}_h)$ and $\mathcal{K}_h \hookrightarrow \mathcal{K}(\widetilde{\Omega}_h)$ obtained by extending by zero the functions defined in Ω or Ω_h, respectively, are continuous.

Lemma 2.3.4 *For any $v_h \in \mathcal{G}_h$,*

$$\overline{v}_h = \nabla\xi + \chi \quad \text{in } \widetilde{\Omega}_h,$$

with $\nabla\xi \in \mathcal{G}(\widetilde{\Omega}_h)$ and $\chi \in \mathcal{K}(\widetilde{\Omega}_h)$. Moreover, there exist constants $C > 0$ and $r_h \in (1/2, 1]$, both independent of v_h, such that $\nabla\xi \in \mathrm{H}^{r_h}(\widetilde{\Omega}_h)$,

$$\|\nabla\xi\|_{r_h, \widetilde{\Omega}_h} \leq C \, \|\mathrm{div}\, v_h\|_{0,\Omega_h}, \tag{2.17}$$

and

$$\|\chi\|_{0,\widetilde{\Omega}_h} \leq C h^{r_h} \, \|\mathrm{div}\, v_h\|_{0,\Omega_h}. \tag{2.18}$$

Proof. Let $\xi \in \mathrm{H}^1(\widetilde{\Omega}_h)/\mathbb{R}$ be the solution of the compatible Neumann problem

$$\begin{cases} \Delta\xi = \mathrm{div}\, \overline{v}_h & \text{in } \widetilde{\Omega}_h, \\ \dfrac{\partial\xi}{\partial\widetilde{\nu}_h} = 0 & \text{on } \partial\widetilde{\Omega}_h. \end{cases}$$

Then, because of the a priori estimate for this problem (see [53]), $\nabla\xi \in \mathrm{H}^{r_h}(\widetilde{\Omega}_h)$ and (2.17) holds with $r_h \in (1/2, 1]$ (in fact, $r_h = 1$ if $\widetilde{\Omega}_h$ has no reentrant corner, and $r_h < \frac{\pi}{\theta_h}$, with θ_h being the largest interior angle of $\widetilde{\Omega}_h$, otherwise).

Let $\chi := \overline{v}_h - \nabla\xi$ in $\widetilde{\Omega}_h$. Then $\chi \in \mathcal{K}(\widetilde{\Omega}_h)$, since $\mathrm{div}\, \chi = 0$ in $\widetilde{\Omega}_h$ and $\chi \cdot \widetilde{\nu}_h = \overline{v}_h \cdot \widetilde{\nu}_h - \nabla\xi \cdot \widetilde{\nu}_h = 0$ on $\partial\widetilde{\Omega}_h$.

On the other hand, since $\overline{v}_h|_{\Omega\setminus\bar{\Omega}_h} = 0$, we have

$$\begin{aligned} \int_{\widetilde{\Omega}_h} |\chi|^2 \, dx &= \int_{\Omega_h} \chi \cdot (v_h - \nabla\xi) \, dx - \int_{\Omega\setminus\bar{\Omega}_h} \chi \cdot \nabla\xi \, dx \\ &= \int_{\Omega_h} \chi \cdot (v_h - R\nabla\xi) \, dx + \int_{\Omega_h} \chi \cdot (R\nabla\xi - \nabla\xi) \, dx \\ &\quad - \int_{\Omega\setminus\bar{\Omega}_h} \chi \cdot \nabla\xi \, dx. \end{aligned}$$

Thus, to prove the lemma, we estimate the three terms in the right hand side of this equality.

For the first one, we note that for $T \in \mathcal{T}_h^\partial$ such that $T \subset \widetilde{T}$ (see Fig. 2.2), we have

$$\int_{\sigma_T} \frac{\partial \xi}{\partial \nu}\, ds + \int_{s_T} \frac{\partial \xi}{\partial \nu_h}\, ds = \int_{\omega_T} \Delta \xi\, dx = \int_{\widetilde{T}\setminus T} \operatorname{div} \overline{v}_h\, dx = 0.$$

Hence,

$$\int_{s_T} \frac{\partial \xi}{\partial \nu_h}\, ds = -\int_{\sigma_T} \frac{\partial \xi}{\partial \nu}\, ds = -\int_{\sigma_T} \frac{\partial \xi}{\partial \widetilde{\nu}_h}\, ds = 0,$$

because $\partial\xi/\partial\widetilde{\nu}_h$ vanishes on the whole $\partial\widetilde{\Omega}_h \supset \sigma_T$. On the other hand, for $T \in \mathcal{T}_h^\partial$ such that $T \supset \widetilde{T}$, we directly have $\partial\xi/\partial\nu_h = \partial\xi/\partial\widetilde{\nu}_h = 0$ on $s_T \subset \partial\Omega_h$. Then, by the definition of R, $(R\nabla\xi)\cdot\nu_h$ vanishes on s_T for all $T \in \mathcal{T}_h^\partial$. Hence $(v_h - R\nabla\xi)\cdot\nu_h = 0$ on $\partial\Omega_h$. In addition we have $\operatorname{div} v_h|_T \in \mathcal{P}_0(T)$ and $\operatorname{div} \nabla\xi|_T = \operatorname{div} v_h|_T$. Then it follows that $\operatorname{div} \nabla\xi|_T \in \mathcal{P}_0(T)$ and, from (2.14),

$$\operatorname{div}(R\nabla\xi)|_T = \operatorname{div} \nabla\xi|_T = \operatorname{div} v_h|_T.$$

Hence $(v_h - R\nabla\xi) \in \mathcal{K}_h \hookrightarrow \mathcal{K}(\widetilde{\Omega}_h)$ and then, since $v_h \in \mathcal{G}_h$ and $\nabla\xi \in \mathcal{G}(\widetilde{\Omega}_h)$, we have

$$\begin{aligned}\int_{\Omega_h} \chi\cdot(v_h - R\nabla\xi)\, dx &= \int_{\Omega_h} v_h\cdot(v_h - R\nabla\xi)\, dx \\ &\quad - \int_{\widetilde{\Omega}_h} \nabla\xi\cdot\overline{(v_h - R\nabla\xi)}\, dx = 0.\end{aligned}$$

For the second term, we use (2.15) and (2.17) to obtain

$$\begin{aligned}\left|\int_{\Omega_h} \chi\cdot(R\nabla\xi - \nabla\xi)\, dx\right| &\le \|\chi\|_{0,\Omega_h} C h^{r_h} \|\nabla\xi\|_{r_h,\Omega_h} \\ &\le C h^{r_h} \|\chi\|_{0,\widetilde{\Omega}_h} \|\operatorname{div} v_h\|_{0,\Omega_h}.\end{aligned}$$

Finally, the last term is bounded by using Lemma 2.3.3 and (2.17) as follows,

$$\begin{aligned}\left|\int_{\Omega\setminus\bar{\Omega}_h} \chi\cdot\nabla\xi\, dx\right| &\le \|\chi\|_{0,\Omega\setminus\bar{\Omega}_h} C h^{r_h} \|\nabla\xi\|_{r_h,\widetilde{\Omega}_h} \\ &\le C h^{r_h} \|\chi\|_{0,\widetilde{\Omega}_h} \|\operatorname{div} v_h\|_{0,\Omega_h}. \ \square\end{aligned}$$

As an immediate consequence of the previous lemma, we have the following result:

Corollary 2.3.1 *There exists a positive constant C such that*

$$\int_{\Omega_h} (\operatorname{div} v_h)^2 \, dx \geq \alpha \|v_h\|^2_{\operatorname{div},\Omega_h} \qquad \forall v_h \in \mathcal{G}_h. \tag{2.19}$$

Proof. Let $v_h \in \mathcal{G}_h$. According to the previous lemma, we have $\overline{v}_h = \nabla\xi + \chi$ and

$$\|v_h\|_{0,\Omega_h} = \|\overline{v}_h\|_{0,\widetilde{\Omega}_h} \leq \|\nabla\xi\|_{0,\widetilde{\Omega}_h} + \|\chi\|_{0,\widetilde{\Omega}_h} \leq C(1+h^{r_h})\|\operatorname{div} v_h\|_{0,\Omega_h},$$

which allows us to conclude the proof. □

Now, we define the discrete analogue of the operator A as follows:

$$\begin{array}{rccl} A_h: & \mathrm{L}^2(\mathbb{R}^2)^2 & \longrightarrow & \mathrm{L}^2(\mathbb{R}^2)^2 \\ & f & \longmapsto & \overline{u}_h: \ \overline{u}_h|_{\Omega_h} = u_h, \end{array}$$

where $u_h \in \mathcal{G}_h$ is the solution of

$$\int_{\Omega_h} \operatorname{div} u_h \operatorname{div} v_h \, dx = \int_{\Omega_h} f \cdot v_h \, dx \qquad \forall v_h \in \mathcal{G}_h \tag{2.20}$$

(recall that $\overline{u}_h$ denotes the extension by zero of u_h to $\mathbb{R}^2$).

Problem (2.20) is well posed because of Corollary 2.3.1. Then, as a consequence of Lax Milgram Lemma, A_h is well defined and we have

$$\|u_h\|_{\operatorname{div},\Omega_h} \leq C\|f\|_{0,\mathbb{R}^2}. \tag{2.21}$$

As in the continuous case, it is simple to show that λ_{hn} is a positive eigenvalue of problem (2.2) if and only if $\mu_{hn} = 1/\lambda_{hn}$ is a positive eigenvalue of the operator A_h, and the corresponding associated eigenfunctions are related by $u_{hn} = \overline{u}_{hn}|_\Omega$. In the following section we study how the eigenvalues and eigenfunctions of A_h approximate those of A.

Remark 2.3.1 *Under the assumption that $\partial\Omega$ is piecewise smooth, the constant r_h in Lemma 2.3.4 satisfies $r_h \to r$ as h goes to zero, with $r \in (1/2, 1]$ being the constant of estimates (2.9) and (2.12). Therefore, if we denote $r'_h := \min\{r, r_h\}$, then r'_h is asymptotically equal to r. Because of this, we will use r'_h instead of r or r_h several times in the following section, just to simplify the notation.*

2.4 Spectral approximation

Our first step is to prove that the operators A_h converge to A in norm as h goes to zero.

From now on and throughout the rest of the chapter, let $f \in \mathrm{L}^2(\mathbb{R}^2)^2$ be a fixed function and let

$$\overline{u} = Af, \quad u = \overline{u}|_\Omega, \quad \overline{u}_h = A_h f, \quad u_h = \overline{u}_h|_{\Omega_h}.$$

Furthermore, C will denote a generic constant independent of the mesh-size as above, but also independent on the particular $f \in \mathrm{L}^2(\mathbb{R}^2)^2$.

We will use in the proofs smooth extensions of functions originally defined in Ω. For $\psi \in \mathrm{H}^s(\Omega)$ $(s > 0)$, let ψ^e denote an extension of ψ to $\mathbb{R}^2$ satisfying $\psi^e \in \mathrm{H}^s(\mathbb{R}^2)$ and

$$\|\psi^e\|_{s,\mathbb{R}^2} \leq C \, \|\psi\|_{s,\Omega} \tag{2.22}$$

(see, for instance, Theorem 1.4.3.1 in [53]). In particular, since according to estimate (2.11) $\operatorname{div} u \in \mathrm{H}^1(\Omega)$, $(\operatorname{div} u)^e$ denotes an extension of $\operatorname{div} u$ satisfying the estimate above for $s = 1$; namely,

$$\|(\operatorname{div} u)^e\|_{1,\mathbb{R}^2} \leq C \, \|\operatorname{div} u\|_{1,\Omega} \, . \tag{2.23}$$

In addition, we introduce a gradient field defined in $\widetilde{\Omega}_h$, closely related to u (as will be shown in Lemma 2.4.1 below). Let $\hat{\varphi} \in \mathrm{H}^1(\widetilde{\Omega}_h)$ be the solution of the following Neumann problem:

$$\begin{cases} \Delta\hat{\varphi} = (\operatorname{div} u)^e + \hat{c} & \text{in } \widetilde{\Omega}_h, \\ \dfrac{\partial\hat{\varphi}}{\partial n} = 0 & \text{on } \partial\widetilde{\Omega}_h, \\ \displaystyle\int_{\widetilde{\Omega}_h} \hat{\varphi} = 0, \end{cases} \tag{2.24}$$

where the constant $\hat{c}$ is taken for the problem to be compatible, i.e.,

$$\hat{c} := -\frac{1}{|\widetilde{\Omega}_h|} \int_{\widetilde{\Omega}_h} (\operatorname{div} u)^e \, dx = -\frac{1}{|\widetilde{\Omega}_h|} \int_{\Omega_h \setminus \bar{\Omega}} (\operatorname{div} u)^e \, dx. \tag{2.25}$$

Then, using Lemmas 2.3.2 and 2.3.3, and estimates (2.23) and (2.11), we have

$$|\hat{c}| \leq \frac{|\Omega_h \setminus \bar{\Omega}|^{1/2}}{|\widetilde{\Omega}_h|} \|(\operatorname{div} u)^e\|_{0,\Omega_h\setminus\bar{\Omega}} \leq Ch^2 \|(\operatorname{div} u)^e\|_{1,\Omega_h} \leq Ch^2 \|f\|_{0,\mathbb{R}^2}. \tag{2.26}$$

Because of the a priori estimate for the Neumann problem (see [53]), $\hat{\varphi} \in \mathrm{H}^{1+r_h}(\widetilde{\Omega}_h)$ and

$$\|\hat{\varphi}\|_{1+r_h,\widetilde{\Omega}_h} \leq C \, \|(\operatorname{div} u)^e + \hat{c}\|_{0,\widetilde{\Omega}_h} \leq C \, \|f\|_{0,\mathbb{R}^2} \, , \tag{2.27}$$

the latter because of (2.23), (2.11), and (2.26). Thus, we define $\hat{u} := \nabla\hat{\varphi}$. Then $\hat{u} \in \mathrm{H}^{r_h}(\widetilde{\Omega}_h)$ and

$$\|\hat{u}\|_{r_h,\widetilde{\Omega}_h} \leq C\|f\|_{0,\mathbb{R}^2}. \tag{2.28}$$

On the other hand, $\operatorname{div} \hat{u} = (\operatorname{div} u)^e + \hat{c} \in \mathrm{H}^1(\widetilde{\Omega}_h)$ and, because of (2.23), (2.11), and (2.26) again,

$$\|\operatorname{div} \hat{u}\|_{1,\widetilde{\Omega}_h} \leq C \|f\|_{0,\mathbb{R}^2}. \tag{2.29}$$

The following lemma shows that $\hat{u}$ is indeed an accurate approximation of u in $\Omega \cap \Omega_h$:

Lemma 2.4.1 *There exists a positive constant C such that*

$$\|u - \hat{u}\|_{\operatorname{div},\Omega\cap\Omega_h} \leq C h^{r+\mathfrak{r}'} \|f\|_{0,\mathbb{R}^2}.$$

Proof. Let $\varphi \in \mathrm{H}^1(\Omega)$ be the solution of the Neumann problem (2.4) for $v = u$, which satisfies $\int_\Omega \varphi = 0$. Then, according to (2.8) and (2.7), $\varphi \in \mathrm{H}^{1+r}(\Omega)$ and $\|\varphi\|_{1+r,\Omega} \leq C \|\operatorname{div} u\|_{0,\Omega} \leq C \|f\|_{0,\mathbb{R}^2}$.

Let φ^e denote an extension to $\mathbb{R}^2$ of $\varphi \in \mathrm{H}^{1+r}(\Omega)$ satisfying (2.22) with $s = 1+r$. Then

$$\|\varphi^e\|_{1+r,\mathbb{R}^2} \leq C \|\varphi\|_{1+r,\Omega} \leq C \|f\|_{0,\mathbb{R}^2}. \tag{2.30}$$

Recalling the weak formulation of problems (2.4) and (2.24), we have

$$\begin{aligned}
\|u - \hat{u}\|^2_{0,\Omega\cap\Omega_h} &= \int_{\Omega\cap\Omega_h} \nabla(\varphi - \hat{\varphi}) \cdot \nabla(\varphi - \hat{\varphi})\, dx \\
&\leq \int_{\widetilde{\Omega}_h} \nabla(\varphi^e - \hat{\varphi}) \cdot \nabla(\varphi^e - \hat{\varphi})\, dx \\
&\leq \int_\Omega \nabla\varphi \cdot \nabla(\varphi - \hat{\varphi})\, dx + \int_{\Omega_h\setminus\bar{\Omega}} \nabla\varphi^e \cdot \nabla(\varphi^e - \hat{\varphi})\, dx \\
&\quad - \int_{\widetilde{\Omega}_h} \nabla\hat{\varphi} \cdot \nabla(\varphi^e - \hat{\varphi})\, dx \\
&\leq -\int_\Omega \operatorname{div} u(\varphi - \hat{\varphi})\, dx + \int_{\widetilde{\Omega}_h} (\operatorname{div} u)^e(\varphi^e - \hat{\varphi})\, dx \\
&\quad + \int_{\widetilde{\Omega}_h} \hat{c}(\varphi^e - \hat{\varphi})\, dx + \int_{\Omega_h\setminus\bar{\Omega}} \nabla\varphi^e \cdot \nabla(\varphi^e - \hat{\varphi})\, dx \\
&= \int_{\Omega_h\setminus\bar{\Omega}} (\operatorname{div} u)^e(\varphi^e - \hat{\varphi})\, dx + \int_{\widetilde{\Omega}_h} \hat{c}(\varphi^e - \hat{\varphi})\, dx \\
&\quad + \int_{\Omega_h\setminus\bar{\Omega}} \nabla\varphi^e \cdot \nabla(\varphi^e - \hat{\varphi})\, dx.
\end{aligned}$$

Now, we estimate the three terms in the previous inequality. For the first one, we use Cauchy-Schwarz inequality, Lemma 2.3.3, (2.23), (2.11), (2.30), and (2.27)

to obtain

$$\begin{aligned}\left|\int_{\Omega_h\setminus\bar{\Omega}} (\operatorname{div} u)^e(\varphi^e-\hat{\varphi})\,dx\right| &\le Ch\,\|(\operatorname{div} u)^e\|_{1,\tilde{\Omega}_h}\,Ch\,\|\varphi^e-\hat{\varphi}\|_{1,\tilde{\Omega}_h}\\ &\le Ch^2\,\|\operatorname{div} u\|_{1,\Omega}\left(\|\varphi^e\|_{1,\Omega}+\|\hat{\varphi}\|_{1,\tilde{\Omega}_h}\right)\\ &\le Ch^2\|f\|^2_{0,\mathbb{R}^2}.\end{aligned}$$

For the second one, we use (2.26), (2.30), and (2.27), to obtain

$$\left|\int_{\tilde{\Omega}_h}\hat{c}(\varphi^e-\hat{\varphi})\,dx\right| \le Ch^2\|f\|_{0,\mathbb{R}^2}\left(\|\varphi\|_{1,\Omega}+\|\hat{\varphi}\|_{1,\tilde{\Omega}_h}\right)\le Ch^2\|f\|^2_{0,\mathbb{R}^2}.$$

For the last term we use Cauchy-Schwarz inequality, Lemma 2.3.3, (2.30) and (2.27) to obtain

$$\begin{aligned}&\left|\int_{\Omega_h\setminus\bar{\Omega}}\nabla\varphi^e\cdot\nabla(\varphi^e-\hat{\varphi})\,dx\right|\\ &\qquad\le Ch^r\,\|\nabla\varphi^e\|_{r,\tilde{\Omega}_h}\,Ch^{r'_h}\,\|\nabla(\varphi^e-\hat{\varphi})\|_{r'_h,\tilde{\Omega}_h}\\ &\qquad\le Ch^{r+r'_h}\,\|f\|_{0,\mathbb{R}^2}\,(\|\varphi\|_{1+r,\Omega}+\|\hat{\varphi}\|_{1+r_h,\mathbb{R}^2})\\ &\qquad\le Ch^{r+r'_h}\,\|f\|^2_{0,\mathbb{R}^2}\,.\end{aligned}$$

Finally, we note that $\operatorname{div}(u-\hat{u})|_{\Omega\cap\Omega_h}=\hat{c}$. Then, using (2.26) and combining the above three inequalities, we have

$$\|u-\hat{u}\|^2_{\operatorname{div},\Omega\cap\Omega_h}=\|u-\hat{u}\|^2_{0,\Omega\cap\Omega_h}+\hat{c}^2\,|\Omega\cap\Omega_h|\le Ch^{r+r'_h}\|f\|^2_{0,\mathbb{R}^2},$$

which allows us to conclude the proof. □

We have now the tools to prove the convergence in norm of A_h to A. As a first step, the following lemma splits a bound of $\|(A-A_h)f\|_{1,\mathbb{R}^2}=\|\,\overline{u}-\overline{u}_h\|_{1,\mathbb{R}^2}$ into several terms which can be dealt with separately:

Lemma 2.4.2 *There exists a positive constant C such that*

$$\begin{aligned}\|\overline{u}-\overline{u}_h\|_{\operatorname{div},\mathbb{R}^2} \le C\Bigg[&\|u-\hat{u}\|_{\operatorname{div},\Omega\cap\Omega_h}+\inf_{v_h\in\mathcal{G}_h}\|\hat{u}-v_h\|_{\operatorname{div},\Omega_h}\\ &+\sup_{w_h\in\mathcal{G}_h}\frac{\left|\int_{\Omega_h}\operatorname{div}(\hat{u}-u_h)\operatorname{div} w_h\,dx\right|}{\|w_h\|_{\operatorname{div},\Omega_h}}\\ &+\|u\|_{\operatorname{div},\Omega\setminus\bar{\Omega}_h}+\|\hat{u}\|_{\operatorname{div},\Omega_h\setminus\bar{\Omega}}\Bigg].\end{aligned}$$

Proof. For all $v_h \in \mathcal{G}_h$

$$\begin{aligned}\|\overline{u}-\overline{u}_h\|^2_{\mathrm{div},\mathbb{R}^2} &= \|u-u_h\|^2_{\mathrm{div},\Omega\cap\Omega_h}+\|u\|^2_{\mathrm{div},\Omega\setminus\bar{\Omega}_h}+\|u_h\|^2_{\mathrm{div},\Omega_h\setminus\bar{\Omega}}\\ &\le 2\left(\|u-v_h\|^2_{\mathrm{div},\Omega\cap\Omega_h}+\|v_h-u_h\|^2_{\mathrm{div},\Omega\cap\Omega_h}\right)\\ &\quad +\|u\|^2_{\mathrm{div},\Omega\setminus\bar{\Omega}_h}+\|u_h\|^2_{\mathrm{div},\Omega_h\setminus\bar{\Omega}}.\end{aligned}$$

Then, using that $\|u_h\|_{\mathrm{div},\Omega_h\setminus\bar{\Omega}} \le \|v_h-u_h\|_{\mathrm{div},\Omega_h\setminus\bar{\Omega}}+\|v_h\|_{\mathrm{div},\Omega_h\setminus\bar{\Omega}}$, we have

$$\begin{aligned}\|\overline{u}-\overline{u}_h\|_{\mathrm{div},\mathbb{R}^2} &\le C\left(\|u-v_h\|_{\mathrm{div},\Omega\cap\Omega_h}+\|v_h-u_h\|_{\mathrm{div},\Omega_h}\right.\\ &\quad \left.+\|u\|_{\mathrm{div},\Omega\setminus\bar{\Omega}_h}+\|v_h\|_{\mathrm{div},\Omega_h\setminus\bar{\Omega}}\right).\end{aligned}$$

Because of the ellipticity estimate (2.19), we have

$$\begin{aligned}\alpha\|v_h-u_h\|^2_{\mathrm{div},\Omega_h} &\le \int_{\Omega_h}\mathrm{div}(v_h-\hat{u})\,\mathrm{div}(v_h-u_h)\,dx\\ &\quad +\int_{\Omega_h}\mathrm{div}(\hat{u}-u_h)\,\mathrm{div}(v_h-u_h)\,dx\\ &\le \|v_h-\hat{u}\|_{\mathrm{div},\Omega_h}\|v_h-u_h\|_{\mathrm{div},\Omega_h}\\ &\quad +\int_{\Omega_h}\mathrm{div}(\hat{u}-u_h)\,\mathrm{div}(v_h-u_h)\,dx,\end{aligned}$$

then

$$\begin{aligned}\|v_h-u_h\|_{\mathrm{div},\Omega_h} &\le \frac{1}{\alpha}\left(\|v_h-\hat{u}\|_{\mathrm{div},\Omega_h}\right.\\ &\quad \left.+\sup_{w_h\in\mathcal{G}_h}\frac{\left|\int_{\Omega_h}\mathrm{div}(\hat{u}-u_h)\,\mathrm{div}\,w_h\,dx\right|}{\|w_h\|_{\mathrm{div},\Omega_h}}\right).\end{aligned}$$

We conclude the proof by combining the above inequalities and the relations

$$\|u-v_h\|_{\mathrm{div},\Omega\cap\Omega_h} \le \|u-\hat{u}\|_{\mathrm{div},\Omega\cap\Omega_h}+\|\hat{u}-v_h\|_{\mathrm{div},\Omega\cap\Omega_h}$$

and

$$\|v_h\|_{\mathrm{div},\Omega_h\setminus\bar{\Omega}} \le \|\hat{u}-v_h\|_{\mathrm{div},\Omega_h}+\|\hat{u}\|_{\mathrm{div},\Omega_h\setminus\bar{\Omega}}.\ \square$$

The first term in the right hand side of the inequality in the previous lemma is directly bounded by Lemma 2.4.1. In what follows we give estimates for the remaining four terms. We begin with the density term in the following lemma:

Lemma 2.4.3 *There exists a positive constant C such that*

$$\inf_{v_h \in \mathcal{G}_h} \|\hat{u} - v_h\|_{\mathrm{div},\Omega_h} \leq C h^{r'_h} \|f\|_{0,\mathbb{R}^2}.$$

Proof. Let $R\hat{u} \in \mathcal{R}_h(\Omega_h)$ be the Raviart-Thomas interpolant of $\hat{u}|_{\Omega_h}$, with its degrees of freedom defined by (2.13). Since $\hat{u} \in \mathrm{H}^{r'_h}(\widetilde{\Omega}_h)$, then $R\hat{u}$ is well defined. However, in general, $R\hat{u} \notin \mathcal{V}_h$ because $\hat{u} \cdot \nu_h$ does not necessarily vanish on the edges s_T corresponding to those boundary triangles $T \in \mathcal{T}_h^{\partial}$ with $T \subset \widetilde{T}$ (see Fig. 2.2).

Then, to define an "interpolant" $\widetilde{R}\hat{u} \in \mathcal{V}_h$, we modify the degrees of freedom of $R\hat{u}$ by explicitly imposing $\widetilde{R}\hat{u} \cdot \nu_h = 0$ on these edges. Namely, let $\widetilde{R}\hat{u}$ be the unique vector field in $\mathcal{R}_h(\Omega_h)$ satisfying

$$\widetilde{R}\hat{u} \cdot \nu_\ell|_\ell = \begin{cases} 0, & \text{if } \ell = s_t \ \text{ for } T \in \mathcal{T}_h^{\partial} : \ T \subset \widetilde{T}, \\ R\hat{u} \cdot \nu_\ell|_\ell, & \text{otherwise,} \end{cases}$$

where ν_ℓ denotes a unit normal to ℓ. Then, $\widetilde{R}\hat{u} \in \mathcal{V}_h$.

In what follows, we bound the difference between this modified Raviart-Thomas interpolant and the standard one:

$$\|\widetilde{R}\hat{u} - R\hat{u}\|^2_{\mathrm{div},\Omega_h} = \sum_{T \in \mathcal{T}_h} \|\widetilde{R}\hat{u} - R\hat{u}\|^2_{\mathrm{div},T} = \sum_{T \in \mathcal{T}_h^{\partial}:\ T \subset \widetilde{T}} \|\widetilde{R}\hat{u} - R\hat{u}\|^2_{\mathrm{div},T}.$$

Let $T \in \mathcal{T}_h^{\partial}$ such that $T \subset \widetilde{T}$; by definition we have

$$(\widetilde{R}\hat{u} - R\hat{u})|_T = \left(\frac{1}{|s_T|} \int_{s_T} \hat{u} \cdot \nu_h \, ds \right) \phi_{s_T},$$

where ϕ_{s_T} is the standard basis function of $\mathcal{RT}_0(T)$ associated to the edge s_T. Hence, straightforward computations yield

$$\|\widetilde{R}\hat{u} - R\hat{u}\|_{\mathrm{div},T} = \left| \frac{1}{|s_T|} \int_{s_T} \hat{u} \cdot \nu_h \, ds \right| \|\phi_{s_T}\|_{\mathrm{div},T} \leq \frac{C}{|s_T|} \left| \int_{s_T} \hat{u} \cdot \nu_h \, ds \right|.$$

On the other hand, since $\int_{\sigma_T} \hat{u} \cdot \nu \, ds = 0$, by using Lemma 2.3.2 we have

$$\int_{s_T} \hat{u} \cdot \nu_h \, ds = \int_{\omega_T} \mathrm{div}\, \hat{u} \, dx \leq |\omega_T|^{1/2} \, \|\mathrm{div}\, \hat{u}\|_{0,\omega_T} \leq C h_T^{3/2} \, \|\mathrm{div}\, \hat{u}\|_{0,\omega_T},$$

and since $|s_T| \geq C h_T$,

$$\|\widetilde{R}\hat{u} - R\hat{u}\|_{\mathrm{div},T} \leq C h_T^{1/2} \, \|\mathrm{div}\, \hat{u}\|_{0,\widetilde{T}\setminus T}.$$

Hence,

$$\|\widetilde{R}\hat{u} - R\hat{u}\|^2_{\mathrm{div},\Omega_h} \leq \sum_{T\in\mathcal{T}_h^\partial:\ T\subset\widetilde{T}} Ch_T \|\mathrm{div}\,\hat{u}\|^2_{0,\widetilde{T}\setminus T} \leq Ch \|\mathrm{div}\,\hat{u}\|^2_{0,\Omega\setminus\bar{\Omega}_h}.$$

Then, because of (2.29), Lemma 2.3.3 yields

$$\|\widetilde{R}\hat{u} - R\hat{u}\|_{\mathrm{div},\Omega_h} \leq Ch^{3/2} \|\mathrm{div}\,\hat{u}\|_{1,\widetilde{\Omega}_h} \leq Ch^{3/2} \|f\|_{0,\mathbb{R}^2}.$$

Hence, we use (2.15), (2.16), (2.28), and (2.29), to obtain

$$\begin{aligned}
\|\hat{u} - \widetilde{R}\hat{u}\|_{\mathrm{div},\Omega_h} &\leq \|\hat{u} - R\hat{u}\|_{\mathrm{div},\Omega_h} + \|R\hat{u} - \widetilde{R}\hat{u}\|_{\mathrm{div},\Omega_h} \\
&\leq Ch^{r'_h}\left(\|\hat{u}\|_{r'_h,\widetilde{\Omega}_h} + \|\mathrm{div}\,\hat{u}\|_{r'_h,\widetilde{\Omega}_h}\right) + Ch^{3/2}\|f\|_{0,\mathbb{R}^2} \\
&\leq Ch^{r'_h}\|f\|_{0,\mathbb{R}^2}.
\end{aligned}$$

Now, let $P : \mathcal{V}_h \longrightarrow \mathcal{K}_h$ be the $\mathrm{H}(\mathrm{div},\Omega_h)$-orthogonal projection and let $v_h := \widetilde{R}\hat{u} - P(\widetilde{R}\hat{u}) \in \mathcal{G}_h$. Then v_h and $P(\widetilde{R}\hat{u}) \in \mathcal{K}_h$ are $\mathrm{H}(\mathrm{div},\Omega_h)$-orthogonal. On the other hand, since $\hat{u} \in \mathcal{G}(\widetilde{\Omega}_h)$, then $\hat{u}|_{\Omega_h}$ and $P(\widetilde{R}\hat{u})$ are also $\mathrm{H}(\mathrm{div},\Omega_h)$-orthogonal. Hence

$$\begin{aligned}
\|\hat{u} - v_h\|^2_{\mathrm{div},\Omega_h} &\leq \|(\hat{u} - v_h)\|^2_{\mathrm{div},\Omega_h} + \|P(\widetilde{R}\hat{u})\|^2_{\mathrm{div},\Omega_h} \\
&= \|(\hat{u} - v_h) - P(\widetilde{R}\hat{u})\|^2_{\mathrm{div},\Omega_h} \\
&= \|\hat{u} - \widetilde{R}\hat{u}\|^2_{\mathrm{div},\Omega_h}.
\end{aligned}$$

Therefore, we conclude the proof by combining the two previous inequalities. □

Now we deal with the consistency term in Lemma 2.4.2:

Lemma 2.4.4 *There exists a positive constant C such that*

$$\int_{\Omega_h} \mathrm{div}(\hat{u} - u_h)\,\mathrm{div}\,w_h\,dx \leq Ch^{r'_h}\|f\|_{0,\mathbb{R}^2}\|w_h\|_{\mathrm{div},\Omega_h} \qquad \forall w_h \in \mathcal{G}_h.$$

Proof. Let $w_h \in \mathcal{G}_h$. Consider the Helmholtz decomposition $\overline{w}_h = \nabla\xi + \chi$ with $\nabla\xi \in \mathcal{G}(\widetilde{\Omega}_h)$ and $\chi \in \mathcal{K}(\widetilde{\Omega}_h)$ as in Lemma 2.3.4. Then, using (2.20) and (2.24), and integrating by parts, we have

$$\begin{aligned}
&\int_{\Omega_h} \mathrm{div}(\hat{u} - u_h)\,\mathrm{div}\,w_h\,dx \\
&\quad= \int_{\widetilde{\Omega}_h} \mathrm{div}\,\hat{u}\,\mathrm{div}\,\overline{w}_h\,dx - \int_{\Omega_h} \mathrm{div}\,u_h\,\mathrm{div}\,w_h\,dx \\
&\quad= \int_{\widetilde{\Omega}_h} \mathrm{div}\,\hat{u}\,\mathrm{div}(\nabla\xi)\,dx - \int_{\Omega_h} f\cdot w_h\,dx \\
&\quad= \int_{\widetilde{\Omega}_h} [(\mathrm{div}\,u)^e + \hat{c}]\,\mathrm{div}(\nabla\xi)\,dx - \int_{\Omega_h} f\cdot\nabla\xi\,dx - \int_{\Omega_h} f\cdot\chi\,dx \\
&\quad= -\int_{\widetilde{\Omega}_h} \nabla\,[(\mathrm{div}\,u)^e]\cdot\nabla\xi\,dx - \int_{\Omega_h} f\cdot\nabla\xi\,dx - \int_{\Omega_h} f\cdot\chi\,dx.
\end{aligned}$$

Hence, using (2.10) we obtain

$$\begin{aligned}\int_{\Omega_h} \operatorname{div}(\hat{u}-u_h)\operatorname{div} w_h\,dx &= -\int_{\Omega_h\setminus\bar{\Omega}} \nabla(\operatorname{div} u)^e\cdot\nabla\xi\,dx \\ &\quad +\int_{\Omega\setminus\bar{\Omega}_h} f\cdot\nabla\xi\,dx \\ &\quad -\int_{\Omega_h\setminus\bar{\Omega}} f\cdot\nabla\xi\,dx-\int_{\Omega_h} f\cdot\chi\,dx.\end{aligned} \tag{2.31}$$

In what follows, we estimate the four terms in the right side above. For the first one we use Lemma 2.3.3, (2.23), (2.11), and (2.17) to obtain

$$\begin{aligned}\left|\int_{\Omega_h\setminus\bar{\Omega}} \nabla(\operatorname{div} u)^e\cdot\nabla\xi\,dx\right| &\le \|(\operatorname{div} u)^e\|_{1,\Omega_h\setminus\bar{\Omega}} Ch^{r'_h}\|\nabla\xi\|_{r'_h,\widetilde{\Omega}_h} \\ &\le Ch^{r'_h}\,\|\operatorname{div} u\|_{1,\Omega}\,\|\operatorname{div} w_h\|_{0,\Omega_h} \\ &\le Ch^{r'_h}\|f\|_{0,\mathbb{R}^2}\|w_h\|_{\operatorname{div},\Omega_h}.\end{aligned}$$

Analogously, for the next two terms, by using Lemma 2.3.3 and (2.17) we have

$$\left|\int_{\Omega\setminus\bar{\Omega}_h} f\cdot\nabla\xi\,dx\right|+\left|\int_{\Omega_h\setminus\bar{\Omega}} f\cdot\nabla\xi\,dx\right| \le Ch^{r'_h}\|f\|_{0,\mathbb{R}^2}\|w_h\|_{\operatorname{div},\Omega_h}.$$

For the last term, we use Cauchy-Schwarz inequality and (2.18) to obtain

$$\left|\int_{\Omega_h} f\cdot\chi\,dx\right| \le \|f\|_{0,\Omega_h}\|\chi\|_{0,\Omega_h} \le Ch^{r'_h}\|f\|_{0,\mathbb{R}^2}\|w_h\|_{\operatorname{div},\Omega_h}.$$

Thus, we conclude the proof. □

It only remains to estimate the last two terms in Lemma 2.4.2. We do it in the following two lemmas:

Lemma 2.4.5 *There exists a positive constant C such that*

$$\|u\|_{\operatorname{div},\Omega\setminus\bar{\Omega}_h} \le Ch^r\|f\|_{0,\mathbb{R}^2}.$$

Proof. Because $u\in \mathrm{H}^r(\Omega)^2$ and $\operatorname{div} u\in \mathrm{H}^1(\Omega)$, we use Lemma 2.3.3 and estimates (2.9) and (2.11) to obtain:

$$\begin{aligned}&\|u\|_{0,\Omega\setminus\bar{\Omega}_h} \le Ch^r\|u\|_{r,\Omega} \le Ch^r\|f\|_{0,\mathbb{R}^2},\\ &\|\operatorname{div} u\|_{0,\Omega\setminus\bar{\Omega}_h} \le Ch\|\operatorname{div} u\|_{1,\Omega} \le Ch\|f\|_{0,\mathbb{R}^2}.\ \square\end{aligned}$$

Lemma 2.4.6 *There exists a positive constant C such that*

$$\|\hat{u}\|_{\mathrm{div},\Omega_h\setminus\bar{\Omega}} \leq Ch^{r'_h}\|f\|_{0,\mathbb{R}^2}.$$

Proof. Because $\hat{u}\in \widetilde{H}^{r'_h}(\widetilde{\Omega}_h)^2$, we use Lemma 2.3.3 and (2.28) to obtain

$$\|\hat{u}\|_{0,\Omega_h\setminus\bar{\Omega}} \leq Ch^{r'_h}\|\hat{u}\|_{r'_h,\widetilde{\Omega}_h} \leq Ch^{r'_h}\|f\|_{0,\mathbb{R}^2}.$$

On the other hand, because of (2.24), $\|\operatorname{div}\hat{u}\|_{0,\Omega_h\setminus\bar{\Omega}} = \|(\operatorname{div}u)^e+\hat{c}\|_{0,\Omega_h\setminus\bar{\Omega}}$. Then, we use Lemma 2.3.3, (2.26), Lemma 2.3.2, (2.23), and (2.11) to obtain

$$\begin{aligned}\|\operatorname{div}\hat{u}\|_{0,\Omega_h\setminus\bar{\Omega}} &\leq \|(\operatorname{div}u)^e\|_{0,\Omega_h\setminus\bar{\Omega}} + |\hat{c}|\left|\Omega_h\setminus\bar{\Omega}\right|^{1/2}\\ &\leq Ch\,\|(\operatorname{div}u)^e\|_{1,\widetilde{\Omega}_h} + Ch^3\,\|f\|_{0,\mathbb{R}^2}\\ &\leq Ch\,\|f\|_{0,\mathbb{R}^2}\,.\ \square\end{aligned}$$

Now we may conclude the convergence in norm of A_h to A:

Lemma 2.4.7 *There exists a positive constant C such that*

$$\|(A-A_h)f\|_{\mathrm{div},\mathbb{R}^2} \leq Ch^{r'_h}\|f\|_{0,\mathbb{R}^2} \qquad \forall f\in \mathrm{L}^2(\mathbb{R}^2)^2.$$

Proof. It is an immediate consequence of the previous six lemmas. $\square$

By virtue of the previous lemma, we are able to apply the spectral approximation theory for compact operators (see [7]) to obtain error estimates for the eigenfunctions.

Let $\mu>0$ be a fixed eigenvalue of A with algebraic multiplicity m. Let $\mathcal{E}$ be the corresponding associated eigenspace. Since Lemma 2.4.7 implies that $\|A-A_h\|_{\mathrm{H}(\mathrm{div},\mathbb{R}^2)}\to 0$ as $h\to 0$, then there exist exactly m eigenvalues of A_h, $\mu_h^{(1)},\ldots,\mu_h^{(m)}$ (repeated accordingly to their respective multiplicities) converging to μ (see [61]). Let $\mathcal{E}_h$ be the direct sum of the corresponding associated eigenspaces.

We recall the definition of the gap $\widehat{\delta}$ between two closed subspaces, $\mathcal{Y}$ and $\mathcal{Z}$, of $\mathrm{H}(\mathrm{div},\mathbb{R}^2)$:

$$\widehat{\delta}(\mathcal{Y},\mathcal{Z}) := \max\left\{\delta(\mathcal{Y},\mathcal{Z}),\delta(\mathcal{Z},\mathcal{Y})\right\},$$

with

$$\delta(\mathcal{Y},\mathcal{Z}) := \sup_{\substack{v\in\mathcal{Y}\\ \|v\|_{\mathrm{div},\mathbb{R}^2}=1}}\left(\inf_{w\in\mathcal{Z}}\|v-w\|_{\mathrm{div},\mathbb{R}^2}\right).$$

Then, the following error estimate holds:

Theorem 2.4.1 *There exist a positive constant C such that*

$$\widehat{\delta}\,(\mathcal{E}_h, \mathcal{E}) \leq C h^{r'_h},$$

with r'_h as defined in Remark 2.3.1.

Proof. It is an immediate consequence of Theorem 7.1 in [7] and Lemma 2.4.7. □

In order to prove a double-order error estimate for the approximate eigenvalues, we will use the following lemma:

Lemma 2.4.8 *There exist a positive constant C such that*

$$\left| \int_{\widetilde{\Omega}_h} (A - A_h) f \cdot g \, dx \right| \leq C h^{2r'_h} \, \|f\|_{0,\mathbb{R}^2} \, \|g\|_{0,\mathbb{R}^2} \qquad \forall f, g \in \mathcal{E}.$$

Proof. Let $f, g \in \mathcal{E}$. We denote

$$\begin{array}{llll} \overline{u} = Af, & u = \overline{u}|_\Omega, & \overline{u}_h = A_h f, & u_h = \overline{u}_h|_{\Omega_h}, \\ \overline{v} = Ag, & v = \overline{v}|_\Omega, & \overline{v}_h = A_h g, & v_h = \overline{v}_h|_{\Omega_h}. \end{array}$$

We have

$$\begin{aligned} \int_{\widetilde{\Omega}_h} (A - A_h) f \cdot g \, dx &= \int_{\widetilde{\Omega}_h} (\overline{u} - \overline{u}_h) \cdot g \, dx \\ &= \int_\Omega \operatorname{div} u \operatorname{div} v \, dx - \int_{\Omega_h} \operatorname{div} u_h \operatorname{div} v_h \, dx \\ &= \int_\Omega \operatorname{div}(u - \overline{u}_h) \operatorname{div}(v - \overline{v}_h) \, dx + \int_{\Omega \cap \Omega_h} \operatorname{div}(u - u_h) \operatorname{div} v_h \, dx \\ &\quad + \int_{\Omega \cap \Omega_h} \operatorname{div} u_h \operatorname{div}(v - v_h) \, dx - \int_{\Omega_h \setminus \bar{\Omega}} \operatorname{div} u_h \operatorname{div} v_h \, dx. \end{aligned} \tag{2.32}$$

In what follows we estimate the terms in the right side of the above equation. Because of Cauchy-Schwarz inequality and Lemma 2.4.7, we have

$$\int_\Omega \operatorname{div}(u - \overline{u}_h) \operatorname{div}(v - \overline{v}_h) \, dx \leq C h^{2r'_h} \, \|f\|_{0,\mathbb{R}^2} \, \|g\|_{0,\mathbb{R}^2}.$$

The next two terms are similar (changing the role of the functions u, u_h, and v_h, by v, v_h, and u_h, respectively). Then we write down the estimate only for the first one.

Since $\overline{u} = Af \in \mathcal{E}$, because of (2.12), $\operatorname{div} u \in \mathrm{H}^{1+r}(\Omega)$. Then, there is an extension $(\operatorname{div} u)^e \in \mathrm{H}^{1+r}(\mathbb{R}^2)$ satisfying (2.22) for $s = 1 + r$; namely,

$$\|(\operatorname{div} u)^e\|_{1+r,\mathbb{R}^2} \leq C \, \|\operatorname{div} u\|_{1+r,\Omega} \leq C \, \|f\|_{0,\mathbb{R}^2}. \tag{2.33}$$

Let $\hat{u} = \nabla\hat{\varphi} \in \mathcal{G}(\widetilde{\Omega}_h)$. with $\hat{\varphi}$ being the solution of (2.24)–(2.25). Then we have

$$\begin{aligned}
&\int_{\Omega\cap\Omega_h} \operatorname{div}(u-u_h)\operatorname{div} v_h\ dx \\
&\quad= \int_{\Omega_h} [(\operatorname{div} u)^e - \operatorname{div} u_h]\operatorname{div} v_h\ dx - \int_{\Omega_h\setminus\bar{\Omega}} (\operatorname{div} u)^e \operatorname{div} v_h\ dx \\
&\qquad+ \int_{\Omega_h\setminus\bar{\Omega}} \operatorname{div} u_h \operatorname{div} v_h\ dx \\
&\quad= \int_{\Omega_h} [(\operatorname{div} u)^e - \operatorname{div}\hat{u}]\operatorname{div} v_h\ dx + \int_{\Omega_h} (\operatorname{div}\hat{u} - \operatorname{div} u_h)\operatorname{div} v_h\ dx \\
&\qquad- \int_{\Omega_h\setminus\bar{\Omega}} (\operatorname{div} u)^e \operatorname{div} v_h\ dx + \int_{\Omega_h\setminus\bar{\Omega}} \operatorname{div} u_h \operatorname{div} v_h\ dx \\
&\quad= \hat{c}\int_{\Omega_h} \operatorname{div} v_h\ dx + \int_{\Omega_h} \operatorname{div}(\hat{u}-u_h)\operatorname{div} v_h\ dx \\
&\qquad- \int_{\Omega_h\setminus\bar{\Omega}} (\operatorname{div} u)^e \operatorname{div} v_h\ dx + \int_{\Omega_h\setminus\bar{\Omega}} \operatorname{div} u_h \operatorname{div} v_h\ dx
\end{aligned}$$

Now, let $\overline{v}_h = \nabla\xi + \chi$ as in Lemma 2.3.4. The second term in the right hand side of this equation can be dealt with by repeating the argument in the proof of Lemma 2.4.4 (see (2.31)). Then we obtain

$$\begin{aligned}
&\int_{\Omega\cap\Omega_h} \operatorname{div}(u-u_h)\operatorname{div} v_h\ dx \\
&\qquad= \hat{c}\int_{\Omega_h} \operatorname{div} v_h\ dx - \int_{\Omega_h\setminus\bar{\Omega}} \nabla(\operatorname{div} u)^e\cdot\nabla\xi\ dx \\
&\qquad\quad+ \int_{\Omega\setminus\bar{\Omega}_h} f\cdot\nabla\xi\ dx - \int_{\Omega\cap\Omega_h} f\cdot\chi\ dx \\
&\qquad\quad- \int_{\Omega_h\setminus\bar{\Omega}} (\operatorname{div} u)^e \operatorname{div} v_h\ dx + \int_{\Omega_h\setminus\bar{\Omega}} \operatorname{div} u_h \operatorname{div} v_h\ dx,
\end{aligned}$$

where we have used that $f|_{\Omega_h\setminus\bar{\Omega}} = 0$. Notice that the last integral also appears in (2.32). Thus, to conclude the lemma, it is enough to estimate each term in the right hand side of the above equation.

Because of (2.26) and (2.21), we have

$$\left|\hat{c}\int_{\Omega_h} \operatorname{div} v_h\ dx\right| \le Ch^2 \|f\|_{0,\mathbb{R}^2} \|v_h\|_{\operatorname{div},\Omega_h} \le Ch^2 \|f\|_{0,\mathbb{R}^2} \|g\|_{0,\mathbb{R}^2}\,.$$

For the second term we use Lemma 2.3.3, (2.33), (2.17), and (2.21) to obtain

$$\begin{aligned}
\left|\int_{\Omega_h\setminus\bar{\Omega}} \nabla(\operatorname{div} u)^e\cdot\nabla\xi\ dx\right| &\le Ch^r \|(\operatorname{div} u)^e\|_{1+r,\widetilde{\Omega}_h} Ch'^{r'_h} \|\nabla\xi\|_{r'_h,\widetilde{\Omega}_h} \\
&\le Ch^{r+r'_h} \|f\|_{0,\mathbb{R}^2} \|g\|_{0,\mathbb{R}^2}\,.
\end{aligned}$$

To estimate the third and forth terms, we use that $\overline{u} = Af = \mu f$ because $f \in \mathcal{E}$. Then $f = \frac{1}{\mu}u$ in Ω. Hence, by using Lemma 2.3.3, (2.9), (2.17), and (2.21) we have

$$\begin{aligned}\left|\int_{\Omega\setminus\bar{\Omega}_h} f\cdot\nabla\xi\,dx\right| &\leq \frac{Ch^r}{\mu}\|u\|_{r,\Omega}\,Ch^{\hbar'}\|\nabla\xi\|_{r'_h,\widetilde{\Omega}_h}\\ &\leq Ch^{r+\hbar'}\|f\|_{0,\mathbb{R}^2}\|g\|_{0,\mathbb{R}^2}.\end{aligned}$$

Regarding the forth term we have

$$\begin{aligned}\int_{\Omega\cap\Omega_h} f\cdot\chi\,dx &= \frac{1}{\mu}\left[\int_{\Omega\cap\Omega_h}(u-\hat{u})\cdot\chi\,dx+\int_{\Omega\cap\Omega_h}\hat{u}\cdot\chi\,dx\right]\\ &= \frac{1}{\mu}\left[\int_{\Omega\cap\Omega_h}(u-\hat{u})\cdot\chi\,dx-\int_{\Omega\setminus\bar{\Omega}_h}\hat{u}\cdot\chi\,dx-\int_{\Omega_h\setminus\bar{\Omega}}\hat{u}\cdot\chi\,dx\right],\end{aligned}$$

the latter because $\int_{\widetilde{\Omega}_h} u\cdot\chi = 0$, from the orthogonality of $\mathcal{G}(\widetilde{\Omega}_h)$ and $\mathcal{K}(\widetilde{\Omega}_h)$. Then, by using Cauchy-Schwarz inequality, Lemmas 2.4.1 and 2.3.3, (2.18), (2.21), and (2.28) we obtain

$$\begin{aligned}\left|\int_{\Omega\cap\Omega_h} f\cdot\chi\,dx\right| &\leq Ch^{2r'_h}\|f\|_{0,\mathbb{R}^2}\,Ch^{r'_h}\|v_h\|_{\mathrm{div},\Omega_h}\\ &\quad +2Ch^{r'_h}\|\hat{u}\|_{r'_h,\widetilde{\Omega}_h}\,Ch^{r'_h}\|v_h\|_{\mathrm{div},\Omega_h}\\ &\leq Ch^{2r'_h}\|f\|_{0,\mathbb{R}^2}\|g\|_{0,\mathbb{R}^2}.\end{aligned}$$

Finally, to estimate the last two terms notice that, because of Lemma 2.4.7,

$$\|v_h\|_{\mathrm{div},\Omega_h\setminus\bar{\Omega}} = \|v_h-\overline{v}\|_{\mathrm{div},\Omega_h\setminus\bar{\Omega}} \leq \|\overline{v}_h-\overline{v}\|_{\mathrm{div},\mathbb{R}^2} \leq Ch^{r'_h}\|g\|_{0,\mathbb{R}^2}$$

and, analogously, $\|u_h\|_{\mathrm{div},\Omega_h\setminus\bar{\Omega}} \leq Ch^{r'_h}\|f\|_{0,\mathbb{R}^2}$. Then, by using Lemma 2.3.3 and (2.33) we have

$$\begin{aligned}\left|\int_{\Omega_h\setminus\bar{\Omega}}(\mathrm{div}\,u)^e\,\mathrm{div}\,v_h\,dx\right| &\leq Ch\|(\mathrm{div}\,u)^e\|_{1,\widetilde{\Omega}_h}\|v_h\|_{\mathrm{div},\Omega_h\setminus\bar{\Omega}}\\ &\leq Ch^{1+r'_h}\|f\|_{0,\mathbb{R}^2}\|g\|_{0,\mathbb{R}^2}\end{aligned}$$

and

$$\begin{aligned}\left|\int_{\Omega_h\setminus\bar{\Omega}}\mathrm{div}\,u_h\,\mathrm{div}\,v_h\,dx\right| &\leq \|u_h\|_{\mathrm{div},\Omega_h\setminus\bar{\Omega}}\|v_h\|_{\mathrm{div},\Omega_h\setminus\bar{\Omega}}\\ &\leq Ch^{2\hbar'}\|f\|_{0,\mathbb{R}^2}\|g\|_{0,\mathbb{R}^2}.\end{aligned}$$

Thus, we conclude the proof. □

Now we are able to establish a double-order error estimate for the approximate eigenvalues. We know that $\lambda = 1/\mu$ is a positive eigenvalue of problem (2.1) with multiplicity m, and $\lambda_h^{(i)} = 1/\mu_h^{(i)}$, $i = 1,\ldots,m$, are the eigenvalues of problem (2.2) converging to λ. Then, the following error estimate holds:

Theorem 2.4.2 *There exist a positive constant C such that*

$$\left|\lambda - \lambda_h^{(i)}\right| \leq Ch^{2r'_h}, \qquad i = 1, \ldots, m.$$

Proof. It is an immediate consequence of the previous lemma, Lemma 2.4.7 and Remark 7.5 in [7]. □

2.5 Numerical Examples

In this section we report the results obtained on two numerical tests which confirm our theoretical statements. One of the tests corresponds to a domain with a smooth boundary and the other to a domain with reentrant corners.

In both tests, we have computed a few eigenvalues on several differently refined meshes in order to estimate the respective orders of convergence. Fig. 2.3 shows the domains and corresponding coarse meshes for each test.

Test 1: Domain with a $\mathcal{C}^\infty$-boundary Test 2: Domain with reentrant corners

Figure 2.3: Domains and meshes.

The results obtained for the annular domain of the first test are reported in Table 2.1. In this case, all the eigenvalues have multiplicity 2. This table shows the approximations of the smallest three double eigenvalues computed on some of the used meshes. Each mesh is identified by its total number of degrees of freedom (d.o.f.). We also include for each eigenvalue the estimated order of convergence and an extrapolated more accurate approximation, both obtained by means of a least square fitting of the computed values. The rate of convergence (in powers of h) is clearly 2, which agrees with the fact that, in this case, $r = 1$.

Figure 2.4 show the pressure corresponding to the first two eigenvalues in Table 2.1.

Table 2.2 shows the corresponding results obtained for the curved L-shaped domain of the second test. In this case, the domain has two reentrant corners of sizes

Table 2.1: Test 1: Numerical results for a domain with a $\mathcal{C}^\infty$-boundary.

d.o.f.	2480	9760	21840	38720	Order	Extrapolated
$\lambda_{h1}^{(1)}$	1.835302	1.835177	1.835154	1.835146	2.03	1.835136
$\lambda_{h1}^{(2)}$	1.835302	1.835177	1.835154	1.835146	2.03	1.835136
$\lambda_{h2}^{(1)}$	7.189809	7.189092	7.188958	7.188915	2.02	7.188856
$\lambda_{h2}^{(2)}$	7.191344	7.189473	7.189132	7.189011	2.02	7.188861
$\lambda_{h3}^{(1)}$	15.674033	15.666375	15.664954	15.664458	2.00	15.663820
$\lambda_{h3}^{(2)}$	15.674033	15.666375	15.664954	15.664458	2.00	15.663820

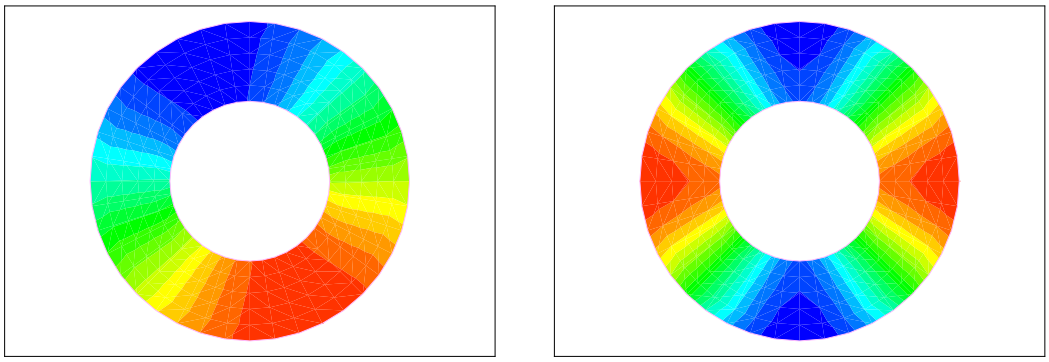

Figure 2.4: Fluid pressure associated to the eigenvalues $\lambda_{h1}^{(1)}$ and $\lambda_{h2}^{(1)}$.

$5\pi/4$ and $3\pi/2$. Because of this, some of the eigenvalues are computed with an order clearly smaller than 2 (in powers of h). Indeed, in this case $r = 2/3$ and then the error estimates proved in the previous section is $|\lambda_i - \lambda_{hi}| \leq Ch^{4/3}$. It can be seen that this order of convergence is practically attained for the two first eigenvalues.

Figure 2.5 and 2.6 show the pressure corresponding to the eigenvalues in Table 2.2.

Table 2.2: Test 2: Numerical results for a domain with a reentrant corner

d.o.f.	3680	14560	32640	57920	Order	Extrapolated
λ_{h1}	1.359828	1.362873	1.363690	1.364048	1.37	1.364792
λ_{h2}	3.349844	3.351317	3.351717	3.351892	1.36	3.352258
λ_{h3}	9.558594	9.562825	9.563608	9.563884	2.00	9.564235
λ_{h4}	9.568797	9.571612	9.572166	9.572368	1.90	9.572643
λ_{h5}	11.035413	11.038415	11.039169	11.039485	1.49	11.040076

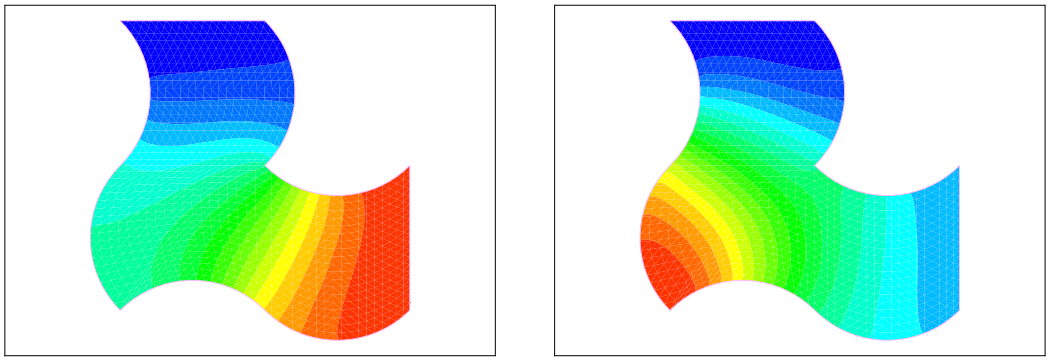

Figure 2.5: Fluid pressure associated to the eigenvalues λ_{h1} and λ_{h2}.

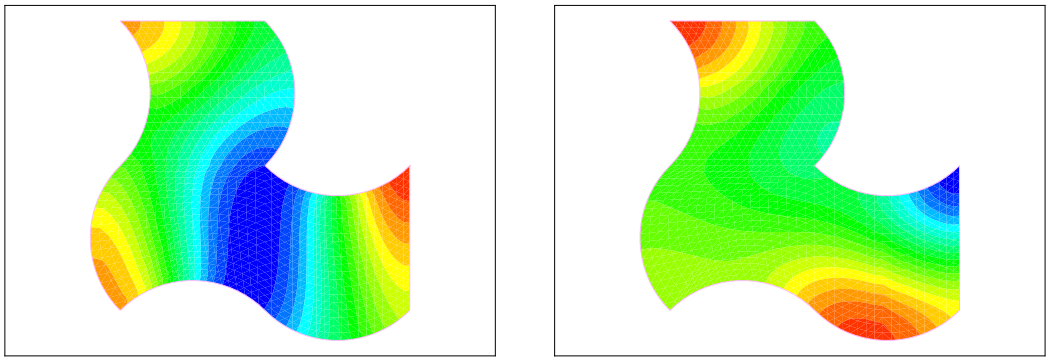

Figure 2.6: Fluid pressure associated to the eigenvalues λ_{h3} and λ_{h4}.

Chapter 3

Error estimates for low-order isoparametric quadrilateral finite elements for plates

This chapter deals with the numerical approximation of the deflection of a plate modeled by Reissner-Mindlin equations. It is well known that, in order to avoid locking, some kind of reduced integration or mixed interpolation has to be used when solving these equations by finite element methods. In particular, one of the most widely used procedures is based on the family of elements called MITC (mixed interpolation of tensorial components). We consider two lowest-order methods of this family on quadrilateral meshes.

Under mild assumptions we obtain optimal H^1 and L^2-error estimates for both methods. These estimates are valid with constants independent of the plate thickness. We also obtain error estimates for the approximation of the plate vibration problem. Finally, we report several numerical experiments showing the very good behavior of the methods, even in some cases not covered by our theory.

3.1 Introduction

The Reissner-Mindlin model is the most widely used for the analysis of thin or moderately thick elastic plates. It is now very well understood that standard finite element methods applied to this problem produce very unsatisfactory results due to the so called locking phenomenon. Therefore, some special method based on reduced integration or mixed interpolation has to be used. Among these methods, the so called *MITC* ones, introduced by Bathe and Dvorkin in [10], or variants of them are very likely the most used in practice.

A great number of papers dealing with the mathematical analysis of these kind of methods have been published (see for example [4, 9, 29, 46, 44, 72, 73, 79]). In those papers optimal order error estimates, valid uniformly in the plate thickness, have been obtained for several methods. However, although one of the most commonly used elements in engineering applications are the isoparametric quadrilaterals (indeed, the original Bathe and Dvorkin paper deals with these elements), no available result seems to exist for this case.

On the other hand, it has been recently noted that the extension to general quadrilaterals of convergence results valid for rectangular elements is not straightforward and, even more, the order of convergence can deteriorate when non-standard finite elements are used in distorted quadrilateral, even if they satisfy the usual shape regularity assumption (see [5, 6]).

The aim of this chapter is to analyze two low-order methods based on quadrilateral meshes. One is the original *MITC4* introduced in [10] while the other one is an extension to the quadrilateral case of a method introduced in [46] for triangular elements (from now on the latter method will be called *DL4*). We are interested not only in load problems but also in the approximation of the vibration modes of the plate.

For nested uniform meshes of rectangles, an optimal order error estimate in H^1 for the *MITC4* has been proved in [9]. However the regularity assumptions on the exact solution required in that paper are not optimal. These assumptions has been weakened in [46] but they are still not optimal. Let us remark that, in order to obtain results for the spectral approximation, it is important to remove this extra regularity assumptions.

On the other hand, for low-order elements as those considered here, an optimal error estimate in L^2 is difficult to obtain because of the consistency term arising in the error equation. For triangular elements this estimate has been proved only recently in [44]. However, the proof given in that paper can not be extended straightforwardly even for the case of rectangular elements. Let us mention also that this L^2 estimate is very important if one wants to prove optimal order convergence for the eigenvalue approximation (see [44]).

In this chapter we prove optimal, both in order and regularity, H^1 and L^2-error estimates for both *MITC4* and *DL4* methods under appropriate assumptions on the family of meshes. As a consequence, following the arguments in [44] we obtain also optimal error estimates for the spectral approximation.

In order to prove the H^1 estimate for the *MITC4* we require an additional assumption on the meshes (which is satisfied, for instance, by uniform refinements of any starting mesh). Instead, for the *DL4* no assumption other than the usual shape

regularity one is needed.

On the other hand, a further assumption on the meshes is made to prove the L^2 estimates and, consequently, the higher order estimate for eigenvalues: the meshes must be formed by higher order perturbations of parallelograms. This restriction is related with approximation properties of the Raviart-Thomas elements which are used in our arguments and do not hold for general quadrilateral elements. However, this assumption is only needed for extremely refined meshes. Indeed, the L^2 estimate holds for any regular mesh as long as the meshsize is comparable with the thickness. Moreover, we believe that this quasi parallelogram assumption is of technical character. In fact, the numerical experiments reported here seem to show that it is not necessary.

The rest of the chapter is organized as follows. In Section 2 we recall Reissner-Mindlin equations for plate vibrations and introduce the two discrete methods. We prove error estimates for both methods in H^1 and L^2 norms in Sections 3 and 4, respectively. In Section 5, prove optimal order convergence for the spectral plate problem. Finally, in Section 6 we report some numerical experiments.

Throughout the chapter we denote by C a positive constant not necessarily the same at each occurrence, but always independent of the mesh-size and the thickness.

3.2 Statement of the problem

3.2.1 Reissner-Mindlin model

Let $\Omega\times(-\frac{t}{2},\frac{t}{2})$ be the region occupied by an undeformed elastic plate of thickness t, where $\Omega\subset\mathbb{R}^2$ is a convex polygonal domain. In order to describe the deformation of the plate, we consider the Reissner-Mindlin model, which is written in terms of the rotations $\beta=(\beta^1,\beta^2)$ of the fibers initially normal to the plate midsurface and the transverse displacement w (see [28, 46]). The following equations describe the plate response to conveniently scaled tranversal and shear loads $f\in L^2(\Omega)$ and $\theta\in L^2(\Omega)^2$:

Find $(\beta,w)\in H_0^1(\Omega)^2\times H_0^1(\Omega)$ *such that:*

$$\begin{cases} a(\beta,\eta)+(\gamma,\nabla v-\eta)=(f,v)+\dfrac{t^2}{12}(\theta,\eta) \qquad \forall(\eta,v)\in H_0^1(\Omega)^2\times H_0^1(\Omega), \\ \gamma=\dfrac{\kappa}{t^2}(\nabla w-\beta), \end{cases} \tag{3.1}$$

where $\kappa:=Ek/2(1+\nu)$ is the shear modulus, in this expression E is the Young modulus, ν stands for the Poisson ratio and k is a correction factor of the shear

stress. We have also introduced the shear stress γ and denoted by $(\cdot,\cdot)$ the standard L^2-inner product. The bilinear form a is $\mathrm{H}_0^1(\Omega)^2$-elliptic and is defined by

$$a(\beta,\eta) := \frac{E}{12(1-\nu^2)} \int_\Omega \left[\sum_{i,j=1}^{2} (1-\nu)\varepsilon_{ij}(\beta)\varepsilon_{ij}(\eta) + \nu \operatorname{div}\beta \operatorname{div}\eta \right],$$

with $\varepsilon_{ij}(\beta)$ being the linear strain tensor.

Let us remark that we have included in our formulation the shear load term $\frac{t^2}{12}(\theta,\eta)$ since it arises naturally when considering the free vibration modes of the plate. In fact, it is simple to see that the plate vibration frequencies and amplitudes are solutions of the following spectral problem:

$$t^3 a(\beta,\eta) + \kappa t \int_\Omega (\nabla w - \beta)\cdot(\nabla v - \eta) = \omega^2 \left[t \int_\Omega \rho\, w v + \frac{t^3}{12} \int_\Omega \rho\, \beta\cdot\eta \right] \qquad \forall (\eta, v) \in \mathrm{H}_0^1(\Omega)^2 \times \mathrm{H}_0^1(\Omega),$$

where ω denotes the angular vibration frequency and ρ the density. Thus, rescaling the problem with $\lambda := \rho\,\omega^2/t^2$, we rewrite it as follows:

Find $\omega > 0$ *and* $0 \neq (\beta, w) \in \mathrm{H}_0^1(\Omega)^2 \times \mathrm{H}_0^1(\Omega)$ *such that:*

$$\begin{cases} a(\beta,\eta) + (\gamma, \nabla v - \eta) = \lambda \left[(w,v) + \dfrac{t^2}{12}(\beta,\eta) \right] & \forall (\eta, v) \in \mathrm{H}_0^1(\Omega)^2 \times \mathrm{H}_0^1(\Omega), \\ \gamma = \dfrac{\kappa}{t^2}(\nabla w - \beta), \end{cases} \tag{3.2}$$

which is the spectral problem associated to (3.1).

This chapter deals with the finite element approximation of both problems, (3.1) and (3.2). It is well known that both are well-posed (see [28] and [44]). Furthermore, we will use the following regularity result for the solution of (3.1) (see [4]):

$$\|\beta\|_{2,\Omega} + \|w\|_{2,\Omega} + \|\gamma\|_{0,\Omega} + t\,\|\gamma\|_{1,\Omega} \leq C \left(t^2 \|\theta\|_{0,\Omega} + \|f\|_{0,\Omega} \right) \leq C\, |(\theta, f)|_t, \tag{3.3}$$

where C denotes a constant independent of t, $\|\cdot\|_{k,O}$ denotes the standard norm of $\mathrm{H}^k(O)$ or $\mathrm{H}^k(O)^2$, as corresponds, for any open subset O of Ω and any integer k, and $|(\cdot,\cdot)|_t$ is the norm in $\mathrm{L}^2(\Omega)^2 \times \mathrm{L}^2(\Omega)$ induced by the weighted inner product in the right hand side of the first equation in (3.1) (see [44]).

3.2.2 Discrete problems

In what follows, we consider two lowest-degree methods on isoparametric quadrilateral meshes for the approximation of the load problem (3.1): the so-called *MITC4*

method (see [10]) and an extension to quadrilaterals of a method introduced in [46] that we call *DL4*. Both methods are based on relaxing the second term in equation (3.1) by introducing an interpolation operator, called *reduction operator*.

Let $\{\mathcal{T}_h\}$ be a family of decompositions of Ω into convex quadrilaterals, satisfying the usual condition of regularity (see for instance [73]); i.e., there exist constants $\sigma > 1$ and $0 < \varrho < 1$ independent of h such that

$$h_K \leq \sigma \rho_K, \quad |\cos\theta_{iK}| \leq \varrho, \quad i = 1,2,3,4, \quad \forall K \in \mathcal{T}_h, \tag{3.4}$$

where h_K is the diameter of K, ρ_K the diameter of the largest circle contained in K, and θ_{iK}, $i = 1,2,3,4$, the four angles of K.

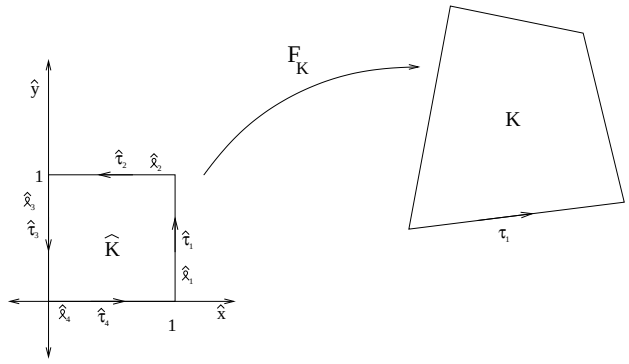

Figure 3.1: Bilinear mapping onto an element $K \in \mathcal{T}_h$.

Let $\widehat{K} := [0,1]^2$ be the reference element. We denote by $Q_{i,j}(\widehat{K})$ the space of polynomials of degree less than or equal to i in the first variable and to j in the second one. Also, we set $Q_k(\widehat{K}) = Q_{k,k}(\widehat{K})$.

Let $K \in \mathcal{T}_h$. We denote by F_K a bilinear mapping of $\widehat{K}$ onto K, with Jacobian matrix and determinant denoted by DF_K and J_{F_K}, respectively. The assumption (3.4) leads to

$$ch_K^2 \leq J_{F_K} \leq Ch_K^2, \tag{3.5}$$

with c and C only depending on σ and ϱ (see [75]). Let $\ell_i \subset \partial K$, $i = 1,\ldots,4$, be the edges of K; then $\ell_i = F_K(\widehat{\ell}_i)$, with $\widehat{\ell}_i$ being the edges of $\widehat{K}$. Let τ_i be a unit tangent vector to the edge ℓ_i of K; then $\tau_i := \frac{DF_K\widehat{\tau}_i}{\|DF_K\widehat{\tau}_i\|}$ with $\widehat{\tau}_i$ being a unit vector tangent to the edge $\widehat{\ell}_i$ on the reference element (see Fig. 3.1).

Let

$$\mathcal{N}(\widehat{K}) := \left\{\widehat{p}\,:\, \widehat{p} \in Q_{0,1}(\widehat{K}) \times Q_{1,0}(\widehat{K})\right\},$$

and, from this space, we define through covariant transformation:

$$\mathcal{N}(K) := \left\{ p : \; p \circ F_K = DF_K^{-T}\widehat{p}, \; \widehat{p} \in \mathcal{N}(\widehat{K}) \right\}.$$

Let us remark that the mapping between $\mathcal{N}(K)$ and $\mathcal{N}(\widehat{K})$ is a kind of "Piola transformation" for the "rot" operator, $\operatorname{rot} p := \partial p/\partial y - \partial p/\partial x$, (the Piola transformation is defined for the "div" operator in, for example, [28]; see also [79, 81] for further details). Then we have the following results which are easily established

$$\int_{\ell_i} p \cdot \tau_i = \int_{\widehat{\ell}_i} \widehat{p} \cdot \widehat{\tau}_i, \quad i = 1, \ldots, 4, \tag{3.6}$$

and

$$(\operatorname{rot} p) \circ F_K = J_{F_K}^{-1} \widehat{\operatorname{rot}} \widehat{p}. \tag{3.7}$$

Then, we define the space (which will be used to approximate the shear stress γ)

$$\Gamma_h := \left\{ \psi \in \mathrm{H}_0(\operatorname{rot}, \Omega) : \; \psi|_K \in \mathcal{N}(K) \; \forall K \in \mathcal{T}_h \right\},$$

that corresponds to the lowest-order rotated Raviart-Thomas space ([75, 81]). We remark that, for $\Gamma_h \subset \mathrm{H}_0(\operatorname{rot}, \Omega)$, the tangential component of a function in Γ_h must be continuous along interelement boundaries and vanish on $\partial\Omega$. In fact, the integrals (3.6) of these tangential components are the degrees of freedom defining an element of Γ_h.

We consider the following "interpolation" operator

$$R : \mathrm{H}^1(\Omega)^2 \cap \mathrm{H}_0(\operatorname{rot}, \Omega) \longrightarrow \Gamma_h,$$

locally defined for each $\psi \in \mathrm{H}^1(\Omega)^2$ by (see [75])

$$\int_\ell R\psi \cdot \tau_\ell = \int_\ell \psi \cdot \tau_\ell \quad \forall \text{ edge } \ell \text{ of } \mathcal{T}_h, \tag{3.8}$$

where, from now on, τ_ℓ denotes a unit vector tangent to ℓ. Clearly, the operator R satisfies

$$\int_K \operatorname{rot}(\psi - R\psi) = 0 \qquad \forall \psi \in \mathrm{H}^1(\Omega)^2, \tag{3.9}$$

for any quadrilateral $K \in \mathcal{T}_h$. Taking into account the rotation mentioned above, it is proved ([52], Chapter III, Theorem XXX) that

$$\| \operatorname{rot} R\psi\|_{0,\Omega} \leq C \|\psi\|_{1,\Omega} \tag{3.10}$$

and

$$\|\psi - R\psi\|_{0,\Omega} \leq Ch \|\psi\|_{1,\Omega}. \tag{3.11}$$

To approximate the tranverse displacements we will use the space of standard bilinear isoparametric elements

$$W_h := \{v \in \mathrm{H}_0^1(\Omega) : \, v|_K \in Q(K) \ \forall K \in \mathcal{T}_h\},$$

where $Q(K) := \{p \in \mathrm{L}^2(K) : \, p \circ F_K \in Q_1(\widehat{K})\}$, for all $K \in \mathcal{T}_h$.

The following lemma establishes some relations between the space Γ_h and W_h:

Lemma 3.2.1 *The following properties hold:*

$$\nabla W_h = \{\mu \in \Gamma_h : \operatorname{rot} \mu = 0\} \subset \Gamma_h.$$

and

$$\forall w \in \mathrm{H}^2(\Omega), \quad R(\nabla w) = \nabla(w^I),$$

where w^I is the Lagrange interpolant of w on W_h.

Proof.

For $\mu \in \Gamma_h$, it follows that $\forall K \in \mathcal{T}_h$

$$\mu|_K \circ F_K = DF_K^{-T}\widehat{\mu}, \ \widehat{\mu} \in \mathcal{N}(\widehat{K}) \quad \text{and} \quad \operatorname{rot} \mu|_K \circ F_K = \frac{1}{J_{F_K}} \widehat{\operatorname{rot}}\widehat{\mu}.$$

Hence, since $J_{F_K} > 0$ because of (3.5), $\operatorname{rot} \mu = 0$ if and only if $\widehat{\operatorname{rot}}\widehat{\mu} = 0$.

On the other hand, note that if $\widehat{\mu} \in \mathcal{N}(\widehat{K})$ then $\widehat{\mu} = (a + b\widehat{y}, c + d\widehat{x})$, with $a, b, c, d \in \mathbb{R}$, and $\widehat{\operatorname{rot}}\widehat{\mu} = d - b$. Therefore, $\widehat{\operatorname{rot}}\widehat{\mu} = 0$ if and only if $\widehat{\mu} = (a + c\widehat{y}, c + d\widehat{x})$ = $\widehat{\nabla}\widehat{v}$, for $\widehat{v} = a\widehat{x} + c\widehat{y} + d\widehat{x}\widehat{y} \in Q_1(\widehat{K})$.

Thus, $\operatorname{rot} \mu|_K = 0$ if and only if $\mu|_K = (DF_K^{-T}\widehat{\mu}) \circ F_K^{-1} = \nabla v$ with $v = \widehat{v} \circ F_K^{-1} \in Q_1(K)$.

To prove the second property, since we have already proved that $\nabla w^I \in \Gamma_h$, is enough to show that the degree of freedom defining $R(\nabla w)$ and ∇w^I coincide. Indeed, for all edge ℓ of $\mathcal{T}_h$,

$$\int_\ell R(\nabla w) \cdot \tau_\ell = \int_\ell \nabla w \cdot \tau_\ell = w(B) - w(A) = w^I(B) - w^I(A) = \int_\ell \nabla w^I \cdot \tau_\ell,$$

where A and B denote the end point of ℓ as in Figure 3.2. □

Let us now specify the methods that we are going to analyze. The two methods that we analyze only differ in the space H_h used to approximate the rotations:

MITC4: We use W_h and Γ_h defined above, whereas for the rotations we use standard isoparametric bilinear functions:

$$H_h^1 := \{\eta \in \mathrm{H}_0^1(\Omega)^2 : \, \eta|_K \in Q(K)^2 \ \forall K \in \mathcal{T}_h\}.$$

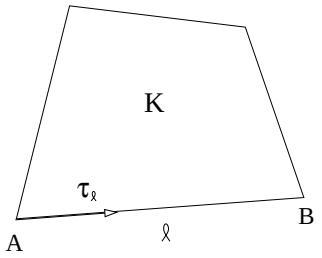

Figure 3.2: Geometry of K.

DL4: While for this method W_h and Γ_h are the same as for *MITC4*, we enrich the space H_h by introducing a rotation of a space used for the approximation of the Stokes problem in [52].

For each edge $\widehat{\ell}_i \subset \widehat{K}$, $i = 1, \ldots, 4$, let $\widehat{q}_i$ be the functions vanishing on $\widehat{\ell}_j$ for $j \neq i$. Namely, $\widehat{q}_1 = \widehat{x}\widehat{y}(1-\widehat{y})$, $\widehat{q}_2 = \widehat{x}\widehat{y}(1-\widehat{x})$, $\widehat{q}_3 = \widehat{y}(1-\widehat{x})(1-\widehat{y})$ and $\widehat{q}_4 = (1-\widehat{x})(1-\widehat{y})$ (see Fig. 3.1). Then we define $\mathbf{p}_i := (\widehat{q}_i \circ F_K^{-1})\tau_i$ and we set

$$H_h^2 := \{\eta \in \mathrm{H}_0^1(\Omega)^2 : \eta|_K \in Q(K)^2 \oplus \langle \mathbf{p}_1, \mathbf{p}_2, \mathbf{p}_3, \mathbf{p}_4 \rangle \ \forall K \in \mathcal{T}_h\}.$$

From now on we use H_h to denote any of the two spaces H_h^1 or H_h^2. In both methods we use R defined by (3.8) as *reduction operator*. Then, the discretization of the load problem (3.1) can be writen in both cases as follows:

Find $(\beta_h, w_h) \in H_h \times W_h$ *such that:*

$$\begin{cases} a(\beta_h, \eta) + (\gamma_h, \nabla v - R\eta) = (f, v) + \dfrac{t^2}{12}(\theta, \eta) & \forall (\eta, v) \in H_h \times W_h, \\ \gamma_h = \dfrac{\kappa}{t^2}(\nabla w_h - R\beta_h). \end{cases} \tag{3.12}$$

Existence and uniqueness of this solution follow easily (see [46]).

On the other hand, the discretization of the spectral problem (3.2) is as follows:

Find $\lambda_h \in \mathbb{R}$ *and* $0 \neq (\beta_h, w_h) \in H_h \times W_h$ *such that:*

$$\begin{cases} a(\beta_h, \eta) + (\gamma_h, \nabla v - R\eta) = \lambda_h \left[(w_h, v) + \dfrac{t^2}{12}(\beta_h, \eta) \right] & \forall (\eta, v) \in H_h \times W_h, \\ \gamma_h = \dfrac{\kappa}{t^2}(\nabla w_h - R\beta_h). \end{cases} \tag{3.13}$$

3.3 H^1–error estimates

To prove optimal error estimates in H^1–norm we use a result from [46]. Let (β, w, γ) and (β_h, w_h, γ_h) be the solutions of the problems (3.1) and (3.12), respectively. By virtue of Lemma 3.2.1, Theorem 3.1 in [46] reads in our case:

Theorem 3.3.1 *Let H_h, W_h, Γ_h, and the operator R be defined as above. If there exist $\widetilde{\beta} \in H_h$ and an operator $\Pi : \mathrm{H}_0(\mathrm{rot}, \Omega) \cap \mathrm{H}^1(\Omega)^2 \longrightarrow \Gamma_h$ satisfaying*

$$\|\beta - \widetilde{\beta}\|_{1,\Omega} \leq Ch\|\beta\|_{2,\Omega}, \tag{3.14}$$

$$\mathrm{rot}\left(\frac{t^2}{\kappa}\Pi\gamma + R\widetilde{\beta}\right) = 0, \tag{3.15}$$

and

$$\|\eta - \Pi\eta\|_{0,\Omega} \leq Ch\|\eta\|_{1,\Omega} \ \ \forall \eta \in \mathrm{H}^1(\Omega)^2 \cap \mathrm{H}_0(\mathrm{rot}, \Omega), \tag{3.16}$$

then, the following error estimates hold:

$$\|\beta - \beta_h\|_{1,\Omega} + t\|\gamma - \gamma_h\|_{0,\Omega} \leq Ch\Big(\|\beta\|_{2,\Omega} + t\|\gamma\|_{1,\Omega} + \|\gamma\|_{0,\Omega}\Big) \tag{3.17}$$

and

$$\|w - w_h\|_{1,\Omega} \leq Ch\Big(\|\beta\|_{2,\Omega} + t\|\gamma\|_{1,\Omega} + \|\gamma\|_{0,\Omega}\Big). \tag{3.18}$$

Our next step is to prove that the theorem above can be applied to both methods.

3.3.1 MITC4

Several studies have been carried out for this method in, for example, [9], [46], and [66]. Since the variational equations for plates have a certain similitude with those of the Stokes problem, the main results are based on the properties already known for the latter. An order h of convergence is obtained in those references only for uniform meshes of square elements. Moreover, more regularity of the solutions is also required. Although these results can be adapted for parallelogram meshes, they cannot be extended to general quadrilateral meshes.

In what follows we obtain error estimates for this method on somewhat more general meshes, optimal in order and regularity. We assume on the meshes specifically the following condition:

Assumption 3.3.1 *The mesh $\mathcal{T}_h$ is a refinement of a coarser partition $\mathcal{T}_{2h}$, obtained by joining the midpoints of each opposite side in each $M \in \mathcal{T}_{2h}$ (called macro-element). In addition, $\mathcal{T}_{2h}$ is a similar refinement of a still coarser regular partition $\mathcal{T}_{4h}$, whose elements are also called macro-elements.*

Let

$$Q_h := \left\{ q_h \in \mathrm{L}^2_0(\Omega) : \, q_h|_K = c_K, \; c_K \in \mathbb{R}, \; \forall K \in \mathcal{T}_h \right\},$$

where $\mathrm{L}^2_0(\Omega) := \{q \in \mathrm{L}^2(\Omega) : \, \int_\Omega q = 0\}$. Note that, for parallelogram meshes, we have $Q_h = \operatorname{rot} \Gamma_h$, but this does not hold for general quadrilateral meshes.

For each macro-element $M \in \mathcal{T}_{2h}$ we introduce four functions q_i, $1 \leq i \leq 4$, taking the values 1 and -1, according to the pattern of Figure 3.3.

Let

$$Q_{h4} := \{q_h \in Q_h : \, q_h|_M = c_M q_4, \; c_M \in \mathbb{R}, \; \forall M \in \mathcal{T}_{2h}\}$$

and $\widetilde{Q}_h$ be its $\mathrm{L}^2(\Omega)$-orthogonal complement on Q_h; i.e.,

$$\widetilde{Q}_h := \{q_h \in Q_h : \, q_h|_M \in \langle q_1, \, q_2, \, q_3 \rangle \; \forall M \in \mathcal{T}_{2h}\}.$$

We associate to these spaces the subspace of H^1_h defined by

$$\widetilde{H}_h := \left\{ \eta_h \in H^1_h : \, \int_\Omega \operatorname{rot} \eta_h \, q_h = 0 \quad \forall q_h \in Q_{h4} \right\}. \tag{3.19}$$

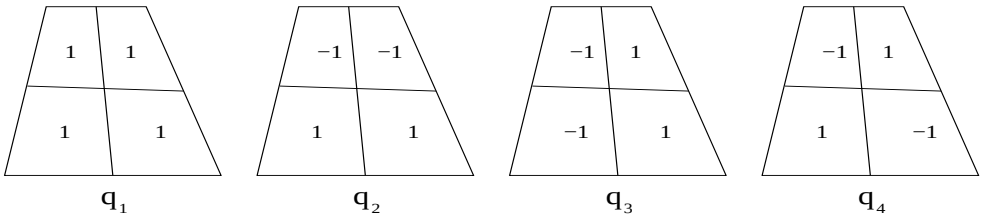

Figure 3.3: Bases for the macro-elements.

The following lemma provides the approximant $\widetilde{\beta}$ required by Theorem 3.3.1. Moreover, this $\widetilde{\beta} \in \widetilde{H}_h$, and this fact will be used below to define the operator Π.

Lemma 3.3.1 *Let $\beta \in \mathrm{H}^1_0(\Omega) \cap \mathrm{H}^2(\Omega)$. There exists $\widetilde{\beta} \in \widetilde{H}_h$ such that*

$$\int_\Omega \operatorname{rot}(\widetilde{\beta} - \beta) q_h = 0 \quad \forall q_h \in \widetilde{Q}_h \tag{3.20}$$

and the estimate (3.14) holds true.

Proof. It follows from the results in section VI.5.4 of [28] by changing "div" by "rot" and rotating 90° the fields, which in its turn are based on the results for isoparametric element in [78] (see also [73]). □

Our next step is to define the operator Π satisfying the requirements of Theorem 3.3.1. To do this, we will use a particular projector $\widetilde{P}$ onto $\operatorname{rot}\Gamma_h$.

We have already mentioned that, in general, $Q_h \neq \operatorname{rot}\Gamma_h$. In fact, it is simple to show that

$$\operatorname{rot}\Gamma_h = \left\{ \sum_{K\in\mathcal{T}_h} \frac{c_K}{J_{F_K}}\chi_K \ : \ c_K \in \mathbb{R}\ \forall K \in \mathcal{T}_h \right\} \cap \mathrm{L}^2_0(\Omega),$$

where χ_K is the characteristic function of K.

For a macro-element $M \in \mathcal{T}_{2h}$, we consider the bilinear mapping F_M, as shown in Fig. 3.4. Therefore, for any $\eta_h \in \Gamma_h$,

$$\operatorname{rot}\eta_h|_M = \frac{1}{J_{F_M}} \sum_{i=1}^{4} c_i \chi_{K_i},$$

where K_i are the four elements in M (see Fig. 3.4). We can write $\sum_{i=1}^4 c_i\chi_{K_i} = \sum_{i=1}^4 d_i q_i$, with d_i related to c_i by an orthogonal matrix, i.e.,

$$\begin{pmatrix} d_1 \\ d_2 \\ d_3 \\ d_4 \end{pmatrix} = \frac{1}{2} \begin{pmatrix} 1 & 1 & 1 & 1 \\ 1 & 1 & -1 & -1 \\ 1 & -1 & -1 & 1 \\ 1 & -1 & 1 & -1 \end{pmatrix} \begin{pmatrix} c_1 \\ c_2 \\ c_3 \\ c_4 \end{pmatrix}, \tag{3.21}$$

and hence

$$|d_i| \leq 2 \max_{1\leq j\leq 4} |c_j|, \quad i = 1,2,3,4. \tag{3.22}$$

Given $p \in \mathrm{L}^2_0(\Omega)$, we define $\widetilde{P} : \mathrm{L}^2_0(\Omega) \longrightarrow \operatorname{rot}\Gamma_h$ as follows:

$$\forall M = \bigcup_{i=1}^{4} K_i \in \mathcal{T}_{2h}, \quad \widetilde{P}p|_M = \sum_{i=1}^{4} \frac{c_i}{J_{F_M}}\chi_{K_i},$$

with c_i chosen such that

$$\begin{cases} \displaystyle\int_M \widetilde{P}p\, q_i = \int_M pq_i, \quad i = 1,2,3, \\ \\ \displaystyle\int_M \widetilde{P}p\, q_4 = 0. \end{cases}$$

Straightforward computations show that $\widetilde{P}$ is well defined by the equation above. As a consequence, we have $\forall M \in \mathcal{T}_{2h}$,

$$\int_M \widetilde{P}p\, q_h = \int_M pq_h \quad \forall q_h \in \widetilde{Q}_h, \quad \text{and} \quad \int_M \widetilde{P}p\, q_h = 0 \quad \forall q_h \in Q_{h4}.$$

The following properties of the operator will be used in the sequel:

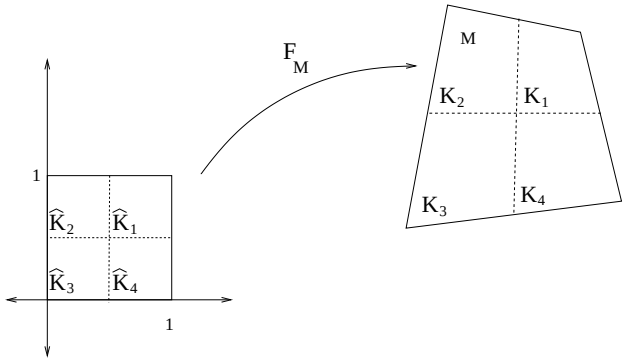

Figure 3.4: Bilinear mapping on macro-elements.

Lemma 3.3.2 *The following estimates hold:*

$$\|p - \widetilde{P}p\|_{0,\Omega} \leq C\|p\|_{0,\Omega} \quad \forall p \in \mathrm{L}^2(\Omega), \tag{3.23}$$

$$\|p - \widetilde{P}p\|_{-1,\Omega} \leq Ch\|p\|_{0,\Omega} \quad \forall p \in \mathrm{L}^2(\Omega). \tag{3.24}$$

Proof. In order to verify (3.23) it is enough to prove that $\|\widetilde{P}p\|_{0,\Omega} \leq C\|p\|_{0,\Omega}$. From the definition of $\widetilde{P}$ we have

$$\int_M (\widetilde{P}p)^2 = \int_M \widetilde{P}p \left(\sum_{i=1}^{4} \frac{c_i}{J_{F_M}\chi_{K_i}} \right) \leq \frac{1}{\min\limits_M J_{F_M}} \int_M \widetilde{P}p \left(\sum_{i=1}^{4} c_i \chi_{K_i} \right)$$

On the other hand, for $d_1, \ldots, d_4$ given by (3.21), from the definition of $\widetilde{P}$ and (3.22) we have

$$\begin{aligned} \int_M \widetilde{P}p \left(\sum_{i=1}^{4} c_i \chi_{K_i} \right) &= \int_M \widetilde{P}p \left(\sum_{i=1}^{4} d_i q_i \right) = \sum_{i=1}^{3} d_i \left(\int_M p q_i \right) \\ &\leq \|p\|_{0,M} \left(\sum_{i=1}^{3} |d_i| \, \|q_i\|_{0,M} \right) \leq C|M|^{1/2}\|p\|_{0,M} \left(\max_{1\leq j\leq 4} |c_j| \right) \\ &\leq C \max_M J_{F_M} \|p\|_{0,M} \|\widetilde{P}p\|_{0,M}, \end{aligned}$$

where we have use that

$$\int_{K_j} (\widetilde{P}p)^2 = c_j^2 \int_{K_j} \frac{1}{J_{F_M}^2} \geq \frac{|K_j|}{\max\limits_M J_{F_M}^2} c_j^2$$

and that $|M| \leq C|K_j|$, $j = 1, 2, 3, 4$, with C only depending on σ and ϱ. Then, using the inequalities above and noting that, for a quadrilateral regular mesh, $\max_M J_{F_M} \leq C \min_M J_{F_M}$ with a constant C independent of h, we obtain (3.23).

To verify (3.24), let $P : L^2(\Omega) \longrightarrow \widetilde{Q}_h$ be the orthogonal projection onto $\widetilde{Q}_h$. Let $v \in H_0^1(\Omega)$ be such that $\|v\|_{1,\Omega} = 1$. By the definition of P, (3.23), and the fact that $\widetilde{Q}_h$ contains the piecewise constants over $\mathcal{T}_{2h}$, we have

$$\begin{aligned}(p - \widetilde{P}p, v) &= (p - \widetilde{P}p, v - Pv) \leq \|p - \widetilde{P}p\|_{0,\Omega}\|v - Pv\|_{0,\Omega} \\ &\leq C\|p\|_{0,\Omega}\|v - Pv\|_{0,\Omega} \leq Ch\|p\|_{0,\Omega}\|v\|_{1,\Omega}.\end{aligned}$$

Thus we conclude (3.24). □

Now we are in order to define an operator Π as required in Theorem 3.3.1:

Lemma 3.3.3 *There exists an operator $\Pi : H_0(\mathrm{rot}, \Omega) \cap H^1(\Omega)^2 \longrightarrow \Gamma_h$ such that (3.15) and (3.16) hold.*

Proof. To define the operator Π we need some previous calculations. The condition (3.9) together with (3.20) yield

$$\int_\Omega \mathrm{rot}[R(\beta - \widetilde{\beta})]\, q_h = 0 \quad \forall q_h \in \widetilde{Q}_h. \tag{3.25}$$

Also, since $\widetilde{\beta} \in \widetilde{H}_h$, from (3.9) and (3.19) we obtain

$$\int_\Omega \mathrm{rot}\, R\widetilde{\beta}\, q_h = \int_\Omega \mathrm{rot}\, \widetilde{\beta}\, q_h = 0 \quad \forall q_h \in Q_{h4}.$$

Then, since $\mathrm{rot}\, R\widetilde{\beta} \in \mathrm{rot}\, \Gamma_h$, by virtue of (3.25) we conclude that

$$\mathrm{rot}\, R\widetilde{\beta} = \widetilde{P}(\mathrm{rot}\, R\beta) = -\frac{t^2}{\kappa}\widetilde{P}(\mathrm{rot}\, R\gamma), \tag{3.26}$$

where we have used that $\mathrm{rot}\, R\gamma = \frac{\kappa}{t^2}\mathrm{rot}\, R(\nabla w - \beta) = \mathrm{rot}\, R\beta$ because of Lemma 3.2.1.

On the other hand, let $\eta \in H_0(\mathrm{rot}, \Omega) \cap H^1(\Omega)^2$. We take $\chi(\eta) = \mathrm{curl}\, \phi := (-\partial\phi/\partial x_2, \partial\phi/\partial x_1)$, where ϕ is the solution of the problem

$$-\Delta\phi = \mathrm{rot}\, R\eta - \widetilde{P}(\mathrm{rot}\, R\eta) \quad \text{in } \Omega,$$

with homogeneous Neumann boundary conditions. Then

$$\mathrm{rot}\, \chi(\eta) = \mathrm{rot}\, R\eta - \widetilde{P}(\mathrm{rot}\, R\eta), \tag{3.27}$$

and

$$\|\chi(\eta)\|_{0,\Omega} \leq \|\operatorname{rot} R\eta - \widetilde{P}(\operatorname{rot} R\eta)\|_{-1,\Omega}, \tag{3.28}$$

$$\|\chi(\eta)\|_{1,\Omega} \leq \|\operatorname{rot} R\eta - \widetilde{P}(\operatorname{rot} R\eta)\|_{0,\Omega}. \tag{3.29}$$

For all $K \in \mathcal{T}_h$, $\operatorname{rot} R\chi(\eta)|_K = \frac{C_{R\chi}}{J_{F_K}}$ and $\operatorname{rot} \chi(\eta)|_K = \frac{C_\chi}{J_{F_K}}$, the latter because $\operatorname{rot} \chi(\eta) \in \operatorname{rot} \Gamma_h$. From (3.9) we have that $\int_K \operatorname{rot}(R\chi(\eta) - \chi(\eta)) = 0$ and, then, $C_{R\chi} = C_\chi$. Hence,

$$\operatorname{rot} R\chi(\eta) = \operatorname{rot} \chi(\eta). \tag{3.30}$$

Now, we set

$$\Pi\eta = R\eta - R\chi(\eta).$$

Therefore, for $\eta = \gamma$ and using (3.30), (3.27), and (3.26), we have

$$\operatorname{rot} \Pi\gamma \;=\; \operatorname{rot} R\gamma - \operatorname{rot} R\chi(\gamma) = \operatorname{rot} R\gamma - \operatorname{rot} \chi(\gamma) = \widetilde{P}(\operatorname{rot} R\gamma) = -\frac{\kappa}{t^2} \operatorname{rot} R\widetilde{\beta},$$

which shows that $\operatorname{rot}(\frac{t^2}{\kappa}\Pi\gamma + R\widetilde{\beta}) = 0$, and hence (3.15) holds true.

Finally, let us verify (3.16). We have

$$\|\eta - \Pi\eta\|_{0,\Omega} \leq \|\eta - R\eta\|_{0,\Omega} + \|R\chi(\eta)\|_{0,\Omega}.$$

The first term in the right hand side is bounded by (3.11) while for the second term we use (3.11), (3.28), (3.29), Lemma 3.3.2, and (3.10) to obtain

$$\begin{aligned}
\|R\chi(\eta)\|_{0,\Omega} &= \|\chi(\eta) - R\chi(\eta)\|_{0,\Omega} + \|\chi(\eta)\|_{0,\Omega} \\
&\leq Ch\|\chi(\eta)\|_{1,\Omega} + \|\chi(\eta)\|_{0,\Omega} \\
&\leq Ch\|\operatorname{rot} R\eta - \widetilde{P}(\operatorname{rot} R\eta)\|_{0,\Omega} + C\|\operatorname{rot} R\eta - \widetilde{P}(\operatorname{rot} R\eta)\|_{-1,\Omega} \\
&\leq Ch\|\operatorname{rot} R\eta\|_{0,\Omega} \leq Ch\|\eta\|_{1,\Omega}.
\end{aligned}$$

Thus, we conclude the proof of the lemma. □

3.3.2 DL4

The convergence of this method follows immediately from the convergence of *MITC4*. But in this case we have an alternative proof, valid for any regular mesh without any further assumption.

In order to prove the hypotheses of Theorem 3.3.1 in this case, we use some known results for the Stokes problem (see Girault & Raviart [52]).

Lemma 3.3.4 *There exists $\widetilde{\beta} \in H_h^2$ such that (3.14) holds. Furthermore, $R\widetilde{\beta} = R\beta$.*

Proof. By using the results of Section 3.1, chapter II in [52], and taking into account a rotation of the space $H(\mathrm{div},\Omega)$, it follows that for $\beta \in H_0^1(\Omega)^2$ there exists $\widetilde{\beta} \in H_h^2$ such that

$$\int_\ell (\widetilde{\beta} - \beta)\cdot\tau = 0 \quad \forall \ell \in \mathcal{T}_h, \tag{3.31}$$

and

$$|\widetilde{\beta} - \beta|_{m,\Omega} \leq C h^{k-m} |\beta|_{k,\Omega}, \quad m = 0,1, \quad k = 1,2. \tag{3.32}$$

In particular, for $k = 2$ and $m = 1$, (3.14) holds. By (3.31) and the definition of R in (3.8), it follows that $R(\widetilde{\beta} - \beta) = 0$. □

Lemma 3.3.5 *There exists an operator* $\Pi : H_0(\mathrm{rot},\Omega) \cap H^1(\Omega)^2 \longrightarrow \Gamma_h$ *such that (3.15) and (3.16) hold.*

Proof. Because of the previous lemma we have $R(\widetilde{\beta} - \beta) = 0$. On the other hand, $\mathrm{rot}\, R(\nabla w) = 0$, because of Lemma 3.2.1. Then, it is enough to take $\Pi = R$ to obtain (3.15), whereas (3.16) follows from (3.11). □

3.3.3 Main result in H^1-norm

Now we are in position to establish the error estimates. As above, in the case of *MITC4*, we consider meshes satisfying Assumption 3.3.1.

Theorem 3.3.2 *Given* $(\theta, f) \in L^2(\Omega)^2 \times L^2(\Omega)$, *let* (β, w) *be the solution of (3.1) and* (β_h, w_h) *the solution of (3.12). Then, there exists a constant* C, *independent of* t *and* h, *such that*

$$\|(\beta, w) - (\beta_h, w_h)\|_{H^1(\Omega)^2 \times H^1(\Omega)} \leq C h |(\theta, f)|_t.$$

Proof. It is a direct consequence of Lemmas 3.3.1, 3.3.3, 3.3.4, 3.3.5, Theorem 3.3.1, and the *apriori* estimate (3.3). □

3.4 L^2-error estimates

Our next goal is to prove L^2-error estimates optimal in order and regularity. To do this we follow the techniques in [44] where a triangular element similar to DL4 is analized. However the arguments therein cannot be directly applied to our case as shown below. Let us remark that, in the case of MITC4, this result completes the analysis carried out in [29, 72] for higher order methods.

First we introduce the dual problem of (3.1). Let $(\varphi, u) \in \mathrm{H}_0^1(\Omega)^2 \times \mathrm{H}_0^1(\Omega)$ be the solution of

$$\begin{cases} a(\eta,\varphi) + (\nabla v - \eta, \delta) = (v, w - w_h) + (\eta, \beta - \beta_h) \quad \forall (\eta, v) \in \mathrm{H}_0^1(\Omega)^2 \times \mathrm{H}_0^1(\Omega), \\ \delta = \dfrac{\kappa}{t^2}(\nabla u - \varphi). \end{cases} \tag{3.33}$$

By taking $\eta = 0$ in (3.33), we have

$$\operatorname{div} \delta = w - w_h. \tag{3.34}$$

The *a priori* estimate analogous to (3.3) yields for this problem:

$$\|\varphi\|_{2,\Omega} + \|u\|_{2,\Omega} + \|\delta\|_{0,\Omega} + t\,\|\delta\|_{1,\Omega} \leq C\Big(\|\beta - \beta_h\|_{0,\Omega} + \|w - w_h\|_{0,\Omega}\Big). \tag{3.35}$$

The arguments in the proof of Lemma 3.4 in [44] can be used in our case yielding the following result:

Lemma 3.4.1 *Given $(\theta, f) \in \mathrm{L}^2(\Omega)^2 \times \mathrm{L}^2(\Omega)$, let (β, w) be the solution of (3.1) and (β_h, w_h) the solution of (3.12). Let (φ, u) be the solution of problem (3.33) and $\delta = \frac{\kappa}{t^2}(\nabla u - \varphi)$ the corresponding shear strain term. Let $\widetilde{\varphi} \in H_h$ be the vector field associated to φ by Lemma 3.3.1 or 3.3.4 for MITC4 or DL4, respectively. Then, there exists a constant C, independent of t and h, such that*

$$\|\beta - \beta_h\|_{0,\Omega} + \|w - w_h\|_{0,\Omega} \leq Ch^2 |(\theta, f)|_t + \frac{|(\beta_h - R\beta_h, \delta)| + |(\gamma, \widetilde{\varphi} - R\widetilde{\varphi})|}{\|\beta - \beta_h\|_{0,\Omega} + \|w - w_h\|_{0,\Omega}}, \tag{3.36}$$

where γ is the shear strain defined in (3.1).

To estimate the consistency terms in (3.36) we cannot proceed as in Lemma 3.3 of [44]. Instead, we have the following lemma:

Lemma 3.4.2 *Given $\zeta \in H(\operatorname{div}, \Omega)$ and $\psi \in \mathrm{H}_0^1(\Omega)^2$, there holds*

$$|(\zeta, \psi - R\psi)| \leq Ch^2 \left(\sum_K |R\psi - \psi|_{1,K}^2\right)^{1/2} \|\operatorname{div} \zeta\|_{0,\Omega} + Ch \|\operatorname{rot}(R\psi - \psi)\|_{0,\Omega}\, \|\zeta\|_{0,\Omega}.$$

Proof. Let $K \in \mathcal{T}_h$. We consider the Neumann problem:

$$\begin{cases} -\Delta s_K &= \operatorname{rot}(R\psi - \psi) & \text{in } K, \\ \dfrac{\partial s_K}{\partial n_K} &= 0 & \text{on } \partial K. \end{cases} \tag{3.37}$$

By virtue of (3.9) we know that the above problem is compatible. Hence, it admits a solution $s_K \in H^1(K)/\mathbb{R}$ which satisfies

$$\| \operatorname{curl} s_K\|_{m+1,K} \leq C \| \operatorname{rot}(R\psi - \psi)\|_{m,K}, \quad m = -1, 0. \tag{3.38}$$

From (3.37) we obtain

$$\operatorname{rot}\Big(\operatorname{curl} s_K - (R\psi - \psi)\Big) = 0,$$

and hence, there exists $r_K \in H^1(K)$ (unique up to an additive constant) such that

$$\nabla r_K = \operatorname{curl} s_K - (R\psi - \psi). \tag{3.39}$$

Moreover, $\nabla r_K \cdot \tau_\ell = -R\psi \cdot \tau_\ell + \psi \cdot \tau_\ell$, for each side ℓ of K. Thus if we define $G \in L^2(\Omega)^2$ such that $G|_K = \nabla r_K$, then $G \in H_0(\operatorname{rot}, \Omega)$ and $\operatorname{rot} G = 0$.

Hence, there exists $r \in H^1(\Omega)/\mathbb{R}$, such that $G = \nabla r$ on Ω. Furthermore, since $G \in H_0(\operatorname{rot}, \Omega)$, then r can be chosen in $H_0^1(\Omega)$ and the additive constant defining r_K can be fixed as to satisfy $r|_K = r_K$.

Let A and B be as in Figure 3.2. Then because of (3.8) we have

$$r(B) = r(A) + \int_\ell \nabla r_K \cdot \tau_\ell = r(A) + \int_\ell (-R\psi + \psi) \cdot \tau_\ell = r(A).$$

Thus, since $r|_{\partial\Omega} = 0$, then r vanishes at all nodes of $\mathcal{T}_h$. Hence, a standard scaling argument on each element K (see [36]) yields $\|r\|_{0,K} \leq Ch^2 |r_K|_{2,K}$ and, then, by using (3.39) and (3.38), we have

$$\begin{aligned} \|r\|_{0,K} &\leq Ch^2 |\nabla r_K|_{1,K} \leq Ch^2 \Big(|\operatorname{curl} s_K|_{1,K} + |R\psi - \psi|_{1,K}\Big) \\ &\leq Ch^2 \Big(C \| \operatorname{rot}(R\psi - \psi)\|_{0,K} + |R\psi - \psi|_{1,K}\Big) \leq Ch^2 |R\psi - \psi|_{1,K}. \end{aligned}$$

On the other hand, let $(\cdot, \cdot)_K$ be the usual inner product in $L^2(K)$ and P the orthogonal projection onto the constant functions. Because of (3.9), we have $\forall \eta \in H_0^1(\Omega)$,

$$\frac{\Big(\operatorname{rot}(R\psi - \psi), \eta\Big)_K}{\|\eta\|_{1,K}} = \frac{\Big(\operatorname{rot}(R\psi - \psi), \eta - P\eta\Big)_K}{\|\eta\|_{1,K}} \leq \frac{\| \operatorname{rot}(R\psi - \psi)\|_{0,K} \|\eta - P\eta\|_{0,K}}{\|\eta\|_{1,K}}.$$

Hence,

$$\| \operatorname{rot}(R\psi - \psi)\|_{-1,K} \leq Ch \| \operatorname{rot}(R\psi - \psi)\|_{0,K}.$$

Now let $S \in \mathrm{L}^2(\Omega)^2$ such that $S|_K = \operatorname{curl} s_K$. Therefore, because of (3.38),

$$\begin{aligned} \|S\|_{0,\Omega}^2 &= \sum_{K\in\mathcal{T}_h} \|\operatorname{curl} s_K\|_{0,K}^2 \le \sum_{K\in\mathcal{T}_h} \|\operatorname{rot}(R\psi-\psi)\|_{-1,K}^2 \\ &\le Ch^2 \sum_{K\in\mathcal{T}_h} \|\operatorname{rot}(R\psi-\psi)\|_{0,K}^2 \le Ch^2 \|\operatorname{rot}(R\psi-\psi)\|_{0,\Omega}^2. \end{aligned} \tag{3.40}$$

Finally, from (3.39) we have

$$|(\zeta, \psi - R\psi)| = \left| \int_\Omega \zeta \cdot \nabla r + \int_\Omega \zeta \cdot S \right| \le \|\operatorname{div}\zeta\|_{0,\Omega}\|r\|_{0,\Omega} + \|\zeta\|_{0,\Omega}\|S\|_{0,\Omega},$$

and using (3.40) and (3.40), the lemma follows. □

On the other hand, the analogous to Theorem 4.3 in [81] applied to our situation in the space $\mathrm{H}(\operatorname{rot},\Omega)$ gives

$$|\varphi - R\varphi|_{1,K} \le C\Big(|\varphi|_{1,K} + h_K|\operatorname{rot}\varphi|_{1,K}\Big) \le \|\varphi\|_{2,K} \tag{3.41}$$

and

$$\|\operatorname{rot}(\varphi - R\varphi)\|_{0,K} \le C\Big(\delta_K h_K^{-1}|\operatorname{rot}\varphi|_{0,K} + h_K|\operatorname{rot}\varphi|_{1,K}\Big), \tag{3.42}$$

where δ_K is a measure of the deviation of the quadrilateral K from a parallelogram defined in Fig. 3.5. For regular meshes clearly $\dfrac{\delta_K}{h_K} \le C$, $\forall K \in \mathcal{T}_h$. A mesh is said *asympotically parallelogram* when $\max\limits_{K\in\mathcal{T}_h} \dfrac{\delta_K}{h_K} \le Ch$.

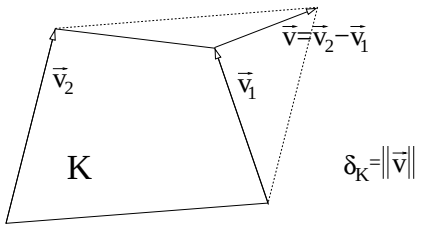

Figure 3.5: Geometric definition of δ_K.

Now we are able to estimate the consistency term in (3.36).

Lemma 3.4.3 *Let β_h, δ, γ and $\widetilde{\varphi}$ be as in Lemma 3.4.1. Then, there holds*

$$\frac{|(\beta_h - R\beta_h, \delta)| + |(\gamma, \widetilde{\varphi} - R\widetilde{\varphi})|}{\|\beta - \beta_h\|_{0,\Omega} + \|w - w_h\|_{0,\Omega}} \le Ch\left(h + t\max_{K\in\mathcal{T}_h}\frac{\delta_K}{h_K}\right)|(\theta, f)|_t. \tag{3.43}$$

Proof. First, we have

$$|(\beta_h - R\beta_h, \delta)| = \Big|\Big((\beta_h - \beta) - R(\beta_h - \beta), \delta\Big)\Big| + |(\beta - R\beta, \delta)|.$$

By using (3.11), Theorem 3.3.2, and (3.35), we obtain

$$\begin{aligned}\Big|\Big((\beta_h - \beta) - R(\beta_h - \beta), \delta\Big)\Big| &\leq C\,h\,\|\beta_h - \beta\|_{1,\Omega}\|\delta\|_{0,\Omega} \leq C\,h^2|(\theta, f)|_t\|\delta\|_{0,\Omega} \\ &\leq C\,h^2|(\theta, f)|_t\Big(\|\beta - \beta_h\|_{0,\Omega} + \|w - w_h\|_{0,\Omega}\Big).\end{aligned}$$

On the other hand, by definition of γ in (3.2) and (3.3), we have

$$|\operatorname{rot}\beta|_{0,K} = t^2|\operatorname{rot}\gamma|_{0,K} \leq Ct|(\theta, f)|_t. \tag{3.44}$$

Then, by using Lemma 3.4.2, (3.41), (3.42), (3.44), (3.3), (3.34), and (3.35), we have

$$\begin{aligned}|(\beta - R\beta, \delta)| &\leq C\,h^2\left(\sum_K |R\beta - \beta|^2_{1,K}\right)^{1/2}\|\operatorname{div}\delta\|_{0,\Omega} + Ch\|\operatorname{rot}(R\beta - \beta)\|_{0,\Omega}\,\|\delta\|_{0,\Omega} \\ &\leq Ch^2\|\beta\|_{2,\Omega}\,\|\operatorname{div}\delta\|_{0,\Omega} + Ch\left(\max_{K\in\mathcal{T}_h}\frac{\delta_K}{h_K}|\operatorname{rot}\beta|_{0,\Omega} + h|\operatorname{rot}\beta|_{1,\Omega}\right)\|\delta\|_{0,\Omega} \\ &\leq Ch^2|(\theta, f)|_t\,\|\operatorname{div}\delta\|_{0,\Omega} + Ch\left(h + t\max_{K\in\mathcal{T}_h}\frac{\delta_K}{h_K}\right)|(\theta, f)|_t\,\|\delta\|_{0,\Omega} \\ &\leq Ch\left(h + t\max_{K\in\mathcal{T}_h}\frac{\delta_K}{h_K}\right)|(\theta, f)|_t\left(\|\beta - \beta_h\|_{0,\Omega} + \|w - w_h\|_{0,\Omega}\right).\end{aligned}$$

The term $|(\gamma, \widetilde{\varphi} - R\widetilde{\varphi})|$ can be bounded almost identically, by using (3.14) to estimate $\|\widetilde{\varphi} - \varphi\|_{1,\Omega}$ and the fact that

$$-\operatorname{div}\gamma = f \quad \text{in } \Omega,$$

which follows by taking $\eta = 0$ in (3.1). By so doing, we obtain

$$|(\gamma, \widetilde{\varphi} - R\widetilde{\varphi})| \leq Ch\left(h + t\max_{K\in\mathcal{T}_h}\frac{\delta_K}{h_K}\right)|(\theta, f)|_t\Big(\|\beta - \beta_h\|_{0,\Omega} + \|w - w_h\|_{0,\Omega}\Big),$$

which concludes the proof of the lemma. □

Now we can prove an optimal $L^2(\Omega)$ error estimate:

Theorem 3.4.1 *Given $(\theta, f) \in L^2(\Omega)^2 \times L^2(\Omega)$, let (β, w) be the solution of (3.1) and (β_h, w_h) the solution of (3.12). Then there exists a constant C, independent of t and h, such that*

$$\|(\beta, w) - (\beta_h, w_h)\|_{L^2(\Omega)^2\times L^2(\Omega)} \leq Ch\left(h + t\max_{K\in\mathcal{T}_h}\frac{\delta_K}{h_K}\right)|(\theta, f)|_t.$$

Proof. It is a direct consequence of Lemmas 3.4.1 and 3.4.3. □

Corollary 3.4.1 *For asymptotically parallelogram meshes the following error estimate holds:*

$$\|(\beta, w) - (\beta_h, w_h)\|_{\mathrm{L}^2(\Omega)^2 \times \mathrm{L}^2(\Omega)} \leq Ch^2 |(\theta, f)|_t.$$

Proof. In this case (3.42) reduces to

$$\|\operatorname{rot}(\varphi - R\varphi)\|_{0,K} \leq Ch_K \|\varphi\|_{2,K},$$

wich yields the estimate. □

Remark 3.4.1 *The asymptotically parallelogram assumption on the meshes is not necessary as long as $h > \alpha t$, for α fixed. Indeed, according to Theorem 3.4.1, for general regular meshes we have*

$$\|(\beta, w) - (\beta_h, w_h)\|_{\mathrm{L}^2(\Omega)^2 \times \mathrm{L}^2(\Omega)} \leq C_\alpha h^2 |(\theta, f)|_t.$$

Notice that $h > \alpha t$ is fulfilled in practice, with a reasonably large value of α.

3.5 The spectral problem

The aim of this section is to study how the eigenvalues and eigenfunctions of problem (3.13) approximate those of problem (3.2). We do this in the framework of the abstract spectral approximation theory as stated, for instance, in the monograph by Babuška and Osborn[7]. In order to use this theory, we define operators T and T_h associated to continuous and discrete spectral problems, respectively, and prove that the operator T_h converge to T in norm as h goes to zero. Let us remark that the results that follow are valid for both methods, MITC4 and DL4, although under the same Assumption 3.3.1 on the meshes as in the previous section for the former.

We consider the operator

$$T : \mathrm{L}^2(\Omega)^2 \times \mathrm{L}^2(\Omega) \to \mathrm{L}^2(\Omega)^2 \times \mathrm{L}^2(\Omega),$$

defined by $T(\theta, f) := (\beta, w)$, where $(\beta, w) \in \mathrm{H}_0^1(\Omega)^2 \times \mathrm{H}_0^1(\Omega)$ is the solution of the continuous load problem (3.1). Clearly T is compact and self-adjoint with respect to $(\cdot, \cdot)_t$. Then, apart from $\mu = 0$, its spectrum consists of a sequence of finite multiplicity real eigenvalues converging to zero. Note that λ is an eigenvalue of (3.2) if and only if $\mu := 1/\lambda$ is an eigenvalue of T with the same multiplicity and corresponding eigenfunctions.

As shown in [44], as the thickness $t \to 0$, each eigenvalue μ of problem (3.1) converge to some limit μ_0. Indeed, μ_0 are the eigenvalues of the operator associated with the Kirchhoff model of the same plate (see Lemma 2.1 in [44]). From now on, for simplicity, we assume that μ is an eigenvalue of T which converges to a simple eigenvalue μ_0 as t goes to zero (see Section 2 in [44] for further discussions).

Now, analogously to the continuous case, we introduce the following operators:

$$T_h : \mathrm{L}^2(\Omega)^2 \times \mathrm{L}^2(\Omega) \longrightarrow \mathrm{L}^2(\Omega)^2 \times \mathrm{L}^2(\Omega),$$

defined by $T_h(\theta, f) := (\beta_h, w_h)$, where $(\beta_h, w_h) \in H_h \times W_h$ is the solution of discrete problem (3.12). In this case T_h is also self-adjoint with respect to $(\cdot,\cdot)_t$. Clearly, the eigenvalues of T_h are given by $\mu_h := 1/\lambda_h$, with λ_h being the strictly positive eigenvalue of problem (3.13), and the corresponding eigenfunctions coincide.

As a consequence of Theorem 3.3.2, for each simple eigenvalue μ of T, there is exactly one aigenvalue μ_h of T_h converging to μ as h goes to zero (see for instance [61]). The following theorem shows optimal t-independent error estimates:

Theorem 3.5.1 *Let T be defined by (3.1) and T_h by (3.12) with $H_h = H_h^1$ or $H_h = H_h^2$. In the case $H_h = H_h^1$ we suppose that the meshes satisfy Assumption 3.3.1. Let μ and μ_h be simple eigenvalues of T and T_h, respectively, such that $\mu_h \to \mu$ as $h \to 0$. Let (β, w) and (β_h, w_h) be the corresponding eigenfunctions normalized in the same manner. Then, there exists $C > 0$ such that, for t and h small enough, there holds*

$$\|(\beta, w) - (\beta_h, w_h)\|_{\mathrm{H}^1(\Omega)^2 \times \mathrm{H}^1(\Omega)} \leq Ch.$$

Furthermore, for asymptotically parallelogram meshes, there holds

$$|\mu - \mu_h| \leq Ch^2$$

and

$$\|(\beta, w) - (\beta_h, w_h)\|_{\mathrm{L}^2(\Omega)^2 \times \mathrm{L}^2(\Omega)} \leq Ch^2.$$

Proof. The proof, which relies on Theorem 3.3.2 and Corrolary 3.4.1, are essentially the same as those of Theorem 2.1, 2.2, and 2.3 in [44]. □

3.6 Numerical experiments

In this section we summarize the numerical experiments carried out with both methods for the spectral problems.

First, we have tested both methods by reproducing all experiments in [44]. The obtained result in both cases are essentially the same as those in that paper. Therefore we do not include them here.

Second, we have tested the two methods by using different meshes, not necessarily satisfying the assumptions made to prove the theorems above. We have considered a square clamped moderately thick plate of side-length L and thickness-to-span ratio $t/L = 0.1$. We present the results for both types of elements using three families of meshes:

$\mathcal{T}_h^U$: The first one consists of uniform subdivisions of the domain into $N \times N$ subsquares, for $N = 4, 8, 16, \ldots$, (see Figure 3.6). Clearly, these are asymptotically parallelogram meshes and they satisfy Assumption 3.3.1.

$\mathcal{T}_h^A$: The second one consists of "uniform" refinements of a non-uniform mesh obtained by splitting the square into four quadrilateral. Each refinement step is obtained by subdividing each quadrilateral into other four, by connecting the midpoints of the opposite edges. Thus we obtain a family of $N \times N$ asymptotically parallelogram, shape regular meshes, as in Figure 3.7. These meshes satisfy Assumption 3.3.1.

$\mathcal{T}_h^T$: The last family consist of a partitions of the domain into $N \times N$ congruent trapezoids, all similar to the trapezoid with vertices $(0, 0)$, $(1/2, 0)$, $(1/2, 2/3)$ and $(0, 1/3)$, as in Figure 3.8. Clearly, these are not asymptotically parallelogram meshes and they do not satisfy Assumption 3.3.1.

Let us remark that the third family of meshes was used in [5, 6], to show that the order of convergence of some finite elements deteriorate on this meshes in spite of the fact that they are shape regular.

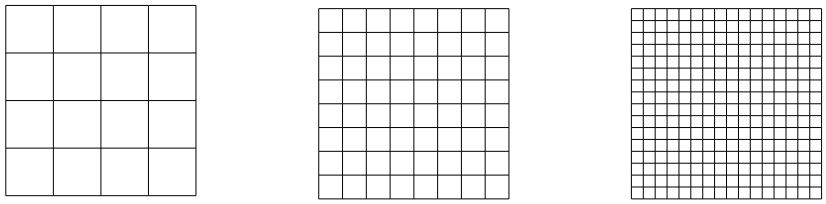

Figure 3.6: Uniform square meshes ($\mathcal{T}_h^U$).

We have computed approximations of the free vibration angular frequencies $\omega = t\sqrt{\lambda/\rho}$ corresponding to the lowest-frequency vibration modes of the plate. In order

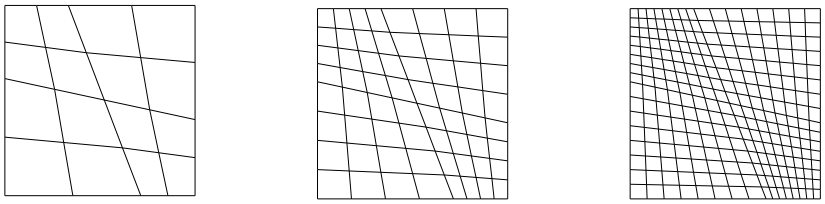

Figure 3.7: Asymptotically parallelogram meshes ($\mathcal{T}_h^A$).

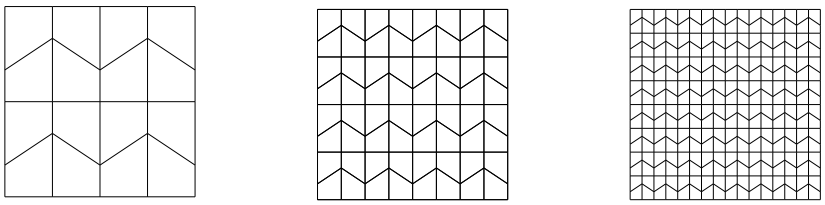

Figure 3.8: Trapezoidal meshes ($\mathcal{T}_h^T$).

to compare the obtained results with those in [3] we present the computed frequencies ω_{mn}^h in the following non-dimensional form:

$$\hat{\omega}_{mn} := \omega_{mn}^h L \left[\frac{2(1+\nu)\rho}{E}\right]^{1/2},$$

m and n being the numbers of half-waves occurring in the modes shapes in the x and y directions, respectively.

Tables 1 and 2 show the four lowest vibration frequencies computed by our method with three different meshes of each type, $\mathcal{T}_h^U$, $\mathcal{T}_h^A$, and $\mathcal{T}_h^T$. Each table includes also the values of the vibration frequencies obtained by extrapolating the computed ones as well as the estimated order of convergence. Finally, it also includes in the last column the results reported in [3]. In every case we have used a Poisson ratio $\nu = 0.3$ and a correction factor $k = 0.8601$. The reported non-dimensional frequencies are independent of the remaining geometrical and physical parameters, except for the thickness-to-span ratio.

It can be clearly seen that none of the two particular assumptions on the meshes (Assumption 3.3.1 and to be asymptotically parallelogram) are actually necessary. Indeed, both methods converge for the three types of meshes with an optimal order $\mathcal{O}(h^2)$.

Table 3.1: *MITC4.*

Mesh	Mode	$N = 16$	$N = 32$	$N = 64$	$extrap$	ORD	[3]
$\mathcal{T}_h^U$	$\hat{\omega}_{11}$	1.6055	1.5946	1.5919	1.5910	2.01	1.591
	$\hat{\omega}_{21}$	3.1042	3.0550	3.0429	3.0389	2.03	3.039
	$\hat{\omega}_{12}$	3.1042	3.0550	3.0429	3.0389	2.03	3.039
	$\hat{\omega}_{22}$	4.3534	4.2850	4.2681	4.2625	2.02	4.263
$\mathcal{T}_h^A$	$\hat{\omega}_{11}$	1.6073	1.5951	1.5921	1.5911	2.01	1.591
	$\hat{\omega}_{21}$	3.1094	3.0563	3.0433	3.0390	2.02	3.039
	$\hat{\omega}_{12}$	3.1190	3.0586	3.0438	3.0390	2.03	3.039
	$\hat{\omega}_{22}$	4.3711	4.2894	4.2692	4.2626	2.02	4.263
$\mathcal{T}_h^T$	$\hat{\omega}_{11}$	1.6112	1.5961	1.5923	1.5910	1.99	1.591
	$\hat{\omega}_{21}$	3.1129	3.0575	3.0436	3.0388	1.99	3.039
	$\hat{\omega}_{12}$	3.1306	3.0618	3.0446	3.0388	2.00	3.039
	$\hat{\omega}_{22}$	4.3916	4.2955	4.2708	4.2622	1.96	4.263

Table 3.2: *DL4.*

Mesh	Mode	$N = 16$	$N = 32$	$N = 64$	$extrap$	ORD	[3]
$\mathcal{T}_h^U$	$\hat{\omega}_{11}$	1.5956	1.5922	1.5913	1.5909	1.97	1.591
	$\hat{\omega}_{21}$	3.0711	3.0470	3.0409	3.0388	1.99	3.039
	$\hat{\omega}_{12}$	3.0711	3.0470	3.0409	3.0388	1.99	3.039
	$\hat{\omega}_{22}$	4.3136	4.2754	4.2657	4.2624	1.98	4.263
$\mathcal{T}_h^A$	$\hat{\omega}_{11}$	1.5929	1.5915	1.5912	1.5911	1.94	1.591
	$\hat{\omega}_{21}$	3.0592	3.0441	3.0402	3.0388	1.96	3.039
	$\hat{\omega}_{12}$	3.0732	3.0476	3.0411	3.0389	1.98	3.039
	$\hat{\omega}_{22}$	4.3136	4.2756	4.2658	4.2624	1.96	4.263
$\mathcal{T}_h^T$	$\hat{\omega}_{11}$	1.5927	1.5914	1.5911	1.5910	2.21	1.591
	$\hat{\omega}_{21}$	3.0606	3.0445	3.0403	3.0388	1.94	3.039
	$\hat{\omega}_{12}$	3.0654	3.0453	3.0405	3.0390	2.05	3.039
	$\hat{\omega}_{22}$	4.3131	4.2754	4.2657	4.2623	1.96	4.263

Chapter 4

Computation of the vibration modes of plates and shells by low-order MITC quadrilateral finite element

This chapter deals with the approximation of the vibration modes of plates and shells using the MITC4 finite element method. We use the classical Naghdi model over a reference domain. We assess the performance of this approach for both structures by means of numerical experiments.

4.1 Introduction.

There is a consensus that there are still many difficulties in analyzing general shell structures. Together with the importance of such structures, this has led to a big amount of work on this subject, during the last years. This work has been made by different communities under different points of view.

In a general framework, following [31], we can classify the shell finite elements in two big families: finite element methods that result from the discretization of shell mathematical models (namely *two-dimensional methods* or *classical methods*), where the unknowns are given on the mid-surface of the shell (see [21, 33, 36]), and methods based on "degenerating" a 3D solid finite element into a shell element by using some kinematic assumptions for describing the variation of displacements across the thickness of the shell structure, namely *general shell elements* (see [8, 11, 23]). Such distinction has caused a significant degree of confusion between the two main communities interested in solving the problem: numerical mathematicians and

engineers.

Indeed, finite element methods derived from a shell model are easier to analyze mathematically. Their solutions can be shown to approximate, with a certain accuracy, the continuous solution of the shell model and, in fact, *a priori* error estimates can be given (see [21]). However, the constants in these estimates depend on the thickness of the shell. This kind of methods are usually chosen by mathematicians. Its main drawback is that it is necessary an explicit knowledge of the chart, since the computation requires an extensive use of it. General shell elements provide more versatility, because they do not require the exact chart and can employ general 3D constitutive laws. However, due precisely to its specific construction, which does not rely on any shell theory, a mathematical analysis of such a procedure is difficult to achieve.

Classical models are not very often encountered in practice. Recently the relationship between these two families of methods has been put into account in [34, 31], where, assuming Reissner-Mindlin hypotheses (i.e., any normal fiber is supposed to remain straight and unstretched during the deformation), it is shown that both models are asymptotically equivalent as regards to their asymptotic solutions when the thickness parameter tends to zero. This result shows the convenience of advancing in the study of classical methods, to find theoretical results that could later be useful for general shell methods. In this context, for the present work, we consider one of the most important classical models: Naghdi, which is based on Reissner-Mindlin hypotheses.

Regarding to the discretization of the problem, MITC finite element methods (introduced by Bathe and Dvorkin in [10]), or variants of them, are very likely the most used in practice. A great number of papers dealing with the mathematical analysis of these methods when applied to discretize Reissner-Mindlin plate equations (what can be understood as a particular simpler case of Naghdi shell model) have been published; see [9, 29, 46, 44, 73], for example. In these papers, optimal order error estimates, valid uniformly on the plate thickness, have been obtained for several methods.

The most commonly used elements in engineering applications are the isoparametric quadrilaterals, which are the basis of the low-order MITC4(indeed, the original Bathe-Dvorkin paper deals with these elements). For plate problems, this element have been mathematically analyzed (see [9, 43]) and optimal error estimates have been provided. Nevertheless, mathematical results when these methods apply to a non-trivial shell are not known.

In this chapter we consider the problem of computing the free vibration modes of a shell. This is a problem of great practical interest, but relatively understud-

ied in the bibliography. We test the efficiency of the MITC4 methods to compute the corresponding vibration frequencies. Since these frequencies are single numbers which depend on the behavior of the whole shell, we believe that the quality of its computation provides an overall assessment of the method.

The outline of the rest of the chapter is as follows. In Section 4.2 we state the vibration problem for the Naghdi shell model and introduce the MITC4 method to discretize it. In Section 4.3 we treat the particular case of plate vibrations. We extend the numerical results in [43] to general boundary conditions and show that, in all cases and for general meshes, the order of convergence is optimal independently of the thickness. Finally, in Section 4.4, we assess the performance of the method by calculating the free vibrations of some benchmark shell cases, suggested in [33].

4.2 Statement of the problem.

Let us briefly recall the classical definitions and notation of differential geometry that we need, see [21, 33] for more details. We employ Greek indexes ranging over 1 and 2. We also use the convention of summation over the repeated indexes up and down.

Let $\Omega \subset \mathbb{R}^2$ be the reference domain. We assume that there exists a single chart ϕ, an one-to-one mapping from $\overline{\Omega}$ into $\mathbb{R}^3$, which transforms Ω on the mid-surface of the shell, $\mathcal{S} = \phi(\overline{\Omega})$ (see Figure 4.1). We denote by t the (constant) thickness of the shell.

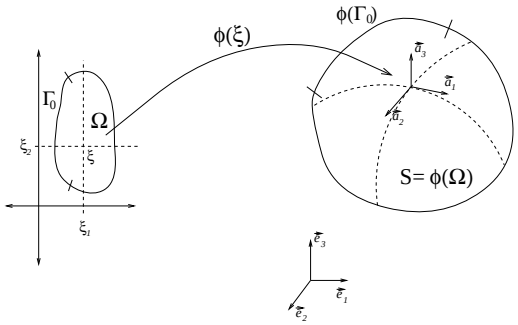

Figure 4.1: middle surface of the shell.

We denote $(a_{\alpha\beta})$ the first fundamental form of the mid-surface, $(a^{\alpha\beta}) := (a_{\alpha\beta})^{-1}$ its contravariant form, and $(b_{\alpha\beta})$ the second fundamental form. We denote $b_\alpha^\beta := a^{\beta\lambda} b_{\lambda\alpha}$. Then, the third fundamental form is given by $c_{\alpha\beta} := b_\alpha^\lambda b_{\lambda\beta}$. Let a be the determinant of the matrix $(a^{\alpha\beta})$.

We need to provide an appropriate functional framework to define the variational formulation. Then we define

$$\mathcal{U} := \{(\vec{u}, \underline{\theta}) : \vec{u} \in \mathrm{H}^1(\Omega)^3,\, \underline{\theta} \in \mathrm{H}^1(\Omega)^2\} \cap \mathcal{BC},$$

where $\mathcal{BC}$ symbolically denotes the essential boundary conditions prescribed, $\vec{u} := (u_1, u_2, u_3)$ denotes a three dimensional vector field that corresponds to the displacement of the mid-surface, and $\underline{\theta} := (\theta_1, \theta_2)$ denotes a two dimensional vector field associated to the rotation of the vector orthogonal to the mid-surface.

The free vibration modes for the Naghdi model of the shell are the solutions of the following spectral problem (see [21]):

SP: *Find* $\omega \in \mathbb{R}^+$ *and* $0 \neq (\vec{u}, \underline{\theta}) \in \mathcal{U}$ *such that*

$$a\Big((\vec{u}, \underline{\theta}), (\vec{v}, \underline{\eta})\Big) = \omega^2 b\Big((\vec{u}, \underline{\theta}), (\vec{v}, \underline{\eta})\Big) \qquad \forall\, (\vec{v}, \underline{\eta}) \in \mathcal{U}.$$

The bilinear form $b(\cdot, \cdot)$ is given by

$$b\Big((\vec{u}, \underline{\theta}), (\vec{v}, \underline{\eta})\Big) := \rho \int_\Omega \left(t a^{\alpha\beta} u_\alpha v_\beta + t u_3 v_3 + \frac{t^3}{12} a^{\alpha\beta} \theta_\alpha \eta_\beta \right) dS,$$

where ρ is the density of the shell and $dS := \sqrt{a}\, d\xi_1\, d\xi_2$ the surface measure.

The bilinear form $a(\cdot, \cdot)$ can be written as the sum of a bending term A, membrane term D^m, and shear term D^s; i.e.,

$$a\Big((\vec{u}, \underline{\theta}), (\vec{v}, \underline{\eta})\Big) := t^3 A\Big((\vec{u}, \underline{\theta}), (\vec{v}, \underline{\eta})\Big) + t D^m(\vec{u}, \vec{v}) + t k D^s\Big((\vec{u}, \underline{\theta}), (\vec{v}, \underline{\eta})\Big),$$

with k being a correction factor for the shear term and

$$\begin{aligned}
A\Big((\vec{u}, \underline{\theta}), (\vec{v}, \underline{\eta})\Big) &:= \int_\Omega \frac{E^{\alpha\beta\lambda\mu}}{12} \chi_{\alpha\beta}(\vec{u}, \underline{\theta}) \chi_{\lambda\mu}(\vec{v}, \underline{\eta})\, dS, \\
D^m(\vec{u}, \vec{v}) &:= \int_\Omega E^{\alpha\beta\lambda\mu} \gamma_{\alpha\beta}(\vec{u}) \gamma_{\lambda\mu}(\vec{v})\, dS, \\
D^s\Big((\vec{u}, \underline{\theta}), (\vec{v}, \underline{\eta})\Big) &:= \int_\Omega G^{\alpha\beta} \varphi_\alpha(\vec{u}, \underline{\theta}) \varphi_\beta(\vec{v}, \underline{\eta})\, dS.
\end{aligned}$$

The bending strain operator χ, the membrane strain operator γ, and the shear strain operator φ, are expressed as

$$\begin{aligned}
\chi_{\alpha\beta}(\vec{u}, \underline{\theta}) &:= \frac{1}{2}\left[\theta_{\alpha|\beta} + \theta_{\beta|\alpha} - b^\mu_\alpha u_\mu - b^\mu_\beta u_\mu\right] + c_{\alpha\beta} u_3, \\
\gamma_{\alpha\beta}(\vec{u}) &:= \frac{1}{2}\left[u_{\alpha|\beta} + u_{\beta|\alpha}\right] + b_{\alpha\beta} u_3, \\
\varphi_\alpha(\vec{u}, \underline{\theta}) &:= u_{3,\alpha} - b^\mu_\alpha u_\mu + \theta_\alpha.
\end{aligned}$$

In the definition above, the vertical bar denotes the covariant differentiation. The tensors present in the stiffness term correspond to the material properties and are given by

$$\begin{aligned} E^{\alpha\beta\lambda\mu} &:= \frac{E}{2(1+\nu)}\left[a^{\alpha\lambda}a^{\beta\mu} + a^{\alpha\mu}a^{\beta\lambda} + \frac{2\nu}{1-\nu}a^{\alpha\beta}a^{\lambda\mu}\right], \\ G^{\alpha\beta} &:= \frac{E}{2(1+\nu)}a^{\alpha\beta}, \end{aligned}$$

where E and ν denote, respectively, Young's modulus and Poisson's ratio for the material.

We use the MITC4 method, introduced in [10], to approximate the solutions of problem **SP**. This method is based on discretizing the bending and membrane terms using the usual isoparametric quadratic finite elements and relaxing the shear term by introducing a reduction operator.

Let us now specify this method in our context. Let $\mathcal{T}_h$ be a family of decompositions of Ω into convex quadrilaterals. Let $\widehat{K}$ be the unit square reference element. We denote by $Q_{i,j}(\widehat{K})$ the space of polynomials of degree less than or equal to i in the first variable and to j in the second one. We set $Q_k(\widehat{K}) = Q_{k,k}(\widehat{K})$.

Let $K \in \mathcal{T}_h$. We denote by F_K the bilinear mapping of $\widehat{K}$ onto K, its Jacobian matrix by DF_K and the determinant of DF_K by J_{F_K}. We set $Q(K) := \{p : p \circ F_K \in Q_1(\widehat{K})\}$ and define the finite element space

$$\mathcal{U}_h := \left\{(\vec{u}_h, \underline{\theta}_h) : \ \vec{u}_h|_K \in Q_1(K)^3, \ \underline{\theta}_h|_K \in Q_1(K)^2 \quad \forall K \in \mathcal{T}_h\right\} \cap \mathcal{BC}.$$

Then, the discretized variational problem is

$\mathbf{SP_h}$: *Find* $\omega_h \in \mathbb{R}^+$ *and* $0 \neq (\vec{u}_h, \underline{\theta}_h) \in \mathcal{U}_h$ *such that*

$$a_h\Big((\vec{u}_h, \underline{\theta}_h), (\vec{v}_h, \underline{\eta}_h)\Big) = \omega_h^2 b\Big((\vec{u}_h, \underline{\theta}_h), (\vec{v}_h, \underline{\eta}_h)\Big) \qquad \forall\, (\vec{v}_h, \underline{\eta}_h) \in \mathcal{U}_h.$$

The bilinear form $a_h(\cdot,\cdot)$ is a perturbed form of $a(\cdot,\cdot)$. It comes from introducing in the shear term a reduction operator $\varphi \longmapsto \mathbf{R}\varphi$, with $\mathbf{R}\varphi|_K \in Q_{0,1}(K) \times Q_{1,0}(K)$, $\forall K \in \mathcal{T}_h$:

$$\begin{aligned} a_h\Big((\vec{u}_h, \underline{\theta}_h), (\vec{v}_h, \underline{\eta}_h)\Big) &:= t^3 A\Big((\vec{u}_h, \underline{\theta}_h), (\vec{v}_h, \underline{\eta}_h)\Big) \\ &\quad + tD^m(\vec{u}_h, \vec{v}_h) + tkD_h^s\Big((\vec{u}_h, \underline{\theta}_h), (\vec{v}_h, \underline{\eta}_h)\Big), \end{aligned}$$

with

$$D_h^s\Big((\vec{u}_h, \underline{\theta}_h), (\vec{v}_h, \underline{\eta}_h)\Big) := \int_\Omega G^{\alpha\beta}\Big(\mathbf{R}\varphi(\vec{u}_h, \underline{\theta}_h)\Big)_\alpha \Big(\mathbf{R}\varphi(\vec{v}_h, \underline{\eta}_h)\Big)_\beta \, dS.$$

Let us emphasize that, since this finite element procedure is based on meshes that are constructed in the reference domain Ω, the numerical computations require an extensive use of the chart ϕ.

4.3 Plates.

The Reissner-Mindlin formulation for plates can be seen as a special case of the general shell formulation. We consider only the plate transversal displacements which, in this case, can be dealt with separately from the in-plane terms. The displacement components u_1 and u_2 of the mid-surface can be written in terms of the rotation of the transverse fiber to the mid-surface of the plate. Then, if we define the finite element space

$$\mathcal{U}_h^P := \left\{(v_h, \underline{\theta}_h) : \ v_h|_K \in Q_1(K), \ \underline{\theta}_h|_K \in Q_1(K)^2 \quad \forall K \in \mathcal{T}_h\right\} \cap \mathcal{BC},$$

the computed free vibration modes for the plate are the solutions of the following problem (see [43]):

PP$_\mathbf{h}$: *Find* $\omega_h \in \mathbb{R}^+$ *and* $0 \neq (u_{3h}, \underline{\theta}_h) \in \mathcal{U}_h^P$ *such that:*

$$\begin{aligned} t^3 a(\underline{\theta}_h, \underline{\eta}_h) \ + \ \kappa t \int_\Omega \mathbf{R}(\nabla u_{3h} - \underline{\theta}_h) \cdot \mathbf{R}(\nabla v_h - \underline{\eta}_h) \\ = \omega_h^2 \rho \left(t \int_\Omega u_{3h} v_h + \frac{t^3}{12} \int_\Omega \underline{\theta}_h \cdot \underline{\eta}_h \right) \qquad \forall (v_h, \underline{\theta}_h) \in \mathcal{U}_h^P. \end{aligned}$$

Here $\kappa := Ek/2(1+\nu)$ is the shear modulus (with k a correction factor), meanwhile the bilinear form a is given by

$$a(\underline{\theta}_h, \underline{\eta}_h) := \frac{E}{12(1-\nu^2)} \int_\Omega \left[\sum_{i,j=1}^{2} (1-\nu) \varepsilon_{ij}(\underline{\theta}_h) \varepsilon_{ij}(\underline{\eta}_h) + \nu \, \mathrm{div}\, \underline{\theta}_h \, \mathrm{div}\, \underline{\eta}_h \right],$$

where ε_{ij} denote the components of the linear strain tensor.

MITC plate elements have a sound mathematical basis and they are reliable and efficient. In particular, for the MITC4 element, a mathematical analysis of convergence is provided in [9], where uniform meshes of square elements are used. This assumption has been weakened in [43], where, by using macro-element techniques, optimal H^1 and L^2 error estimates are proved. However, the L^2-estimates are obtained by assuming that the meshes are formed by higher order perturbations of parallelograms (i.e., asymptotically parallelogram meshes). All these estimates are independent of the mesh size h and of the plate thickness t. Moreover, in the same reference and under the same assumptions on the meshes, it is also proved that the order of convergence for the vibration frequencies of the corresponding vibration problem is optimal when the MITC4 method is used.

On the other hand, it has been recently put into account that error estimates valid for meshes of rectangles cannot be directly extended to meshes of general quadrilaterals. Even more, the order of convergence can deteriorate when non-standard finite

elements are used in distorted quadrilaterals, even if they fulfill the usual shape regularity assumption (see [5, 6]). Then, it is important to verify if the hypotheses on the meshes in [43] are essential or if they are just a technicality.

Numerical experiments for clamped plates have been reported in [43]. They show that the order of convergence for the method is optimal, even in some cases not covered by the theory. In the rest of this section we report numerical experiments with more general boundary conditions and different meshes, not all satisfying the assumptions in [43].

We consider square plates of side-length L and thickness-to-span ratio ranging from moderately thick to very thin. We report the results for boundary conditions S-C-S-F (S stands for hard simply supported, C for clamped and F for free). We use four different families of meshes:

$\mathcal{T}_h^U$: Uniform subdivisions of the domain into $N \times N$ sub-squares, for $N = 4, 8, 16, \ldots$, (see Figure 4.2).

$\mathcal{T}_h^A$: Asymptotic parallelogram meshes given by "uniform" refinements of a non-uniform mesh obtained by splitting the original square into four quadrilaterals. Each refinement step is obtained by subdividing each quadrilateral into other four by connecting the midpoints of the opposite edges (see Figure 4.3).

$\mathcal{T}_h^T$: Partitions of the domain into $N \times N$ congruent trapezoids, all similar to the trapezoid with vertexes $(0,0)$, $(1/2,0)$, $(1/2,2/3)$ and $(0,1/3)$, as in Figure 4.4 (see [5]). These meshes do not satisfy the assumptions in [43].

$\mathcal{T}_h^R$: Random partitions of the domain with N element edges in each side of the plate, as in Figure 4.5. These meshes do not satisfy the assumptions in [43].

Note that in all cases $h \approx C/N$, with C a positive constant.

Let us remark that the third family of meshes was used in [5, 6] to show that the order of convergence of some finite elements deteriorate on this meshes, in spite of the fact that they are shape regular.

We have computed approximations of the free vibration angular frequencies corresponding to the lowest-frequency vibration modes of the plate. In order to compare the obtained results with those in [3], we present the computed frequencies, ω_{mn}^h, in the following non-dimensional form:

$$\hat{\omega}_{mn} := \omega_{mn}^h L \left[\frac{2(1+\nu)\rho}{E}\right]^{1/2},$$

m and n being the number of half-waves occurring in the modes shapes in the x and y directions, respectively.

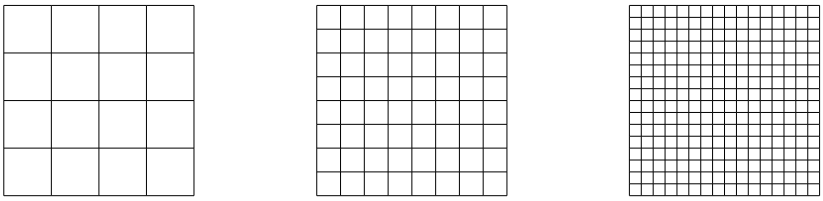

Figure 4.2: Uniform square meshes $\mathcal{T}_h^U$.

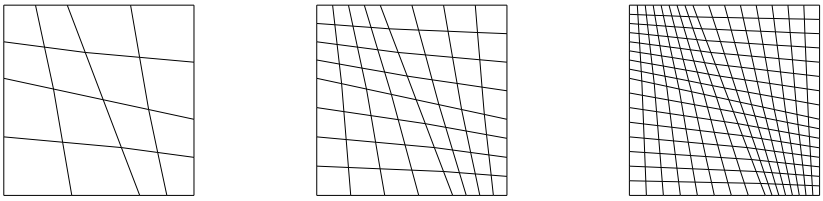

Figure 4.3: Asymptotically parallelogram meshes $\mathcal{T}_h^A$.

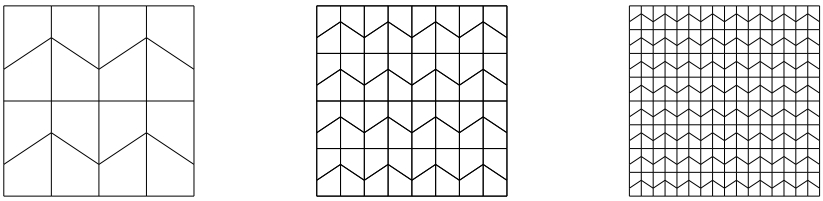

Figure 4.4: Trapezoidal meshes $\mathcal{T}_h^T$.

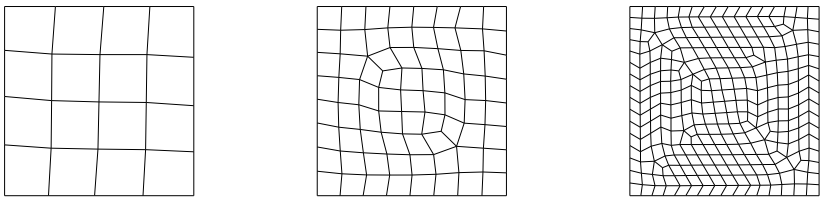

Figure 4.5: Random meshes $\mathcal{T}_h^R$.

We consider first the case of a plate with thickness-to-span ratio t/L=0.1. This choice was made to allow for comparison with the result of [3]. Table 4.1 shows

the four lowest vibration frequencies, $\hat{\omega}_{11}$, $\hat{\omega}_{12}$, $\hat{\omega}_{21}$, and $\hat{\omega}_{22}$, computed with our code with four different meshes of each type $\mathcal{T}_h^U$, $\mathcal{T}_h^A$, $\mathcal{T}_h^T$, and $\mathcal{T}_h^R$. The table also includes more accurate values of the vibration frequencies obtained by extrapolating the frequencies computed with highly refined meshes. Finally, it includes in the last column the corresponding results reported in [3], too. We have used a Poisson ratio $\nu = 0.3$ and a correction factor $k = 0.822$. The reported non-dimensional frequencies are independent of the remaining geometrical and physical parameters, except for the thickness-to-span ratio.

It can be clearly seen from Table 4.1 that the method converges to the correct solution even for arbitrary isoparametric quadrilateral meshes like those of Figures 4.4 and 4.5, and for arbitrary boundary conditions. Let us remark that the available mathematical analysis for this method is valid only for clamped plates and does not cover this kind of meshes (see [9, 43]).

Table 4.1: Vibration frequencies for the moderately thick plate ($t/L = 0.1$).

Mesh	Mode	$N = 16$	$N = 32$	$N = 64$	Extrap.	[3]
$\mathcal{T}_h^U$	$\hat{\omega}_{11}$	0.6004	0.5983	0.5977	0.5975	0.598
	$\hat{\omega}_{21}$	1.4955	1.4860	1.4835	1.4826	1.483
	$\hat{\omega}_{12}$	1.9172	1.8922	1.8859	1.8838	1.884
	$\hat{\omega}_{22}$	2.7596	2.7300	2.7224	2.7198	2.721
$\mathcal{T}_h^A$	$\hat{\omega}_{11}$	0.6009	0.5984	0.5977	0.5975	0.598
	$\hat{\omega}_{21}$	1.4975	1.4866	1.4836	1.4826	1.483
	$\hat{\omega}_{12}$	1.9212	1.8932	1.8862	1.8838	1.884
	$\hat{\omega}_{22}$	2.7669	2.7320	2.7229	2.7198	2.721
$\mathcal{T}_h^T$	$\hat{\omega}_{11}$	0.6017	0.5986	0.5978	0.5975	0.598
	$\hat{\omega}_{21}$	1.4996	1.4871	1.4838	1.4829	1.483
	$\hat{\omega}_{12}$	1.9281	1.8950	1.8866	1.8838	1.884
	$\hat{\omega}_{22}$	2.7803	2.7356	2.7239	2.7196	2.721
$\mathcal{T}_h^R$	$\hat{\omega}_{11}$	0.6009	0.5983	0.5977	0.5975	0.598
	$\hat{\omega}_{21}$	1.4978	1.4865	1.4837	1.4827	1.483
	$\hat{\omega}_{12}$	1.9183	1.8918	1.8859	1.8842	1.884
	$\hat{\omega}_{22}$	2.7699	2.7317	2.7229	2.7203	2.721

Figures 4.6–4.9 show the vibration shapes and the error curves for each vibration mode computed with the four families of meshes. Notice that in all cases the method

converges with an optimal quadratic order.

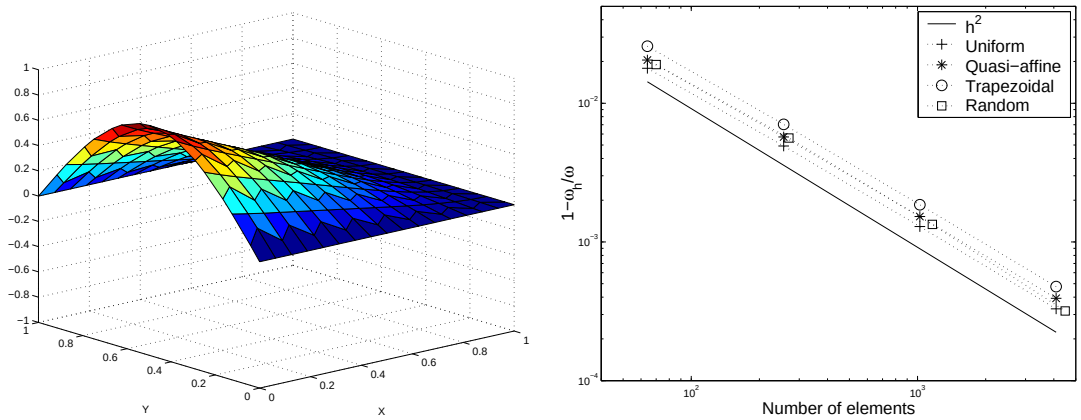

Figure 4.6: First mode of the moderately thick plate. Deformed plate and error curve.

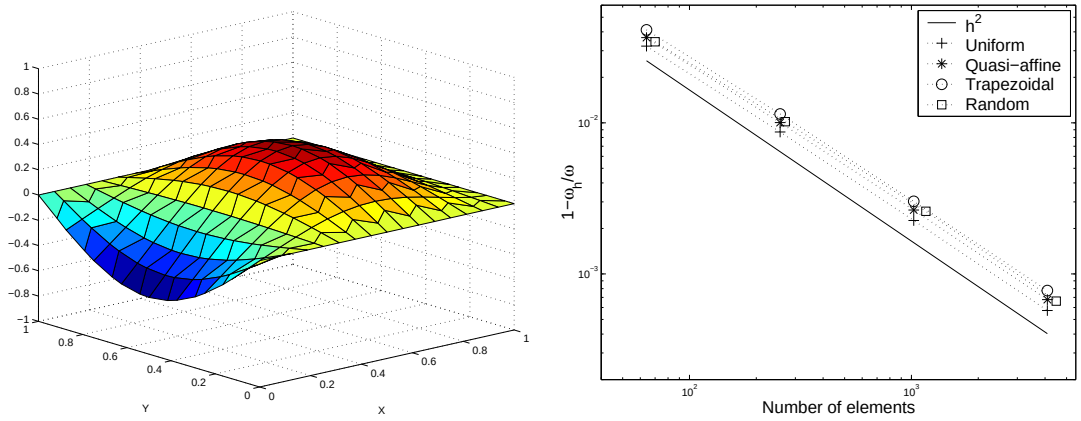

Figure 4.7: Second mode of the moderately thick plate. Deformed plate and error curve.

In order to assess the quality of the method for very thin plates, we consider a thickness-to-span ratio $t/L = 0.0001$. Table 4.2 shows the four lowest computed vibration frequencies. As in the previous case, extrapolated more accurate values are included. Note that the discrepancy between these extrapolated values and those obtained with the coarsest meshes are less than 5% in all cases.

Figures 4.10–4.13 show the vibration shapes and the error curves for the four lowest-frequency vibration modes in this case. For this very thin plate, the uniform and quasi-affine meshes produce slightly better approximations than the other two

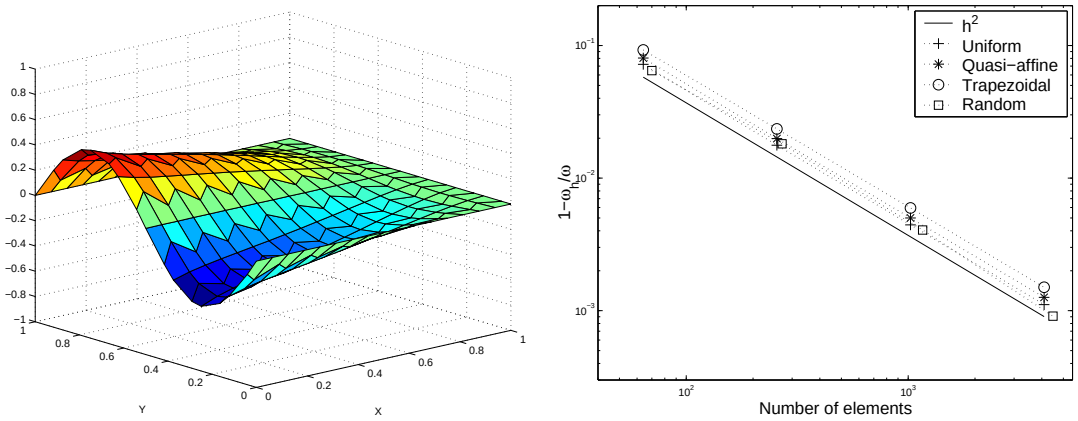

Figure 4.8: Third mode of the moderately thick plate. Deformed plate and error curve.

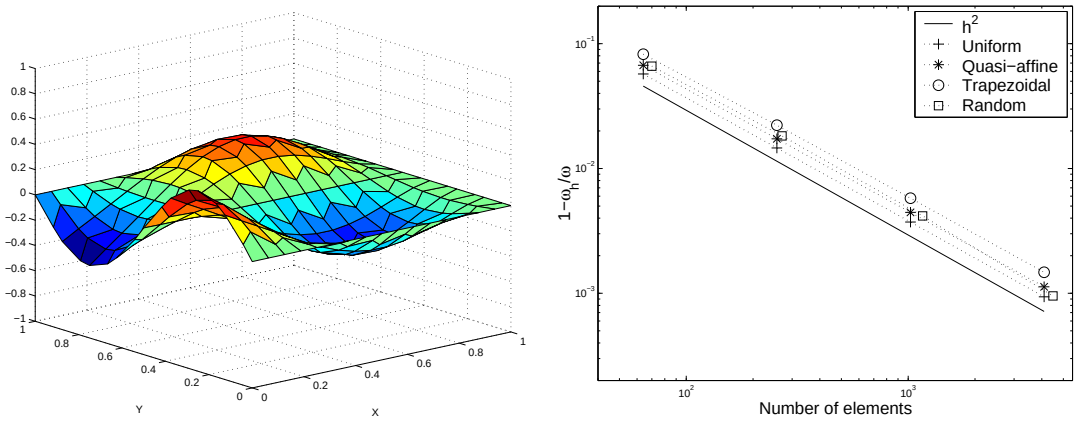

Figure 4.9: Fourth mode of the moderately thick plate. Deformed plate and error curve.

general quadrilateral meshes. Moreover, the order of convergence for uniform and quasi-affine meshes is exactly 2, whereas for the other two meshes it ranges between 1.8 and 1.9.

4.4 Shells.

In this section we report numerical results corresponding to the solution of problem $\mathbf{SP_h}$. We consider two different numerical examples: a free cylindrical shell and a clamped hemispherical one. Both are suggested and analyzed in [33], where load problems are considered.

Table 4.2: Vibration frequencies for the thin plate ($t/L = 0.0001$).

Mesh	Mode	$N = 16$	$N = 32$	$N = 64$	Extrap.
$\mathcal{T}_h^U$	$\hat{\omega}_{11}$	0.6213×10^{-3}	0.6196×10^{-3}	0.6192×10^{-3}	0.6190×10^{-3}
	$\hat{\omega}_{21}$	1.6255×10^{-3}	1.6164×10^{-3}	1.6141×10^{-3}	1.6134×10^{-3}
	$\hat{\omega}_{12}$	2.0721×10^{-3}	2.0440×10^{-3}	2.0371×10^{-3}	2.0350×10^{-3}
	$\hat{\omega}_{22}$	3.1200×10^{-3}	3.0860×10^{-3}	3.0776×10^{-3}	3.0749×10^{-3}
$\mathcal{T}_h^A$	$\hat{\omega}_{11}$	0.6217×10^{-3}	0.6197×10^{-3}	0.6192×10^{-3}	0.6190×10^{-3}
	$\hat{\omega}_{21}$	1.6274×10^{-3}	1.6169×10^{-3}	1.6142×10^{-3}	1.6134×10^{-3}
	$\hat{\omega}_{12}$	2.0765×10^{-3}	2.0451×10^{-3}	2.0374×10^{-3}	2.0350×10^{-3}
	$\hat{\omega}_{22}$	3.1282×10^{-3}	3.0880×10^{-3}	3.0781×10^{-3}	3.0749×10^{-3}
$\mathcal{T}_h^T$	$\hat{\omega}_{11}$	0.6233×10^{-3}	0.6203×10^{-3}	0.6194×10^{-3}	0.6190×10^{-3}
	$\hat{\omega}_{21}$	1.6313×10^{-3}	1.6181×10^{-3}	1.6146×10^{-3}	1.6133×10^{-3}
	$\hat{\omega}_{12}$	2.0926×10^{-3}	2.0518×10^{-3}	2.0396×10^{-3}	2.0351×10^{-3}
	$\hat{\omega}_{22}$	3.1499×10^{-3}	3.0948×10^{-3}	3.0800×10^{-3}	3.0745×10^{-3}
$\mathcal{T}_h^R$	$\hat{\omega}_{11}$	0.6218×10^{-3}	0.6197×10^{-3}	0.6192×10^{-3}	0.6190×10^{-3}
	$\hat{\omega}_{21}$	1.6283×10^{-3}	1.6171×10^{-3}	1.6143×10^{-3}	1.6131×10^{-3}
	$\hat{\omega}_{12}$	2.0734×10^{-3}	2.0437×10^{-3}	2.0371×10^{-3}	2.0340×10^{-3}
	$\hat{\omega}_{22}$	3.1333×10^{-3}	3.0882×10^{-3}	3.0782×10^{-3}	3.0741×10^{-3}

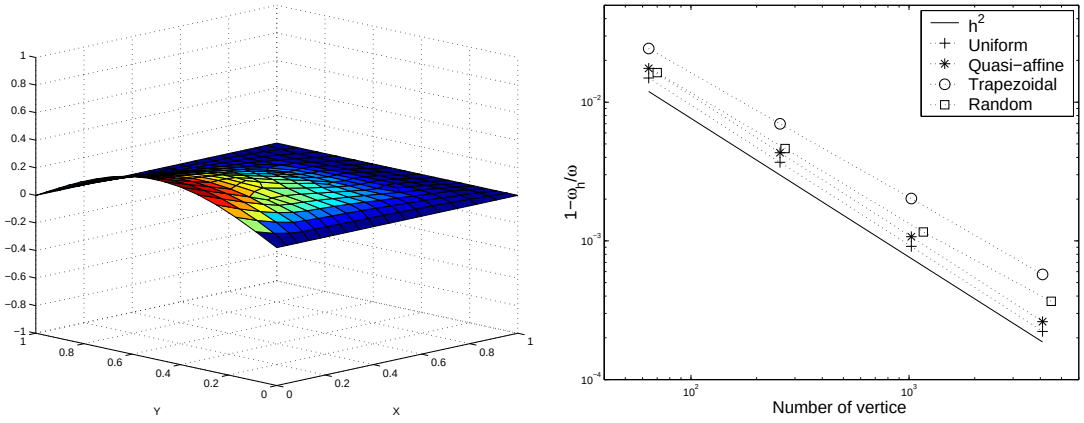

Figure 4.10: First mode of the thin plate. Deformed plate and error curve.

The first example consists of a cylinder of length 10 m and radius 1.8 m with free ends. We take the following values for the physical parameters of the cylinder,

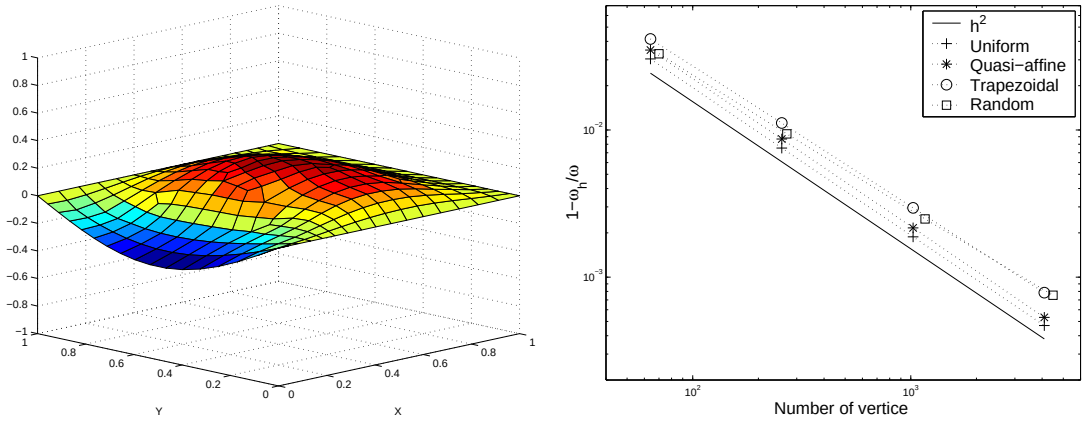

Figure 4.11: Second mode of the thin plate. Deformed plate and error curve.

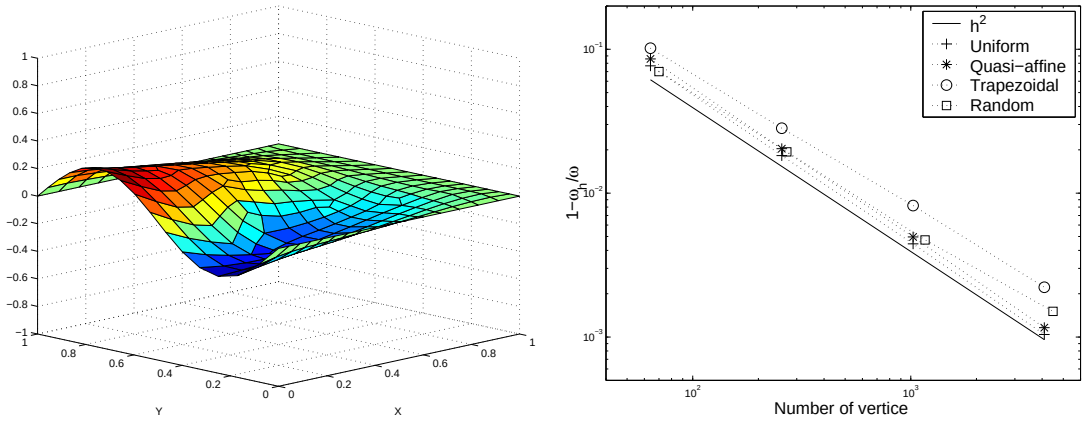

Figure 4.12: Third mode of the thin plate. Deformed plate and error curve.

which correspond to a type of steel:

- density: $\rho = 8000$ Kg/m^3,
- Young modulus: $E = 200 \times 10^9$ Pa,
- Poisson coefficient: $\nu = 0.3$.

By using cylindrical coordinates we are led to a reference domain $\Omega = [0,1] \times [0,1]$. We take uniform meshes of squares with N elements on each side. The correction factor in the shear term is taken as $k = \frac{5}{6}$.

First, we validate our code by comparing the results that we obtain with those in [32] for a moderately thick cylinder of thickness $t = 0.4$ m. The values in this

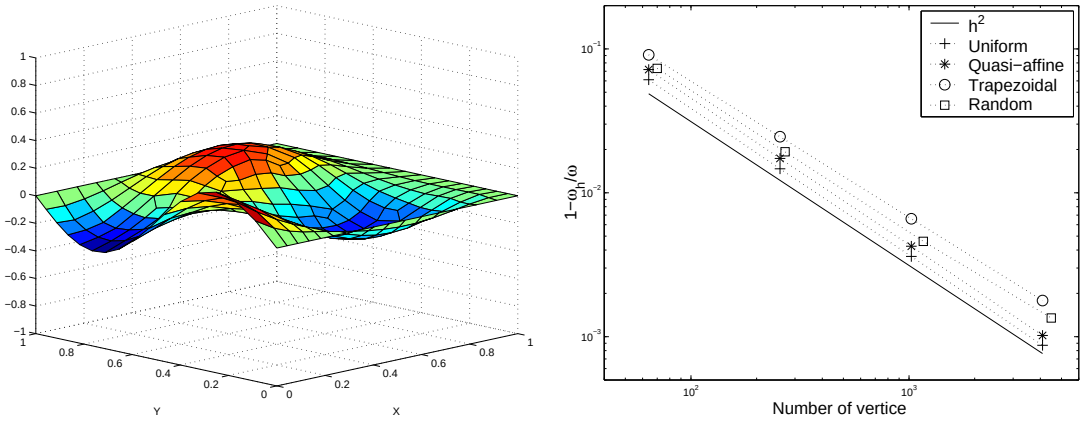

Figure 4.13: Fourth mode of the thin plate. Deformed plate and error curve.

reference have been obtained by using Q_2 3D-elements with a single layer of elements across the thickness, which is equivalent to a general shell model.

Table 4.3 shows some of the lowest vibration frequencies of the cylinder that we have computed. They are ordered according to their circumferential and axial mode numbers n and m, respectively. This table also includes more accurate values of the vibration frequencies obtained by extrapolating the frequencies computed with highly refined meshes. Finally, it includes the results in [32], too.

Second, we evaluate the behavior of MITC4 with respect to the thickness of the shell, by considering a similar cylinder but with thickness $t = 0.0004$ m. Table 4.4 shows some of the lowest vibration frequencies of this thin cylinder. We also include more accurate extrapolated values.

It can be seen from Tables 4.3 and 4.4 that the method is locking-free for the computation of the vibration modes with low circumferential number (n=0 and n=1) as well as for torsional modes. Instead, for larger circumferential numbers (n=2, n=3, etc) the computed values of the vibration frequencies are close to the exact ones only for highly refined meshes and for not very thin shells. Indeed, for these modes, the discrepancy between the computed frequencies becomes more remarkable as the thickness diminishes. This shows that the method locks for circumferential numbers greater than 1 in the case of free cylindrical shells.

Figures 4.14 and 4.15 show the deformed shells and the displacement vector fields associated to the first torsional mode and to the mode n=0, m=0, respectively.

As a second numerical example, we consider a fully clamped hemisphere of radius $R = 10$ m. The physical parameters of the material are the same as in the previous example and we take $k = \frac{5}{6}$ as correction factor for the shear term.

We describe the hemisphere by means of a stereographic projection onto the

Table 4.3: Vibration frequencies for the free cylindrical shell with thickness $t = 0.4$ m.

Mode	$N = 10$	$N = 20$	$N = 40$	Extrap.	[32]
torsion	156.6354	156.1536	156.0333	155.9930	155.05
n=0, m=0	246.3435	245.5347	245.3311	245.2629	243.50
torsion	317.1372	313.2679	312.3042	311.9879	310.17
n=0, m=1	412.2772	409.9354	409.3174	409.0949	377.46
n=0, m=2	437.4810	436.6099	436.3766	436.2912	394.29
n=1, m=0	157.4533	147.3331	144.8173	143.9885	150.58
n=1, m=1	242.0222	234.4688	232.5655	231.9264	223.17
n=1, m=2	322.4530	314.9537	313.0779	312.4533	296.79
n=2, m=0	192.0059	111.8841	85.9812	73.6300	63.26
n=2, m=1	195.1902	115.0604	89.3939	77.2358	67.16
n=2, m=2	216.3747	142.1747	120.7520	112.0132	107.63
n=2, m=3	267.0965	206.3499	190.7752	185.3610	185.23
n=3, m=0	445.6543	264.8193	221.1085	207.2203	173.99
n=3, m=1	449.5729	269.2100	225.4787	211.3448	179.06
n=3, m=2	466.4737	287.7182	232.5564	208.1327	200.99

unit circle, which is the reference domain of our problem (see Figure 4.16). We use differently refined meshes as those shown in Figure 4.16. In all cases, the refinement parameter $N \approx C/h$.

First we compare again our results with those in [32] for a shell of thickness $t = 0.4$ m; in this case, the values in [32] have been obtained with eight Q_2-Fourier-axisymmetric elements.

Table 4.5 shows some of the lowest vibration frequencies of the hemisphere, ordered according to their circumferential and axial mode numbers n and m, respectively. This table includes also extrapolated values of the vibration frequencies, as well as the results in [32] in the last column.

In this case the performance of the method is very good for all circumferential numbers. Indeed, even for rather coarse meshes like those in the first column of Table 4.5 the computed vibration frequencies are reasonably close to the exact ones.

Figures 4.17-4.20 show the vibration shapes corresponding to the lowest frequencies in each circumferential mode n=0,1,2,3.

Table 4.4: Vibration frequencies for the free cylindrical shell with thickness $t = 0.0004$ m.

Mode	$N = 10$	$N = 20$	$N = 40$	Extrap.
torsion	155.6818	155.2029	155.0833	155.0433186
n=0, m=0	246.2266	245.4206	245.2177	245.1494377
torsion	315.2095	311.3635	310.4057	310.0913697
n=1, m=0	156.7888	146.7250	144.2246	143.3999878
n=1, m=1	239.7767	232.3576	230.4811	229.8411165
n=2, m=0	163.5245	76.8020	37.7935	5.7321978
n=2, m=1	164.6616	77.3584	38.0643	5.7905892
n=2, m=2	179.4784	100.9416	73.9391	59.7825430
n=3, m=0	278.7239	124.6618	60.4295	14.3015611
n=3, m=1	279.1710	125.2854	60.7556	13.7934255
n=3, m=2	285.2548	131.6391	69.7290	27.8425332

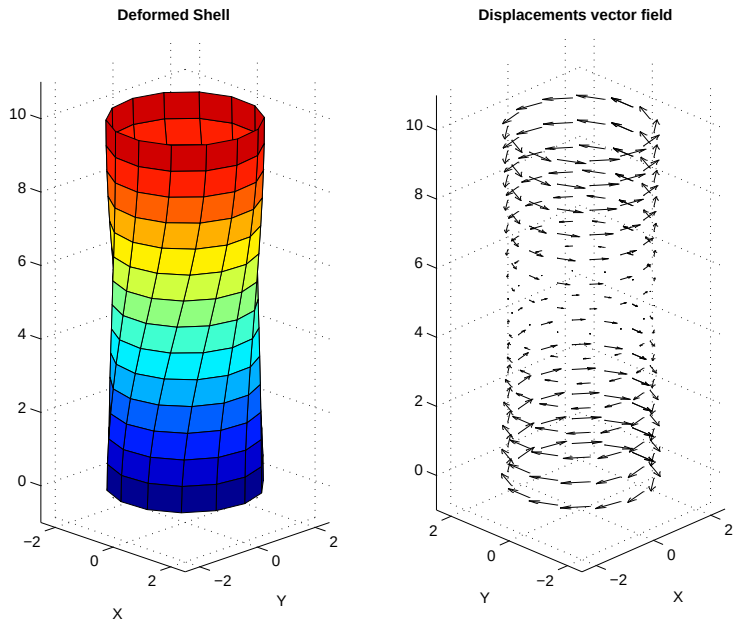

Figure 4.14: Free cylindrical shell. First torsional mode.

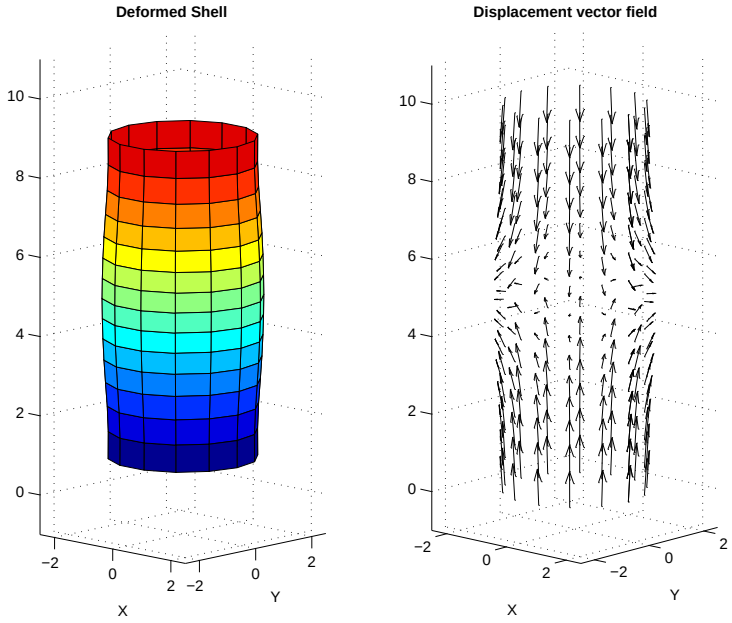

Figure 4.15: Free cylindrical shell. Mode n=0, m=1.

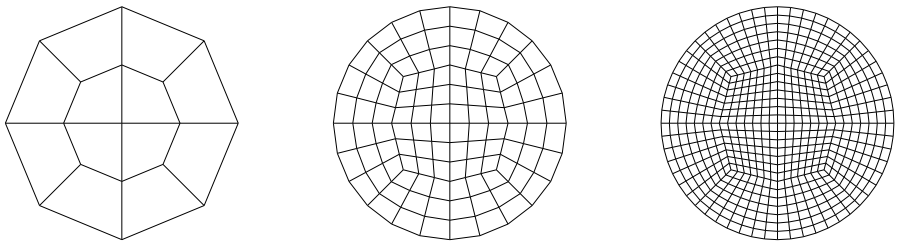

Figure 4.16: Meshes on the reference domain for the hemispherical shell.

For this numerical test, we have also compared the results obtained using the MITC4 method with a purely displacement method (denoted Q_1). The last one consists in solving the spectral problem **SP** by using the same isoparametric quadratic finite elements without relaxing the shear term (i.e., no reduction operator is used); see [33].

Figures 4.21-4.24 show error curves in terms of the refinement parameter N for both methods, MITC4 and Q_1. Now, for each vibration mode, we consider two different thicknesses of the shell: $t = 0.4$ m and $t = 0.004$ m. Once more, it can be observed that the order of convergence for MITC4 is almost quadratic.

Table 4.5: Vibration modes for the clamped hemispherical shell with thickness $t = 0.4$ m.

Mode	$N = 4$	$N = 8$	$N = 12$	$N = 18$	Extrap.	[32]
n=0, m=1	68.5975	64.8487	64.2319	63.9871	63.8196	62.3596
n=0, m=2	90.4970	83.4000	81.9532	81.3665	80.9562	78.6232
n=1, m=1	49.9516	47.6657	47.2893	47.1397	47.0373	59.2177
n=1, m=2	81.8682	76.5863	75.6759	75.3123	75.0616	75.2207
n=2, m=1	76.3073	74.3285	73.9148	73.7484	73.6329	71.5254
n=2, m=2	92.0576	85.5341	84.4929	84.0813	83.7994	81.1326
n=3, m=1	86.1210	81.1263	80.2976	79.9660	79.7358	77.1851
n=3, m=2	101.8573	94.4224	92.4195	91.6757	91.1933	88.1218

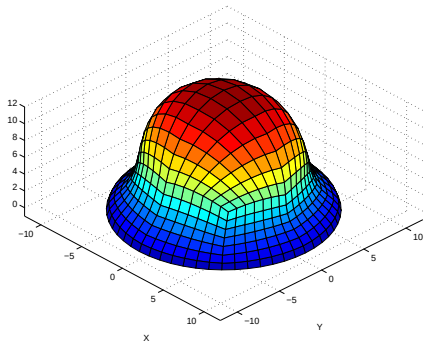

Figure 4.17: Deformed hemispherical shell. Mode: n=0, m=1.

The locking phenomenon arising from the displacement method Q_1 can be clearly appreciated in these figures. Instead, MITC4 is quite free of locking for clamped hemispherical shells.

4.5 Conclusions.

We have assessed the efficiency of MITC4 finite element method applied to the classical Naghdi shell model for the vibration modes of slender structures. First we have tested the method for plates with arbitrary isoparametric meshes and boundary condition. We have considered moderately thick as well as very thin plates. The

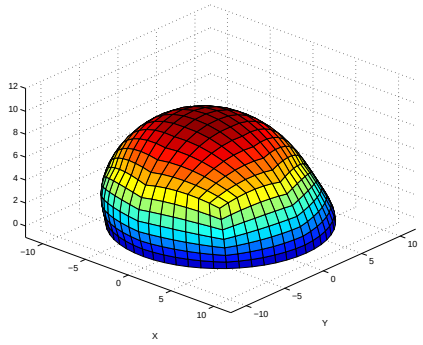

Figure 4.18: Deformed hemispherical shell. Mode: n=1, m=1.

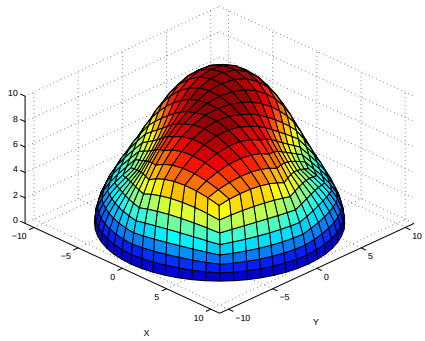

Figure 4.19: Deformed hemispherical shell. Mode n=2, $m = 1$.

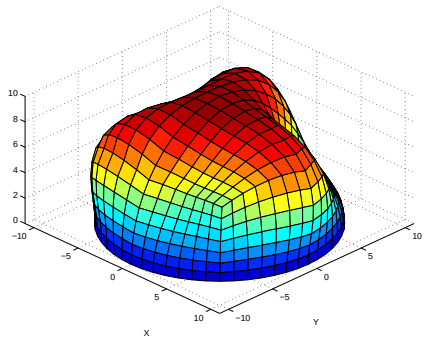

Figure 4.20: Deformed hemispherical shell. Mode n=3, $m = 1$.

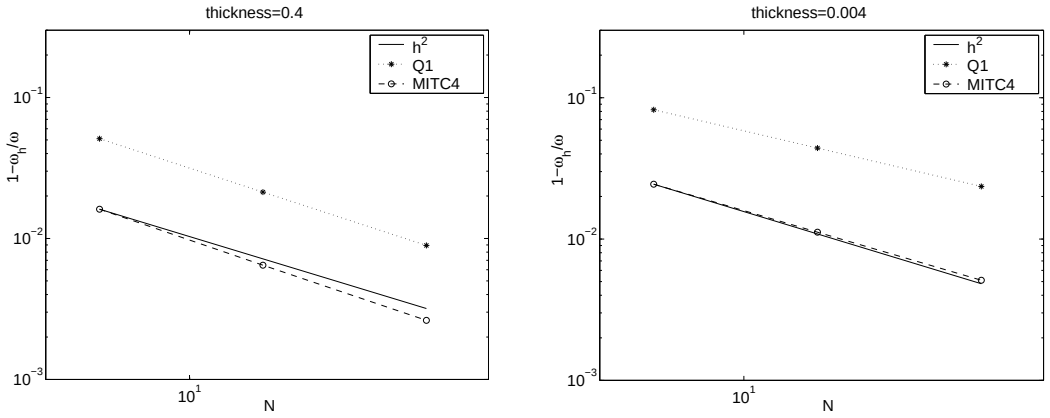

Figure 4.21: Clamped hemispherical shell. Mode n=0, m=1.

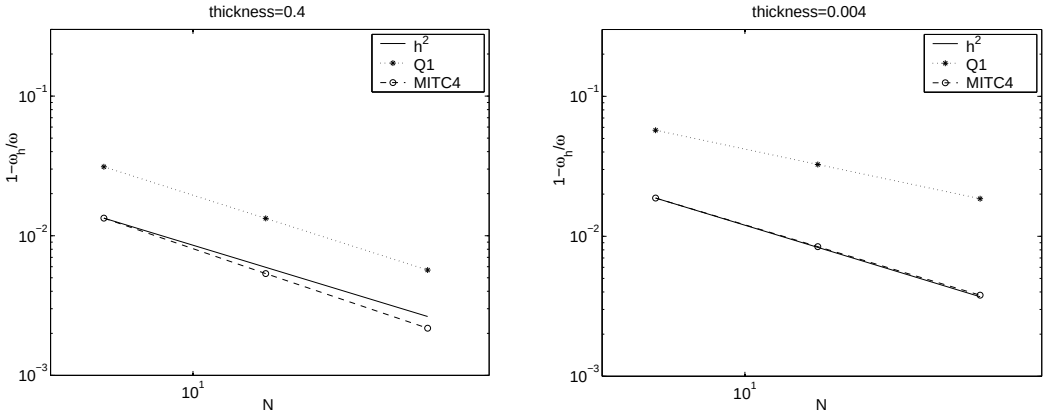

Figure 4.22: Clamped hemispherical shell. Mode n=1, m=1.

obtained results show that the method is completely locking-free in all cases. Second, we have applied the method to two particular shells: the free cylinder and the clamped hemisphere. Each shell has been tested with different thicknesses. In the first case we have found that the method is locking free only for low circumferential numbers. In the second one, the method is always locking-free.

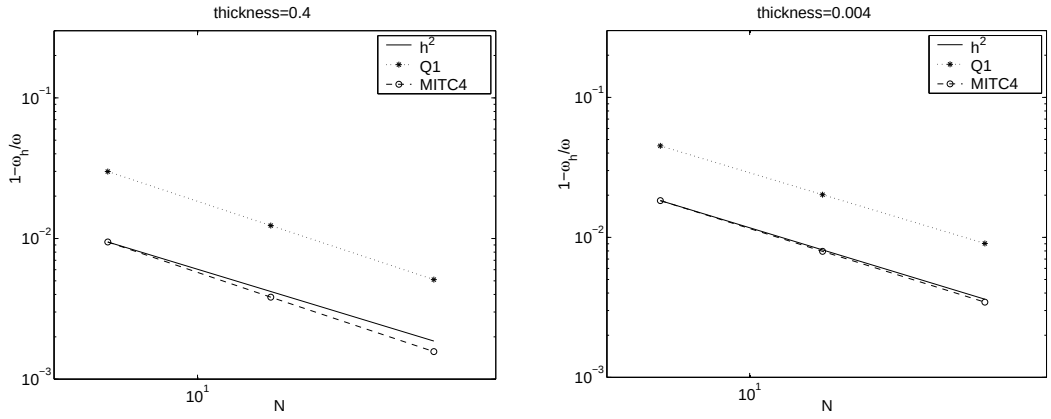

Figure 4.23: Clamped hemispherical shell. Mode n=2, m=1.

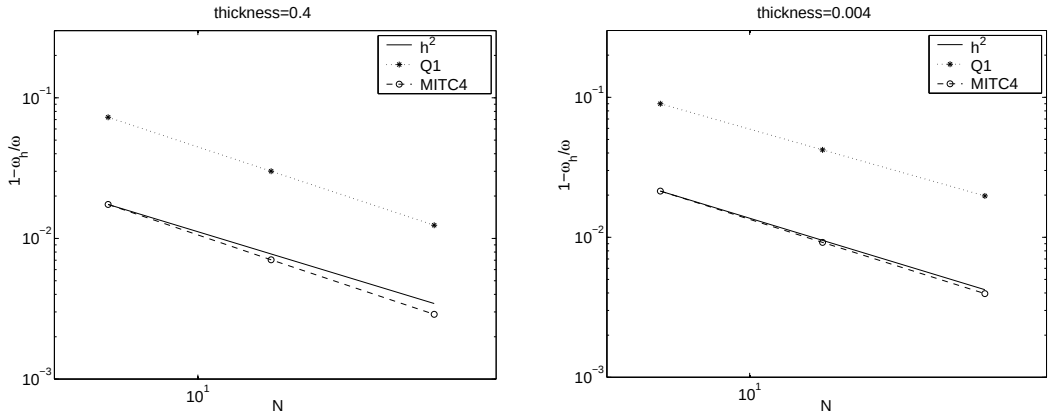

Figure 4.24: Clamped hemispherical shell. Mode n=3, m=1.

Chapter 5

Approximation of the vibration modes of a plate coupled with a fluid by low-order isoparametric finite elements

We analyze an isoparametric finite element method to compute the vibration modes of a plate, modeled by Reissner-Mindlin equations, in contact with a compressible fluid, described in terms of displacement variables. To avoid locking in the plate, we consider a low-order method of the so called MITC (Mixed Interpolation of Tensorial Component) family on quadrilateral meshes. To avoid spurious modes in the fluid, we use a low-order hexahedral Raviart-Thomas element and a non conforming coupling is used on the fluid-structure interface.

Applying a general approximation theory for spectral problems, under mild assumptions, we obtain optimal order error estimates for the computed eigenfunctions, as well as a double order for the eigenvalues. These estimates are valid with constants independent of the plate thickness. Finally, we report several numerical experiments showing the behavior of the methods.

5.1 Introduction

This chapter deals with the numerical computation of the vibration modes of a fluid-structure interaction problem in a 3D-domain. This is a very important engineering problem (e.g. for treatment of noise in cars or planes). It is well known that a large amount of work has been devoted to this subject (see for example [68]).

We are interested in one of problems of this kind: to compute elastoacoustic vibrations when the structure is an elastic plate and the fluid is ideal and compressible, both with small displacements.

In the framework of plate theory, we consider the most commonly used model to describe small as well as moderately thin plates: Reissner-Mindlin equations. It is well known that standard finite element methods produce unsatisfactory result when applied to this model, even for the plate alone; this phenomenon is due to numerical locking. To avoid this drawback, some special method based on reduced integration or mixed interpolation has to be used. One of the most used methods of this type is the MITC (Mixed Interpolation of Tensorial Component) methods introduced by Bathe and Dvorkin in [10]. A great number of papers dealing with the mathematical analysis of this method have been published in the context of load problem (see for example [4, 9, 29, 46, 79]) and for the plate vibration spectral problem (see [44, 43]).

To determining the vibration modes of the fluid, usually the pressure is chosen as primary variable; however, for coupled systems, the use of displacement vector fields present some advantageous properties like, for example, that compatibility and equilibrium through the fluid-structure interface are satisfied automatically. Though, it is well known that the displacement formulation suffers from the presence of zero-frequency spurious modes with no physical meaning. An alternative approach has been introduced and analyzed in [12] to avoid the spurious modes; it consists in the use of lowest-order Raviart-Thomas element. Non-existence of spurious modes and optimal error estimates for two dimensional fluid-structure problem have been proved in [12] and [74].

The problem of a plate coupled with a fluid has been mathematically analyzed in [45], by using DL3 triangular finite element for the plate and tetrahedral Raviart-Thomas element for the fluid. Optimal order error estimates for the eigenvalues and eigenvectors valid uniformly on the thickness parameter have been obtained in that reference and no spurious modes are present with this discretization.

In this chapter we have extended the results in [45] by considering a discretization of the coupled problem involving the lowest-order quadrilateral MITC4 finite element for the bending of the plate (the original Bathe and Dvorkin's paper deals with this element) and lowest-order hexahedral Raviart-Thomas element (see [81]) for the fluid. On the fluid-plate interface a non-conforming coupling is used; i.e., equal normal displacement for the fluid and plate is imposed in a weak sense. Let us remark that although the isoparametrical finite element are the most used element in engineering applications (quadrilateral in 2D and hexahedral in 3D), no available result seems to exist for this case.

The rest of the chapter is organized as follow. In Section 2 we introduce the spectral problem to describe the free vibration modes for the coupled system. In Section 3, we describe the finite element method to solve the problem. We prove optimal order error estimates for the approximation . In Section 4 and 5 we prove error estimates for the spectral plate-fluid vibration problem. Finally, in Section 6, we report some numerical experiments.

Throughout the chapter we denote by C a positive constant not necessarily the same at each occurrence, but always independent of the mesh-size and the plate thickness.

5.2 Statement of the problem

We consider the problem of determining the free vibration modes of a three-dimensional cavity enclosing and ideal inviscid barotropic fluid. The walls of this cavity are considered to be all rigid, except for one of them which is an elastic plate. Let Ω be the domain occupied by the fluid and $\Gamma \times \left(-\frac{t}{2}, \frac{t}{2}\right)$, that of the plate, where Γ is its middle surface of the plate of constant thickness $t > 0$.

We consider that Ω is a polyhedral convex three-dimensional domain. Its boundary $\partial\Omega$ is the union of the convex surfaces Γ_0, Γ_1, ... , Γ_J. We assume that Γ_0 is in contact with the plate, whereas the remaining surfaces are assumed to be perfectly rigid walls. We denote by n the unit outward normal vector to $\partial\Omega$.

Throughout this chapter we make use of the standard notation for Sobolev spaces $H^k(\Omega)$, $H_0^1(\Gamma)$, $H(\mathrm{div}, \Omega)$, $H_0(\mathrm{rot}, \Gamma)$, etc. and their respective norms (see for instance [52]). We also denote $\mathcal{H} := L^2(\Gamma) \times L^2(\Gamma)^2 \times L^2(\Omega)^3$, $\mathcal{X} := H_0^1(\Gamma) \times H_0^1(\Gamma)^2 \times H(\mathrm{div}, \Omega)$ and $\|\cdot\|$ the product norm of the latter.

In that follows, we introduce the coupled problem. For more details see [45].

In order to describe the deformation of the plate, we consider the Reissner-Mindlin model, which is written in terms of the rotations $\beta = (\beta^1, \beta^2)$ of the fibers initially normal to the plate midsurface and the transverse displacement w (see [28, 46]). The following equations describe the dynamic response of the plate to a pressure load q exerted on one of its faces with $(w, \beta) \in H_0^1(\Gamma) \times H_0^1(\Gamma)^2$ being such that

$$\begin{aligned} t^3 a(\beta, \eta) + \kappa t \int_\Gamma (\nabla w - \beta) \cdot (\nabla v - \eta) \qquad\qquad (5.1) \\ + t \int_\Gamma \rho_{\mathrm{P}} \ddot{w} v + \frac{t^3}{12} \int_\Gamma \rho_{\mathrm{P}} \ddot{\beta} \cdot \eta \;\; = \;\; \int_\Gamma q v \qquad \forall (v, \eta) \in H_0^1(\Gamma) \times H_0^1(\Gamma)^2 \end{aligned}$$

(see for instance [60]). In the previous equation, the double dot means second derivatives with respect to time, ρ_{P} is the density of the plate, $\kappa := \frac{Ek}{2(1+\nu)}$, where E is the

Young modulus, ν the Poisson ratio of the plate and k a correction factor which is usually taken as $5/6$ (see [1] for a justification of the use of this coefficient); finally, a is the bilinear form $H_0^1(\Gamma)^2$-elliptic defined by

$$a(\beta,\eta) := \frac{E}{12(1-\nu^2)} \int_\Gamma \left[\sum_{i,j=1}^{2} (1-\nu)\varepsilon_{ij}(\beta)\varepsilon_{ij}(\eta) + \nu \operatorname{div}\beta \operatorname{div}\eta \right].$$

On the other hand, to describe the governing equations for the free small amplitude motions of an inviscid compressible fluid contained in Ω, we consider the displacement formulation

$$\int_\Omega \rho_{\text{F}}\, \ddot{u}\cdot\phi + \int_\Omega \rho_{\text{F}}\, c^2 \operatorname{div} u \operatorname{div}\phi = -\int_\Gamma p\, \phi\cdot n. \tag{5.2}$$

where p is the pressure, u the displacement field, ρ_{F} the density and c the acoustic speed of the fluid.

Since the fluid is considered inviscid, only the normal component of the displacement vanishes on the rigid part of the cavity boundary $\Gamma_{\text{R}} := \Gamma_1 \cup \cdots \cup \Gamma_J$:

$$u\cdot n = 0 \quad \text{on } \Gamma_{\text{R}}. \tag{5.3}$$

Since the transverse displacement of the plate does not depend on the z-coordinate, it can be considered that Γ (instead of Γ_0) is one of the components of $\partial\Omega$. Then, the interface condition reads

$$u\cdot n = w \quad \text{on } \Gamma. \tag{5.4}$$

Finally, in our coupled problem, the unique load q exerted on the plate is the pressure p of the fluid.

Then, the space of kinematically admissible displacements of the coupled system is

$$\mathcal{V} := \{(v,\eta,\phi)\in\mathcal{X} :\ \phi\cdot n = 0 \text{ on } \Gamma_{\text{R}} \ \text{ and } \ \phi\cdot n = v \text{ on } \Gamma\},$$

and, by adding (5.1) to (5.2), for all $(v,\eta,\phi)\in\mathcal{V}$ we have

$$\begin{aligned} t^3 a(\beta,\eta) + \kappa t \int_\Gamma (\nabla w-\beta)\cdot(\nabla v-\eta) + \int_\Omega \rho_{\text{F}}\, c^2 \operatorname{div} u \operatorname{div}\phi \\ = -t\int_\Gamma \rho_{\text{P}}\, \ddot{w} v - \frac{t^3}{12}\int_\Gamma \rho_{\text{P}}\, \ddot{\beta}\cdot\eta - \int_\Omega \rho_{\text{F}}\, \ddot{u}\cdot\phi. \end{aligned} \tag{5.5}$$

The free vibration modes of this coupled problem are obtained by seeking harmonic in time solutions of (5.5). By so doing we obtain the following spectral problem (see for instance [68]):

Find $\lambda \in \mathbb{R}$ *and* $0 \neq (w, \beta, u) \in \mathcal{V}$ *such that*

$$t^3 a(\beta, \eta) + \kappa t \int_\Gamma (\nabla w - \beta) \cdot (\nabla v - \eta) + \int_\Omega \rho_{\mathrm{F}} c^2 \operatorname{div} u \operatorname{div} \phi \tag{5.6}$$
$$= \lambda \left(t \int_\Gamma \rho_{\mathrm{P}} w v + \frac{t^3}{12} \int_\Gamma \rho_{\mathrm{P}} \beta \cdot \eta + \int_\Omega \rho_{\mathrm{F}} u \cdot \phi \right) \qquad \forall (v, \eta, \phi) \in \mathcal{V},$$

where λ is the square of the angular vibration frequency.

As usual, when a displacement formulation is used for the fluid, $\lambda = 0$ is a solution of this problem with eigenspace given by

$$\mathcal{K} := \Big\{ (0, 0, \phi) \in \mathcal{V} : \ \operatorname{div} \phi = 0 \text{ in } \Omega \ \text{ and } \ \phi \cdot n = 0 \text{ on } \partial\Omega \Big\}. \tag{5.7}$$

The eigenfunctions corresponding to non-zero eigenvalues belong to the orthogonal complement of $\mathcal{K}$ in $\mathcal{V}$ with respect to the symmetric bilinear form in the right hand side of (5.6). This orthogonal complement consist of the conservative displacement fields in the fluid, namely

$$\mathcal{G} := \Big\{ (v, \eta, \phi) \in \mathcal{V} : \ \phi = \nabla q \text{ for some } q \in H^1(\Omega) \Big\}, \tag{5.8}$$

with

$$\|\phi\|_{1,\Omega} \leq C \left(\|v\|_{1/2,\Gamma} + \|\operatorname{div} \phi\|_{0,\Omega} \right). \tag{5.9}$$

We observe that $\mathcal{K}$ and $\mathcal{G}$ are also orthogonal with respect to the bilinear form in the left hand side from (5.6). Hence, to obtain the eigenpairs corresponding to non-zero eigenvalues we can seek the solution of problem (5.6) restricted to $\mathcal{G}$ (i.e., with $\mathcal{V}$ substituted by $\mathcal{G}$).

For the theoretical analysis we consider

$$\|(v, \eta, \phi)\|_\bullet := \left(\|v\|_{1,\Gamma}^2 + \|\eta\|_{1,\Gamma}^2 + \|\operatorname{div} \phi\|_{0,\Omega}^2 \right)^{1/2}, \tag{5.10}$$

which is a norm on $\mathcal{G}$ equivalent to $\|\cdot\|$ (see [45]).

On the other hand, in static problems, the loads are typically assumed to depend adequately on the thickness in order to obtain a family of problems with uniformly bounded solutions: volumetric forces are supposed to be proportional to t^3 and surface loads to t^2 (see for instance [28]). For this reason, we assume that the densities for both, fluid and solid, are related with the thickness of the plate as follows:

$$\rho_{\mathrm{F}} = \hat{\rho}_{\mathrm{F}} t^3, \qquad\qquad \rho_{\mathrm{P}} = \hat{\rho}_{\mathrm{P}} t^2.$$

Hence, we consider the following rescaled problem, for the non-zero eigenvalues of (5.6):

Find $\lambda \in \mathbb{R}$ *and* $0 \neq (w, \beta, u) \in \mathcal{G}$ *such that*

$$s_t\Big((w,\beta,u),(v,\eta,\phi)\Big) = \lambda r_t\Big((w,\beta,u),(v,\eta,\phi)\Big) \qquad \forall (v,\eta,\phi) \in \mathcal{G}. \tag{5.11}$$

with

$$s_t\Big((w,\beta,u),(v,\eta,\phi)\Big) := a(\beta,\eta) + \frac{\kappa}{t^2}\int_\Gamma (\nabla w - \beta)\cdot(\nabla v - \eta) + \int_\Omega \hat{\rho}_{\mathrm{F}} c^2 \operatorname{div} u \operatorname{div}\phi$$

and

$$r_t\Big((w,\beta,u),(v,\eta,\phi)\Big) := \int_\Gamma \hat{\rho}_{\mathrm{P}} wv + \frac{t^2}{12}\int_\Gamma \hat{\rho}_{\mathrm{P}}\beta\cdot\eta + \int_\Omega \hat{\rho}_{\mathrm{F}} u\cdot\phi.$$

We consider the operator T_t defined by

$$\begin{array}{rccc} T_t: & \mathcal{H} & \longrightarrow & \mathcal{G} \\ & (f,\theta,g) & \longmapsto & (w,\beta,u) \end{array}$$

with $(w, \beta, u) \in \mathcal{G}$ being the solution of

$$s_t\Big((w,\beta,u),(v,\eta,\phi)\Big) = r_t\Big((f,\theta,g),(v,\eta,\phi)\Big) \qquad \forall (v,\eta,\phi) \in \mathcal{G}. \tag{5.12}$$

This problem is well posed and the operator turns out to be uniformly bounded on t (see [45]). Furthermore, as a consequence of (5.9), $\mathcal{G}$ is compactly included in $\mathcal{H}$ and, therefore, $T_t : \mathcal{H} \longrightarrow \mathcal{H}$ is a compact operator. Moreover, since s_t and r_t are symmetric and semipositive definite, the spectrum of T_t, apart from $\mu = 0$, consists of a sequence of positive finite multiplicity eigenvalues converging to zero. Note that λ is an eigenvalue of (5.11) if and only if $\mu = \frac{1}{\lambda}$ is an eigenvalue of T_t with the same multiplicity and corresponding eigenfunctions.

We will use the following regularity result for the solution of (5.12) (see [45]):

Theorem 5.2.1 *Let* $(f,\theta,g) \in \mathcal{H}$, $(w,\beta,u) = T_t(f,\theta,g)$ *and* $\gamma = \frac{\kappa}{t^2}(\nabla w - \beta)$. *Then,* $(w,\beta,u) \in H^2(\Gamma)\times H^2(\Gamma)^2 \times H^1(\operatorname{div},\Omega)$, $\gamma \in L^2(\Gamma)$ *and the following estimate holds*

$$\|w\|_{2,\Gamma} + \|\beta\|_{2,\Gamma} + \|u\|_{H^1(\operatorname{div},\Omega)} + \|\gamma\|_{0,\Gamma} \leq C|(f,\theta,g)|_t,$$

with $C > 0$ *independent of* t.

5.3 Discretization

Let $\{\mathcal{T}_h\}$ be a family of partitions in hexahedra of Ω and $\{\mathcal{T}_h^\Gamma\}$ be a family of decomposition of Γ into convex quadrilaterals. Note that, although each $\mathcal{T}_h$ induces a decomposition on Γ, we do not assume that $\mathcal{T}_h^\Gamma$ is this induced mesh. That is each pair of meshes $\mathcal{T}_h$ and $\mathcal{T}_h^\Gamma$ do not need to be compatible. Here h stands for the maximum diameter of the elements in $K \in \mathcal{T}_h^\Gamma$ or $\mathbf{K} \in \mathcal{T}_h$, respectively.

Let $\widehat{\mathbf{K}} := [0,1]^3$ be the reference element for the partition $\mathcal{T}_h$. We denote by $Q_{i,j,k}(\widehat{\mathbf{K}})$ the space of polynomials of degree less than or equal to i in the first variable, to j in the second one, and to k in the third one. Also, we set $Q_k(\widehat{\mathbf{K}}) = Q_{k,k,k}(\widehat{\mathbf{K}})$. Similarly, for $\widehat{K} := [0,1]^2$ the reference element for the partition $\mathcal{T}_h^\Gamma$, we define $Q_{i,j}(\widehat{K})$ and $Q_k(\widehat{K})$.

Let $\mathbf{K} \in \mathcal{T}_h$. We denote by $\mathbf{F}_K$ a trilinear mapping of $\widehat{\mathbf{K}}$ onto $\mathbf{K}$, with Jacobian matrix and determinant denoted by $D\mathbf{F}_K$ and $J_{\mathbf{F}_K}$ respectively (see Fig. 5.1). Analogously, let $K \in \mathcal{T}_h^\Gamma$, we denote by F_K the bilinear mapping of $\widehat{K}$ onto K, with Jacobian DF_K and determinant of the Jacobian J_{F_K} (see Fig. 5.2).

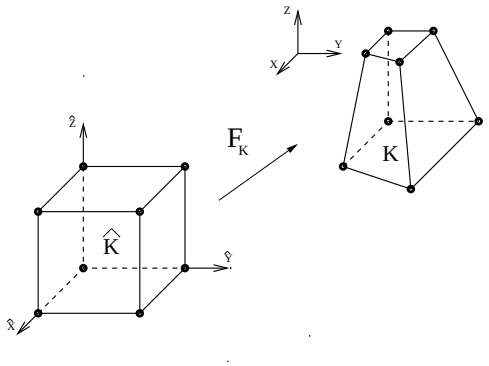

Figure 5.1: Trilinear mapping onto an element $\mathbf{K} \in \mathcal{T}_h$.

We consider *regular meshes* in the sense that there exist constants c and C independent of the elements K or $\mathbf{K}$ such that

$$ch_K^2 \leq J_{F_K} \leq Ch_K^2 \quad \forall\ K \in \mathcal{T}_h^\Gamma$$

and

$$ch_{\mathbf{K}}^3 \leq J_{\mathbf{F}_K} \leq Ch_{\mathbf{K}}^3 \quad \forall\ \mathbf{K} \in \mathcal{T}_h,$$

respectively.

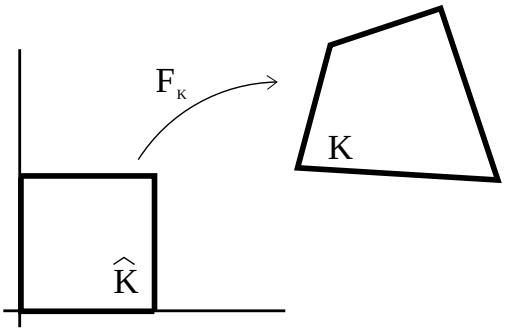

Figure 5.2: Bilinear mapping onto an element $K \in \mathcal{T}_h^\Gamma$.

Furthermore, according to [43] and [50], we assume that the meshes are *asymptotically paralelogramic*, i.e. the above mapping verify

$$\frac{|\widehat{\nabla} J_{\mathbf{F}_K}|}{J_{\mathbf{F}_K}} \leq C h_{\mathbf{K}},$$

$$|\widehat{\nabla}(J_{\mathbf{F}_K} D\mathbf{F}_K{}^{-1})| \leq C h_{\mathbf{K}}^3,$$

and

$$|\widehat{\nabla}(DF_K^{-1})| \leq C h_K^2,$$

for all $\mathbf{K} \in \mathcal{T}_h$ and $K \in \mathcal{T}_h^\Gamma$, respectively. Here, $|\cdot|$ denote the standard euclidean norm and the corresponding matrix norm. Moreover, in the plate we assume that the mesh $\mathcal{T}_h^\Gamma$ is a refinement of a coarser partition $\mathcal{T}_{2h}^\Gamma$, obtained by joining the midpoints of each opposite side in each $M \in \mathcal{T}_{2h}^\Gamma$ (called macro-element). In addition, $\mathcal{T}_{2h}^\Gamma$ is a similar refinement of a still coarser regular partition $\mathcal{T}_{4h}^\Gamma$ (see [28]).

To approximate the fluid displacements, we use lowest order Raviart-Thomas elements (see [81]). Let

$$\mathcal{R}T(\widehat{\mathbf{K}}) := \left\{ \widehat{q} : \widehat{q} \in Q_{1,0,0}(\widehat{\mathbf{K}}) \times Q_{0,1,0}(\widehat{\mathbf{K}}) \times Q_{0,0,1}(\widehat{\mathbf{K}}) \right\}$$

and, from this space, we define through the contravariant transformation known as the *Piola's transformation*,

$$\mathcal{R}T(\mathbf{K}) := \left\{ q : q \circ \mathbf{F}_K = J_{\mathbf{F}_K}^{-1} D\mathbf{F}_K \widehat{q}, \quad \widehat{q} \in \mathcal{R}T(\widehat{\mathbf{K}}) \right\}$$

Note that the *Piola transform* associated with $\mathbf{F}_K$ allows to transforming vector fields from the current element to the reference one (see the definition of the space

$\mathcal{R}T(\widehat{K})$), leaving invariant its flux through any surface; i.e., for each face S of $\mathbf{K} = \mathbf{F}_K(\widehat{\mathbf{K}})$ we have

$$\int_S q \cdot n = \int_{\widehat{S}} \widehat{q} \cdot \widehat{n}, \tag{5.1}$$

where n is the normal unit vector to S.

Then, we define the lowest-order Raviart-Thomas space (see [81, 75])

$$R_h := \left\{ \phi_h \in H(\mathrm{div}, \Omega) : \ \phi_h|_K \in \mathcal{R}T(\mathbf{K}) \ \ \forall \mathbf{K} \in \mathcal{T}_h \right\}. \tag{5.2}$$

We remark that, for $R_h \subset H(\mathrm{div}, \Omega)$, the normal component of a function in R_h must be continuous along interelement boundaries and vanish on $\partial\Omega$. In fact, the integrals (5.1) of these normal components are the degrees of freedom defining an element of R_h.

For the plate we consider a method MITC4, introduced by Bathe and Dvorkin (see [10]) and analyzed in [9, 46, 43]. It is based on different finite element spaces for the rotations, the transverse displacement and the shear strain.

Let

$$\mathcal{N}(\widehat{K}) := \left\{ \widehat{p} : \ \widehat{p} \in Q_{0,1}(\widehat{K}) \times Q_{1,0}(\widehat{K}) \right\},$$

and, from this space, we define through covariant transformation:

$$\mathcal{N}(K) := \left\{ p : \ p \circ F_K = DF_K^{-T} \widehat{p}, \ \ \widehat{p} \in \mathcal{N}(\widehat{K}) \right\}.$$

Let us remark that the mapping between $\mathcal{N}(K)$ and $\mathcal{N}(\widehat{K})$ is a kind of *Piola transform* for the "rot" operator, r*ot* $p := \partial p/\partial y - \partial p/\partial x$ and, in this case, there holds

$$\int_\ell p \cdot \tau = \int_{\hat{\ell}} \widehat{p} \cdot \widehat{\tau}, \tag{5.3}$$

for all edge ℓ of the element $K = F(\widehat{K})$, where τ is the unit vector tangential to ℓ. Then, we define the space (which will be used to approximate the shear stress γ)

$$Z_h := \left\{ \psi \in H_0(\mathrm{rot}, \Gamma) : \ \psi|_K \in \mathcal{N}(K) \ \forall K \in \mathcal{T}_h^\Gamma \right\},$$

that corresponds to the lowest-order rotated Raviart-Thomas space ([75, 81]). We remark that, for $Z_h \subset H_0(\mathrm{rot}, \Gamma)$, the tangential component of a function in Z_h must be continuous along interelement boundaries and vanish on $\partial\Gamma$. In fact, the integrals (5.3) of these tangential components are the degrees of freedom defining an element of Z_h.

We consider the *reduction operator*

$$\Pi : H^1(\Gamma)^2 \cap H_0(\mathrm{rot}, \Gamma) \longrightarrow Z_h,$$

locally defined for each $\psi \in H^1(\Gamma)^2$ by (see [28, 75])

$$\int_\ell \Pi\psi \cdot \tau = \int_\ell \psi \cdot \tau, \tag{5.4}$$

for every edge ℓ of the triangulation (τ being a unit tangent vector along ℓ). It can be shown that this operator satisfies ([28, 75])

$$\|\psi - \Pi\psi\|_{0,\Gamma} \leq Ch\|\psi\|_{1,\Gamma}. \tag{5.5}$$

For the transverse displacements we take standard bilinear isoparametric elements, namely,

$$W_h := \Big\{ v_h \in H_0^1(\Gamma) : \ \ v_h|_K \in Q(K) \ \forall K \in \mathcal{T}_h^\Gamma \Big\},$$

where $Q(K) := \{p \in \mathrm{L}^2(K) : \ p \circ F_K \in Q_1(\widehat{K})\}$, for all $K \in \mathcal{T}_h$.

Finally, the finite element spaces for the rotations are defined by

$$H_h := \Big\{ \eta \in H_0^1(\Gamma)^2 : \ \eta|_K \in Q(K)^2 \ \forall K \in \mathcal{T}_h^\Gamma \Big\}.$$

The approximation of the plate problem by using the spaces W_h, H_h, Z_h, and the reduction operator Π, corresponds to the method MITC4.

We impose weakly the interface condition (5.4), because doing it strongly (i.e., $u_h \cdot n = w_h$ on Γ) is too stringent (see [19]). Let $\mathcal{C}_h := \{\mathcal{F} : \ \mathcal{F}$ is a face of the fluid meshes lying on $\Gamma\}$. Then, we take as discrete space for the coupled problem

$$\mathcal{V}_h := \Big\{ (v_h, \eta_h, \phi_h) \in W_h \times H_h \times R_h : \ \phi_h \cdot n = 0 \text{ on } \Gamma_{\mathrm{R}} \ \text{ and } \ \int_{\mathcal{F}} \phi_h \cdot n = \int_{\mathcal{F}} v_h \ \forall \mathcal{F} \in \mathcal{C}_h \Big\}.$$

The corresponding discrete eigenvalue problem is:

Find $\lambda_h \in \mathbb{R}$ *and* $0 \neq (w_h, \beta_h, u_h) \in \mathcal{V}_h$ *such that*

$$\left\{ \begin{array}{l} a(\beta_h, \eta_h) + \dfrac{\kappa}{t^2} \displaystyle\int_\Gamma (\nabla w_h - \Pi\beta_h) \cdot (\nabla v_h - \Pi\eta_h) + \int_\Omega \hat{\rho}_{\mathrm{F}} c^2 \operatorname{div} u_h \operatorname{div} \phi_h \\ \\ \qquad = \lambda_h \left(\displaystyle\int_\Gamma \hat{\rho}_{\mathrm{P}} w_h v_h + \frac{t^2}{12} \int_\Gamma \hat{\rho}_{\mathrm{P}} \beta_h \cdot \eta_h + \int_\Omega \hat{\rho}_{\mathrm{F}} u_h \cdot \phi_h \right) \qquad \forall (v_h, \eta_h, \phi_h) \in \mathcal{V}_h, \end{array} \right. \tag{5.6}$$

Note that the fact that $\mathcal{V}_h \not\subset \mathcal{V}$ and the use of the reduction operator Π lead to two variational crimes for our method.

Analogously to the continuous case, $\lambda_h = 0$ is an eigenvalue of this problem, with corresponding eigenspace

$$\mathcal{K}_h := \{(0,0,\phi_h) \in \mathcal{V}_h : \ \operatorname{div}\phi_h = 0 \text{ in } \Omega \ \text{ and } \ \phi_h \cdot n = 0 \text{ on } \partial\Omega\}.$$

Hence, for the theoretical analysis, we may restrict the discrete eigenvalue problem to the space $\mathcal{G}_h$ given by the orthogonal complement of $\mathcal{K}_h$ in $\mathcal{V}_h$ with respect to r_t. We write

Find $\lambda_h \in \mathbb{R}$ and $0 \neq (w_h, \beta_h, u_h) \in \mathcal{G}_h$ such that

$$\begin{aligned} s_{th}\Big((w_h,\beta_h,u_h),(v_h,\eta_h,\phi_h)\Big) & \\ = \lambda_h r_t\Big((w_h,\beta_h,u_h),(v_h,\eta_h,\phi_h)\Big) & \qquad \forall (v_h,\eta_h,\phi_h) \in \mathcal{G}_h, \end{aligned} \tag{5.7}$$

with

$$\begin{aligned} s_{th}\Big((w_h,\beta_h,u_h),(v_h,\eta_h,\phi_h)\Big) &:= a(\beta_h,\eta_h) \\ &+\frac{\kappa}{t^2}\int_\Gamma (\nabla w_h - \Pi\beta_h)\cdot(\nabla v_h - \Pi\eta_h) + \int_\Omega \hat{\rho}_{\mathrm{F}} c^2 \operatorname{div} u_h \operatorname{div}\phi_h. \end{aligned}$$

Because ϕ_h is not necessarily a gradient, for $(v_h,\eta_h,\phi_h) \in \mathcal{G}_h$, we have that $\mathcal{G}_h \not\subset \mathcal{G}$, and then a third variational crime for our methods.

To define the arises discrete analogue of the operator T, we need the following lemma which provides a Helmholtz decomposition for the discrete fluid displacements.

Lemma 5.3.1 *For any $(v_h,\eta_h,\phi_h) \in \mathcal{G}_h$, ϕ_h can be written as*

$$\phi_h = \nabla\xi + \chi,$$

with ξ and χ satisfying $(v_h,\eta_h,\nabla\xi) \in \mathcal{G}$ and $\operatorname{div}\chi = 0$. Moreover, there exists a constant C, independent of h, such that

$$\|\nabla\xi\|_{1,\Omega} \ \leq \ C\Big(\|\operatorname{div}\phi_h\|_{0,\Omega} + \|v_h\|_{1,\Gamma}\Big), \tag{5.8}$$

$$\|\chi\|_{0,\Omega} \ \leq \ Ch\Big(\|\operatorname{div}\phi_h\|_{0,\Omega} + \|v_h\|_{1,\Gamma}\Big). \tag{5.9}$$

Proof. We do not include it here since it is essentially identical to those of Theorem 1.6.1 in [50] □

As a consequence of the previous lemma, $\|\cdot\|_\bullet$ and $\|\cdot\|$ are equivalent on $\mathcal{G}_h$ (with equivalence constants not depending on h). On the other hand, $a(\beta_h,\eta_h)+$

$\frac{\kappa}{t^2}\int_\Gamma(\nabla w_h-\Pi\beta_h)\cdot(\nabla v_h-\Pi\eta_h)$ is known to be uniformly coercive on $H_h\times W_h$ (see [46]). Then, clearly, the bilinear form s_{th} are coercive on $\mathcal{G}_h$, with coerciveness constant independent of t and h.

We introduce the following operator T_{th} by

$$\begin{array}{rccc} T_{th}: & \mathcal{H} & \longrightarrow & \mathcal{G}_h \\ & (f,\theta,g) & \longmapsto & (w_h,\beta_h,u_h) \end{array}$$

with $(w_h,\beta_h,u_h)\in\mathcal{G}_h$ being the solution of

$$s_{th}\Big((w_h,\beta_h,u_h),(v_h,\eta_h,\phi_h)\Big)=r_t\Big((f,\theta,g),(v_h,\eta_h,\phi_h)\Big)\qquad\forall(v_h,\eta_h,\phi_h)\in\mathcal{G}_h. \tag{5.10}$$

These operators are uniformly bounded in t and h. Moreover, the non-zero eigenvalues μ_h of T_{th} are related with the eigenvalues λ_h of Problem (5.7) by $\mu_h=\frac{1}{\lambda_h}$.

5.4 Convergence of the discrete operators

We are going to prove that the operator T_{th} converge to T_t in norm as h goes to zero, in both $\|\cdot\|$ and the norm induced by $r_t(\cdot,\cdot)$. This fact will be used in the next section to prove the spectral convergence.

From now on and throughout this section, we consider $(f,\theta,g)\in\mathcal{H}$ fixed and denote

$$\begin{aligned} &(w,\beta,u):=T_t(f,\theta,g), && (w_h,\beta_h,u_h):=T_{th}(f,\theta,g),\\ &\gamma:=\frac{\kappa}{t^2}(\nabla w-\beta), && \gamma_h:=\frac{\kappa}{t^2}(\nabla w_h-\Pi\beta_h). \end{aligned}$$

From (5.10) and the definition of s_t we have

$$\begin{aligned} a(\beta-\beta_h,\eta_h)+\int_\Gamma(\gamma-\gamma_h)\cdot(\nabla v_h-\Pi\eta_h)+\int_\Omega\hat\rho_{\text{F}}\,c^2\,\mathrm{div}\,(u-u_h)\,\mathrm{div}\,\phi_h \qquad (5.1)\\ =\int_\Gamma\gamma\cdot(\eta_h-\Pi\eta_h)+M_h(v_h,\eta_h,\phi_h)\qquad\forall(v_h,\eta_h,\phi_h)\in\mathcal{G}_h, \end{aligned}$$

where

$$M_h(v_h,\eta_h,\phi_h):=s_t\Big((w,\beta,u),(v_h,\eta_h,\phi_h)\Big)-r_t\Big((f,\theta,g),(v_h,\eta_h,\phi_h)\Big).$$

Note that, two consistency terms appear in the error equation. The first one due of the use of the reduction operator Π in s_{th} and the last one because the space $\mathcal{G}_h\not\subset\mathcal{G}$).

The argument to prove that the consistency terms are bounded and the corresponding convergence of the operators, have been used in [45] for similar methods on triangular and tetrahedral meshes. The proof are essentially identical to those of that reference. However, for the sake of completeness, we include some of these.

By using (5.5), we can easily estimate the term $\int_\Gamma \gamma \cdot (\eta_h - \Pi\eta_h)$ in the equation above. For the second consistency term we have:

Lemma 5.4.1 *There holds*

$$|M_h(v_h, \eta_h, \phi_h)| \leq Ch\, \|g\|_{0,\Omega} \|(v_h, \eta_h, \phi_h)\|_\bullet \qquad \forall (v_h, \eta_h, \phi_h) \in \mathcal{G}_h.$$

Proof. See Lemma 5.1 in [45]. □

Now, we prove that the spaces $\mathcal{G}_h$ provide suitable approximations for (w, β, u):

Lemma 5.4.2 *There exists $(\hat{w}, \hat{\beta}, \hat{u}) \in \mathcal{G}_h$ such that*

$$\|(\hat{w}, \hat{\beta}, \hat{u}) - (w, \beta, u)\| \leq Ch\, |(f, \theta, g)|_t.$$

Moreover, if $\hat{\gamma} := \dfrac{\kappa}{t^2}(\nabla\hat{w} - \Pi\hat{\beta})$, the following estimate also holds

$$t\, \|\hat{\gamma} - \gamma\|_{0,\Gamma} \leq Ch\, |(f, \theta, g)|_t.$$

Proof. According with Theorems 3.7 and 3.1 in [43], there exist $\hat{\beta} \in H_h$ and an operator $\widetilde{\Pi} : H_0(\mathrm{rot}, \Gamma) \cup H^1(\Gamma)^2 \longrightarrow Z_h$ such that

$$\|\hat{\beta} - \beta\|_{1,\Gamma} \leq Ch\|\beta\|_{2.\Gamma}$$

and

$$\mathrm{r}ot\left(\Pi\hat{\beta} - \frac{t^2}{\kappa}\widetilde{\Pi}\gamma\right) = 0.$$

By virtue of the last equality and Lemma 2.1 in that paper, there exist $\hat{w} \in W_h$ such that $\nabla\hat{w} = \frac{t^2}{\kappa}\widetilde{\Pi}\gamma - \Pi\hat{\beta}$. Then for $\hat{\gamma} = \widetilde{\Pi}\gamma = \frac{\kappa}{t^2}(\nabla\hat{w} - \Pi\hat{\beta})$ we have $\|\hat{\gamma} - \gamma\|_{0,\Gamma} \leq Ch\|\gamma\|_{1,\Gamma}$.

On the other hand, because

$$\nabla(w - \hat{w}) = \frac{t^2}{\kappa}(\gamma - \hat{\gamma}) + \Pi\hat{\beta} - \beta = \frac{t^2}{\kappa}(\gamma - \hat{\gamma}) + \Pi(\hat{\beta} - \beta) + (\Pi\beta - \beta)$$

by using (5.5) and the previous estimates we have $\|\hat{w} - w\|_{1,\Gamma} \leq Ch\,(\|\gamma\|_{1,\Gamma} + \|\beta\|_{2,\Gamma})$.

Arguing as in Theorem 5.2 of [12] we can find $u^I \in R_h$ such that $(\hat{w}, \hat{\beta}, u^I) \in V_h$ and $\|u^I - u\|_{H(\mathrm{div},\Omega)} \leq Ch\left[\|w\|_{2,\Gamma} + \|u\|_{H^1(\mathrm{div},\Omega)}\right]$.

Now, let $(0,0,u_{\mathcal{K}_h})$ be the r_t projection of $(\hat{w},\hat{\beta},u^I)$ onto $\mathcal{K}_h$. Hence, for $\hat{u} := u^I - u_{\mathcal{K}_h}$, $(\hat{w},\hat{\beta},\hat{u}) \in \mathcal{G}_h$. Moreover, since $u_{\mathcal{K}_h}$ and $(\hat{u}-u)$ are orthogonal in $H(\mathrm{div},\Omega)$, we have

$$\|\hat{u}-u\|_{H(\mathrm{div},\Omega)} \le \|(\hat{u}-u)+u_{\mathcal{K}_h}\|_{H(\mathrm{div},\Omega)} = \|u^I-u\|_{H(\mathrm{div},\Omega)}.$$

Therefore, by applying the *a priori* estimate in Theorem 5.2.1 we conclude the proof. □

The following lemma establishes convergence for the discrete operators in $\|\cdot\|_\bullet$. As a byproduct we obtain convergence for the shear strains, which will be used in the next section.

Lemma 5.4.3 *There holds*

$$\|w-w_h\|_{1,\Gamma} + \|\beta-\beta_h\|_{1,\Gamma} + t\,\|\gamma-\gamma_h\|_{0,\Gamma} + \|\,\mathrm{div}\,(u-u_h)\|_{0,\Omega} \le Ch\,|(f,\theta,g)|_t.$$

Proof. See Lemma 5.3 in [45]. □

Now, we may prove the claimed convergence:

Theorem 5.4.1 *There exists a constant C such that, for any $(f,\theta,g)\in\mathcal{H}$, there holds*

$$\|(T_t - T_{th})(f,\theta,g)\| \le Ch\,|(f,\theta,g)|_t. \tag{5.2}$$

Proof. The theorem is an immediate consequence of Lemma 5.4.3 and Lemma 5.4 in [45]. □

Finally, we obtain the following estimate:

Theorem 5.4.2 *There exists a constant C such that, for any $(f,\theta,g)\in\mathcal{H}$, there holds*

$$\Big|r_t\Big((T_t - T_{th})(f,\theta,g),(f,\theta,g)\Big)\Big| \le Ch^2\,|(f,\theta,g)|_t. \tag{5.3}$$

Proof. We consider a decomposition of u_h according to the lemma 5.3.1; i.e., $u_h = \nabla\xi + \chi$. Recalling the equation (6.2) in [45] we have

$$\begin{aligned} r_t\Big((T_t - T_{th})(f,\theta,g),(f,\theta,g)\Big) \qquad\qquad (5.4)\\ = a(\beta-\beta_h,\beta-\beta_h) + \frac{t^2}{\kappa}\int_\Gamma |\gamma-\gamma_h|^2 + \int_\Omega \hat{\rho}_{\mathrm{F}}c^2(\,\mathrm{div}\,u - \,\mathrm{div}\,u_h)^2\\ - 2\int_\Omega \hat{\rho}_{\mathrm{F}} g\cdot\chi - 2\int_\Gamma \gamma\cdot(\beta_h - \Pi\beta_h). \end{aligned}$$

Because of continuity of $a(\cdot,\cdot)$ and lemmas 5.4.3, only remains to estimate the two last terms in the right hand side of the equation above.

The proof in the lemmas 4.2 and 4.3 in [43] can be easily adapted to prove the estimate for the last term. In fact, this term has been analyzed in that paper in order to obtain optimal L^2 error estimate for the MITC4 methods for a clamped plate.

On the other hand, since $(f,\theta,g) \in \mathcal{G}$, then $g = \nabla q$ and, because of (5.9), $q \in H^2(\Omega)^2$ with

$$\|q\|_{2,\Omega} \leq C\left(\|f\|_{1/2,\Gamma} + \|\operatorname{div} g\|_{0,\Omega}\right) \leq C\|(f,\theta,g)\|.$$

Now, since $\operatorname{div}\chi = 0$ and $\chi = u_h - \nabla\xi$, we have

$$\int_\Omega \hat{\rho}_{\mathrm{F}}\, g\cdot\chi = \int_{\partial\Omega} \hat{\rho}_{\mathrm{F}}\, q\,(u_h - \nabla\xi)\cdot n = \int_\Gamma \hat{\rho}_{\mathrm{F}}\, q\,(u_h\cdot n - w_h)\,,$$

the latter because of $(w_h,\beta_h,\nabla\xi) \in \mathcal{G}$. Since $(w_h,\beta_h,u_h) \in \mathcal{G}_h$, then $P(u_h\cdot n) = P(w_h)$, with P being the $L^2(\Gamma)$-projection onto the piecewise constant functions on $\mathcal{C}_h$. Hence,

$$\begin{aligned}
\left|\int_\Omega \hat{\rho}_{\mathrm{F}}\, g\cdot\chi\right| &= \left|\int_\Gamma \hat{\rho}_{\mathrm{F}}[q - P(q)]\,[u_h\cdot n - P(u_h\cdot n) + P(w_h) - w_h]\right| \\
&\leq \|q - P(q)\|_{0,\Gamma}(\|u_h\cdot n - P(u_h\cdot n)\|_{0,\Gamma} + \|P(w_h) - w_h\|_{0,\Gamma}) \\
&\leq Ch\|q\|_{1,\Gamma}(\|u_h\cdot n - P(u_h\cdot n)\|_{0,\Gamma} + \|P(w_h) - w_h\|_{0,\Gamma}),
\end{aligned}$$

and $\|q\|_{1,\Gamma} \leq C\|q\|_{2,\Omega} \leq C\|(f,\theta,g)\|$. Then, we estimates the remainder two terms. The proof of Lemma 1.6.8 in [50] can be easily adapted to prove that

$$\|u_h\cdot n - P(u_h\cdot n)\|_{0,\Gamma} \leq Ch\|(f,\theta,g)\|.$$

For the last term, we have

$$\begin{aligned}
\|P(w_h) - w_h\|_{0,\Gamma} &\leq \|P(w_h - w)\|_{0,\Gamma} + \|Pw - w\|_{0,\Gamma} + \|w - w_h\|_{0,\Gamma} \\
&\leq \|Pw - w\|_{0,\Gamma} + C\|w - w_h\|_{0,\Gamma} \\
&\leq Ch\|w\|_{1,\Gamma} + Ch\|(f,\theta,g)\| \\
&\leq Ch\|(f,\theta,g)\|,
\end{aligned}$$

where we have used Lemmas 5.2.1 and 5.4.3. Thus, we conclude proof. □

Remark 5.4.1 *According to [43], the macroelement assumption on the mesh $\mathcal{T}_h^\Gamma$ for the MITC4 method is only used to prove an optimal order estimate for the last*

terms in the right hand side of the equation (5.4) in the proof of the theorem above. However, a modification of this method is introduced in this reference.It consists of enriching the discrete space H_h by means of a rotation of a space used for the approximation of the Stokes problem. For these methods, which is called DL4, the macroelement assumption is not necessary.

5.5 Spectral approximation

It is shown in [45], that as the thickness $t \to 0$, each eigenvalue μ of problem (5.6) converge to some limit μ_0. Indeed, μ_0 are the eigenvalues of the operator associated with the classical Kirchhoff model of the same plate coupled with the fluid (see Theorem 3.2 in [45]). From now on, for simplicity, we assume that μ is an eigenvalue of T_t which converges to a simple eigenvalue μ_0 as t goes to zero (see Section 3 in [45] for further discussions).

As a consequence of Theorem 5.4.1, for each simple eigenvalue μ of T_t, there is exactly one eigenvalue μ_h of T_{th} converging to μ as h goes to zero (see for instance [45]). The following theorem shows optimal t-independent error estimates:

Theorem 5.5.1 *Let μ and μ_h be simple eigenvalues of T_t and T_{th}, respectively, such that $\mu_h \to \mu$ as $h \to 0$. Let (w, β, u) and (w_h, β_h, u_h) be the eigenfunctions corresponding to μ and μ_h, respectively, both normalized in the same manner. Then, there exists $C > 0$ such that, for t and h small enough, there holds*

$$\|(w, \beta, u) - (w_h, \beta_h, u_h)\| \leq Ch, \tag{5.1}$$

and

$$|\mu_t - \mu_{th}| \leq Ch^2. \tag{5.2}$$

PROOF. The proofs, which rely on Theorems 5.4.1 and 5.4.2, are essentially the same as those of Theorem 6.2 and 6.3 in [45]. □

5.6 Numerical experiments

In this section we present numerical results obtained with a implementation of the method.

We have tested the methods by reproducing the experiments in [45]. In that paper, the problem is approximated by using triangular and tetrahedral finite elements; more precisely, using DL3 for plate and hexahedral Raviart-Thomas elements for the fluid.

We remark that it is well know that, from the point of view of efficiency, for the same number of degrees of freedom, hexahedral element approach the exact solution better than tetrahedral ones for structural problems (see for instance [16]). In fact, using Raviart-Thomas elements, the number of faces (degree of freedom for this element) for hexahedral approximation is about one quarter that for tetrahedral ones, on meshes with same vertices (see [16]).

We have considered a steel 3D cavity completely filled with water with all of its walls being perfectly rigid, except for one of them which is an elastic plate. The geometric data are given in Figure 5.3. The physical parameters of plate and fluid are the following ones:

- density of the plate: $\rho_{\text{P}} = 7700\,\text{kg/m}^3$,
- Young modulus: $E = 1.44 \times 10^{11}\,\text{Pa}$,
- Poisson coefficient: $\nu = 0.35$,
- density of the fluid: $\rho_{\text{F}} = 1000\,\text{kg/m}^3$,
- sound speed: $c = 1430\,\text{m/s}$,

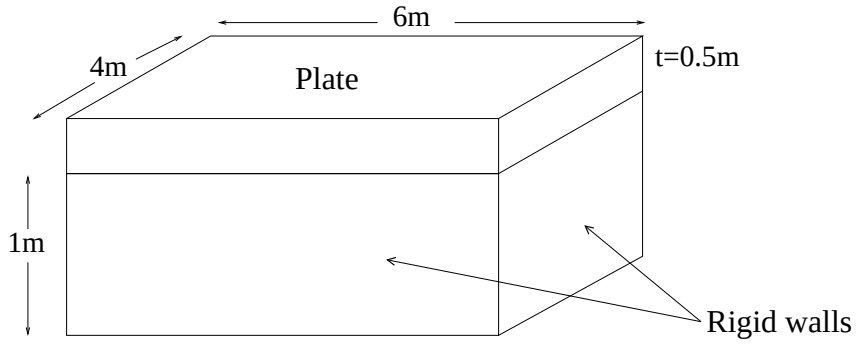

Figure 5.3: Cavity filled with fluid.

The method have been used on several successively refinements of the initial mesh (see Figure 5.4). The refinement parameter N stand for the number of layer of element for the fluid domain in the vertical direction. The number of layers in the other two direction being $2N$ and $3N$, as show the Figure 5.4.

We have computed approximations of the free vibration angular frequencies corresponding to the lowest-frequency vibration modes of the coupled system.

Table I show the five lowest vibration frequencies computed by our method for the plate coupled with water. The table includes also the value of the vibration frequencies obtained by extrapolating the computed ones (ω_m^h) as well as the estimated

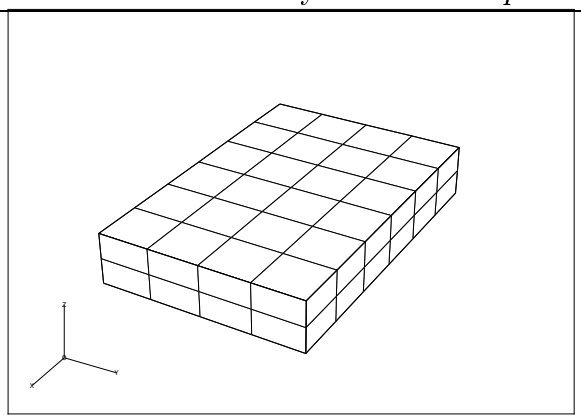

Figure 5.4: Fluid mesh with N=2.

order of convergence α. Such values have been obtained by means of a least square fitting of the model

$$\omega_m^h \approx \omega_m \left(1 + C_m h^\alpha\right)$$

for the frequencies calculated on three different meshes ($N = 4,\ 5,\ 6$).

The obtained result compare perfectly well with those in [45, 16].

Table I: Angular vibration frequencies of a steel plate in contact with water.

Mode	$N = 4$	$N = 5$	$N = 6$	α	ω_m
ω_1^h	703.4418	701.3463	700.1963	1.95	697.5025809
ω_2^h	1046.7326	1035.0140	1028.7364	2.07	1015.0498050
ω_3^h	1096.3214	1091.2521	1088.4428	1.90	1081.6537906
ω_4^h	1329.5584	1325.0901	1322.6234	1.92	1316.7369551
ω_5^h	1513.5155	1492.4589	1481.2156	2.08	1456.8201771

Figures 5.5 to 5.8 show the deformed plate and the fluid pressure for some of these vibration modes.

According to [45], we also check the stability of the method as the thickness becomes small. Table II and III show the results obtained for the first and second frequency vibration modes, for plates with different thicknesses. To allow for comparison we scale the frequencies by using the assumption made in Section 2 on the densities of the plate and fluid (namely, $\rho_{\text{F}} = \hat{\rho}_{\text{F}} t^3$ and $\rho_{\text{P}} = \hat{\rho}_{\text{P}} t^2$). Note that the convergence behavior does not depend on the thickness.

Table II: First vibration ω_1^h for plates of different thickness coupled with fluid.

t	$N=4$	$N=5$	$N=6$	α	ω_1
0.5	703.4418	701.3463	700.1963	1.95	697.5025809
0.05	747.5121	746.6361	746.1595	1.99	745.0693080
0.005	747.5326	746.6569	746.1806	1.99	745.0908998
0.0005	747.5328	746.6571	746.1808	1.99	745.0911159

Table III: Second vibration ω_2^h for plates of different thickness coupled with fluid.

t	$N=4$	$N=5$	$N=6$	α	ω_1
0.5	1046.7326	1035.0140	1028.7364	2.07	1015.0498050
0.05	1128.5113	1125.7410	1124.2345	1.99	1120.7874465
0.005	1128.5296	1125.7600	1124.2539	1.99	1120.8077413
0.0005	1128.5298	1125.7602	1124.2541	1.99	1120.8079442

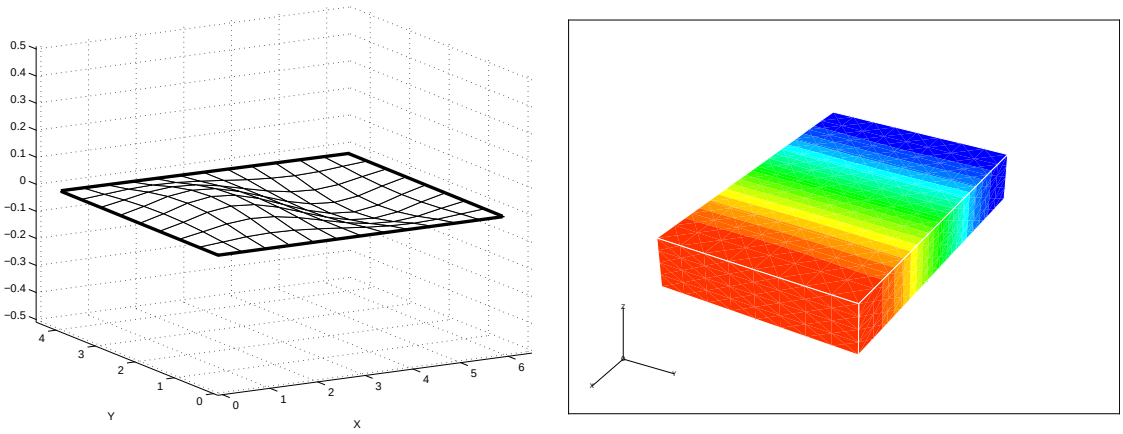

Figure 5.5: Deformed plate and fluid pressure for the mode ω_1.

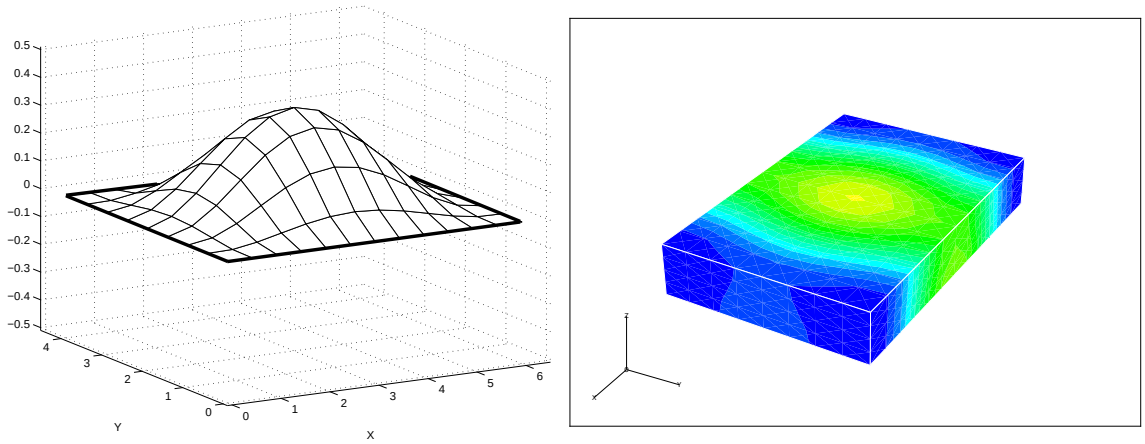

Figure 5.6: Deformed plate and fluid pressure for the mode ω_2.

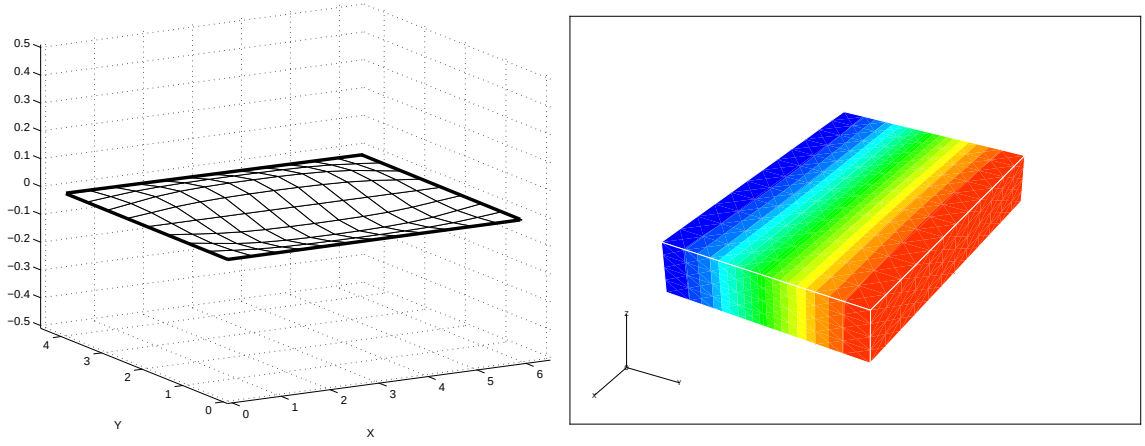

Figure 5.7: Deformed plate and fluid pressure for the mode ω_3.

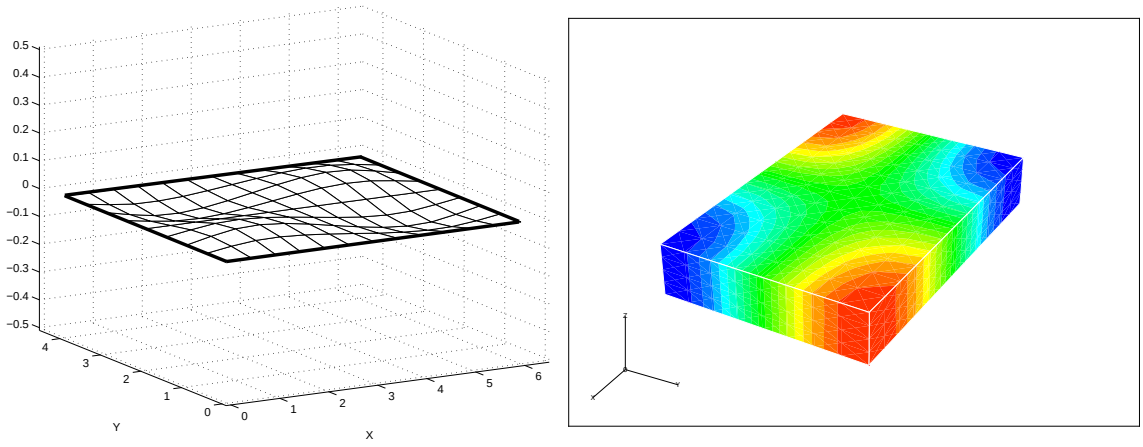

Figure 5.8: Deformed plate and fluid pressure for the mode ω_4.

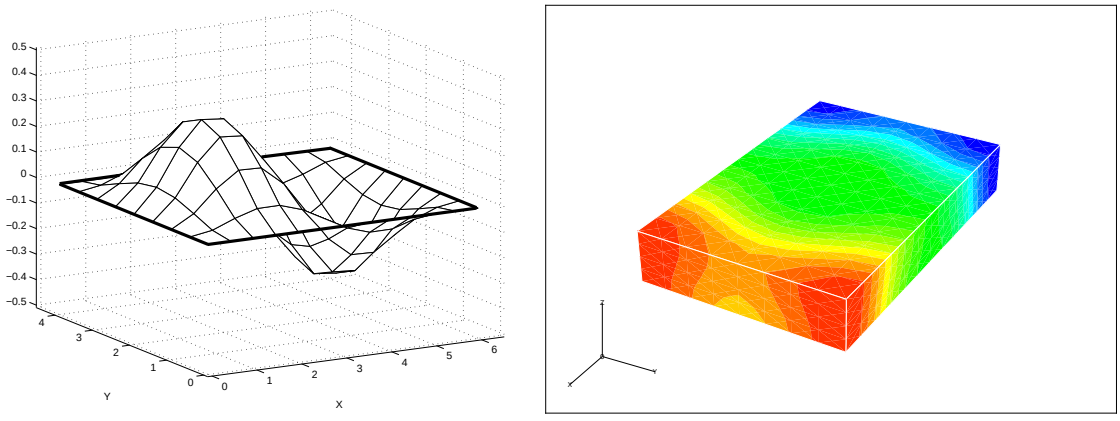

Figure 5.9: Deformed plate and fluid pressure for the mode ω_5.

Chapter 6

Computation of the vibration modes of plates and shells coupled with a fluid

We consider a method to compute the vibration modes of an elastic thin structure (shell or plate) in contact with a compressible fluid. We use the classical Naghdi model over a reference domain and its approximation using the MITC4 finite element method for the structure. The equations for the fluid are discretized with Raviart-Thomas elements, and a non conforming coupling is used on the fluid-solid interface. We report numerical experiments assessing the efficiency of this coupled scheme.

6.1 Introduction

This chapter deals with the numerical computation of the vibration modes of a fluid-structure interaction problem in a 3D-domain. This is a very important engineering problem (e.g., for treatment of noise in cars or planes) and a large amount of work has been devoted to this subject (see for example [68]).

We are interested in one problem of this kind: to compute elastoacoustic vibrations when the structure is an elastic shell and the fluid is ideal and compressible, both subject to small displacements.

In the framework of thin structures, a big amount of work has been developed during the last years by different communities under different points of view. There exist two main ways of approximating shell problems: finite element methods resulting from the discretization of classical shell models (namely, *two dimensional methods*) (see [21, 33]) and methods based on "degenerating" a 3D solid finite element into a shell element using some kinematical assumption in the thickness direction

(see [8, 11])

For the present work, we consider one of the most important classical two-dimensional shell models: Naghdi equations, which are based on Reissner-Mindlin hypotheses. To discretize them we use the MITC (Mixed Interpolation of Tensorial Component) finite element methods, introduced by Bathe and Dvorkin in [10], which are very likely the most used in practice.

Some mathematical analysis can be found for these elements applied to Reissner-Mindlin plate equations (see, for example, [45, 43, 46]). In particular, we use the low-order MITC4 method, which is the most common isoparametric quadrilateral element of this family. The performance of this approach has been recently tested for both, plates and shells vibration problems [58].

To determining the vibration modes of a fluid, usually the pressure is chosen as primary variable. However, for coupled systems, the displacement vector field presents some important properties like, for example, the fact that compatibility and equilibrium through the fluid-structure interface satisfy automatically. Though, it is well known that the displacement formulation suffers from the presence of zero-frequency spurious modes with no physical meaning. An alternative approach has been introduced and analyzed in [12, 19] to avoid such spurious modes; it consists in the use of lowest-order Raviart-Thomas elements. The degrees of freedom of these elements are located at the element faces and represent the normal component of the field through them.

On the fluid-solid interface a non conforming coupling is used: the kinematic constraint (i.e., equal normal displacement for fluid and shell) is imposed in a weak sense. In fact, because of this, the fluid and shell meshes do not need to be compatible on the common interface.

In this chapter we consider the problem of computing the vibration modes of a shell in contact with a fluid. In Section 2 we state the vibration coupled problem. In Section 3 we treat the particular case when the shell is plane (i.e., a plate). Finally, in Section 4, we apply the method to calculate the vibrations of a thin cylinder full of fluid.

6.2 Statement of the problem.

We consider the problem of determining the free vibration modes of a three-dimensional cavity enclosing and ideal inviscid barotropic fluid. The walls of this cavity are either rigid or linearly elastic shells.

Let Ω be the three-dimensional domain occupied by the fluid. We consider that $\partial\Omega$ is the union of the 2D surfaces Γ_0, $\Gamma_1, \ldots, \Gamma_J$ and we assume that Γ_0 is in

contact with the shell, whereas the remaining surfaces are in contact with perfectly rigid walls.

To describe the free small amplitude motions of the fluid, we consider the displacement formulation; we denote by $W = (W_1, W_2, W_3)$ the displacement fluid field.

For the shell, we assume that there exists a single chart ϕ that is a one-to-one mapping, which applies a 2D domain Γ onto the midsurface of the shell. Then, we consider the Naghdi shell model, which is written in terms of the rotations $\Theta = (\Theta_1, \Theta_2)$ of the fibers initially normal to the shell midsurface and the three dimensional vector field $U = (U_1, U_2, U_3)$ which corresponds to the displacement of the midsurface. Note that these vectors are function defined on the reference domain Γ. Moreover, by simplicity we suppose that the fluid is in contact with the midsurface Γ.

The space of kinematically admissible virtual displacements is denoted by $\mathcal{U}$ and defined by

$$\mathcal{U} := \Big\{ (U, \Theta, W) : \ U, \ \Theta, \ W \text{ sufficiently smooth and } (U_3 \circ \phi^{-1}) = W \cdot \mathrm{n} \Big\} \cap \mathcal{BC},$$

where $\mathcal{BC}$ symbolically denotes the prescribed essential boundary conditions. The expression $(U_3 \circ \phi^{-1}) = W \cdot \mathrm{n}$, denotes the equality of the normal displacements of both medium.

The governing formulation for the free small amplitude motions of the coupled system in the frequency domain is the following:

SP: *Find* $\omega > 0$ *and* $0 \neq (U, \Theta, W) \in \mathcal{U}$ *such that*

$$a\Big((U, \Theta, W), (V, \Upsilon, Z)\Big) = \omega^2 b\Big((U, \Theta, W), (V, \Upsilon, Z)\Big) \qquad \forall\, (V, \Upsilon, Z) \in \mathcal{U}.$$

The bilinear form $b(\cdot, \cdot)$ is given by

$$b\Big((U, \Theta, W), (V, \Upsilon, Z)\Big) := \int_\Gamma \rho_S \Big(t a^{\alpha\beta} U_\alpha V_\beta + t U_3 V_3 + \frac{t^3}{12} a^{\alpha\beta} \Theta_\alpha \Upsilon_\beta \Big) \sqrt{\det(a)} + \int_\Omega \rho_F W \cdot Z$$

where ρ_S and ρ_F are the density of the shell and the fluid, respectively. Here, the matrix $(a^{\alpha\beta})$ is the contravariant form of the first fundamental form of the midsurface of the shell (see [21, 33] for further details); Greek indices range over 1 and 2, the convention of summation over indices repeated up and down is used.

The bilinear form $a(\cdot, \cdot)$ can be written as the sum of one term for the fluid stiffness and other for the shell stiffness; the latter also splits into a bending term D^b, a membrane term D^m, and a shear term D^s; i.e.,

$$\begin{aligned} a\Big((U, \Theta, W), (V, \Upsilon, Z)\Big) \ := \ & A(W, Z) + t^3 D^b\Big((U, \Theta), (V, \Upsilon)\Big) \\ & + t D^m(U, V) + t k D^s\Big((U, \Theta), (V, \Upsilon)\Big), \end{aligned}$$

with k being a correction factor for the shear term and

$$\begin{aligned} A(W,Z) &:= \int_\Omega \rho_F c^2 \operatorname{div} W \operatorname{div} Z \\ D^b\Big((U,\Theta),(V,\Upsilon)\Big) &:= \int_\Gamma \frac{E^{\alpha\beta\lambda\mu}}{12} \chi_{\alpha\beta}(U,\Theta)\chi_{\lambda\mu}(V,\Upsilon)\sqrt{\det(a)}, \\ D^m(U,V) &:= \int_\Gamma E^{\alpha\beta\lambda\mu}\gamma_{\alpha\beta}(U)\gamma_{\lambda\mu}(V)\sqrt{\det(a)}, \\ D^s\Big((U,\Theta),(V,\Upsilon)\Big) &:= \int_\Gamma G^{\alpha\beta}\varphi_\alpha(U,\Theta)\varphi_\beta(V,\Upsilon)\sqrt{\det(a)}. \end{aligned}$$

Here, c is the sound speed in the fluid, the tensors χ, γ, and φ are the well-known bending, membrane, and shear strain operators, respectively (see Chapter 4, section 2, of this thesis). The tensors present in the stiffness term, $E^{\alpha\beta\lambda\mu}$ and $G^{\alpha\beta}$ correspond to the material properties and depend on Young's modulus and Poisson's ratio for the structure, E and ν, respectively.

The spectrum of **SP** consists of the frequency $\omega = 0$ and a sequence of finite multiplicity positive frequencies converging to infinity. In the first case, the associated eigenfunctions belong to an infinite-dimensional subspace that consists of pure rotational fluid motions inducing neither variations of the pressure in the fluid nor vibrations in the shell. In fact, they do not correspond to free vibrations modes of the fluid-shell system, but arise because no irrotational constraint is imposed to fluid displacements. The rest of the spectrum are strictly positive frequencies which correspond to actual vibration modes of the fluid-solid system. Moreover, the corresponding fluid displacements are irootational.

According to [12, 19], to avoid typical spurious modes in the fluid-solid coupled system, the approximation of the fluid displacement vector field is made by using Raviart-Thomas element. This element discretize the whole vector field instead of each of its components separately (see [16], for further details).

On the other hand, we use MITC4 elements for the shell structure. This method is based on discretizing the bending and membrane terms using the usual isoparametric quadratic finite elements and relaxing the shear term by using reduced integration.

Let us now specify this method in our context. Let $\{\mathcal{T}_h\}$ be a family of partitions in hexahedra of Ω and $\{\mathcal{T}_h^\Gamma\}$ be a family of decompositions of Γ into convex quadrilaterals. Note that, although each mesh $\mathcal{T}_h$ induces a decomposition on Γ, a non compatible new mesh $\{\mathcal{T}_h^\Gamma\}$ can also be used. Here h stands for the maximum diameter of the elements in $K \in \mathcal{T}_h^\Gamma$ or $\mathbf{K} \in \mathcal{T}_h$, respectively.

Let $\widehat{K}$ be the unit square reference element. We denote by $Q_{i,j}(\widehat{K})$ the space of polynomials of degree less than or equal to i in the first variable and to j in the

second one. We set $Q_k(\widehat{K}) := Q_{k,k}(\widehat{K})$. We denote by F_K the bilinear mapping of $\widehat{K}$ onto K, and we set $Q(K) := \{p : \ p \circ F_K \in Q_1(\widehat{K})\}$.

For the definition of admissible discrete variables, we impose weakly the kinematic interface constraint because to do it strongly would be too stringent (see [19]). The integrals to do this are imposed on the fluid mesh faces in contact with the shell. More precisely, let $\mathcal{C}_h := \{\mathcal{F} : \ \mathcal{F}$ is a face of the fluid meshes lying on $\Gamma\}$, we consider

$$\mathcal{U}_h := \Big\{ (U_h, \Theta_h, W_h) : \ U_h|_K \in Q_1(K)^3, \ \Theta_h|_K \in Q_1(K)^2 \ \ \forall K \in \mathcal{T}_h^\Gamma,$$
$$W_h|_{\mathbf{K}} \in RT(\mathbf{K}) \ \forall \mathbf{K} \in \mathcal{T}_h, \ \textit{and} \ \int_{\mathcal{F}} (U_{3h} \circ \phi^{-1}) = \int_{\mathcal{F}} W_h \cdot \mathrm{n} \ \ \forall \mathcal{F} \in \mathcal{C}_h \Big\} \cap \mathcal{BC},$$

where $RT(\mathbf{K})$ denotes the lowest-order Raviart-Thomas hexahedron, whose degrees of freedom are the fluxes through each of the six faces of $\mathbf{K}$. Recall that $\mathcal{BC}$ denotes the prescribed essential boundary conditions.

Then, the discrete variational problem reads:

$\mathbf{SP_h}$: *Find* $\omega_h > 0$ *and* $0 \neq (U_h, \Theta_h, W_h) \in \mathcal{U}_h$ *such that*

$$a_h\Big((U_h, \Theta_h, W_h), (V_h, \Upsilon_h, Z_h)\Big) = \omega_h^2 b\Big((U_h, \Theta_h, W_h), (V_h, \Upsilon_h, Z_h)\Big) \ \forall\, (V_h, \Upsilon_h, Z_h) \in \mathcal{U}_h.$$

The bilinear form $a_h(\cdot, \cdot)$ is a perturbed form of $a(\cdot, \cdot)$; more precisely, it comes from introducing in the shear term D^s an appropiated reduction operator $\varphi \longmapsto \mathbf{R}\varphi$. In this particular case, the operator $\mathbf{R}$ is defined such that $\mathbf{R}\varphi|_K \in Q_{0,1}(K) \times Q_{1,0}(K)$ $\forall K \in \mathcal{T}_h^\Gamma$ (For details in the case of plate see, for example, [43], and for cylindrical shell see [67]). Thus we obtain

$$\begin{aligned} a_h\Big((U_h, \Theta_h, W_h), (V_h, \Upsilon_h, Z_h)\Big) \ &:= \ A(W_h, Z_h) + t^3 D^b\Big((U_h, \Theta_h), (V_h, \Upsilon_h)\Big) \\ &\quad + tD^m(U_h, V_h) + tkD_h^s\Big((U_h, \Theta_h), (V_h, \Upsilon_h)\Big), \end{aligned}$$

with

$$D_h^s\Big((U_h, \Theta_h), (V_h, \Upsilon_h)\Big) := \int_\Omega G^{\alpha\beta} \Big(\mathbf{R}\varphi(U_h, \Theta_h)\Big)_\alpha \Big(\mathbf{R}\varphi(V_h, \Upsilon_h)\Big)_\beta \sqrt{\det(a)}.$$

Let us emphasize that, for the shell structure, this MITC4 finite element procedure is based on meshes that are constructed in a reference 2D domain, and the numerical computations require an extensive use of the chart ϕ.

6.3 Plates

In this section, we consider that the shell is plane (i.e. a plate). The Reissner-Mindlin formulation for plates can be seen as a special case of the Naghdi shell model,

where the plate transversal displacement terms appear separately from the in-plane terms. Moreover, the in-plane motions do not interact with the fluid. Therefore they can be solved separately. Thus the fluid-solid interaction can be expressed in terms only of the plate transversal displacement, the fiber rotations and the fluid displacements. If we choose a coordinate system in which the plate lies in the x, y plane, then the finite element space is

$$\mathcal{U}_h^P := \Big\{ (U_{3h}, \Theta_h, W_h) : \ U_{3h}|_K \in Q_1(K), \ \Theta_h|_K \in Q_1(K)^2 \ \ \forall K \in \mathcal{T}_h^\Gamma, \\ W_h|_{\mathbf{K}} \in RT(\mathbf{K}) \ \ \forall \mathbf{K} \in \mathcal{T}_h, \ \textit{and} \ \int_{\mathcal{F}} U_{3h} = \int_{\mathcal{F}} W_h \cdot \mathrm{n} \Big\} \cap \mathcal{BC},$$

Then to compute the free vibration modes we must solve the following problem (see [45, 55]):

$\mathbf{PP_h}$: *Find $\omega_h > 0$ and $0 \neq (U_{3h}, \Theta_h, W_h) \in \mathcal{U}_h^P$ such that:*

$$t^3 \tilde{a}(\Theta_h, \Upsilon_h) + \kappa t \int_\Omega \mathbf{R}(\nabla U_{3h} - \Theta_h) \cdot \mathbf{R}(\nabla V_{3h} - \Upsilon_h) + \int_\Omega \rho_F c^2 \operatorname{div} W_h \operatorname{div} Z_h \\ = \omega_h^2 \rho \left(t \int_\Omega U_{3h} V_{3h} + \frac{t^3}{12} \int_\Omega \Theta_h \cdot \Upsilon_h \right) + \int_\Omega \rho_F W_h \cdot Z_h \qquad \forall (V_{3h}, \Upsilon_h, Z_h) \in \mathcal{U}_h^P.$$

Here $\kappa := Ek/2(1+\nu)$ is the shear modulus (we recall that E is the Young modulus, ν the Poisson ratio, and k a correction factor), meanwhile the bilinear form a is defined by

$$\tilde{a}(\Theta_h, \Upsilon_h) := \frac{E}{12(1-\nu^2)} \int_\Omega \left[\sum_{i,j=1}^{2} (1-\nu) \varepsilon_{ij}(\Theta_h) \varepsilon_{ij}(\Upsilon_h) + \nu \operatorname{div} \Theta_h \operatorname{div} \Upsilon_h \right],$$

where ε_{ij} denotes the components of the linear strain tensor.

This coupled problem have been mathematically analyzed in [45], where tetrahedral Raviart-Thomas elements for the fluid and MITC3 elements for the plate have been used. These results have been extended to MITC4 and Raviart-Thomas hexahedra in [55]. In both papers, optimal order error estimates have been obtained for the solution of $\mathbf{PP_h}$, which are valid uniformly on the plate thickness t.

As a test of the performance of this method, we have considered a steel 3D cavity completely filled with water with all of its walls being perfectly rigid, except for one of them which is a plate. The geometric parameters are given in Figure 6.1. The physical parameters of plate and fluid are the following ones:

- density of the plate: $\rho_{\mathrm{P}} = 7700\,\mathrm{kg/m^3}$,
- Young modulus: $E = 1.44 \times 10^{11}\,\mathrm{Pa}$,

- Poisson coefficient: $\nu = 0.35$,
- density of the fluid: $\rho_{\text{F}} = 1000\,\text{kg/m}^3$,
- sound speed: $c = 1430\,\text{m/s}$.
- correction factor: $k = 5/6$.

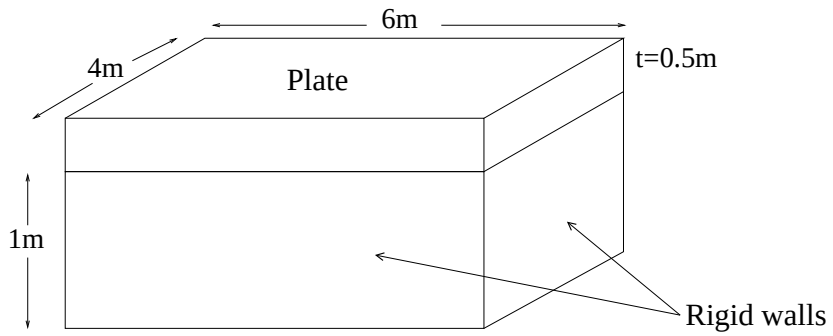

Figure 6.1: 3D cavity filled with fluid.

Table 6.1 shows the frequencies of the three lowest-frequency vibration modes computed on different meshes. Here, N stands for the number of layers of elements for the fluid domain in the vertical direction. The number of layers in the other two direction being $2N$ and $3N$ (see Fig. 6.2). The plate meshes are induced by the fluid meshes. We also include more accurate values computed by extrapolating those obtained with the most refined meshes. The obtained results compare perfectly well with those in [16, 45, 55].

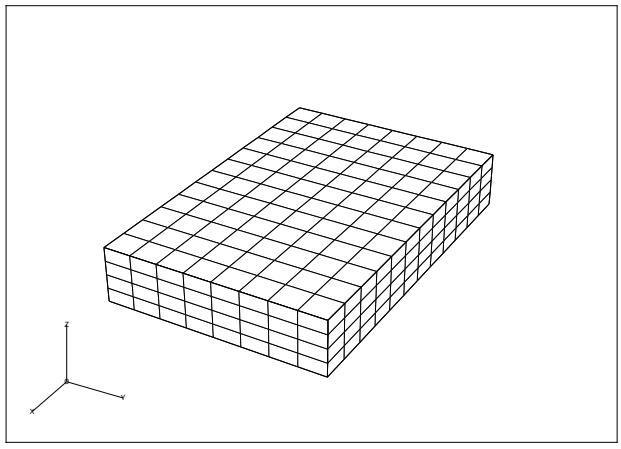

Figure 6.2: Mesh on the fluid for N=4.

Table 6.1: Lowest vibration frequencies of a steel plate in contact with water.

Mode	$N = 4$	$N = 5$	$N = 6$	$N = 7$	"exact"
ω_1	745.5411	744.6309	744.1355	743.8364	743.002848
ω_2	1126.6920	1123.8563	1122.3137	1121.3828	1118.786303
ω_3	1354.1576	1351.3917	1349.8881	1348.9811	1346.471972

Table 6.2 shows the results obtained for the lowest-frequency vibration mode for plates of different thickness. To allow for comparison we scale the frequencies, like in Chapter 5 section 3. Note that the convergence behavior does not depend on the plate thickness.

Table 6.2: Scaled lowest vibration frequency for plates of different thickness coupled with fluid.

Thickness	$N = 4$	$N = 5$	$N = 6$	$N = 7$	"exact"
0.5	745.54	744.63	744.13	743.83	743.0028
0.05	747.51	746.63	746.15	745.87	745.0697
0.005	747.53	746.65	746.18	745.89	745.0913
0.0005	747.53	746.65	746.18	745.89	745.0915

Figures 6.3 and 6.4 show the deformed plate and the fluid pressure field for the two first modes in Table 6.1.

6.4 Shells

In this section we present numerical results corresponding to the solution of problem $\mathbf{SP_h}$ in the case of circular cylindrical shells filled with fluid. First, to validate our code, we compare the results with those in [63]. As a second test, to show the clear advantage of using a 2D model for the structure, we apply our method to a problem considered in [17].

By using cylindrical coordinates, we are led to a reference domain $\Omega = [0, 2\pi] \times [0, H]$, with H being the height of the cylindrical shell. We have used uniform meshes of rectangles with 2^{N+2} and 2^{N+1} element edges on each side of Ω, respectively (see Fig. 6.7). For a given mesh (i.e., a fixed N), we denote by d.o.f. its total number

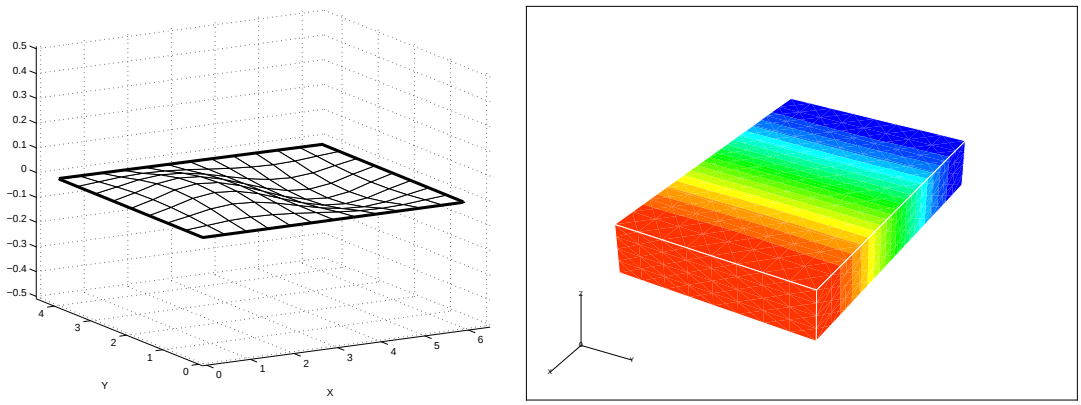

Figure 6.3: Vibration mode of frequency ω_1. Deformed plate and fluid pressure.

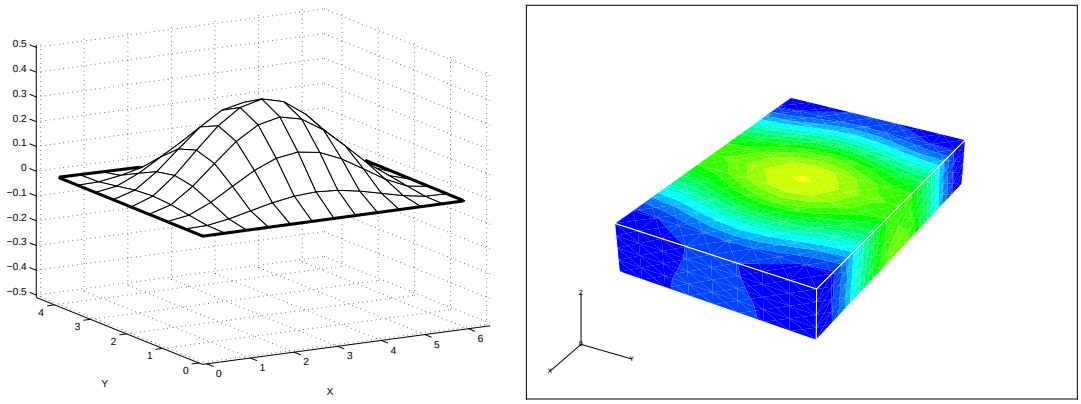

Figure 6.4: Vibration mode of frequency ω_2. Deformed plate and fluid pressure.

of degrees of freedom. We have used three meshes in both experiments, those corresponding to $N = 3$ (4956 d.o.f.), $N = 4$ (11168 d.o.f.), and $N = 5$ (21100 d.o.f.).

In the first case, we have considered a clamped circular cylindrical thin shell completely filled with a compressible fluid (see Figure 6.6). The dimensions of the shell are radius 0.1 m, height 0.3 m, and thickness 0.002 m. The physical properties of the materials, which correspond to aluminum and water, are the following:

- density of the shell: $\rho_{\text{P}} = 2700\,\text{kg/m}^3$,
- Young modulus: $E = 69 \times 10^9\,\text{Pa}$,
- Poisson coefficient: $\nu = 0.3$,
- density of the fluid: $\rho_{\text{F}} = 1000\,\text{kg/m}^3$,
- sound speed: $c = 1483\,\text{m/s}$.
- correction factor: $k = 5/6$.

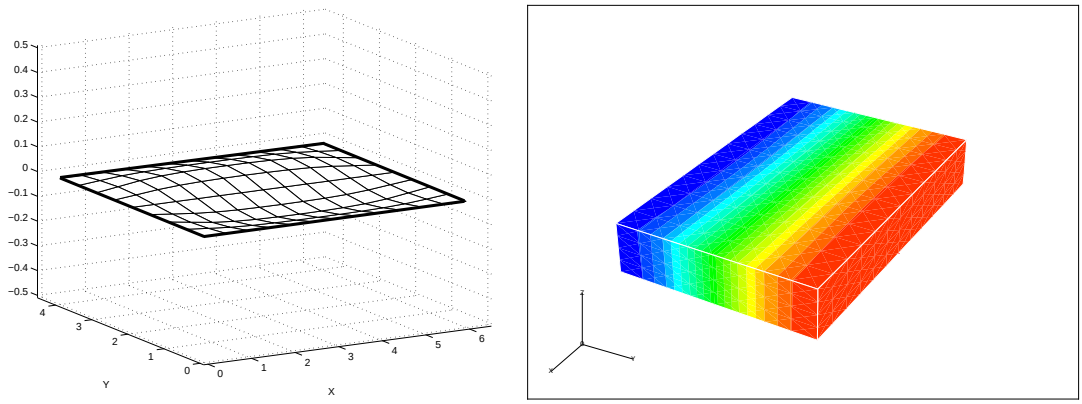

Figure 6.5: Vibration mode of frequency ω_2. Deformed plate and fluid pressure.

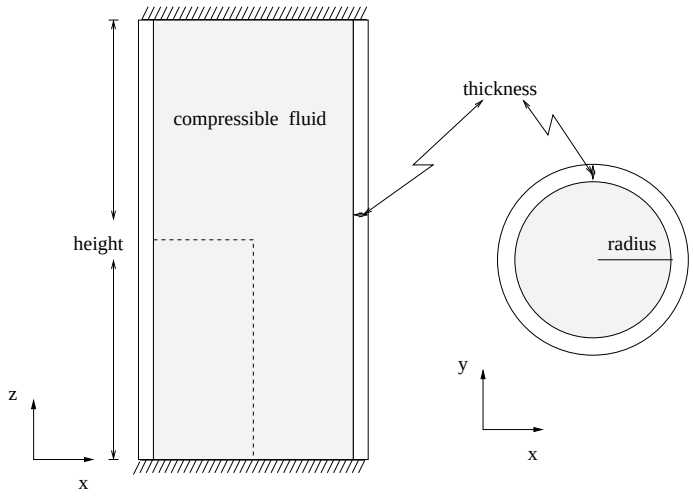

Figure 6.6: Cylinder filled with fluid.

Table 6.3 shows the computed lowest vibration frequencies. They are ordered according to their circumferential and axial mode numbers n and m, respectively (see Figures 6.8 and 6.9). This table also includes "exact" values of the vibration frequencies obtained by extrapolating the frequencies computed with these meshes. In the last column, we include the results reported in [63], which are obtained with an analytical method based on a finite Fourier series expansion. Note that in all cases the difference between the "exact" values and those in [63] are smaller than 3.0%.

It can be seen from Table 6.3 that the method appears locking-free for the computation of vibration modes with low circumferential number ($n = 0$ and $n = 1$). Instead, for larger circumferential numbers ($n = 2$, $n = 3$, etc.), the computed values

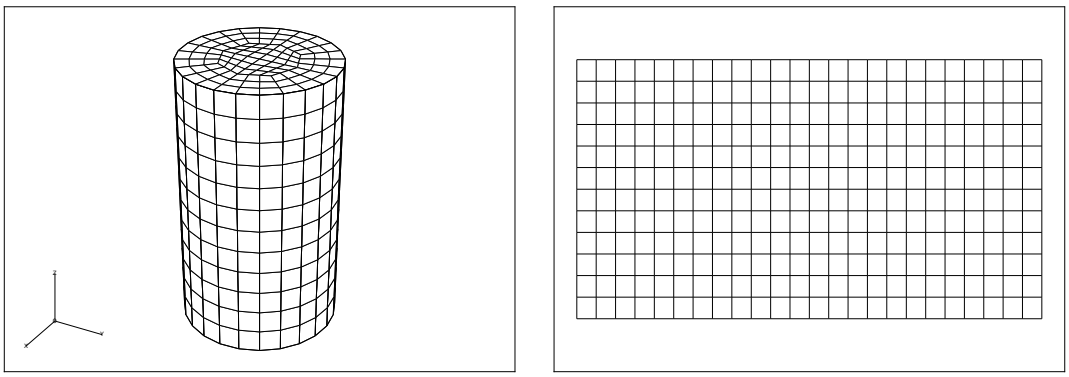

Figure 6.7: Used meshes for N=3.

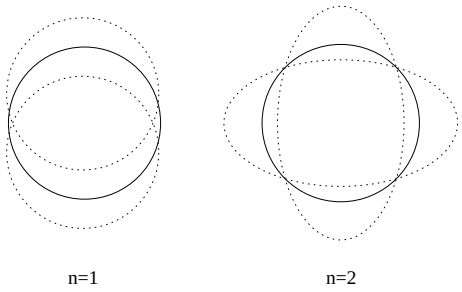

Figure 6.8: Circumferential modes.

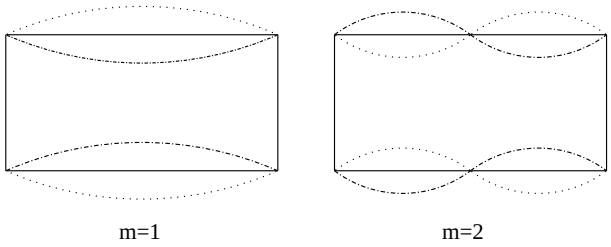

Figure 6.9: Axial modes.

of the vibration frequencies are close to the exact ones only for highly refined meshes. This suggests that the method locks for circumferential numbers greater than 1 in this case. This observation agrees with the results reported in [58] for a cylindrical shell in vacuum.

For the second test, we have considered a moderately thick circular cylinder clamped by both ends and filled with fluid. We have used the same material properties as in the example of the plate from the previous section; i.e., a steel structure filled with water. The height of the cylinder is 3.5 m, its inner diameter length is

Table 6.3: Vibration frequencies for a thin cylindrical shell filled with fluid.

Mode	$N = 3$	$N = 4$	$N = 5$	"exact"	[63]
$n = 1$, $m = 1$	1020.3491	1013.3759	1010.1519	1004.4146433	1007.5
$n = 1$, $m = 2$	1727.6673	1713.7354	1707.3111	1695.9488040	1699.5
$n = 2$, $m = 1$	841.9886	792.0624	768.7160	726.1533379	728.6
$n = 2$, $m = 2$	1539.8293	1499.4937	1481.1173	1449.6221483	1453.9
$n = 3$, $m = 1$	956.2804	793.6864	712.6670	539.6201194	553.0
$n = 3$, $m = 2$	1433.4752	1310.1966	1253.4812	1153.8148361	1156.2
$n = 4$, $m = 1$	1337.5487	1023.6297	863.8526	502.6526781	516.8
$n = 4$, $m = 2$	1631.5230	1355.9940	1226.7993	989.8001371	985.5
$n = 5$, $m = 1$	1935.2604	1425.5616	1176.4975	668.9915372	644.0
$n = 5$, $m = 2$	2133.8595	1644.8755	1415.2789	994.6122312	974.5

2.0 m, and its thickness 0.1 m.

Table 6.4 shows the lowest vibration frequencies computed with the method described in this paper. We have used the same meshes as in the previous example. We denote by ω_s^i and ω_f^i the shell and fluid mode, respectively. We also include the "exact" values of the vibration frequencies obtained by extrapolating the computed frequencies. In the last column we include the discrepancy (in %) between the values computed on the finest mesh and the "exact" values. Let us remark that ω_s^2 is a shell mode with circumferential number $n = 2$; this is the reason why the discrepancy is larger for this mode.

Table 6.4: Vibration frequencies for a moderately thick cylindrical shell filled with fluid.

mode	$N = 3$	$N = 4$	$N = 5$	"exact"	discrepancy
ω_f^1	1162.5606	1160.2396	1159.1665	1157.2567655	0.165%
ω_f^2	2288.0000	2270.9296	2263.1405	2249.6966024	0.597%
ω_s^1	1213.3284	1204.3192	1200.1554	1192.8062219	0.616%
ω_s^2	1014.5626	948.2604	916.9248	858.3380240	6.825%

To allow for comparison, we reproduce in Table 6.5 some results reported in [17]. In this reference, the same problem has been solved, but considering the structure

as a three-dimensional elastic solid. The total numbers of d.o.f. used in each mesh are also given in the table. Let us recall that the corresponding numbers of d.o.f. of the meshes in Table 6.4 are 4956, 11168, and 21100, respectively. The impressive advantage of using the present 2D model can be clearly observed.

Table 6.5: Vibration frequencies reported in [17].

mode	Mesh 1 (8544 d.o.f.)	Mesh 2 (57720 d.o.f.)	Mesh3 (183840 d.o.f.)
ω_f^1	1188.4430	1166.6490	1158.6870
ω_f^2	2348.5520	2281.9990	2255.3540
ω_s^1	1311.8430	1237.6660	1219.2640
ω_s^2	1701.5000	1153.6710	1009.3770

Finally, Figures 6.10 and 6.11 show the deformed shell and the fluid pressure field for the two lowest-frequency vibration modes in Table 6.4.

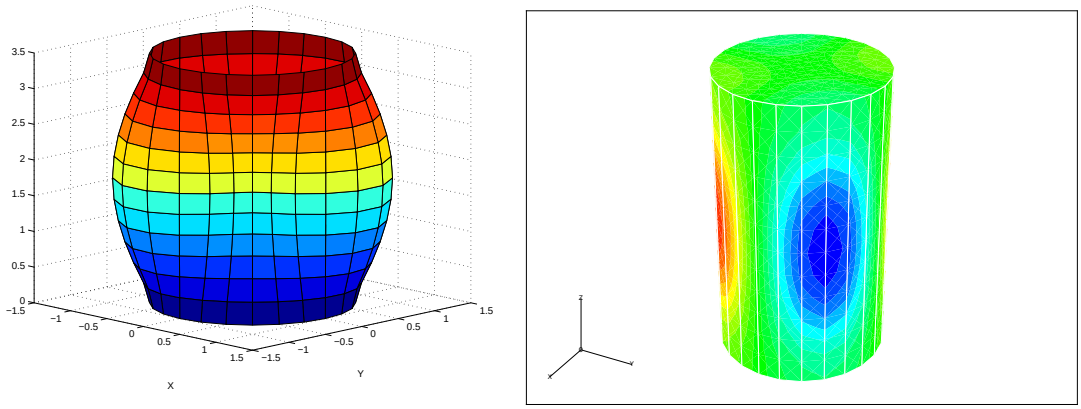

Figure 6.10: Vibration mode of frequency ω_s^1. Deformed shell and fluid pressure.

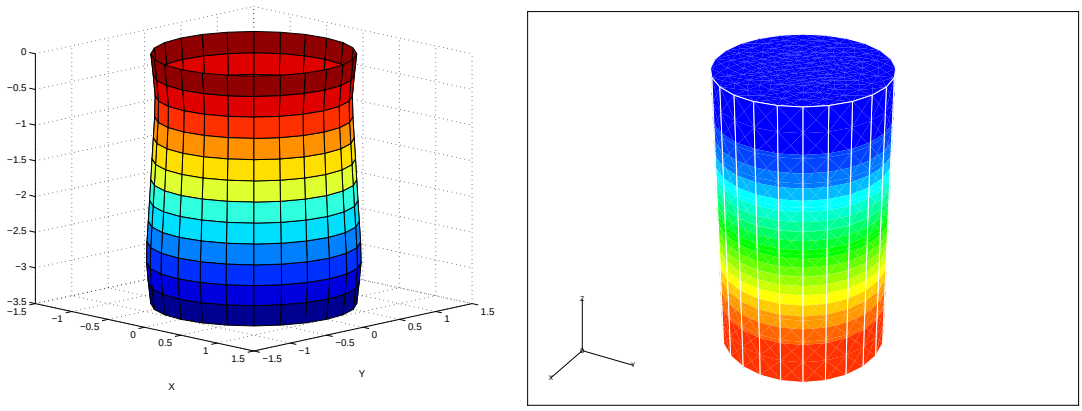

Figure 6.11: Vibration mode of frequency ω_f^1. Deformed shell and fluid pressure.

Bibliography

[1] S.M. Alessandrini, D.N. Arnold, R.S. Falk, and A.L. Madureira, *Derivation and justification of plate models by variational methods*, in "Plates and Shells", CRM Proc. & Lect. Notes Ser., Vol. 21, M. Fortin, ed., AMS, Providence, 1999, pp. 1-20.

[2] A. Alonso, A. Dello Russo, and V. Vampa, *A posteriori error estimates in finite element acoustic analysis*, J. Comput. Appl. Math. **117** (2000) 105–119.

[3] B.S. Al Janabi and E. Hinton, *A study of the free vibrations of square plates with various edge conditions*, in *Numerical Methods and Software for Dynamic Analysis of Plates and Shells*, E. Hinton, ed., Pineridge Press, Swansea, 1987.

[4] D.N. Arnold and R.S. Falk, *A uniformly accurate finite element method for the Reissner-Mindlin plate*, SIAM J. Numer. Anal., **26** (1989) 1276–1290.

[5] D.N. Arnold, D. Boffi, and R.S. Falk, *Approximation by quadrilateral finite elements*, Math. Comp., **71** (2002) 909–922.

[6] D.N. Arnold, D. Boffi, R.S. Falk, and L. Gastaldi, *Finite element approximation on quadrilateral meshes*, Comm. Numer. Methods Eng., **17** (2001) 805–812.

[7] I. Babuška and J. Osborn, *Eigenvalue problems* in *Handbook of Numerical Analysis*, Vol II, P.G. Ciarlet and J.L. Lions, eds., North Holland, Amsterdam, 1991, pp. 641–787.

[8] K.J. Bathe, Finite Element Procedures. Prentice Hall,Englewood Cliffs, NJ, 1996.

[9] K.J. Bathe and F. Brezzi, *On the convergence of a four-node plate bending element based on Mindlin/Reissner plate theory and a mixed interpolation* in *Mathematics of Finite Elements an Applications V*, J.R. Whiteman, ed., Academic Press, London, 1985, pp. 491–503.

[10] K.J. Bathe and E.N. Dvorkin, *A four-node plate bending element based on Mindlin/Reissner plate theory and a mixed interpolation*, Internat. J. Numer. Methods Eng., **21** (1985) 367–383.

[11] K.J. Bathe, A. Iosilevich and D. Chapelle, *An evaluation of the MITC shell elements.* Compt. Struc., **75** 2000 1–30.

[12] A. Bermúdez, R. Durán, M.A. Muschietti, R. Rodríguez and J. Solomin, *Finite element vibration analysis of fluid-solid systems without spurious modes*, SIAM J. Numer. Anal., **32** (1995) 1280–1295.

[13] A. Bermúdez, R. Durán, and R. Rodríguez, *Finite element solution of incompressible fluid-structure vibration problems*, Internat. J. Numer. Methods Eng., **40** (1997) 1435–1448.

[14] A. Bermúdez, R. Durán, and R. Rodríguez, *Finite element analysis of compressible and incompressible fluid-solid systems*, Math. Comp., **67** (1998) 111–136.

[15] A. Bermúdez, R. Durán, R. Rodríguez, and J. Solomin, *Finite element analysis of a quadratic eigenvalue problem arising in dissipative acoustics*, SIAM J. Numer. Anal., **38** (2000) 267–291.

[16] A. Bermúdez, P. Gamallo, and R. Rodríguez. *An hexahedral face element method for the displacement formulation of structural acoustics problems*, J. Comp. Acoustics, **9** (2001) 911-918.

[17] A. Bermúdez, L. Hervella-Nieto, and R. Rodríguez, *Finite element computation of three dimensional elastoacoustic vibrations*, J. Sound Vib.,**219** (1999) 277–304.

[18] A. Bermúdez, L. Hervella-Nieto and R. Rodríguez, *Finite element computation of the vibrations of a plate-fluid system with interface damping*, Comp. Methods Appl. Mech. Eng., **190** (2001) 3021-3038.

[19] A. Bermúdez and R. Rodríguez, *Finite element computation of the vibration modes of a fluid-solid system*, Comp. Methods Appl. Mech. Eng., **119** (1994) 355-370.

[20] A. Bermúdez, R. Rodríguez, *Modelling and numerical solution of elastoacoustic vibrations with interface damping*, Internat. J. Numer. Methods Eng., **46** (1999) 1763-1779.

[21] M. Bernadou, *Finite Element Methods for Thin Shell Problems*, J. Wiley & Sons, 1996.

[22] C. Bernardi, *Optimal finite-element interpolation on curved domain*, SIAM J. Numer. Anal., **5** (1989) 1212–1240.

[23] M. Bischoff and E. Ramm, *Shear deformable shell elements for large strains and rotations.* Internat. J. Numer. Methods Engrg., **40** (1997) 4427–4449.

[24] D. Boffi, F. Brezzi, and L. Gastaldi, *On the convergence of eigenvalues for mixed formulations*, Ann. Scuola Norm. Sup. Pisa, **25** (1997) 131–154.

[25] D. Boffi, F. Brezzi, and L. Gastaldi, *On the problem of spurious eigenvalues in the approximation of linear elliptic problems in mixed form*, Math. Comp., **69** (2000) 121–140.

[26] S. Brenner and L.R. Scott, *The mathematical theory of finite element methods*, Springer-Verlag, New York, 1994.

[27] J.H. Bramble and J.T. King, *A robust finite element method for nonhomogeneous Dirichlet problems in domains with curved boundaries*, Math. Comp., **63** (1994) 1–17.

[28] F. Brezzi and M. Fortin, Mixed and Hybrid Finite Element Methods. Springer-Verlag, New York, 1991.

[29] F. Brezzi, M. Fortin and R. Stenberg, *Quasi-optimal error bounds for approximation of shear-stresses in Mindlin-Reissner plate models*, Math. Models Methods Appl. Sci., **1** (1991) 125–151.

[30] M.L. Bucalem and K.J. Bathe, *Finite element analysis of shell structures*, Arch. Comput. Methods Engrg., **4** (1997) 3–61.

[31] D. Chapelle, *Some new results and current challenges in the finite element analysis of shells.* Acta Numerica, (2000) 215–250.

[32] D. Chapelle, *Personal Communication.*

[33] D. Chapelle and K.J. Bathe, *Fundamental considerations for the finite element analysis of shell structures*, Compt. Struc., **66** (1998) 19–36.

[34] D. Chapelle and K.J. Bathe., *The mathematical shell model underlying general shell elements.* Internat. J. Numer. Methods Engrg., **48(2)** (2000) 289–313.

[35] H.C. Chen and R.L. Taylor, *Vibration analysis of fluid-solid systems using a finite element displacement formulation*, Internat. J. Numer. Methods Eng., **29** (1990) 683–698.

[36] P.G. Ciarlet, *Basic error estimates for elliptic problems*, in *Handbook of Numerical Analysis*, Vol. II, P.G. Ciarlet and J.L. Lions, eds., North Holland, Amsterdam, 1991, pp. 17–351.

[37] P.G. Ciarlet, Mathematical Elasticity - Volume III: Theory of Shells. North-Holland, 2000.

[38] P.G. Ciarlet and P.A. Raviart, *Interpolation theory over curved elements with applications to finite element methods*, Comput. Methods Appl. Mech. Engrg., **1** (1972) 217–249.

[39] C. Conca, J. Planchard and M. Vanninathan, *Fluids and Periodic Structures*, Masson, Paris, 1992 (Recherches en Mathématiques Appliquées. Vol. 38).

[40] J. Descloux, N. Nassif and J. Rappaz, *On spectral approximation. Part. 1: The problem of convergence. Part. 2: Error estimates for the Galerkin methods*, R.A.I.R.O. Anal. Numér. **12** (1978) 97–119.

[41] T. Dupont and R. Scott, *Polynomial approximation of functions in Sobolev spaces*, Math. Comp., **34** (1980) 441–463.

[42] R.G. Durán, L. Gastaldi, and C. Padra, *A posteriori error estimators for mixed approximations of eigenvalue problems*, Math. Models Methods Appl. Sci., **9** (1999) 1165–1178.

[43] R. Durán, E. Hernández, L. Hervella-Nieto, E. Liberman and R. Rodríguez, *Error estimates for low-order isoparametric quadrilateral finite element for plates*, SIAM J. Numer. Anal., submitted.

[44] R. Durán, L. Hervella-Nieto, E. Liberman, R. Rodríguez, J. Solomin, *Approximation of the vibration modes of a plate by Reissner-Mindlin equations*, Math. Comp., **68** (1999) 1447–1463.

[45] R. Durán, L. Hervella-Nieto, E. Liberman, R. Rodríguez and J. Solomin, *Finite element analysis of the vibration problem of a plate coupled with a fluid*, Numer. Math., **86** (2000) 591-616.

[46] R. Durán and E. Liberman, *On mixed finite element methods for the Reissner-Mindlin plate model*, Math. Comp., **58** (1992) 561–573.

[47] G.C. Everstine, *A symmetric potential formulation for fluid-structure interaction*, J. Sound Vib., **79** (1981) 157–160.

[48] M. Feistauer, *On the finite element approximation of functions with noninteger derivatives* Numer. Funct. Anal. and Optim., **10** (1989) 91–110.

[49] M. Feistauer and A. Ženíšek, *Finite element solution of nonlinear elliptic problems*, Numer. Math., **50** (1987) 451–475.

[50] P. Gamallo, *Métodos numéricos de elementos finitos en problemas de interacción fluido-estructura* , Phd. Thesis, U. de Santiago de Compostela, Spain (2002).

[51] L. Gastaldi, *Mixed finite element methods in fluid-structure systems*, Numer. Math., **74** (1996) 153–176.

[52] V. Girault and P.A. Raviart, *Finite element methods for Navier-Stokes equations*, Springer-Verlag, Germany, Berlin, 1986.

[53] P. Grisvard, *Elliptic Problems On Nonsmooth Domains*, Pitman, Boston, London, Melbourne, 1985.

[54] M. Hamdi, Y. Ousset, and G. Verchery, *A displacement method for the analysis of vibrations of coupled fluid-structure systems*, Internat. J. Numer. Methods Eng., **13** (1978) 139–150.

[55] E. Hernández, *Approximation of the vibration modes of a plate coupled with a fluid by low-order isoparametric finite elements*, (in redaction) (2002).

[56] E. Hernández and R. Rodríguez, *Finite element approximation of spectral problems with Neumann boundary conditions on curved domains*, Math. Comp., (in press).

[57] E. Hernández and R. Rodríguez, *Finite element approximation of spectral acoustic problems on curved domains*, Numer. Math., (submitted).

[58] E. Hernández, L. Hervella-Nieto, and R. Rodríguez, *Computation of the vibration modes of plates and shells by low order MITC quadrilateral finite elements*, Compt. Struc., (in press).

[59] E. Hernández, L. Hervella-Nieto, and R. Rodríguez, *Computation of the vibration modes of plates and shells coupled with a fluid*, Procedings of the First South-American Congress on Computational Mechanics, Santa Fe - Paraná, Argentina, 2002.

[60] T.J.R. Hughes, *The Finite Element Method: Linear Static and Dinamic Finite Element Analysis*, Prentice-Hall, Englewood Cliffs, NJ, 1987.

[61] T. Kato, *Perturbation Theory for Linear Operators*, Lecture Notes in Mathematics **132**, Springer Verlag, Berlin, 1966.

[62] L. Kiefling and G.C. Feng, *Fluid-structure finite element vibrational analysis*, AIAA J., **14** (1976) 199–203.

[63] J. Kyeong-Hoon and K. Kwi-Ja, *Free vibration of a circular cylindrical shell filled with bounded compressible fluid*, J. Sound Vib., **217** (1998) 197–221.

[64] M.P. Lebaud, *Error estimate in an isoparametric finite element eigenvalue problem*, Math. Comp., **63** (1994) 17–40.

[65] P. Le Tallec and S. Mani, *Numerical analysis of a linearised fluid-structure interaction problem*, Numer. Math., **87** (2000) 317–354.

[66] E. Liberman, Sobre la convergencia de métodos de elementos finitos para el modelo de placas de Reissner-Mindlin. Ph. D. Thesis, Universidad Nacional de la Plata, Argentina (1995).

[67] M. Malinen and J. Pitkäranta, *A benchmark study of reduced-strain shell finite elements: quadratic shemes*, Internat. J. Numer. Methods Eng., **48** (2000) 1637–1671.

[68] H.J-P. Morand and R. Ohayon, *Fluid Structure Interaction*, J. Wiley & Sons, 1995.

[69] R. Ohayon and C. Soize, *Structural acoustics and vibration*, Academic Press, 1998.

[70] L.G. Olson and K.J. Bathe, *A study of displacement-based fluid finite elements for calculating frequencies of fluid and fluid-structure systems*, Nucl. Eng. Design, **76** (1983) 137–151.

[71] J. Osborn, *Spectral approximation for compact operators*, Math. Comp., **29** (1965) 712–725.

[72] P. Peisker and D. Braess, *Uniform convergence of mixed interpolated elements for Reissner-Mindlin plates*, M^2AN, **26** (1992) 557–574.

[73] J. Pitkäranta and M. Suri, *Design principles and error analysis for reduced-shear plate-bending finite elements*, Numer. Math., **75** (1996) 223–266.

[74] R. Rodríguez and J. Solomin, *The order of convergence of eigenfrequencies in finite element approximations of fluid-structure interaction problems*, Math. Comp., **65** (1996) 1463–1475.

[75] P.A. Raviart and J.M. Thomas, *A mixed finite element method for second order elliptic problems*, in *Mathematical Aspects of Finite Element Methods*, Springer Verlag, 1977, pp. 292–315. (Lecture Notes in Mathematics. Vol. 606).

[76] P.A. Raviart and J.M. Thomas, *Introduction à l'Analyse Numérique des Equations aux Dérivées Partielles*, Masson, Paris, 1983.

[77] R. Scott, *Interpolated boundary conditions in the finite element method*, SIAM J. Numer. Anal., **12** (1975) 440–427.

[78] R. Stenberg, *AAnalysis of mixed finite element methods for the Stokes problem: a unified approach*, Math. Comp., **42** (1984) 9–23.

[79] R. Stenberg and M. Suri, *An hp error analysis of MITC plate elements*, SIAM J. Numer. Anal., **34** (1997) 544–568.

[80] G. Strang and G. Fix, *An Analysis of the Finite Element Method*, Prentice-Hall, Englewood Cliffs, 1973.

[81] J.M. Thomas, *Sur l'analyse numérique des méthodes d'éléments finis hybrides et mixtes*, Thèse de Doctorat d'Etat, Université Pierre et Marie Curie, Paris 6, France (1977).

[82] M. Vanmaele and A. Ženíšek, *External finite element approximations of eigenvalue problems*, M^2AN, **27** (1993) 565–589.

[83] M. Vanmaele and A. Ženíšek, *External finite-element approximations of eigenfunctions in the case of multiple eigenvalues*, J. Comput. Appl. Math., **50** (1994) 51–66.

[84] M. Vanmaele and A. Ženíšek, *The combined effect of numerical integration and approximation of the boundary en the finite element methods for the eigenvalue problems*, Numer. Math., **71** (1995) 253–273.

[85] X. Wang and K.J. Bathe, *Displacement/pressure based mixed finite element formulation for acoustic fluid-structure interaction problems*, Internat. J. Numer. Methods Eng. **40** (1997) 2001–2017.

[86] A. Ženíšek, *Nonlinear Elliptic and Evolution Problems and Their Finite Element Approximation*, Academic Press, London, 1990.

[87] O. C. Zienkiewicz and R. L. Taylor, *The Finite Element Method*, Vol. 2, McGraw-Hill, London, 1991.

[88] M. Zlámal, *Curved elements in the finite element method I*, SIAM J. Numer. Anal., **10** (1973) 228–240.